November 2016

Cell Modulation Using Functionalized Nanoparticles

Rui Tang
University of Massachusetts Amherst

CELL MODULATION USING FUNCTIONALIZED NANOPARTICLES

A Dissertation Presented

by

RUI TANG

Submitted to the Graduate School of the
University of Massachusetts Amherst in partial fulfillment
of the requirements for the degree of

DOCTOR OF PHILOSOPHY

September 2016

Chemistry

Cell Modulation Using Functionalized Nanoparticles

A Dissertation Presented

by

RUI TANG

Approved as to style and content by:

_____
Vincent M. Rotello, Chair

_____
Richard W. Vachet, Member

_____
Alejandro P. Heuck, Member

_____
Craig T. Martin, Department Head
Department of Chemistry

DEDICATION

To my beloved family and friends

ACKNOWLEDGMENTS

I am very grateful to my advisor, Prof. Vincent Rotello, for sharing his enthusiasm for science and inspiring a bit in me, and for giving out all the knowledge possible every time. I would like to thank him for the patience, trust and encouragement.

I would like to thank my dissertation committee members, Prof. Richard Vachet and Prof. Alejandro Heuck. I appreciate their time and effort advising and helping me.

I would like to express my gratitude to Prof. Jeanne Hardy and Prof. Qiaobing Xu at Tufts University for our successful collaboration work. Their help is essential for my PhD research.

I am very thankful to all past and current Rotello lab members. My labmates are passionate, knowledgeable and dedicated. Dr. Xiaochao Yang was my first mentor in the lab and helped me set up my directions for my whole PhD research. Dr. Apiwat Chompoosor was my second mentor who guided me to the research of protein delivery. Dave extensively discussed with me about improving the quality of my research at my junior time. Dr. Zhengjiang Zhu, Dr. Bo Yan, Dr. Changsoo Kim, Dr. Subinoy Rana, Dr. Yi-cheun Yeh, Dr. Chandramouleeswaran Subramani, Dr. Eunhee Jeoung, Dr. Sungtae Kim and Dr, Youngdo Jeong are my great seniors that I feel very lucky to collaborate with them. I also learned quite much from Dr. Oscar Miranda, Dr. Chaekyu Kim, Dr. Myoung-Hwan Park, Dr. Sarit Agasti, Dr. Xi Yu, Dr. Xiaoning Li, Dr. Krishnendu Saha, Dr. Brian Creran, Dr. Tsukasa Miruhara and Dr. Tatsuyuki Yoshii. Brad and Daniel are my incredible batchmates. I improved much being with them. I am also very glad to work with many great juniors. Moumita was my mentee and we together accomplished great achievements. Ying, Gülen, Rubul, NLe, Ryan, Li-Sheng, Akash, Riddha, Yuanchang, Joe, Mahdieh, Yi-Wei, Yingying, Yuqing, Singyuk and Ziwen either collaborated with me or offered me help in different ways. Thank you all!

I appreciate my outside collaborators, Dr. Elih M Velázquez-Delgado and Dr. Ming Wang for their sincere help.

Finally, I would like to thank my family for their unconditional love throughout the years. My wife scarified herself for the family and her support during hard times greatly helped me to move forward. My daughter cheered my up and made me energetic every time when I encountered difficulties. She is my angel. My parents and parents-in-law always encouraged me to pursue my goal in science. Especially, my mother-in-law frequently traveled between China and US taking care of my family these years. This thesis would not be possible without their selfless devotion to the family.

ABSTRACT

CELL MODULATION USING FUNCTIONALIZED NANOPARTICLES

SEPTEMBER 2016

RUI TANG

B. Eng., SICHUAN UNIVERSITY, CHINA

M. Eng., SICHUAN UNIVERSITY, CHINA

Ph.D., UNIVERSITY OF MASSACHUSETTS AMHERST

Directed by: Professor Vincent M. Rotello

Monolayer functionalized ultra-small gold nanoparticles (AuNPs) provide a versatile platform for applications in cell research. Through rational design of surface ligands, the chemistry of AuNPs are precisely regulated at atomic level. In this dissertation, applications of AuNPs in cell modulation are discussed. The topics are split into two categories. In the first category, functionalized AuNPs are harnessed to generate a robust monolayer on cell culture surface for cell modulation. The proliferation and behavior of different types of cancer cells and normal cells are modulated by tuning the surface ligands of AuNPs. Fate decision of mesenchymal stem cells are also modulated using the same strategy. In the second category, AuNPs are assembled to nanoparticle stabilized capsules (NPSCs) for the delivery of a variety of proteins to cytosol of cells. Using this method, phenotype of cells are rapidly switched without genomic disturbance. In addition, subcellular localization of proteins are also controlled by the combination of subcellular localization signals and NPSC delivery platform. The first non-peptide synthetic nuclear localization signal based on boronate is discovered using NPSC delivery platform as well.

TABLE OF CONTENTS

Page

ACKNOWLEDGMENTS v

ABSTRACT vii

LIST OF TABLES xii

LIST OF FIGURES xiii

CHAPTER

1 NANOMATERIALS FOR CELL MODULATION 1

1.1 An overview of cell modulation 1
1.2 Nanotechnology for cell modulation 3

1.2.1 Nanotechnology 3
1.2.2 Nanotechnology for drug delivery 4
1.2.3 Nanotechnology for External Cell Modulation 6

1.3 Gold nanoparticles 6

1.3.1 Synthesis of gold nanoparticles 7
1.3.2 Functionalization of monolayer protected gold nanoparticles 8
1.3.3 Biomedical applications of gold nanoparticles 9

1.4 Nanoparticle stabilized capsule 10

1.4.1 Theoretical base of nanoparticle stabilized capsule (NPSC) 11
1.4.2 Applications of NPSCs 12

1.5 Dissertation overview 13
1.6 References 16

2 RAPID COATING OF SURFACES WITH FUNCTIONALIZED NANOPARTICLES FOR REGULATION OF CELL BEHAVIOR 20

2.1. Introduction 20
2.2. Methods 21

2.2.1. Syntheses of Ligands and AuNPs. 21
2.2.2 Synthesis of T-Phe ligand 21
2.2.3 Synthesis of T-Adman ligand 21
2.2.4 Syntheses of Functionalized AuNPs 22

2.2.5 AuNP Coating 22
2.2.6 Characterizations 22
2.2.7 Cell culture 23
2.2.8 Cell viability assay 23

2.3 Results and Discussion 24
2.4 References 34

3 MODULATION OF STEM CELL DIFFERENTIATION BY NANOPARTICLE FUNCTIONALIZED SURFACES 37

3.1 Introduction 37
3.2 Methods 39

3.2.1 AuNP coating 39
3.2.2 AFM imaging 39
3.2.3 Cell culture 40
3.2.4 Cell differentiation 40
3.2.5 AuNPs cell-uptake test 40
3.2.6 Cell viability assay 41
3.2.7 Cell fixation 41
3.2.8 Characterizations for osteogenesis 42
3.2.9 Characterizations for adipogenesis 42

3.3. Results and Discussion 43
3.4 Conclusion 53
3.5 References 54

4 DIRECT DELIVERY OF FUNCTIONAL PROTEINS AND ENZYMES TO THE CYTOSOL USING NANOPARTICLE-STABILIZED NANOCAPSULES 56

4.1 Introduction 56
4.2 Methods 58

4.2.1 Protein-NPSC complex preparation 58
4.2.2 GFP expression and purification 58
4.2.3 Caspase-3 expression and purification 59
4.2.4 Cell culture 59
4.2.5 Cell transfection and selection 60
4.2.6 Fluorescence titration 60
4.2.7 GFP delivery 60
4.2.8 CASP3 delivery 61
4.2.9 Cell viability assay (Alamar Blue) 61
4.2.10 In vitro caspase-3 activity assay 61
4.2.11 Live cell imaging 62

4.3 Results and Discussions 62

4.3.1 Nanoparticle-stabilized capsule fabrication 62
4.3.2 Therapeutic protein delivery with NPSCs 65
4.3.3 GFP delivery using NPSCs 67
4.3.4 Intracellular targeting of delivered proteins 72

4.4 Conclusion 75
4.5 References 75

5 QUANTITATIVE TRACKING OF PROTEIN TRAFFICKING TO THE NUCLEUS ENABLED BY CYTOSOLIC PROTEIN DELIVERY 77

5.1 Introduction 77
5.2 Results and Disscussions 78
5.3 Methods 86

5.3.1 Construction of plasmids and *Escherichia coli* strains 86
5.3.2 Protein Expression 87
5.3.3 Protein-NPSC Complex Formation 88
5.3.4 Cell viability assay (Alamar Blue) 88
5.3.5 Cell culture 89
5.3.6 NLS-eGFP Delivery 89
5.3.7 Cell Imaging 89
5.3.8 Live Cell Imaging 89
5.3.9 ATP Depletion 90
5.3.10 Image Analysis 90

5.4 Conclusion 90
5.5 References 90

6 EFFECTIVE NUCLEAR LOCALIZATION OF PROTEINS WITH BORONATE TARGETING SIGNALS 92

6.1 Introduction 92
6.2 Methods 94

6.2.1 GFP expression 94
6.2.2 Protein modification 95
6.2.3 Protein-NPSC Complex Formation 95
6.2.4 Cell culture 96
6.2.5 Cell synchronization 96
6.2.6 Cell viability assay (Alamar Blue) 97
6.2.7 Protein delivery 97
6.2.8 Importin α/β inhibition 97
6.2.10 ATP Depletion 98
6.2.11 Image Analysis 98

6.3 Results 98

6.3.1 RNase A-NBC accumulates in the nucleus after NPSC delivery 98
6.3.2 NBC tag drives nuclear accumulation 103
6.3.3 NBC mediated nuclear localization is independent of cell synchronization, cell type, delivery vehicle and protein size 111
6.3.4 Pathways involved in NBC nuclear accumulation 114

6.4 Discussion 117
6.5 References 118

7 INTRACELLULAR DELIVERY OF LARGE PROTEINS USING NANOPARTICLE-STABILIZED CAPSULES 120

7.1 Introduction 120
7.2 Methods 121

7.2.1 Preparation of GIPA Ligand 121
7.2.2 Gold nanoparticle (AuNP) synthesis and functionalization with GIPA Ligand 125
7.2.3 Cell culture 126
7.2.4 Fluorescence titration 127
7.2.5 Protein-NPSC complex formation 127
7.2.6 Protein delivery 127
7.2.7 X-gal staining 128
7.3 Results and Discussion 128

7.4 Conclusion 133
7.5 References 133

BIBLIOGRAPHY 136

LIST OF TABLES

Table Page

1.1. Examples of commercialized nanoscale systems for disease therapies..... 5

5.1. Primers for PCR cloning 80

5.2. Sequences of NLS-eGFPs (NLSs have been labeled with color) 81

5.3. Primers for PCR cloning 87

6.1. Quantitative analysis of individual cells after RNase A-NBC delivery..... 101

6.2. Quantitative analyses of individual cells after RNase A-ACO delivery 102

6.3. Quantitative analyses of individual cells after GFP-NBC delivery..... 106

6.4. Quantitative analysis of individual cells after GFP-CPB delivery 108

6.5. Quantitative analysis of individual cells after GFP-NC delivery..... 108

6.6. Quantitative analysis of individual cells after GFP delivery..... 109

6.7. Quantitative analysis of individual cells after GFP-NBC delivery in the presence of ivermectin..... 115

6.8. Quantitative analysis of individual cells after GFP-NBC delivery with ATP depletion. 116

6.9. Quantitative analysis of individual cells after GFP-NC delivery in the presence of ivermectin..... 117

LIST OF FIGURES

Figure Page

1.1. Schematic representing different approaches for cell modulation. 2

1.2. Preparation of monolayer-protected AuNPs using the Brust–Schiffrin reaction, and functionalization using the Murray's place-exchange reaction.[63] 7

1.3. Structure of monolayer stabilized AuNP 8

1.4. AuNPs for biological applications. 9

1.5. Formation of Pickering emulsion. 10

1.6. Fabrication of stable nanoscale NPSCs. 11

1.7. External and internal modulation of cells using functionalized nanoparticles 14

2.1. Preparation and characterization of TTMA AuNP layer on the polystyrene-plate surface. a) Schematic representation of the strategy to generate a AuNP monolayer on the cell-culture plate. b) Angle-resolved XPS detection of the polystyrene-plate surface with the AuNP layer. Relative atomic concentrations of C, N, O and Au are listed in the table. c) AuNPs attached to the plate with or without plasma treatment under cell-culture conditions. Each bar represents the amount of gold left in one well of a 96-well plate. The error bars represent the standard deviation of three measurements. 25

2.2. Characterizations of cell culture plate surface after TTMA AuNP coating. Untreated surface and surface treated with water without AuNPs were used as controls. a) AFM images and related roughness measurements. b) Mean roughness values with triplicate determinations. 26

2.3. AuNPs amount taken up by cells and left on the cell culture plate surface after one week culture of HepG2 cells (started at 30,000 cells/well). The cell culture media were replaced every other day. 27

2.4. Attachment of HepG2 cells after 80 min incubation on cell culture plates a) without or b) with TTMA AuNP coating. Bar: 100 µm 28

2.5. Optical images of HepG2 cell grown on a) plasma-treated plate and b) TTMA AuNP coated surface. Bar: 100 µm 28

2.6. HepG2 cell culture for 24 h on plates with and without the TTMA AuNP layer. a) Optical image of HepG2 cell grown on a plasma-treated plate. b) Optical image of HepG2 cell grown on a TTMA AuNP monolayer. c) Fluorescent image of Figure 2.6a. F-actin was stained by Oregon Green labeled phallotoxin, and the nuclei were stained by Hoechst 33342. d) Fluorescent image of Figure 2.6b. The staining conditions were the same as in Figure 2.6c. The arrow indicates filopodia of the cell. e) Cell-uptake test of TTMA AuNP monolayer. The cells were cultured on the TTMA AuNP monolayer in a 24-well plate for 24 h. A 24-well plate coated with TTMA AuNPs without cells cultured on the surface was used as a control. 29

2.7. HepG2 cells growing on TTMA CdSe quantum dots coated surface for 24 h showed similar morphology as those growing on TTMA AuNP coated surface. Bar: 100 µm 30

2.8. Cell viability assay for 26 different AuNP coatings (morphology changes of HepG2 cell were shown in Figure 2.9). a) A heat map of cell viability influenced by different AuNP coatings. b) Structures of ligands on the AuNPs. 'Blank' represents the cell viability on plasma-treated surface without any pretreatment, and 'Water' represents the cell viability on the surface pretreated with water only (no AuNP added) for 3 h and without post deposition of AuNPs. 31

2.9. Morphologies of HepG2 cell in the presence of AuNPs listed in Figure 2.8. Bar: 100 µm 32

2.10. Cell viability variations induced by different kinds of AuNP coatings. R^2 values of linear fitting are -0.012, 0.175, 0.012 and 0.067 for HepG2, MCF7, HeLa and 3T3 groups, respectively. 34

3.1. Schematic representation of the strategy developed to control MSC differentiation using tunable AuNP-coated surfaces. 39

3.2. AFM image and cross section profile of untreated cell culture plate, water-treated cell culture plate and TTMA AuNP-treated cell culture plate. The RMS roughness was obtained from three cross section profiles in each image (0.5 nm ± 0.1 nm, 0.2 nm ± 0.1 nm, 0.2 nm ± 0.1 nm, respectively). 44

3.3. Cell-uptake test of TTMA AuNP monolayer. The cells were cultured on the TTMA AuNP monolayer in a 24-well plate under adipogenic or osteogenic induction conditions for one week. A 24-well plate coated with TTMA AuNPs without cells cultured on the surface was used as a control. 44

3.4. MSCs grown on differential functional positively charged AuNP-coated surfaces for 1 hr. Scale bars: 100 µm. 45

3.5. Proliferation assay of MSCs grown on surfaces functionalized with different positively charged AuNPs for 1 day, 3 days and 7 days. 46

3.6. MSCs grown on differential functional positively charged AuNP-coated surfaces for 24 hr. Scale bars: 100 µm. 46

3.7. MSCs grown on differential functional positively charged AuNP-coated surfaces for 7 days. Scale bars: 100 µm.. 47

3.8. Proliferation assay of MSC on various positively charged AuNP-coated surfaces after 7 days induction in differentiation media: a) Adipogenic inducing media; b) Osteogenic inducing media. 48

3.9. Vector® Blue staining for alkaline phosphatase activity after osteogenic induction for 14 days. Scale bars: 100 µm. 49

3.10. Osteogenesis of MSCs is modulated by AuNP-coated surfaces. a) Normalized differentiation ratio of induced cells grown on AuNP-coated surfaces after 14 days, marked by alkaline phosphatase expression level. b) Normalized calcium mineralization of osteoblasts, determined by Alizarin Red S staining. 50

3.11. Cells stained with Alizarin S (red) and Vector® Blue (blue) after osteogenic induction for 14 days. Scale bars: 100 µm. 51

3.12. Adipogenesis of MSCs is modulated by AuNP-coated surfaces. a) FABP4 expression of induced cells grown on AuNP-coated surfaces after 7 days. b) FABP4 expression of induced cells grown on AuNP-coated surfaces after 14 days. c) Normalized differentiation ratio determined by Oil Red O staining..... 52

3.13. Oil Red O staining of cells after adipogenic induction for 14 days. Scale bars: 50 µm. 53

4.1. Design and preparation of nanoparticle-stabilized capsules (NPSCs). (a) Schematic showing the preparation of the protein-NPSC complex containing caspase-3 or GFP and proposed delivery mechanism. The oil was a 1:1 mixture of linoleic acid (LA) and decanoic acid (DA). (b) TEM image of the dried GFP-NPSC. (c) Dynamic light scattering (DLS) histogram of GFP-NPSCs indicating an average diameter of 130 ± 40 nm. 63

4.2. DLS (left) and TEM (right) results of CASP3-NPSCs. 63

4.3. Determination of the interaction between GFP and HKRK AuNPs. (a) Fluorescence titration of HKRK AuNPs in the presence of 100 nM GFP in 5 mM phosphate buffer (pH = 7.4). The binding constant (Ks) and association stoichiometry (n) were calculated through the fitting using the model of single set of identical binding sites.[33] (b) Fluorescence recovery of 100 nM GFP quenched by 100 nM HKRK AuNPs in the presence of 500 mM NaCl or phosphate buffer (control). 65

4.4. (a) Fluorescence recovery of GFP quenched by NPSC. The concentrations of both GFP and AuNP are 400 nM in 100 µL mixture. The concentration of NaCl is 500 mM and that of Tween-20 is 0.5% by volume. (b) In vitro activity assay of CASP3 in the presence or absence of HKRK AuNPs. 65

4.5. Delivery of caspase-3 into HeLa cells. Cells were incubated for 1 h with (a) CASP3-NPSC, (b) NPSC without CASP3, and (c) only CASP3 without NPSC. Subsequently, cells were stained using Yopro-1 (green fluorescence) and 7-AAD (red fluorescence) for 30 min, and the overlapped images are presented as apoptotic. (d) Apoptosis ratios of the cells after CASP3 delivery. Scale bars: 100 µm; the error bars represent the standard deviations of three parallel measurements. 67

4.6. Delivery of GFP into HeLa cells. (a) Confocal image showing GFP delivery into HeLa cells by NPSCs. (b) Confocal images showing the colocalization of delivered GFP with expressed mCherry in HeLa cell. (c) Flow cytometry results of HeLa cells treated with GFP-NPSCs (red), or GFP alone (blue) for 2 h, using untreated HeLa cells as the control (black). Scale bars: 20 µm. 68

4.7. Co-incubation of empty NPSC and GFP with HeLa cells for 1 hr. The bar represent 20 µm. 69

4.8. HeLa cells stably express mCherry (control group for Figure 2d in context). The scale bar represents 20 µm. 69

4.9. (a) Colocalization of GFP and Hoechst 33342 in a HeLa cell. (b) Magnified from boxes of Figure 4.9a. The scale bars represent 20 µm. 69

4.10. Flow cytometry results of HeLa cells cultured with GFP-HKRK AuNPs for 2 h, using untreated HeLa cells as the control. 70

4.11. Confocal image of the colocalization of GFP with late endosomes and lysosomes after 1 hr of delivery by HKRK AuNPs. The scale bar represents 20 µm. 71

4.12. Viability of HeLa cells at different concentrations of GFP-NPSC complexes measured by Alamar Blue assay. 71

4.13. Live cell imaging of rapid GFP release into the cytosol of HeLa cell by NPSCs. “0 min” label represents the starting point of release. The arrow indicates a GFP-NPSC at the cell membrane prior to delivery of payload. Scale bar: 20 µm. 72

4.14. GFP fused with PTS1 motif..... 73

(a) Sequence of C-terminal of GFP from the plasmid (sequence:
MASHHHHHHMVSKGEELFTGVVPILVELDGDVNGHKFSVSGEGEGDATYGKLTLKFI
CTTGKLPVPWPTLVTTFTYGVQCFSRYPDHMKQHDFFKSAMPEGYVQERTIFFKDD
GNYKTRAEVKFEGDTLVNRIELKGIDFKEDGNILGHKLEYNYNSHNVYIMADKQKNGI
KVNFKIRHNIEDGSVQLADHYQQNTPIGDGPVLLPDNHYLSTQSALSKDPNEKRDHM
VLLEFVTAAGITHGMDELYK). 73

(b) Sequence of C-terminal of GFP fused with PTS1 motif from the plasmid (sequence:
MASHHHHHHMVSKGEELFTGVVPILVELDGDVNGHKFSVSGEGEGDATYGKLTLKFI
CTTGKLPVPWPTLVTTFTYGVQCFSRYPDHMKQHDFFKSAMPEGYVQERTIFFKDD
GNYKTRAEVKFEGDTLVNRIELKGIDFKEDGNILGHKLEYNYNSHNVYIMADKQKNGI
KVNFKIRHNIEDGSVQLADHYQQNTPIGDGPVLLPDNHYLSTQSALSKDPNEKRDHM
VLLEFVTAAGITHGMDELYK**SKL**)..... 73

4.15. Peroxisome targeting in HeLa cells transfected with RFP-PTS1 plasmid. (a) Colocalization of GFP-PTS1 fusion protein with the peroxisomal indicator (RFP-PTS1) expressed by the cell. (b) No colocalization of GFP was observed without PTS1 motif. Scale bars: 20 µm. 74

4.16. (a) Delivery of GFP-PTS1 into HeLa cells by NPSCs. (b) Untreated cells under the same exposure conditions. The scale bars represent 20 µm. 74

5.1. Delivery of eGFP fused with nuclear localization signals (NLS) to cells using NPSCs. (**a**) Schematic representing the cytosolic delivery and nuclear accumulation of proteins with NLSs. (**b**) Structure of eGFP fused with NLSs. (**c**) LSCM images showing different cellular distribution patterns of eGFP fused with NLSs. Bars: 20 µm. (**d**) Statistical analysis revealing nuclear importing efficiency (6 cells per group). 79

5.2. SDS-PAGE analysis of five NLS-eGFPs..... 80

5.3. Dynamic Light Scattering measurements for NLS-eGFP-NPSC complexes. 80

5.4. Viability of HeLa cells at different concentrations of NPSC-NLS$^{c\text{-}Myc}$-eGFP complexes measured by Alamar Blue assay..... 83

5.5. Large scale images of NLS-eGFPs delivered into HeLa cells. Bars: 20 µm. 83

5.6. Typical results of quantitative fluorescence intensity analyses of NLS-eGFPs in single cells. Quartiles of pixel intensities were illustrated as box plots. 84

5.7. LSCM image showing cellular distribution pattern of eGFP without NLS. Bar: 20 µm. 84

5.8. Nuclear import of eGFP fused with NLS is rapid and ATP dependent. (**a**) Time-lapse fluorescent microscopic images show nuclear accumulation of $NLS^{c\text{-}Myc}$-eGFP starts within 1 minute after presenting in cytosol. (**b,c**) Time-lapse LSCM images unveil the kinetics of nuclear import of $NLS^{c\text{-}Myc}$-eGFP. (**d**) No nuclear accumulation of $NLS^{c\text{-}Myc}$-eGFP is observed after the delivery following ATP depletion in the presence of 3 mg/mL NaN_3 and 50 mM 2-deoxyglucose. Bars: 20 µm..... 85

5.9. Typical results of quantitative fluorescence intensity analyses of NLSc-Myc-eGFPs in single cell at different time scales. Quartiles of pixel intensities were illustrated as box plots. 85

5.10. A comparison between the cytosolic delivery of (a) NLSc-Myc-eGFP at ATP depletion condition and (b) eGFP without NLS into HeLa cells. Bars: 20 µm. (c,d) Quartiles of pixel intensities were illustrated as box plots. For (d) Analysis of the boxed cell in b. 86

6.1. Schematic diagram showing delivery of RNase A-NBC-NPSC complex to the cytosol and into the nucleus of cells..... 94

6.2. Viability of HeLa cells at different concentrations of NPSC measured by Alamar Blue assay. 94

6.3. Delivery complex of RNase A-NBC labeled with FITC and NPSCs. (a) Mass spectrometry of RNase A-NBC labeled with FITC. (b) Dynamics light scattering results of the size of the delivery complex..... 99

6.4. Delivery of RNase A-NBC into HeLa cells using the NPSC delivery platform. (a) LSCM image showing RNase A-NBC delivery into HeLa cells by NPSCs. Arrows indicate granular structures of RNase A-NBC formed in the nucleus. (b) Quantitative analysis of fluorescence intensities in a. (c) Colocalization of RNase A-NBC with Hoechst 33342, a DNA staining dye. (d) Colocalization of RNase A-NBC with Pyronin Y, a dsRNA staining dye. Scale bars: 10 µm. 100

6.5. LSCM image showing RNase A delivery into HeLa cells by NPSCs: (a) RNase A-NBC and (b) RNase A-ACO. Scale bar: 20 µm. 100

6.6. Quantitative analysis of an individual cell in Figure 1b after RNase A-NBC delivery. (a) Analysis result after R processing. (b) Different parts of the image were split for the analysis..... 101

6.7. Z-stack overlap of RNase A-NBC with Pyronin Y. Green: RNase A-NBc; Red: Pyronin Y. Scale bar: 20 µm. 103

6.8. Nuclear accumulation of eGFP relies on the NBC label. (a) LSCM image of a HeLa cell after the delivery of eGFP-NBC. (b) LSCM image of a HeLa cell after the delivery of eGFP-CPB. (c) LSCM image of a HeLa cell after the delivery of eGFP-NC. (d) LSCM image of a HeLa cell after the delivery of normal eGFP. Scale bars: 20 μm. (e) Quantitative analysis of the increased fluorescence intensity of eGFP in the nucleus. Six random cells representing different intensities were analyzed in each group. ** indicates P value of t-test less than 0.01. 104

6.9. Mass spectrometry of both native and tagged GFP. 105

6.10. Large scale LSCM images of HeLa cells after delivery of GFP with different labels. Native GFP was delivered as a control. Scale bars: 20 μm. 106

6.11. Quantitative analysis of individual cells in Figure 6.8. 106

6.12. GFP-NBC dose not accumulate into nucleoli of the HeLa cell. Scale bars: 20 μm. 107

6.13. Flow cytometry results of GFP delivery with or with without tags to HeLa cells. (a) Flow cytometry data. (b) Ratio of GFP positive cells in each group. (c) Average fluorescence intensity of cells in each group. 109

6.14. Delivery of dsRed with or without NBC tag to HeLa cells. (a) SDS-PAGE gel of dsRed before Brilliant Blue staining. (b) SDS-PAGE gel after Brilliant Blue staining. Under denaturing condition to break the tetramer structure, samples were denatured with 2-mercaptoethanol at 95 °C for 5 min. Under semi-denaturing condition to keep the tetramer structure, samples were loaded without treatment of 2-mercaptoethanol or heating. Protein amount for each lane: 20 μg. (c) Large scale LSCM images of HeLa cells after 1 hr delivery of dsRed with NBC tag. (d) Large scale LSCM images of HeLa cells after 1hr delivery of dsRed without NBC tag. Scale bars: 20 μm. 110

6.15. Large fluorescent protein dsRed was accumulated in nucleus after labeling with NBC tag. (a) deRed-NBC accessed nucleus of HeLa cell after 1 hr delivery. (b) dsRed without NBC tag did not enter nucleus of HeLa cell after 1 hr delivery. (c) 8 hr after dsRed-NBC delivery to HeLa cells. Scale bars: 20 μm 112

6.16. Flow cytometry after cell synchronizations. 112

6.17. NBC mediated nuclear localization is independent of cell synchronization, cell type and delivery vehicle. (a) eGFP-NBC delivery after cells being synchronized to G0/G1 phase and (b) to the beginning of S phase. (c) eGFP-NBC delivery to human mesenchymal stem cell. (d) eGFP-NBC delivery using Arginine AuNP NPSCs as the vehicle. Scale bars: 20 μm. 112

6.18. Large scale LSCM images of MSCs after delivery of GFP tagged with NBC. Scale bar: 20 μm. 113

6.19. Inhibition of active import to nucleus significantly reduces nuclear accumulation of NBC-tagged eGFP. (a) eGFP-NBC delivery before and (b) after inhibition of importin α/β pathway. (c) eGFP-NBC delivery after inhibition of all active import pathway by ATP depletion. (d) eGFP-NC delivery before and (e) after inhibition of importin α/β pathway. (f) eGFP-NC delivery after inhibition of all active import pathway by ATP depletion. Scale bars: 20 µm. (g) Quantitative analysis of increased fluorescence intensity of eGFP-NBC and eGFP-NC in the nucleus after delivery with or without pretreatment using six cells in each group. 115

6.20. Quantitative analyses of individual cells in Figure 6. 116

7.1. Schematic illustration of a new platform of intracellular protein (dsRed and *β*-galactosidase) delivery using GIPA AuNPs-stabilized capsule. 121

7.2. Synthetic scheme of GIPA ligand. 122

7.3. TEM image of GIPA-functionalized AuNPs. The black scale bar is 20 nm as denoted. 126

7.4. DLS histogram of GIPA-functionalized AuNPs, demonstrating the hydrodynamic diameter distribution of nanoparticles. 126

7.5. Fluorescence titrations of AuNPs in the presence of fluorescent proteins. 129

7.6. DLS histogram of dsRed-NPSCs indicating an average diameter of 130 ± 50 nm. 130

7.7. Delivery of dsRed to cytosol of HeLa cells. a) Flow cytometry results of dsRed delivery by GIPA NPSCs. b) Quantification of average fluorescence intensity of cells. c) Flow cytometry results of dsRed delivery by HKRK NPSCs. d) Quantification indicates GIPA NPSC has much higher efficiency for the delivery of dsRed. e) LSCM image showing dsRed delivery into HeLa cells by GIPA NPSCs. f) Z-stack image of dsRed delivery. Scale bars: 20 µm. 131

7.8. DLS histogram of *β*-Gal-NPSCs indicating an average diameter of 110 ± 50 nm. 132

7.9. Distribution of *β*-gal in HeLa cells after delivery. a) LSCM image showing FITC- *β*-gal delivery. Scale bar: 10 µm. b) X-gal staining of delivered *β*-gal in HeLa cells. c) X-gal staining of cells incubated with free *β*-gal alone. d) X-gal staining of cells incubated with NPSCs alone. Scale bars: 100 µm. 133

CHAPTER 1

NANOMATERIALS FOR CELL MODULATION

1.1 An overview of cell modulation

Cell is the fundamental unit of structure and function in living organisms. Generally, cells are responsible for basic functions such as growth, metabolism and reproduction. Cells with similar functions form tissues and organs that are responsible for the vitality of higher organisms such as human beings. Dysfunction of cells is associated with numerous infectious[1-3] and noncommunicable[4-6] diseases. Therefore, cells are primary targets in multiple clinical applications, such as organ transplantation,[7] tissue regeneration and engineering,[8] wound healing[9] and disease therapies.[10]

Modulation of cells naturally occurs and has been broadly used in research and clinical applications. Literally, processes that modify cell genotype, phenotype, behavior, signaling and viability are categorized to cell modulation. Modulation of cells in nature associates with development,[11] cell maturation,[12] organ and tissue renewal[13] and senescent cell clearance.[14] For example, during the development of embryo, cells in blastocyst are modulated to different fates for further tissue and organ formation;[15] in hematogenesis, hematopoietic stem cells are modulated by surrounding niches for the generation of different types of terminal blood cells;[16] old cells or abnormal cells are modulated to death by themselves, microenvironment or killer cells through the activation of apoptosis signals[17] or the intracellular delivery of killing proteins such asgranzymes.[18]

Cell modulation has been extensively investigated in research (Figure 1.1). As a basic biological technique, cell culture is a typical and one of the oldest example of in vitro cell modulation. Since the success of HeLa cell culture, numerous cell types have been isolated from

tissues and are eternally growing in laboratories and factories all over the world. To effectively culture cells, an appropriate environment and enough nutrient must be supplied. Additional supplements may also be required including chemical and biological compounds to induce the proliferation and maintain or change phenotypes of cells. Adapted from nature, different kinds of signaling proteins originated as in vivo cell modulators have been heavily harnessed,[19, 20] such as epidermal growth factor, transforming growth factors and bone morphogenetic proteins, Cytokines and leukemia inhibitory factor. Chemical compounds including inhibitors, inducers and other types of regulators have been employed for phenotypical and behavioral modulations as well. Dexamethasone, a steroid medication, is an indispensable compound for osteoblast generation[21] and immune cell modulation;[22] CHIR99021, a GSK3α/β inhibitor, has been used for stem cell maintenance and differentiation;[23] a cocktail of chemicals alone was reported to reprogram somatic cells to induced pluripotent stem cells in 2013.[24]

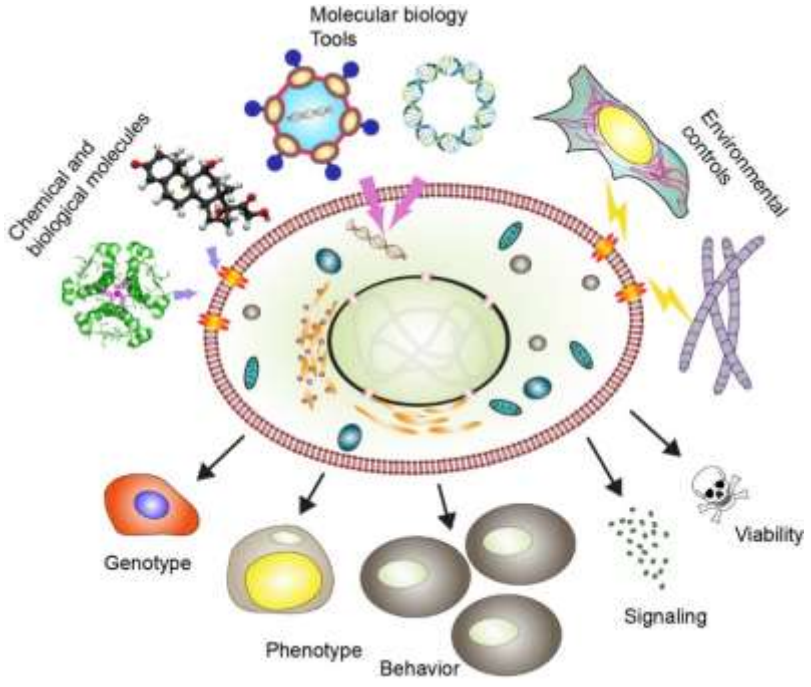

Figure 1.1. Schematic representing different approaches for cell modulation.

Another classical set of approaches is to deliver genes, mRNAs, siRNAs and proteins to cells to modify the genotype or phenotype of cells. Introduction or deletion of genes by virus,[25] plasmids[26] and genomic editing proteins[27] provides a powerful means to modify cell behaviors and functions, thus greatly facilitate the fundamental discovery and development of therapeutic methods. A representative example is the reprogramming of induced pluripotent stem cells from somatic cells. Yamanaka et al successfully induced fibroblasts to pluripotent stem cells by transfection of four genes with viral vectors in 2006.[28] After that, numerous other delivery vectors have been thoroughly studied for reprogramming various types of cells.[29]

In recent years, environment based controls have been an emerging technique for the modulation of cells, especially for the control of cell phenotype, behaviors and fate decision.[30] To this end, different environmental controlling strategies have been developed.[31] A straightforward way is to mimic the in vivo conditions using chemical or biological materials. For example, collagen and derivatives have been used to reconstruct the extracellular matrix for cell growth.[32] Synthetic polymers have also been developed to simulate the extracellular matrix for better cell maintenance or modulations.[33] More recently, organs have been decellularized with surfactants and repopulated with specific cell types for regeneration. Regenerated organs can be transplanted back to animals and regain functions.[34] Without a doubt, cell modulation will play a major role for the clinical practice in the future for disease therapy and wound healing.

1.2 Nanotechnology for cell modulation

1.2.1 Nanotechnology

In 1959, Late Nobel Laureate Richard Feynman raised nanotechnology in his revolutionary lecture “There's plenty of room at the bottom”.[35] In the lecture, manipulating small-scale

molecules for large-scale benefits was discussed. Since then, nanotechnology, a discipline composed of science, technology and engineering manipulating at nanoscale, has attracted attentions from both research and industry sectors. Properties of nanostructured materials differ from their bulk counterparts. At nanoscale, materials bear reduced elastic modulus, decreased melting points, increased diffusion, enhanced solid solubility, lower thermal conductivity and novel optical property.[36] Due to such difference, nanotechnology has been rapidly developing in multiple disciplines, including chemistry, biology, physics, materials science, and engineering. Nanotechnology covers a series of aspects including nanomaterials, a set of substances where at least one dimension is at nanoscale,[37] and nanofabrication, a collection of techniques that generates reproducible patterns whose elements have sizes of 100nm or less in at least one dimension.[38]

Nanotechnology has greatly broadened the application of materials in biological and clinical applications. Besides widely sold gold nanoparticle based pregnancy test strips, numerous nanomaterials and nanodevices have been commercialized or in clinical trials (Table 1.1). In addition, nanomaterials have been exploited as magnetic resonance imagining contrast agents[39] and optical/fluorescent imaging agents,[40] as well as various disease detection sensors.[41]

1.2.2 Nanotechnology for drug delivery

Delivery of functional molecules to cells belongs to one category of cell modulation. Delivery of drugs alters cell viability and behavior, as well as induces cell death. Delivery of macromolecules, such as proteins, DNA and RNA, modifies the phenotype or genotype of cells. Due to their large surface to mass ratio, facile cellular internalization, nanomaterials especially nanoparticles are ideal vehicles for delivery of functional molecules to cells.[42] Through nanomaterials based delivery vehicles, drugs target diseases with increased efficiencies.[43]

Amongst vast amount of nanovehicles, some have been commercialized for clinical uses, such as Doxil, a liposome based doxorubicin drug for cancer therapy.[44] More examples can be found in Table 1.1. Successes in commercialization of these drugs greatly inspired the development of this area. A number of new nanovehicles for drug delivery is created every year,[45] including nanoparticles, polymers, dendrimers and liposomes and lipids.

Table 1.1. Examples of commercialized nanoscale systems for disease therapies[46, 47]

Drug product	Active ingredient	Indications
Doxil (Caelyx)	Pegylated doxorubicin	Ovarian/breast cancer
Abraxane	Albumin-bound Paclitaxel nanospheres	Various cancers
	Nab paclitaxel in combination with gemcitabine	Metastatic pancreatic cancer
Myocet	Liposome encapsulated Doxorubicin	Breast cancer
DaunoXome	Liposome-encapsulated Daunorubicin	HIV-related Kaposi sarcoma
DepoCyt	Liposomal Cytarabine	Lymphomatous meningitis
Oncaspar	PEGasparaginase	Acute Lymphocytic Leukemia
Marqibo	Vincristine	Philadelphia chromosome-negative lymphoblastic leukemia
Genexal-PM	Paclitaxel-loaded polymeric micelle	Breast cancer/small cell lung cancer
Ontak	Diphtheria toxin	Cutaneous T-cell
ThermoDox	Heat-activated liposomal encapsulation of doxorubicin	Breast cancer, primary liver cancer
Rexin-G	Targeting protein tagged phospholipid/microRNA-122	Sarcoma, osteosarcoma, pancreatic cancer, and other solid tumor
Resovist	Iron oxide nanoparticles coated with carboxydextran	Liver/spleen lesion imaging
Feridex	Iron oxide nanoparticles coated with dextran	Liver/spleen lesion imaging
Endorem	Iron oxide nanoparticles coated with dextran	Liver/spleen lesion imaging

1.2.3 Nanotechnology for External Cell Modulation

Modulating the proliferation and function of cells through external stimulation have been achieved using nanotechnology as well. Nanomaterials show high potential for the modulation of cells. Recently, Mooney et al reported that elasticity of nanoporous hydrogel controls transplanted-stem-cell-mediated bone formation.[48] Ding et al discovered that by spatial organization of cell-adhesive ligands on nanoparticles as well as matrix stiffness direct the fate decision of stem cells.[49] In another research conducted by Di Carlo et al, nanomagnets was found to engineer the polarity of neuron, yielding new insights into mechanotransduction in neural networks.[50] Through nanopartterning, shape,[51] growth[52] and differentiation[53] of cells were modulated. Although techniques or materials of nanotechnology employed for cell research vary, they all take advantage of the interactions between cells and support materials at nanoscale. Through ratinal design, physical, chemical and biological properties of materials can be harnessed for precise modulation of cells for both research and applications.

1.3 Gold nanoparticles

The use of gold nanoparticles (AuNPs) can be backtracked to ancient Egypt and Roman times.[54] AuNPs bear advantageous physical, chemical and biological properties that have been adopted in immense applications.[55] AuNPs are optically differed from bulk gold. The surface plasmon resonance of AuNPs leads to strong electromagnetic fields on the particle surface and consequently enhances all the radiative properties of both light absorption and scattering.[56] AuNPs are relatively inert in biological environment, making them compatible for biomedical applications.[57] In addition, size, shape, and surface properties of AuNPs can be facilely modulated for specific purposes.[58] These properties confer AuNPs a versatile platform for a spectrum of biological applications.

1.3.1 Synthesis of gold nanoparticles

In general, the synthesis of AuNPs includes the nucleation of AuNP cores and stabilization of AuNPs with a shell to prevent aggregation. AuNPs can be synthesized in both aqueous solution and organic solvents. For the synthesis in aqueous solution, stabilizer are chosen from small molecules, such as citrate[59] and polyphenols,[60] to macromolecules,[61] including polymers, proteins and DNA. However, direct synthesis of AuNPs in aqueous solution has intrinsic drawbacks. Particularly, once AuNPs are wrapped with stabilizers, they are difficult to be further functionalized, limiting their further applications.

Phase transfer is an alternative strategy for the synthesis of AuNPs with the ease of preparation, purification and further functionalization. Phase transfer technique includes two basic steps, nucleation and stabilization (Figure 1.2). Apart from aqueous synthesis, these two steps occur in organic solvents. For example, in the classical Brust–Schiffrin method,[62] tetraoctylammonium bromide (TOAB) was employed to transfer hydrogen tetrachloroaurate ($HAuCl_4$) from aqueous phase to the organic phase and then sodium borohydride ($NaBH_4$) was used to reduce the gold salt to AuNPs. Immediately after the nucleation, the surfaces of AuNPs were protected with a monolayer of thiols for stabilization. This monolayer can be readily displaced with functionalized ligands for further applications (Figure 1.2).

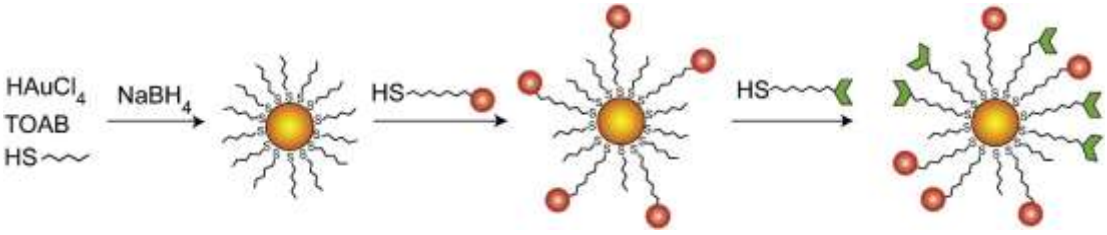

Figure 1.2. Preparation of monolayer-protected AuNPs using the Brust–Schiffrin reaction, and functionalization using the Murray's place-exchange reaction.[63]

1.3.2 Functionalization of monolayer protected gold nanoparticles

AuNPs synthesized with phase transfer method are covered with labile capping agents on the surface, such as thiols. These agents, however, can be displaced by rationally designed functional ligands thereafter. Since 1996, Murray et al have studied the ligand substitution, or place exchange, on AuNP surface in a series of research and paved the way for precise functionalization of ultra-small AuNPs.[64, 65]

Place exchange is a process that substitutes anchored primary ligands on AuNP surface with secondary free ligands. In the pioneer research done by Murray et al,[65] two important principles were drawn: (1) more polar ligands displace less polar ligands; (2) Ligands with longer chain displace ligands with shorter chain. Based on these principles, Rotello et al further developed a series of ligands for place exchange that both well protects and precisely functionalizes AuNPs. A representative structure of such ligand is shown in Figure 1.3. This type of ligand is composed of a thiol terminal for interaction with the AuNP core, a hydrophobic chain for stability, an oligo(ethylene glycol) layer for biocompatibility, and terminal residues for functions.[66] By tuning the terminal residues, the function of AuNPs can be specified. This approach standardized the preparation of functionalized AuNPs with tunable functions, thus opening up a new avenue for the use of AuNPs in different scenarios.

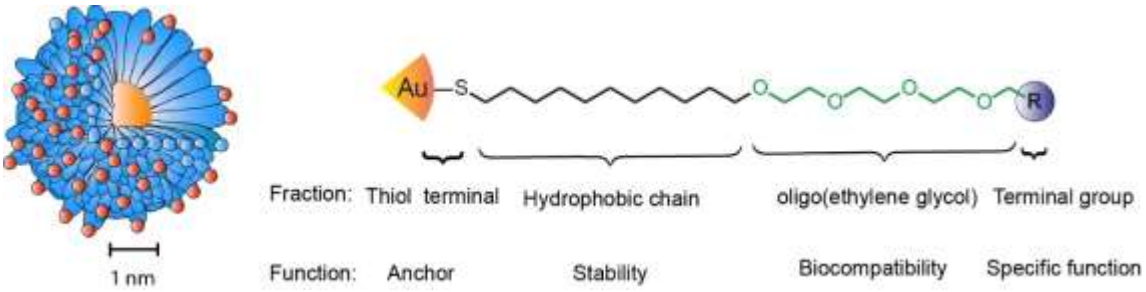

Figure 1.3. Structure of monolayer stabilized AuNP

1.3.3 Biomedical applications of gold nanoparticles

AuNP is one of the earliest commercialized nanomaterials for biomedical applications. In recent years, a number of new applications of AuNPs have been developed, such as sensors, heating sources and delivery vehicles.[67] As pioneers in this field, Rotello et al applied monolayer protected AuNPs to numerous applications by taking advantage of the interactions between AuNPs and biological substrates (Figure 1.4). Interactions between AuNPs and biological molecules have been thoroughly analyzed.[68-72] AuNPs have also been utilized as a versatile sensing probe for the detection of different kinds of analytes, such as proteins,[66] bacteria[73] and cells.[74] In another series of research, AuNPs were exploited as carriers for intracellular delivery of various molecules, such as drugs,[75] proteins[76] and DNA.[77] By designing terminal residue of surface ligand, interactions of AuNPs with delivery payloads are readily modulated. Through cell uptake, various payloads have been successfully delivered to cells for specific functions. Decorating the surface of AuNPs with zwitterion ligands further modulates cell uptake, thus potentially affecting delivery and sensing strategies using AuNPs.[78]

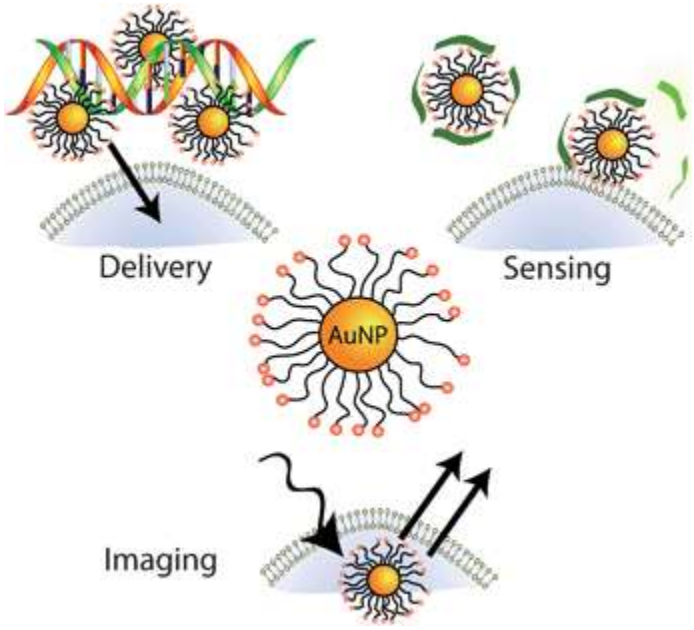

Figure 1.4. AuNPs for biological applications.[79]

1.4 Nanoparticle stabilized capsule

In 1907, S. U. Pickering described an emulsion type that is consist of a hydrophobic core and a shell of solid particles adsorbed onto the interface between two phases (Figure 1.5). In Pickering emulsion system, the oil droplet is stabilized by a reduction of the bare oil-water interface by adsorption of solid particles wetted by both water and oil.[80, 81] This old system is reviving recently due to its unique structure with the three interfacial interactions. For example, in 2002, Dinsmore et al developed a colloidosome system based on Pickering emulsion.[82] Microencapsulation by colloidosome enables controlled release of active compounds in various industrial and research sectors including medicine, food, home and personal care products, agrochemicals and cosmetics.[83] This technique allows the delivery of a range of actives such as drugs, pesticides and fragrances for specific functions.

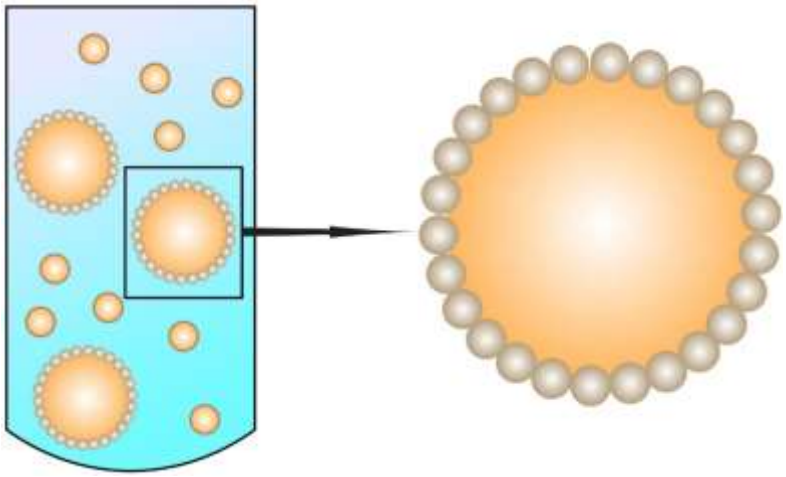

Figure 1.5. Formation of Pickering emulsion.

Traditionally, Pickering emulsion based systems are in microscale, limiting their applications for biomedical use. In 2010, Rotello et al developed a nanostructure based on Pickering emulsion, namely nanoparticle stabilized capsule (NPSC) that is composed of an oil core

and a nanoparticle shell (Figure 1.6).[84] Through rational design of the nanoparticle surface, this structure maintains a nanometer size and is capable of delivering drugs and macromolecules into cells in a rapid diffusion fashion.

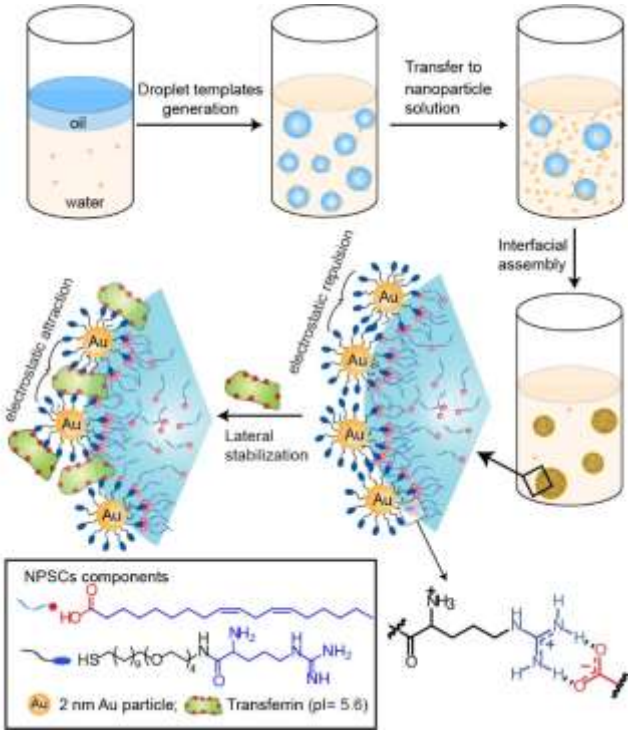

Figure 1.6. Fabrication of stable nanoscale NPSCs.[84]

1.4.1 Theoretical base of nanoparticle stabilized capsule (NPSC)

There are three different interfaces in the Pickering emulsion, including solid particle/water, solid particle/oil and oil/water interfaces. The stabilization of Pickering emulsion can be described using the following Pieranski Equation:[85]

$$\Delta E = -\frac{\pi r^2}{\gamma_{o/w}}[\gamma_{o/w} - (\gamma_{p/w} - \gamma_{p/o})]$$

Where r is the effective radius of the solid particle, $\gamma_{o/w}$ is the surface tension at oil/water interface, $\gamma_{p/w}$ is the surface tension at solid particle/water interface and $\gamma_{p/o}$ is the surface tension

at solid particle/oil interface. Clearly, change of interfacial energy is related to both the effective radius of the solid particle and the surface tensions of the above three interfaces.

A major challenge to reduce the size of Pickering emulsion is the use of ultra-small nanoparticles as the emulsifier. According to the equation, it is difficult to maintain the NPSC structure if the size of the nanoparticle is too small. To overcome this problem, other interactions must be introduced into the NPSC system. By designing the surface ligand, the interaction between the oil core of the capsule with the nanoparticle that constitute the shell to access nanoscale assemblies was engineered. The NPSC structure was therefore stabilized through lateral particle-particle interactions and particle-protein interactions.[84] This development has been proven as a direct technique for the formation of NPSCs featuring diameters around 100 nm that are stable in both buffer and cell culture medium.

1.4.2 Applications of NPSCs

The NPSC system has been successfully used in intracellular delivery of a variety of molecules. As a demonstration, Nile Red, a hydrophobic fluorescent dye, was rapidly delivered to cytosol of HeLa cells. Mechanism study revealed that the payload was transferred through membrane fusion from the NPSC to the cell without endocytosis. Delivery of paclitaxel to cells indicated that the release of therapeutic drugs from the NPSC is efficient.[84]

Following this research, NPSCs were investigated for the delivery of macromolecules. In 2013, proteins were delivered into cytosol of cells without sequestration in endosomes.[86] In 2014, NPSCs through a set of orthogonal supramolecular interactions were generated for the co-delivery of hydrophobic endosome-disrupting agents and fluorescent proteins to cells, thereby creating a system featuring stimuli-responsive release of a payload into the cytosol with fluorescence monitoring.[87] In 2015, siRNA/NPSC nanocomplex was developed for efficient

cytosolic delivery of siRNA.[88] Using this structure, siRNA was rapidly delivered into the cytosol through membrane fusion and 90% knockdown was observed. Co-delivery of anti-cancer drug and proteins for apoptosis was achieved using NPSCs as well.[89] Higher cytotoxicity than either of the single agent was shown, with synergistic action established using combination index values. This NPSC platform has also been used for efficient eradication of bacterial biofilms while promoting fibroblast proliferation in a mixed bacteria/mammalian cell system,[90] making it promising for wound healing applications.

1.5 Dissertation overview

Monolayer functionalized ultra-small AuNPs provide a versatile platform for applications in cell research. Through rational design of surface ligands, the chemistry of AuNPs are precisely regulated at atomic level. In this dissertation, applications of AuNPs in cell modulation are split into two categories (Figure 1.7). In the first category, functionalized AuNPs are harnessed to generate a robust monolayer on cell culture surface, thus modulating cell viability, behavior and fate decision. In the second category, AuNPs are assembled to NPSCs for the delivery of a variety of proteins to cytosol of cells. Using this method, phenotype of cells are rapidly switched without genomic disturbance. In addition, subcellular localization of proteins are also controlled by the combination of subcellular localization signals and NPSC delivery platform. The first non-peptide synthetic nuclear localization signal has been discovered using NPSC delivery platform as well.

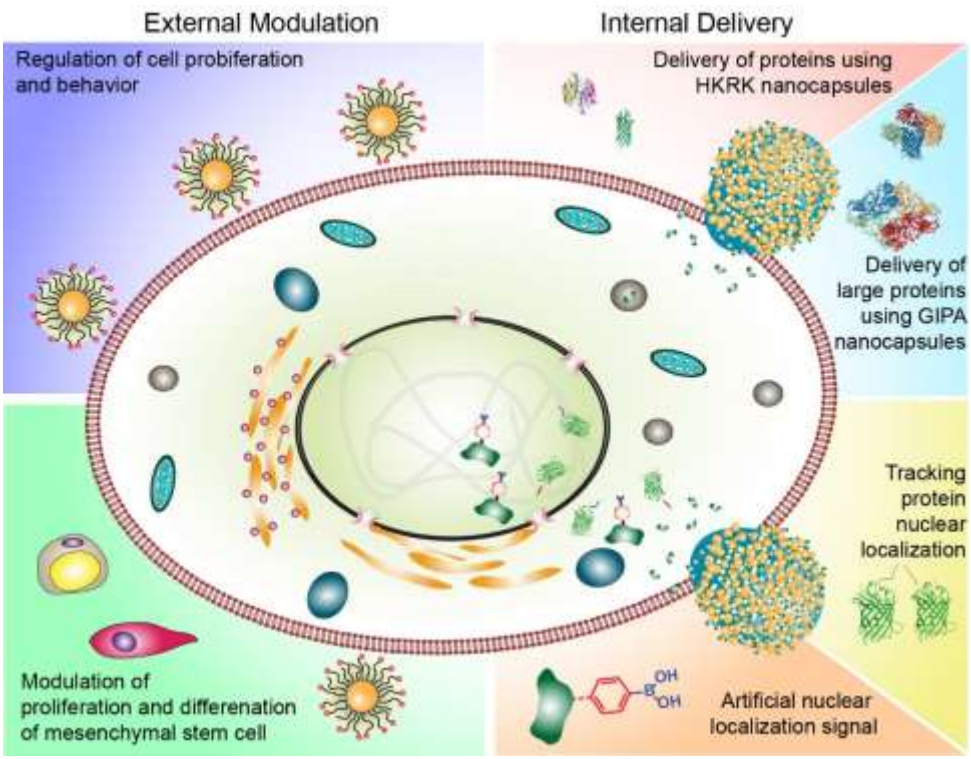

Figure 1.7. External and internal modulation of cells using functionalized nanoparticles.

In Chapter 2, a robust monolayer of nanoparticles formed via dip-coating of cell culture plates has been developed. The coating is robust under cell culture conditions, and a negligible amount of AuNPs can be taken up by cells. Cell behaviors, such as morphologenesis, adhesion and proliferation, can be regulated through extracellular stimulation by the AuNP coating. The properties of the AuNP coated surfaces can be precisely tuned to regulate the cell behaviors and to selectively support cell growth.

In Chapter 3, a defined chemical environment for stem cells has been prepared through dip-coating functionalized gold nanoparticles (AuNPs) onto cell culture plates. Modulation of mesenchymal stem cell (MSC) proliferation and differentiation has been achieved by precisely controlling the chemical structures of surface ligands on AuNPs. This generalized strategy opens up a facile way to adjust chemical clues for the modulation of stem cell growth.

In Chapter 4, a general strategy for direct delivery of functional proteins to the cytosol using nanoparticle-stabilized capsules (NPSCs) has been discussed. Intracellular protein delivery is an important tool for both therapeutic and fundamental applications. Effective protein delivery faces two major challenges: efficient cellular uptake and avoiding endosomal sequestration. NPSCs developed in this chapter were formed and stabilized via supramolecular interactions between the nanoparticle, the protein cargo, and the fatty acid capsule interior. The NPSCs were ~130 nm in diameter and featured low toxicity and excellent stability in serum. The effectiveness of these NPSCs as therapeutic protein carriers was demonstrated through the delivery of fully functional caspase-3 to HeLa cells with concomitant apoptosis. Analogous delivery of green fluorescent protein (GFP) confirmed cytosolic delivery as well as intracellular targeting of the delivered protein, demonstrating the utility of the system for both therapeutic and imaging applications.

In Chapter 5, a method for quantitative monitoring of subcellular protein trafficking using NPSCs for protein delivery has been described. This method has provided rapid delivery of the protein into the cytosol, eliminating complications from protein homeostasis processes observed with cellularly expressed proteins. After delivery, nuclear protein trafficking was followed by real time microscopic imaging. Quantitative analyses of the accumulation percentage and the import dynamics of the nuclear protein trafficking, demonstrated the utility of this method for studying intracellular trafficking systems.

In Chapter 6, the first non-peptide moiety that recruits intracellular transporting machineries for nuclear targeting has been discussed. In nature, a limited set of signaling peptides have been used to direct intracellular localization. Proteins synthetically modified with an aromatic boronic acid motif were effectively directed to the nucleus after cytosolic delivery using a nanoparticle-stabilized capsule system. Mechanistic studies revealed that active transport to

the nucleus occurd through the interaction between boronic acid and importin α/β, while the aromatic ring synergistically enhanced nuclear accumulation. Proteins too large to passively diffuse through nuclear pores were imported into the nucleus after being tagged with this aromatic boronic acid motif, further confirming an active transport mechanism. This purely synthetic methodology is a promising alternative strategy for directing subcellular localization for therapeutic and fundamental applications.

In Chapter 7, an alternative NPSC system with simplified ligand structure has been developed for efficient delivery of proteins with large size into cytosol. Through weak interactions, proteins with high molecular weight were effectively delivered into cytosol without endosomal sequestration and maintained their natural structures and functions after delivery. This platform opens up new opportunities for efficient intracellular delivery of large proteins.

1.6 References

1. S.-J. Kee, Y.-S. Kwon, Y.-W. Park, Y.-N. Cho, S.-J. Lee, T.-J. Kim, S.-S. Lee, H.-C. Jang, M.-G. Shin, J.-H. Shin, S.-P. Suh, D.-W. Ryang, *Infect. Immun.* **2012**, *80*, 2100.
2. J. Huang, Y. Yang, M. Al-Mozaini, P. S. Burke, J. Beamon, M. F. Carrington, K. Seiss, J. Rychert, E. S. Rosenberg, M. Lichterfeld, X. G. Yu, *J. Infect. Dis.* **2011**, *204*, 1557.
3. A. Pinzon-Charry, T. Woodberry, V. Kienzle, V. McPhun, G. Minigo, D. A. Lampah, E. Kenangalem, C. Engwerda, J. A. López, N. M. Anstey, M. F. Good, *J. Exp. Med.* **2013**, *210*, 1635.
4. M. E. Cerf, *Front. Endocrinol.* **2013**, *4*, 37.
5. A. Pinzon-Charry, T. Maxwell, J. A. Lopez, *Immunol. Cell Biol.* **2005**, *83*, 451.
6. A. Lerman, A. M. Zeiher, *Circulation* **2005**, *111*, 363.
7. R. Matesanz, in *Stem Cell Transplantation*, (Eds: C. López-Larrea, A. López-Vázquez, B. Suárez-Álvarez), Springer US, New York, NY 2012, 1.
8. S. W. Lane, D. A. Williams, F. M. Watt, *Nat Biotech* **2014**, *32*, 795.
9. M. P. Rodero, K. Khosrotehrani, *Int. J. Clin. Exp. Pathol.* **2010**, *3*, 643.
10. S. Li, A. L. J. Symonds, T. Miao, I. Sanderson, P. Wang, *Front. Immunol.* **2014**, *5*, 293.
11. E. J. de la Rosa, F. de Pablo, *Trends Neurosci.* **2000**, *23*, 454.
12. T.-L. Hsu, Y.-C. Chang, S.-J. Chen, Y.-J. Liu, A. W. Chiu, C.-C. Chio, L. Chen, S.-L. Hsieh, *J. Immunol.* **2002**, *168*, 4846.
13. S. Blanco, M. Frye, *Curr. Opin. Cell Biol.* **2014**, *31*, 1.
14. A. Lujambio, *Inside the Cell* **2016**, *1*, 87.
15. A. I. Mihajlović, V. Thamodaran, A. W. Bruce, *Sci Rep* **2015**, *5*, 15034.
16. G. Ghiaur, S. Yegnasubramanian, B. Perkins, J. L. Gucwa, J. M. Gerber, R. J. Jones, *Proc. Natl. Acad. Sci. U. S. A.* **2013**, *110*, 16121.

17. M. R. Elliott, K. S. Ravichandran, *J. Cell Biol.* **2010**, *189*, 1059.
18. I. Rousalova, E. Krepela, *Int. J. Oncol.* **2010**, *37*, 1361.
19. M. Kawamura, M. R. Urist, *Dev. Biol.* **1988**, *130*, 435.
20. Z. He, J. J. Li, C. H. Zhen, L. Y. Feng, X. Y. Ding, *Acta Pharmacol. Sin.* **2006**, *27*, 80.
21. K. Yamanouchi, Y. Gotoh, M. Nagayama, *J. Bone Miner. Metab.*, *15*, 23.
22. L. M. Schwiebert, R. P. Schleimer, S. F. Radka, S. J. Ono, *Cell. Immunol.* **1995**, *165*, 12.
23. Y. Wu, Z. Ai, K. Yao, L. Cao, J. Du, X. Shi, Z. Guo, Y. Zhang, *Exp. Cell Res.* **2013**, *319*, 2684.
24. P. Hou, Y. Li, X. Zhang, C. Liu, J. Guan, H. Li, T. Zhao, J. Ye, W. Yang, K. Liu, J. Ge, J. Xu, Q. Zhang, Y. Zhao, H. Deng, *Science* **2013**, *341*, 651.
25. J. L. Stilwell, R. J. Samulski, *Mol. Ther.* **2004**, *9*, 337.
26. Y. Takahashi, M. Shintani, N. Takase, Y. Kazo, F. Kawamura, H. Hara, H. Nishida, K. Okada, H. Yamane, H. Nojiri, *Environ. Microbiol.* **2015**, *17*, 134.
27. A. A. Dominguez, W. A. Lim, L. S. Qi, *Nat. Rev. Mol. Cell Biol.* **2016**, *17*, 5.
28. K. Takahashi, S. Yamanaka, *Cell*, *126*, 663.
29. N. Malik, M. S. Rao, *Methods Mol. Biol. (Clifton, N.J.)* **2013**, *997*, 23.
30. S. A. Lelièvre, M. J. Bissell, in *Reviews in Cell Biology and Molecular Medicine*, Wiley-VCH Verlag GmbH & Co. KGaA, 2006.
31. C. A. Custodio, R. L. Reis, J. F. Mano, *Adv. Healthcare Mater.* **2014**, *3*, 797.
32. M. Yamamoto, K. Yamamoto, T. Noumura, *Exp. Cell Res.* **1993**, *204*, 121.
33. C. Frantz, K. M. Stewart, V. M. Weaver, *J. Cell Sci.* **2010**, *123*, 4195.
34. H. C. Ott, T. S. Matthiesen, S.-K. Goh, L. D. Black, S. M. Kren, T. I. Netoff, D. A. Taylor, *Nat. Med.* **2008**, *14*, 213.
35. S. Kyle, S. Saha, *Adv. Healthcare Mater.* **2014**, *3*, 1703.
36. B. S. Murty, P. Shankar, B. Raj, B. B. Rath, J. Murday, in *Textbook of Nanoscience and Nanotechnology*, Springer Berlin Heidelberg, Berlin, Heidelberg 2013, 29.
37. Y. N. Xia, P. D. Yang, Y. G. Sun, Y. Y. Wu, B. Mayers, B. Gates, Y. D. Yin, F. Kim, Y. Q. Yan, *Adv. Mater.* **2003**, *15*, 353.
38. X.-M. Zhao, Y. Xia, G. M. Whitesides, *J. Mater. Chem.* **1997**, *7*, 1069.
39. J. Estelrich, M. J. Sánchez-Martín, M. A. Busquets, *Int. J. Nanomed.* **2015**, *10*, 1727.
40. V. Pansare, S. Hejazi, W. Faenza, R. K. Prud'homme, *Chem. Mat.* **2012**, *24*, 812.
41. Y. Y. Broza, H. Haick, *Nanomedicine* **2013**, *8*, 785.
42. W. H. De Jong, P. J. A. Borm, *Int. J. Nanomed.* **2008**, *3*, 133.
43. K. B. Sutradhar, M. L. Amin, *ISRN Nanotechnology* **2014**, *2014*, 12.
44. H.-I. Chang, M.-K. Yeh, *Int. J. Nanomed.* **2012**, *7*, 49.
45. S. R. Mudshinge, A. B. Deore, S. Patil, C. M. Bhalgat, *Saudi Pharm. J.* **2011**, *19*, 129.
46. G. Pillai, *SOJ Pharm. Pharm. Sci.* **2014**, *1*, 13.
47. R. B. Wang, P. S. Billone, W. M. Mullett, *J. Nanomater.* **2013**.
48. N. Huebsch, E. Lippens, K. Lee, M. Mehta, S. T. Koshy, M. C. Darnell, R. M. Desai, C. M. Madl, M. Xu, X. Zhao, O. Chaudhuri, C. Verbeke, W. S. Kim, K. Alim, A. Mammoto, D. E. Ingber, G. N. Duda, D. J. Mooney, *Nat. Mater.* **2015**, *14*, 1269.
49. K. Ye, X. Wang, L. Cao, S. Li, Z. Li, L. Yu, J. Ding, *Nano Lett.* **2015**, *15*, 4720.
50. A. Kunze, P. Tseng, C. Godzich, C. Murray, A. Caputo, F. E. Schweizer, D. Di Carlo, *ACS Nano* **2015**, *9*, 3664.
51. T. Vignaud, R. Galland, Q. Tseng, L. Blanchoin, J. Colombelli, M. Thery, *J. Cell Sci.* **2012**, *125*, 2134.
52. L. Richert, F. Vetrone, J. H. Yi, S. F. Zalzal, J. D. Wuest, F. Rosei, A. Nanci, *Adv. Mater.* **2008**, *20*, 1488.

53. X. Wang, S. Li, C. Yan, P. Liu, J. Ding, *Nano Lett.* **2015**, *15*, 1457.
54. P. Sciau, *Nanoparticles in Ancient Materials: The Metallic Lustre Decorations of Medieval Ceramics*, Vol. 115, INTECH Open Access Publisher, 2012.
55. A. S. Thakor, J. Jokerst, C. Zavaleta, T. F. Massoud, S. S. Gambhir, *Nano Lett.* **2011**, *11*, 4029.
56. X. Huang, M. A. El-Sayed, *J. Adv. Res.* **2010**, *1*, 13.
57. X. Zhang, *Cell Biochem. Biophys.* **2015**.
58. G. Doria, J. Conde, B. Veigas, L. Giestas, C. Almeida, M. Assunção, J. Rosa, P. V. Baptista, *Sensors* **2012**, *12*, 1657.
59. Y. Ding, Z. Jiang, K. Saha, C. S. Kim, S. T. Kim, R. F. Landis, V. M. Rotello, *Mol. Ther.* **2014**, *22*, 1075.
60. V. Sanna, N. Pala, G. Dessì, P. Manconi, A. Mariani, S. Dedola, M. Rassu, C. Crosio, C. Iaccarino, M. Sechi, *Int. J. Nanomed.* **2014**, *9*, 4935.
61. A. Dzimitrowicz, P. Jamroz, K. Greda, P. Nowak, M. Nyk, P. Pohl, *J. Nanopart. Res.* **2015**, *17*, 185.
62. M. Brust, M. Walker, D. Bethell, D. J. Schiffrin, R. Whyman, *J. Cheml Soci. Chem. Commun.* **1994**, 801.
63. S. Rana, A. Bajaj, R. Mout, V. M. Rotello, *Adv. Drug Deliv. Rev.* **2012**, *64*, 200.
64. M. J. Hostetler, S. J. Green, J. J. Stokes, R. W. Murray, *J. Am. Chem. Soc.* **1996**, *118*, 4212.
65. M. J. Hostetler, A. C. Templeton, R. W. Murray, *Langmuir* **1999**, *15*, 3782.
66. C.-C. You, O. R. Miranda, B. Gider, P. S. Ghosh, I.-B. Kim, B. Erdogan, S. A. Krovi, U. H. F. Bunz, V. M. Rotello, *Nat. Nanotechnol.* **2007**, *2*, 318.
67. R. A. Sperling, P. Rivera Gil, F. Zhang, M. Zanella, W. J. Parak, *Chem. Soc. Rev.* **2008**, *37*, 1896.
68. G. Han, N. S. Chari, A. Verma, R. Hong, C. T. Martin, V. M. Rotello, *Bioconjugate Chem.* **2005**, *16*, 1356.
69. H. Bayraktar, P. S. Ghosh, V. M. Rotello, M. J. Knapp, *Chem. Commun.* **2006**, 1390.
70. G. Han, C. C. You, B. J. Kim, R. S. Turingan, N. S. Forbes, C. T. Martin, V. M. Rotello, *Angew. Chem. Int. Ed.* **2006**, *45*, 3165.
71. B. J. Jordan, R. Hong, B. Gider, J. Hill, T. Emrick, V. M. Rotello, *Soft Matter* **2006**, *2*, 558.
72. R. Mout, G. Y. Tonga, M. Ray, D. F. Moyano, Y. Q. Xing, V. M. Rotello, *Nanoscale* **2014**, *6*, 8873.
73. O. R. Miranda, X. N. Li, L. Garcia-Gonzalez, Z. J. Zhu, B. Yan, U. H. F. Bunz, V. M. Rotello, *J. Am. Chem. Soc.* **2011**, *133*, 9650.
74. S. Rana, A. K. Singla, A. Bajaj, S. G. Elci, O. R. Miranda, R. Mout, B. Yan, F. R. Jirik, V. M. Rotello, *ACS Nano* **2012**, *6*, 8233.
75. S. S. Agasti, A. Chompoosor, C. C. You, P. Ghosh, C. K. Kim, V. M. Rotello, *J. Am. Chem. Soc.* **2009**, *131*, 5728.
76. P. Ghosh, X. C. Yang, R. Arvizo, Z. J. Zhu, S. S. Agasti, Z. H. Mo, V. M. Rotello, *J. Am. Chem. Soc.* **2010**, *132*, 2642.
77. P. S. Ghosh, C. K. Kim, G. Han, N. S. Forbes, V. M. Rotello, *ACS Nano* **2008**, *2*, 2213.
78. R. F. Landis, R. Tang, S. Hou, M. Yazdani, Y. Lee, V. M. Rotello, *Phosphorus Sulfur Silicon Relat. Elem.* **2015**, *190*, 2302.
79. Y. C. Yeh, B. Creran, V. M. Rotello, *Nanoscale* **2012**, *4*, 1871.
80. C. C. Berton-Carabin, K. Schroen, *Annu. Rev. Food Sci. Technol.* **2015**, *6*, 263.
81. Y. Chevalier, M. A. Bolzinger, *Colloid Surf. A-Physicochem. Eng. Asp.* **2013**, *439*, 23.
82. A. D. Dinsmore, M. F. Hsu, M. G. Nikolaides, M. Marquez, A. R. Bausch, D. A. Weitz, *Science* **2002**, *298*, 1006.
83. K. L. Thompson, M. Williams, S. P. Armes, *J. Colloid Interface Sci.* **2015**, *447*, 217.

84. X.-C. Yang, B. Samanta, S. S. Agasti, Y. Jeong, Z.-J. Zhu, S. Rana, O. R. Miranda, V. M. Rotello, *Angew. Chem. Int.l Ed.* **2011**, *50*, 477.
85. P. Pieranski, *Phys. Rev. Lett.* **1980**, *45*, 569.
86. R. Tang, C. S. Kim, D. J. Solfiell, S. Rana, R. Mout, E. M. Velázquez-Delgado, A. Chompoosor, Y. Jeong, B. Yan, Z.-J. Zhu, C. Kim, J. A. Hardy, V. M. Rotello, *ACS Nano* **2013**, *7*, 6667.
87. Y.-C. Yeh, R. Tang, R. Mout, Y. Jeong, V. M. Rotello, *Angew. Chem. Int.l Ed.* **2014**, *53*, 5137.
88. Y. Jiang, R. Tang, B. Duncan, Z. Jiang, B. Yan, R. Mout, V. M. Rotello, *Angew. Chem. Int.l Ed.* **2015**, *54*, 506.
89. C. S. Kim, R. Mout, Y. Zhao, Y.-C. Yeh, R. Tang, Y. Jeong, B. Duncan, J. A. Hardy, V. M. Rotello, *Bioconjugate Chem.* **2015**, *26*, 950.
90. B. Duncan, X. Li, R. F. Landis, S. T. Kim, A. Gupta, L.-S. Wang, R. Ramanathan, R. Tang, J. A. Boerth, V. M. Rotello, *ACS Nano* **2015**, *9*, 7775.

CHAPTER 2

RAPID COATING OF SURFACES WITH FUNCTIONALIZED NANOPARTICLES FOR REGULATION OF CELL BEHAVIOR

2.1. Introduction

Material properties such as surface morphology,[1] chemistry,[2, 3] hydrophobicity,[4, 5] and elasticity[6, 7] can be used to regulate cell growth. With proper surface modification, cells can grow on materials otherwise biologically incompatible including plastics and inorganic platforms, such as polyester, polycaprolactone, polyetheretherketone, alumina and calcium phosphate.[8-11] These modified surfaces have been used for *in vitro* cell culture, [12] tissue regeneration and organ rebuilding.[13-15] Selectivity of cell proliferation on surfaces is an additional requirement for multiple applications, including wound healing,[16] tissue repair,[17] cell residence and development, as well as differentiation.[18, 19] The capability of such surfaces to dictate cellular fate can be obtained by precisely defining surface components and structures. For example, RGD peptide has been used to selectively stimulate specific cell growth.[20] Topography has also been harnessed to selectively trigger cell fate decisions.[21]

Specifically tailoring surfaces to support growth of specific cell types is challenging, particularly in the context of processes amenable to manufacturing.[22] While cells respond to their supporting microenvironment,[23] developing a general strategy for precisely tuning the surface to optimize biocompatibility of specific cell type is currently unfeasible. Challenges for development include identifying appropriate surfaces, while manufacturing is complicated by the use of complex coating processes such as layer-by-layer deposition[24, 25] and nanopatterning[26] that are costly and time consuming and therefore challenging to implement for large-scale production.

Herein, we describe a rapid and scalable strategy to deposit a monolayer of functionalized gold nanoparticles (AuNPs) onto commercial polystyrene cell-culture plates. By tuning the terminal group of the ligand, the properties of AuNPs and hence the resulting surface can be precisely modulated to regulate cellular behavior. This control of surface functionality yields surfaces that show cell type selectivity in cell viability.

2.2. Methods

2.2.1. Syntheses of Ligands and AuNPs.

The syntheses of most ligands have been reported elsewhere[27-31] except T-Phe and T-Adman ligands.

2.2.2. Synthesis of T-Phe ligand

The synthesis of T-Phe ligand was similar to that of T-Arg ligand. Briefly, trityl protected amine (Trt-C11-TEG-NH_2) was firstly coupled with Boc-Phe-OH through EDC coupling. Then the resulting protected T-Phe was cleaved by trifluoroacetic acid (TFA) in the presence of triisopropylsilane (TIPS). T-Phe ligand was purified by washing the crude product with hexane and diethylether for three times, respectively. ^{1}H NMR (400MHz, $CDCl_3$, δ): 7.35-7.31 (5H, m, Ar), 5.32 (1H, s, -NH-), 4.12-4.08 (1H, m, -CH-), 3.76-3.28 (19H, -OCH_2-, CH_2Ar), 3.08-3.02 (1H, s, -CH_2Ar), 2.53 (2H, q, J = 7.5 Hz, -SCH_2-), 1.65-1.54 (4H, m, -CH_2-), 1.41-1.27 (14H, m, -CH_2-). MS (ESI, m/z): M^+ calcd for C28H50N2O5S, 526.3; found, 526.5.

2.2.3. Synthesis of T-Adman ligand

The synthesis of T-Adman ligand also followed the previous published method. Briefly, trityl protected methanesulphonate (Trt-C11-TEG-MS) was reacted with

dimethyladamantaneamine in mixed solution of dichloromethane (DCM) and ethanol (1:3, v/v) at 40 °C for 72 h. The product was then washed by hexane and hexane/DCM mixture (10:1, v/v) for five times, respectively. After that, T-Adman ligand was obtained by cleaving the washed product using TFA and TIPS followed by hexanes washing for three times. ^{1}H NMR (400MHz, $CDCl_3$, δ): 3.97 (br, 2H, -OCH_2-(CH_2N)-), 3.74-3.58 (m, 14H, -CH_2O- + -CH_2N-), 3.46 (t, 2H, -CH_2O-), 3.07 (s, 6H, -$(CH_3)_2N$-), 2.78 (s, 3H, CH_3SO^{-3}-), 2.58 (q, 2H, -CH_2S-), 2.36-2.12 (br, 9H, HAdamantane), 1.92-1.70 (br, 6H, HAdamantane), 1.51-1.12 (m, 18H, -(SCH_2)CH_2 + -CH_2(CH_2O)- + SH + -CH2-). MS (ESI, m/z): M^+ calcd for C31H60NO4S, 542.4; found, 542.5.

2.2.4. Syntheses of Functionalized AuNPs

The syntheses of functionalized AuNPs were accomplished by place exchange in the presence of purified ligands as described before.[32]

2.2.5. AuNP Coating

AuNPs were dissolved in MilliQ water at a concentration of 100 nM prior to coating. Then 500 µL of AuNP solution were incubated in one well of a 24-well plate at 37 °C for 3 h (125 µL for 96-well plate). Excess AuNPs were washed away with water three times followed by complete drying at 37 °C.

2.2.6. Characterizations

For both AFM and XPS characterization, the bottom of the plate coated by AuNPs was carefully removed. AFM imaging was performed on a DI Dimension-3100 AFM. Both height and phase images were collected. The average roughness of the determined sample area was calculated by Gwyddion, a freeware with the agreement of GNU General Public License. XPS

analysis was performed on a Physical Electronics Quantum 2000 spectrometer using a monochromatic Al Kα excitation at a spot size of 10 mm with pass energy of 46.95 eV at take-off angles of 15°, 45°, and 75°. For stability testing, the TTMA AuNP coating process was performed on a 96-well plate with or without plasma treatment. After washing with PBS three times, the surface was incubated with DMEM media containing 10% serum at 37 °C for 24 h, followed by treatment with trypsin for 5 min. AuNPs left on the plates were dissolved by using aqua regia for inductively coupled plasma mass spectrometry detection.

2.2.7. Cell culture

Cells were cultured in a humidified atmosphere (5% CO_2) at 37 °C, and grown in Dulbecco's Modified Eagle's Medium (DMEM, low glucose) supplemented with 10% fetal bovine serum (FBS) and 1% antibiotics (100 U/mL penicillin and 100 µg/mL streptomycin). To culture cells on the plates, 30,000 or 7,500 cells were plated on 24- or 96-well plates for a desired time (80 min, 24 h or one week), respectively.

2.2.8. Cell viability assay

7,500 cells were cultured in a 96-well plate for 24 h with or without AuNP coating. Cells were then incubated with 200 µL DMEM containing 10% Alamar Blue. Cells growing in untreated wells were set as "Blank" group. The "Untreated" group was set by adding the same volume of the Alamar Blue media into the untreated wells without cells. After 3 h incubation, the fluorescence intensity (FI) of reduced Alamar Blue at 590 nm from each well was recorded with an excitation wavelength of 535 nm. By defining the cell viability of Blank as 100%, the viabilities of cells growing on AuNP coated wells were calculated using the following equation:

$$\text{Cell viability } (\%) = \frac{\text{FI} - \text{FI}_{\text{Untreated}}}{\text{FI}_{\text{Blank}} - \text{FI}_{\text{Untreated}}} \times 100\%$$

Where FI_{Blank} is the average fluorescence intensity of “Blank” group and $FI_{untreated}$ is the average fluorescence intensity of “Untreated” group.

2.3 Results and Discussion

The first step for our modulation strategy is the "painting" of the surfaces using AuNPs. For our studies, AuNPs with 2 nm cores were functionalized with a variety of surface ligands. These ligands were designed to prevent protein fouling, maximizing the role of the particle in dictating cellular interactions.[33] In our previous approach to NP-mediated surface modification, AuNPs with defined ligands were immobilized onto surfaces through chemical crosslinking.[34] However, this method requires extra steps. In addition, the crosslinking reagents are cytotoxic and the residual after the reaction cannot be completely removed. In the current approach particles were deposited through simple dip coating of the particles onto commercial plasma-oxidized polystyrene cell-culture plates in an aqueous solution. (Figure 2.1a). Interactions between the plate and the AuNPs provided irreversible particle deposition (*vide infra*). The process was also self-passivating: after formation of an AuNP monolayer, no further deposition onto the surface was observed due to electrostatic repulsion between particles.

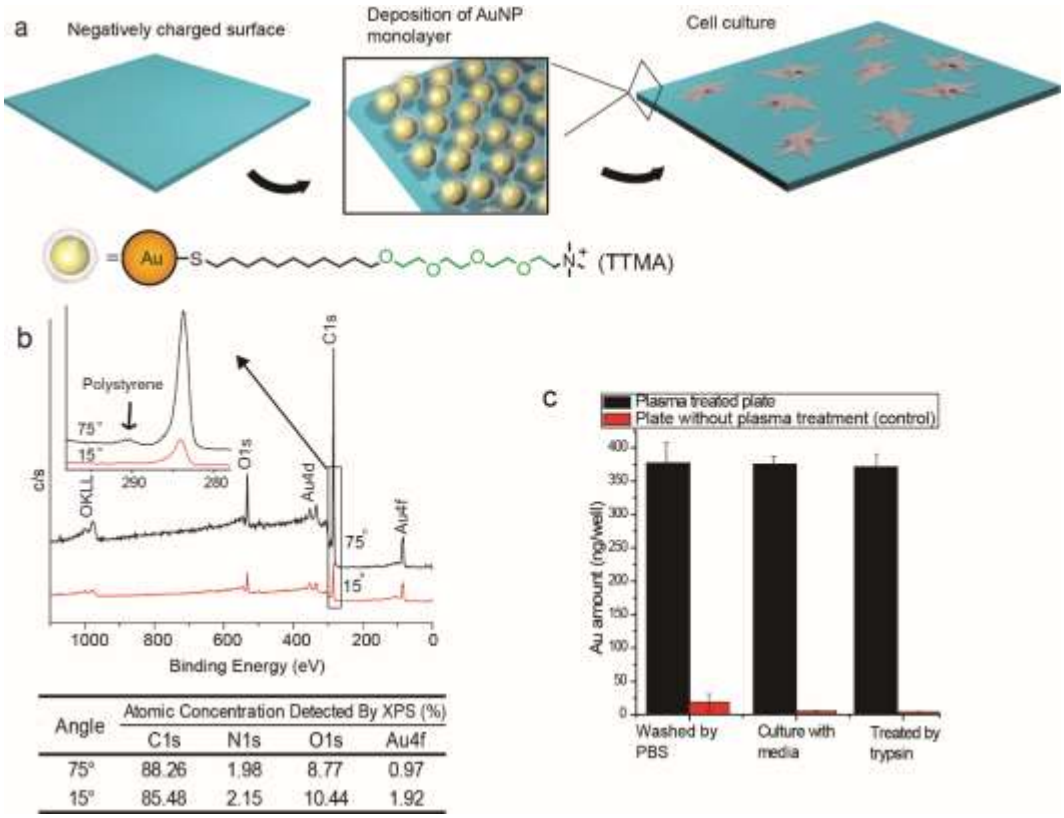

Angle	Atomic Concentration Detected By XPS (%)			
	C1s	N1s	O1s	Au4f
75°	88.26	1.98	8.77	0.97
15°	85.48	2.15	10.44	1.92

Figure 2.1. Preparation and characterization of TTMA AuNP layer on the polystyrene-plate surface. a) Schematic representation of the strategy to generate a AuNP monolayer on the cell-culture plate. b) Angle-resolved XPS detection of the polystyrene-plate surface with the AuNP layer. Relative atomic concentrations of C, N, O and Au are listed in the table. c) AuNPs attached to the plate with or without plasma treatment under cell-culture conditions. Each bar represents the amount of gold left in one well of a 96-well plate. The error bars represent the standard deviation of three measurements.

A TTMA AuNP layer (see Figure 2.1a) was generated to characterize the AuNP-modified surfaces. The AuNP layer was formed by dipping a plasma-treated polystyrene culture plate surface into 100 nM aqueous solution of TTMA AuNPs. No significant differences in surface morphology and roughness between untreated and TTMA AuNP coated surfaces were observed (Figure 2.2) as detected by Atomic Force Microscopy (AFM). The AuNP layer on the template was then characterized by depth profiling using angle-resolved X-ray photoelectron spectroscopy (XPS).[35] As shown in Figure 2.1b, there was a strong angular dependence of the Au peak and other

peaks associated with the AuNP signal. Particularly, the C/Au ratio increased from 45 (15°) to 91 (75°) with increasing take-off angle. This angle-dependent increase coupled with the shake-up peak from the π-π interaction of polystyrene observed at 75° (inset of Figure 2.1b), confirms the detection of the polystyrene substrate. Considering the detection depth of XPS is *ca.* 5 nm,[36] the thickness of the AuNP layer can be estimated to be less than 5 nm, consistent with a monolayer of particles.

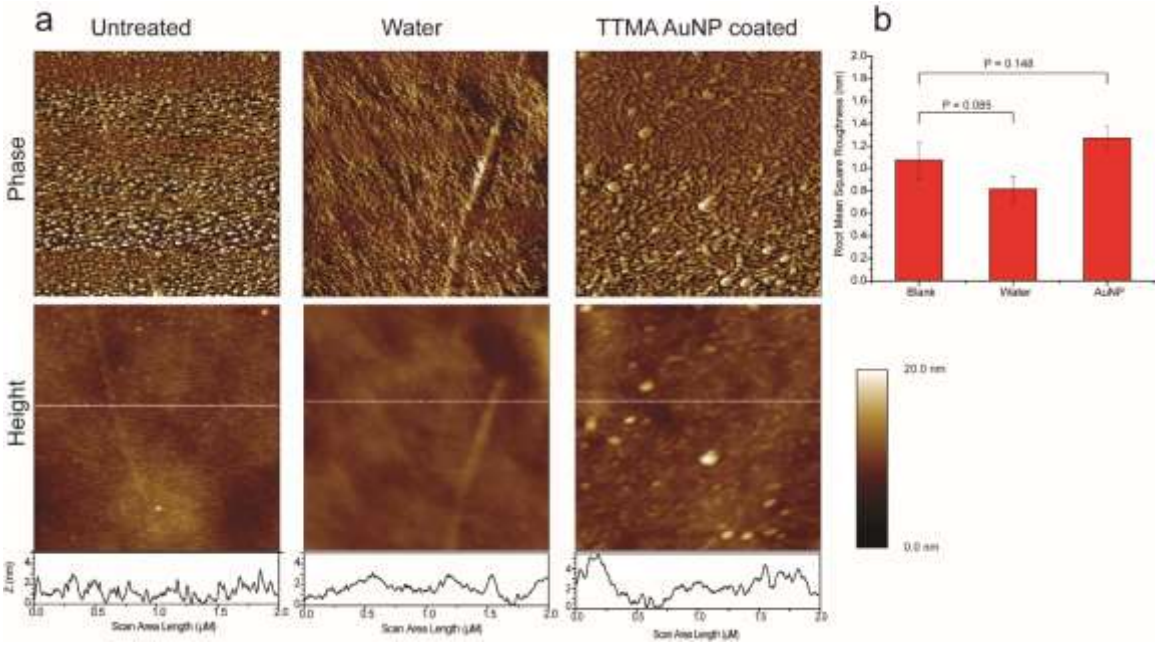

Figure 2.2. Characterizations of cell culture plate surface after TTMA AuNP coating. Untreated surface and surface treated with water without AuNPs were used as controls. a) AFM images and related roughness measurements. b) Mean roughness values with triplicate determinations.

The TTMA AuNP film was robust under cell-culture conditions: after washing with phosphate buffered saline (PBS) three times, the surface was incubated with Dulbecco's Modified Eagle Medium (DMEM) containing 10% serum at 37 °C for 24 h, followed by treatment with trypsin for 5 min. After this treatment, the loss of the AuNPs from the surface was negligible, as determined by inductively-coupled plasma mass spectrometry (ICP-MS) (Figure 2.1c). Even after

one week of culture replacing the media every other day, minimal AuNP uptake was detected, while a substantial amount of AuNPs (86.7%) remained in the plate (Figure 2.3). In contrast, without plasma treatment, TTMA AuNPs were easily washed away indicating that plasma treatment of the polystyrene surface is essential for creation of a stable monolayer of AuNPs.

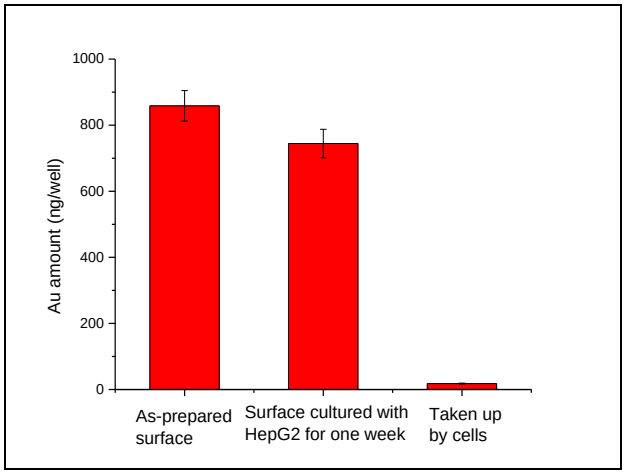

Figure 2.3. AuNPs amount taken up by cells and left on the cell culture plate surface after one week culture of HepG2 cells (started at 30,000 cells/well). The cell culture media were replaced every other day.

Preliminary insight into the interaction of particle-modified surfaces and cells was obtained using surfaces coated with TTMA AuNPs. HepG2 cells were grown in the cell-culture plates with or without a TTMA AuNP coating. After 80 min incubation, cells cultured on the TTMA AuNP treated surface have already adhered and filopodia started to form. In contrast, few cells attached to the plate surface without AuNP layer at the same time point (Figure 2.4). After 24 h incubation, cells cultured on the TTMA AuNP treated surface exhibit distinctly different morphologies, with TTMA-treated surfaces encouraging cell spreading relative to the untreated control (Figure 2.5 and Figure 2.6). Staining with phallotoxin to specifically target F-actin demonstrates that cells grown on the AuNP surface have more filopodia than those grown on a plasma-treated surface (Figure 2.6c-d), indicative of enhanced adhesion.[37, 38] Taken together,

these results reveal that TTMA AuNP monolayers can be successfully used to enhance the adhesion of cells. It is notable that ICP-MS indicated no loss of AuNPs from the polystyrene surface (Figure 2.6e), despite the fact that positively charged nanoparticles are known to be readily taken up by cells.[39] Substitution of the AuNP for a TTMA CdSe quantum dot (core diameter ≈ 3 nm) also showed a stimulatory effect on cell morphogenesis that resembled that of the TTMA AuNPs (Figure 2.7). Thus it is clear that it is the surface ligand, rather than the core of the nanoparticle, that plays an important role in regulating the cell behavior.

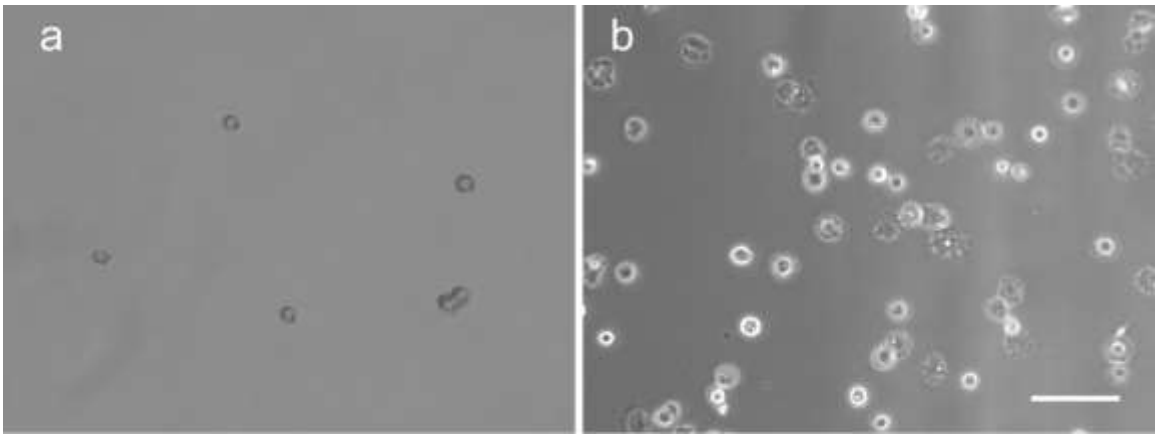

Figure 2.4. Attachment of HepG2 cells after 80 min incubation on cell culture plates a) without or b) with TTMA AuNP coating. Bar: 100 µm

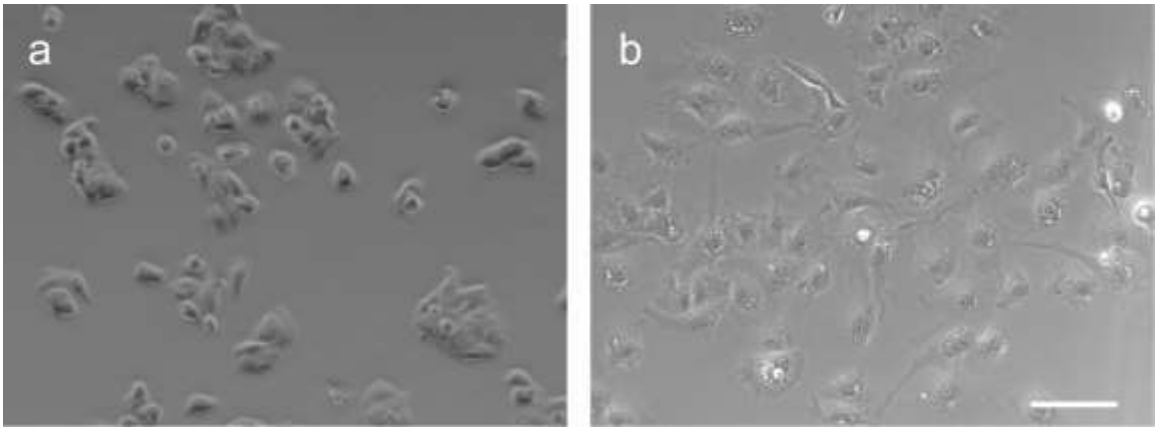

Figure 2.5. Optical images of HepG2 cell grown on a) plasma-treated plate and b) TTMA AuNP coated surface. Bar: 100 µm

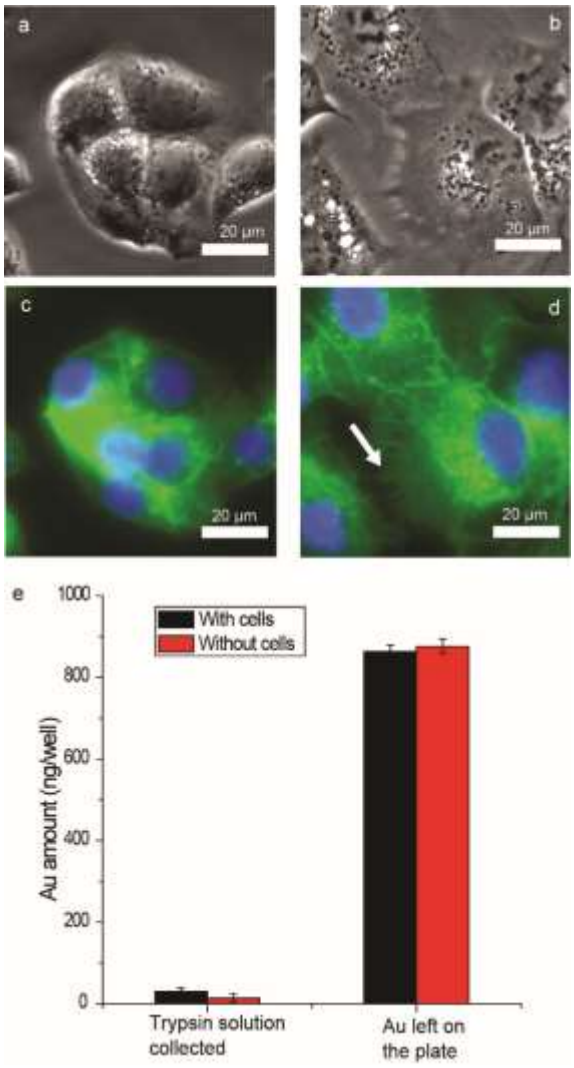

Figure 2.6. HepG2 cell culture for 24 h on plates with and without the TTMA AuNP layer. a) Optical image of HepG2 cell grown on a plasma-treated plate. b) Optical image of HepG2 cell grown on a TTMA AuNP monolayer. c) Fluorescent image of Figure 2.6a. F-actin was stained by Oregon Green labeled phallotoxin, and the nuclei were stained by Hoechst 33342. d) Fluorescent image of Figure 2.6b. The staining conditions were the same as in Figure 2.6c. The arrow indicates filopodia of the cell. e) Cell-uptake test of TTMA AuNP monolayer. The cells were cultured on the TTMA AuNP monolayer in a 24-well plate for 24 h. A 24-well plate coated with TTMA AuNPs without cells cultured on the surface was used as a control.

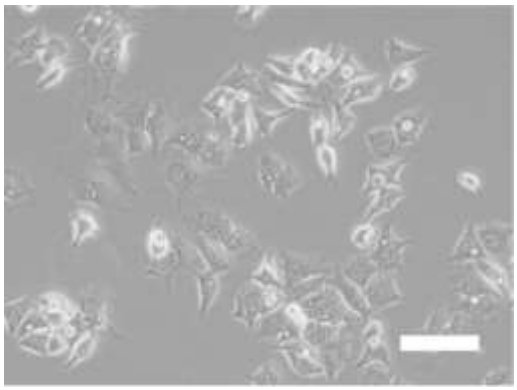

Figure 2.7. HepG2 cells growing on TTMA CdSe quantum dots coated surface for 24 h showed similar morphology as those growing on TTMA AuNP coated surface. Bar: 100 µm

Variation of surface ligands on AuNPs can be used to control surface properties,[40] providing a potential tool to regulate cellular behavior. To test this hypothesis, the effects of AuNP coatings on the viability on four kinds of cells from different organs was determined, namely HepG2 (human liver), HeLa (human cervix), MCF7 (human breast), and 3T3 (murine fibroblast). To perform this study, 26 kinds of functionalized AuNPs were screened, with different types of ligands of varying hydrophobic, stereoelectronic, constitutional, and aromatic characteristics (Figure 2.8).

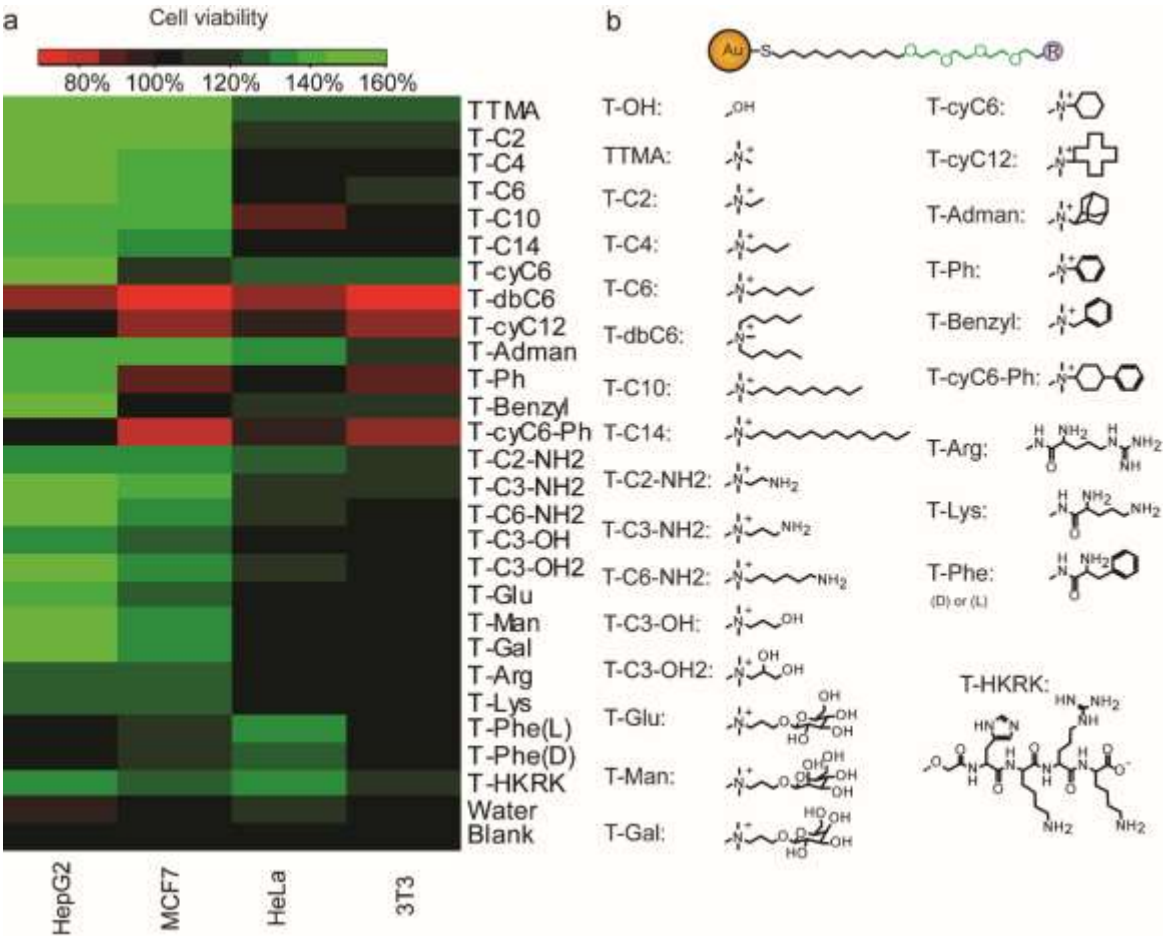

Figure 2.8. Cell viability assay for 26 different AuNP coatings (morphology changes of HepG2 cell were shown in Figure 2.9). a) A heat map of cell viability influenced by different AuNP coatings. b) Structures of ligands on the AuNPs. 'Blank' represents the cell viability on plasma-treated surface without any pretreatment, and 'Water' represents the cell viability on the surface pretreated with water only (no AuNP added) for 3 h and without post deposition of AuNPs.

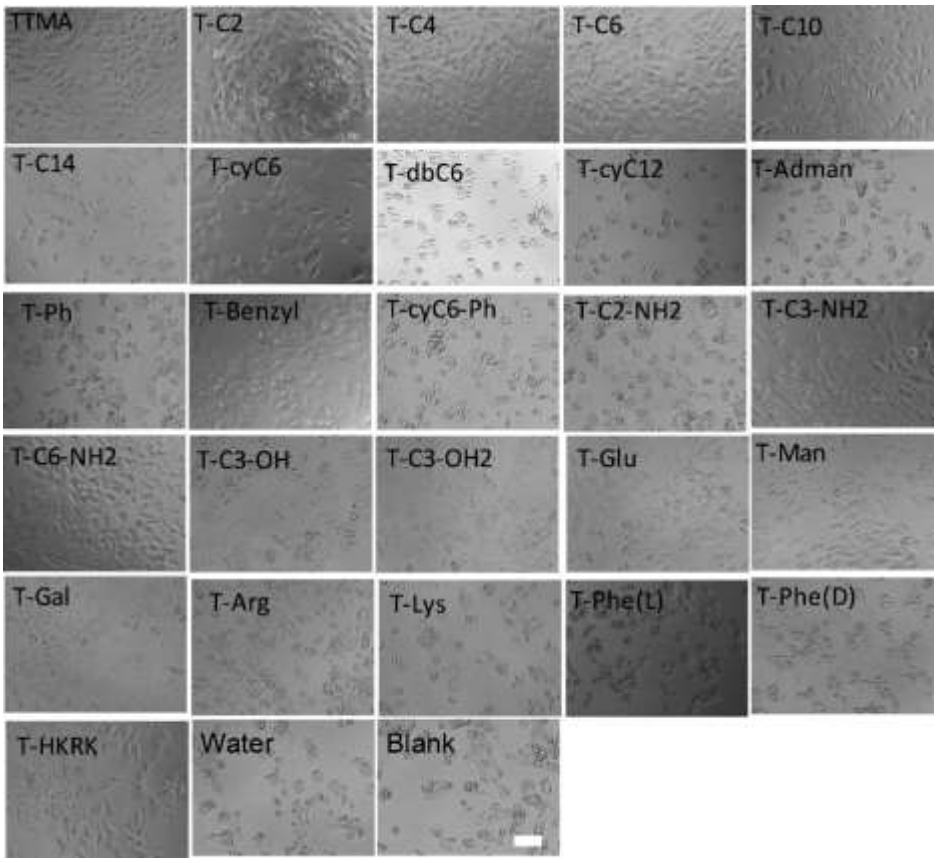

Figure 2.9. Morphologies of HepG2 cell in the presence of AuNPs listed in Figure 2.8. Bar: 100 μm

Cell viability was determined using an Alamar blue assay (Figure 2.8). The matrix of the 26 nanoparticles against the four cell lines indicated that different AuNPs had marked and selective effects on the viability of the different cell lines. It is evident that these cationic NPs (TTMA) dramatically increased the viability of HepG2 cells and to a lesser extent MCF7 cells, while having minimal effect on HeLa and 3T3 cells. These differences among cell types may be due to the sensitivity of the cells responding to the environment. However, this tendency was not universal and certain cationic nanoparticles promoted the growth of specific cell lines while inhibiting others, for example aromatic functionalities (T-Ph and T-Benzyl) that significantly

boosted the viability of HepG2 comparative to the other the cell lines. A similar case was observed when the hydrophobicity of the ligand increases. While the more hydrophilic NPs (TTMA to T-C6, and T-C2-NH2 to T-C3-OH2) boosted the viability of both HepG2 and MCF7, the more hydrophobic NPs (T-C14 to T-dbC6) increased the viability only for HepG2, as MCF7 is apparently more sensitive to the cytotoxic properties of the hydrophobic moieties.

Constitutional isomerism has a significant effect on the viability pattern of the cells, with T-cyC6 inhibiting the growth of MCF7 while increasing HeLa and 3T3 viability, contrasting with T-C6 that only boosted the growth of MCF7. On the other hand, the stereoisomeric nature of the terminal group had little effect on the preferential cell viability, as demonstrated by comparing the cases of the two T-Phe NPs (L and D), as well as the three different sugar functionalized NPs (T-Glu, T-Man and T-Gal). This observation was surprising, as a dissimilar behavior was expected to arise from the different levels of specific receptors at the surfaces of the cells, *e.g.*, HepG2 cell contains galactose receptor while HeLa cell does not.[41] It is important to note that despite the fact that the surface coverage with the AuNPs may be affected by the differences in the chemical nature of the ligand, the coverage (Figure 2.10, measured by ICP-MS) has a weak correlation with the observed changes in cell viability, strengthening our hypothesis that the principle factor to control the cell behavior is the chemistry at the AuNP surface.

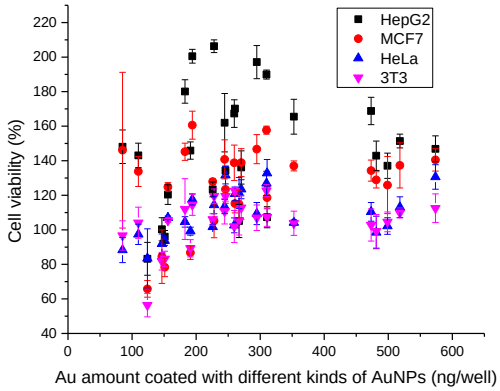

Figure 2.10. Cell viability variations induced by different kinds of AuNP coatings. R^2 values of linear fitting are -0.012, 0.175, 0.012 and 0.067 for HepG2, MCF7, HeLa and 3T3 groups, respectively.

In conclusion, we developed a facile strategy to generate robust surfaces coated with AuNP monolayers. As shown by our preliminary studies, the surfaces are tunable in an "atom-by-atom" fashion, allowing the exploration of a wide variety of surface chemistries. The ability to foster the selective growth of specific cell types makes these surfaces promising for medical applications such as wound healing and transplantation. Finally, the ready scalability of the deposition process makes these surfaces attractive for real-world manufacturing.

2.4 References

1. L. Qi, N. Li, R. Huang, Q. Song, L. Wang, Q. Zhang, R. Su, T. Kong, M. Tang, G. Cheng, *PLoS One* **2013**, *8*, e59022.
2. W. F. Zheng, W. Zhang, X. Y. Jiang, *Adv. Healthcare Mater.* **2013**, *2*, 95.
3. M. Mrksich, *Chem. Soc. Rev.* **2000**, *29*, 267.
4. B. Valamehr, S. J. Jonas, J. Polleux, R. Qiao, S. Guo, E. H. Gschweng, B. Stiles, K. Kam, T.-J. M. Luo, O. N. Witte, X. Liu, B. Dunn, H. Wu, *Proc. Natl. Acad. Sci. U. S. A.* **2008**, *105*, 14459.
5. Y. Arima, H. Iwata, *Biomaterials* **2007**, *28*, 3074.
6. A. Skardal, D. Mack, A. Atala, S. Soker, *J. Mech. Behav. Biomed. Mater.* **2013**, *17*, 307.
7. T. Kawano, Y. Nakamichi, S. Fujinami, K. Nakajima, H. Yabu, M. Shimomura, *Biomacromolecules* **2013**, *14*, 1208.
8. Y.-P. Jiao, F.-Z. Cui, *Biomed. Mater.* **2007**, *2*, R24.
9. Z. Ma, Z. Mao, C. Gao, *Colloids Surf. B* **2007**, *60*, 137.

10. S. I. Roohani-Esfahani, S. Nouri-Khorasani, Z. F. Lu, M. H. Fathi, M. Razavi, R. C. Appleyard, H. Zreiqat, *Mater. Sci. Eng. C* **2012**, *32*, 830.
11. J. H. Lee, H. L. Jang, K. M. Lee, H.-R. Baek, K. Jin, K. S. Hong, J. H. Noh, H.-K. Lee, *Acta Biomater.* **2013**, *9*, 6177.
12. D. Mazia, *J. Cell Biol.* **1975**, *66*, 198.
13. T. M. Meese, Y. Hu, R. W. Nowak, K. G. Marra, *J. Biomater. Sci.- Polym. Ed.* **2002**, *13*, 141.
14. R. M. P. da Silva, J. F. Mano, R. L. Reis, *Trends Biotechnol.* **2007**, *25*, 577.
15. R. Sipehia, G. Martucci, J. Lipscombe, *Artificial Cells, Blood Substitutes, and Biotechnology* **1996**, *24*, 51.
16. C. M. Stanford, *Int. J. Mol. Sci.* **2010**, *11*, 354.
17. J. L. García, A. Asadinezhad, J. Pacherník, M. Lehocký, I. Junkar, P. Humpolíček, P. Sáha, P. Valášek, *Molecules* **2010**, *15*, 2845.
18. N. Li, X. Zhang, Q. Song, R. Su, Q. Zhang, T. Kong, L. Liu, G. Jin, M. Tang, G. Cheng, *Biomaterials* **2011**, *32*, 9374.
19. J. E. Phillips, T. A. Petrie, F. P. Creighton, A. J. García, *Acta Biomater.* **2010**, *6*, 12.
20. U. Hersel, C. Dahmen, H. Kessler, *Biomaterials* **2003**, *24*, 4385.
21. Y. Engel, J. D. Schiffman, J. M. Goddard, V. M. Rotello, *Mater. Today* **2012**, *15*, 478.
22. F. Variola, J. B. Brunski, G. Orsini, P. Tambasco de Oliveira, R. Wazen, A. Nanci, *Nanoscale* **2011**, *3*, 335.
23. J. M. Berg, J. L. Tymoczko, L. Stryer, Springer Science + Business Media, 2013.
24. H. Lee, Y. Jang, J. Seo, J.-M. Nam, K. Char, *ACS Nano* **2011**, *5*, 5444.
25. J. Fukuda, A. Khademhosseini, J. Yeh, G. Eng, J. Cheng, O. C. Farokhzad, R. Langer, *Biomaterials* **2006**, *27*, 1479.
26. L. Bacakova, E. Filova, M. Parizek, T. Ruml, V. Svorcik, *Biotechnol. Adv.* **2011**, *29*, 739.
27. O. R. Miranda, H.-T. Chen, C.-C. You, D. E. Mortenson, X.-C. Yang, U. H. F. Bunz, V. M. Rotello, *J. Am. Chem. Soc.* **2010**, *132*, 5285.
28. C.-C. You, O. R. Miranda, B. Gider, P. S. Ghosh, I.-B. Kim, B. Erdogan, S. A. Krovi, U. H. F. Bunz, V. M. Rotello, *Nat. Nanotechnol* **2007**, *2*, 318.
29. P. Ghosh, X. Yang, R. Arvizo, Z.-J. Zhu, S. S. Agasti, Z. Mo, V. M. Rotello, *J. Am. Chem. Soc.* **2010**, *132*, 2642.
30. X.-C. Yang, B. Samanta, S. S. Agasti, Y. Jeong, Z.-J. Zhu, S. Rana, O. R. Miranda, V. M. Rotello, *Angew. Chem. Int. Ed.* **2010**, *50*, 477.
31. S. G. Elci, D. F. Moyano, S. Rana, G. Y. Tonga, R. L. Phillips, U. H. F. Bunz, V. M. Rotello, *Chem. Sci.* **2013**, *4*, 2076.
32. V. M. R. D. F. Moyano, *Cellular and subcellular nanotechnology : methods and protocols*, Humana Press ; Springer, New York 2013.
33. D. F. Moyano, V. M. Rotello, *Langmuir* **2011**, *27*, 10376.
34. M.-H. Park, C. Subramani, S. Rana, V. M. Rotello, *Adv. Mater.* **2012**, *24*, 5862.
35. J. Wen, G. Somorjai, F. Lim, R. Ward, *Macromolecules* **1997**, *30*, 7206.
36. T. L. Barr, *Modern ESCA: the Principles and Practice of X-Ray Photoelectron Spectroscopy*, CRC Press, Boca Raton 1994.
37. C. Schäfer, B. Borm, S. Born, C. Möhl, E.-M. Eibl, B. Hoffmann, *Exp. Cell Res.* **2009**, *315*, 1212.
38. H. C. Tsui, K. L. Lankford, W. L. Klein, *Proc. Natl. Acad. Sci. U. S. A.* **1985**, *82*, 8256.
39. Z.-J. Zhu, R. Carboni, M. J. Quercio, B. Yan, O. R. Miranda, D. L. Anderton, K. F. Arcaro, V. M. Rotello, R. W. Vachet, *Small* **2010**, *6*, 2261.
40. C. Subramani, K. Saha, B. Creran, A. Bajaj, D. F. Moyano, H. Wang, V. M. Rotello, *Small* **2012**, *8*, 1209.

41. T. Satoh, S. Kakimoto, H. Kano, M. Nakatani, S. Shinkai, T. Nagasaki, *Carbohydr. Res.* **2007**, *342*, 1427.

CHAPTER 3

MODULATION OF STEM CELL DIFFERENTIATION BY NANOPARTICLE FUNCTIONALIZED SURFACES

3.1. Introduction

Stem cells are a promising platform for regenerative therapies due to their intrinsic self-renewal properties and ability to differentiate into diverse cell types.[1] Modulation of stem cell proliferation and differentiation into a specific cell type is typically achieved through the use of defined culture media containing specific growth factors and small molecule effectors.[2] Recently, studies revealed that supporting matrices also play an important role in controlling stem cell proliferation and differentiation.[3-5] Matrix stiffness,[6] roughness,[7, 8] nanotopography,[9, 10] and chemical structure[11, 12] all uniquely influence the interactions between stem cells and substrates, thereby dictating subsequent stem cell behavior.

Tuning the matrix surface chemistry is a potent strategy to precisely control the cellular growth microenvironment at the molecular level.[13] The chemical properties of supporting materials for stem cells are generally controlled through the inherent structural design of the material itself[12] or surface post-modification.[11] Surface modification provides facile access to the functionalization of the supporting matrix and offers more versatility than other methods.[14] For example, polytetrafluoroethylene sequentially treated with multiple types of plasma exhibited enhanced osteogenesis in mesenchymal stem cells (MSCs).[15] Furthermore, glass surfaces dip-coated with different functional groups induced stem cell differentiation.[16] However, due to the restricted range of conjugation strategies between substrata and coating layers, dip-coating is typically restricted to glass,[17] silicon[18] and gold[19] surfaces. Developing more general dip-coating

approaches for the modulation of stem cell proliferation and differentiation would greatly improve the versatility of this method.

We have recently developed a facile strategy to rapidly generate robust monolayers of positively charged 2-nm gold nanoparticles (AuNPs) on plastic cell culture plates via a dip-coating process.[20] Attached through strong and stable electrostatic interactions, these AuNP-coated surfaces featured tunable functionality, and could be used to provide cell type-specific modulation of growth without uptake of AuNPs into the supported cells. This method enables the surface fabrication with minimal mechanic modulation through a monolayer of 2-nm gold nanoparticles. We hypothesized that the ability to control cellular responses by these nanomaterial surfaces could be extended to the modulation of stem cell differentiation. Herein, we report an alternative surface functionality-dependent strategy to modulate the proliferation and differentiation of MSCs using tunable AuNP-coated surfaces (Figure 3.1). We show that the differentiation of MSCs into adipocytes and osteoblasts can be readily controlled via choice of AuNP surface modifier, therefore providing a versatile approach for the control of stem cell differentiation.

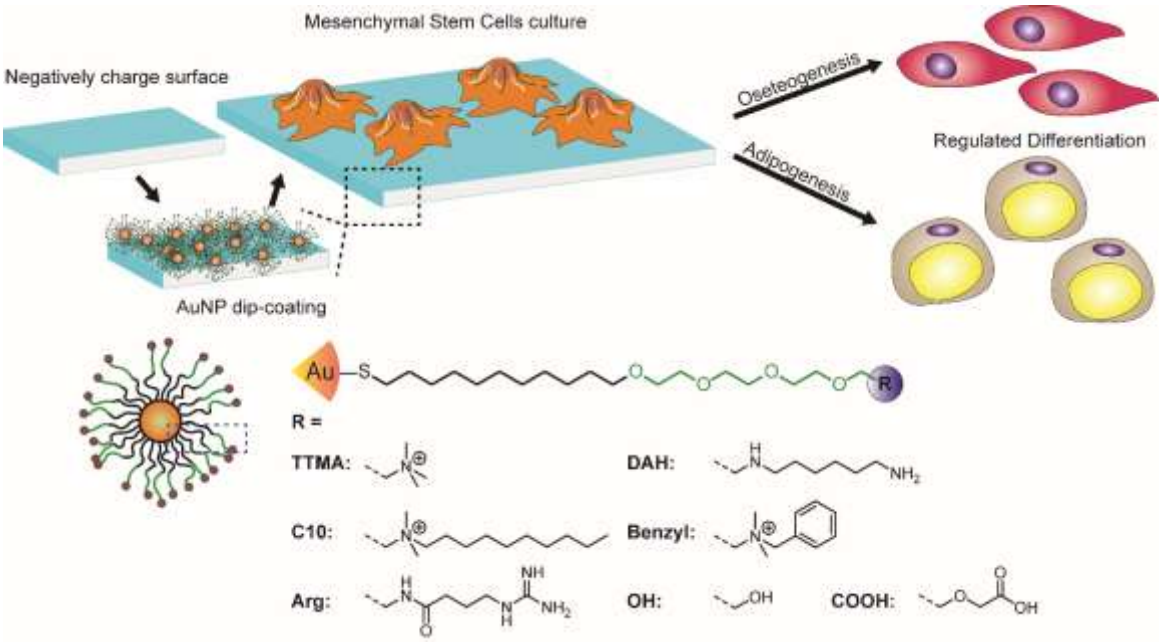

Figure 3.1. Schematic representation of the strategy developed to control MSC differentiation using tunable AuNP-coated surfaces.

3.2 Methods

3.2.1 AuNP coating

2-nm AuNPs were synthesized according to our previous report.[20] AuNPs were dissolved in Milli-Q water at a concentration of 100 nM prior to coating. Then 500 µL of AuNP solution were incubated in one well of a 24-well plate at 37 °C for 3 h (125 µL for 96-well plate). Excess AuNPs were washed away with water three times followed by complete drying at 37 °C.

3.2.2 AFM imaging

For AFM characterization, the bottom of the plate coated by AuNPs was carefully removed and collected. AFM imaging was performed on a DI Dimension-3100 AFM. The AFM images and cross section profiles were processed using Gwyddion, a freeware with the agreement of GNU General Public License.

3.2.3 Cell culture

hTERT mesenchymal stem cells were cultured in a humidified atmosphere (5% CO2) at 37 °C, and grown in Dulbecco's Modified Eagle's Medium (DMEM, low glucose) supplemented with 10% fetal bovine serum (FBS), 1× non-essential amino acids, 1 mM sodium pyruvate and 1% antibiotics (100 U/mL penicillin and 100 µg/mL streptomycin). To culture cells on the plates, 30,000 or 7,500 cells were plated on 24- or 96-well plates for a desired time (24 hrs, 3, 7 or 14 days), respectively.

3.2.4 Cell differentiation

After 24 hrs culture on plates, the media of cells were replaced with induction media that containing base media (R&D Systems, CCM007) and differentiation supplements (R&D Systems, CCM011 for adipogenesis or R&D Systems, CCM008 for osteogenesis). Differentiation media were replaced every 3.5 days until reaching 7- or 14-day point.

3.2.5 AuNPs cell-uptake test

Cells were cultured on TTMA AuNP coated plate under undifferentiated condition for one day, allowing them to reside on the surface. Then the media were changed to adipogenic or osteogenic media and replaced with fresh ones after 3 days. With the culture for another 3 days, cells were trypsinized and collected. For sample preparation for inductively coupled plasma mass spectrometry (ICP-MS), collected trypsin solutions were transferred to eppendorf tubes and 1 mL aqua regia was added for digestion for 15 minutes. Leftover plates were digested by 0.5 mL aqua regia for 15 minutes as well. Then all the samples were transferred to 15 mL centrifuge tubes prewashed in 5% nitric acid solution for 2 days and were diluted to 10 mL with milli-Q water. The ICP-MS analyses were performed on a Perkin-Elmer NexION 300X ICP mass spectrometer. 197Au

was measured under standard mode. Operating conditions were as follows: nebulizer flow rate: 0.95 L/min; rf power: 1600 W; plasma Ar flow rate: 18 L/min; dwell time: 50 ms. A series of standard gold solutions (concentration: 0, 0.2, 0.5, 1, 2, 5, 10, and 20 ppb) were prepared to draw for quantification.

3.2.6 Cell viability assay

7,500 cells were cultured in a 96-well plate for 24 hrs with or without AuNP coating. Cells were then incubated with 200 µL DMEM containing 10% Alamar Blue. Cells growing in untreated wells were set as "Blank" group. The "Untreated" group was set by adding the same volume of the Alamar Blue media into the untreated wells without cells. After 3 hrs incubation, the fluorescence intensity (FI) of reduced Alamar Blue at 590 nm from each well was recorded with an excitation wavelength of 535 nm. By defining the cell viability of Blank as 100%, the viabilities of cells growing on AuNP coated wells were calculated using the following equation:

$$Cell\ viability\ (\%) = \frac{FI - FI_{Untreated}}{FI_{Blank} - FI_{Untreated}} \times 100\%$$

Where FI_{Blank} is the average fluorescence intensity of "Blank" group and $FI_{untreated}$ is the average fluorescence intensity of "Untreated" group.

3.2.7 Cell fixation

Before fixation, cells were washed 3 times with PBS. The cells were then fixed with 4% (w/v) paraformaldehyde for 10 min at room temperature. After that, paraformaldehyde solution was removed and cells were washed with PBS for 3 times for further tests.

3.2.8 Characterizations for osteogenesis

For alkaline phosphatase activity assay, fixed cells were stained with Vector® Blue substrate (Vector Laboratories, SK-5300) following its protocol. To stain for calcium deposits, fixed cells were incubated in 0.5 % Alizarin Red S solution (pH 4.3) for 30 min at room temperature. After removing the staining solution, cells were washed with PBS for 3 times followed by optical microscope imaging. After that, cells were dried and 200 µL 10% acetic acid solution was employed for each well in 24 well plate to extract the dye. Calcium deposits were quantified by measuring the absorbance of Alizarin S at 556 nm.

3.2.9 Characterizations for adipogenesis

For Oil Red O staining, fixed cells were stained with 0.3% Oil Red O in 60% isopropanol solution for 20 min. After removal of the staining solution, cells were immediately washed with MilliQ water for 4 times followed by optical microscope imaging. After that, cells were dried and Oil Red O were extracted by isopropanol. The amount of fat droplets in cells after adipogenesis was quantified by measuring the absorbance of Oil Red O at 570 nm. For western blot analysis, fresh cells in 24 well plates were first washed once with cold PBS, and then lyzed by 100 µL freshly prepared RIPA buffer supplemented with protease inhibitor cocktails (Promega, G6521). The lysates were then clarified by centrifugation for 10 min. at 4 °C. The protein concentration was determined using BCA Protein Assay Kit (Pierce, 23227). Total cell lysate protein (30 µg) was separated on 12% SDS PAGE gel and then transferred to a PVDF membrane (200 mA for 120 min). After blocking the blot with 5% non-fat milk in Tris buffered saline with Tween-20 (TBST, pH 7.4) for 1 hr, the membrane was incubated with rabbit anti-FABP4 (GeneTex, GTX116036; 1:500) or anti-β-actin (BioSS, bs-0061R; 1:1000) in 5% non-fat milk TBST solution for overnight. After

incubation in 5% non-fat milk in TBST with goat anti-rabbit IgG-HRP antibody (1:10000) for 1 hr, bands were then visualized using the ECL system.

3.3. Results and Discussion

The surfaces used for MSC culture were generated by dip-coating positively charged AuNPs onto the surface of negatively charged commercial cell culture plates. The coating materials and procedures were the same with our developed method. Briefly, the cell culture plate surface was incubated with 100 nM AuNP solution for 3 hrs to provide a monolayer of AuNPs. Surface analysis using atomic force microscopy revealed similar surface roughness before and after AuNP coating (Figure 3.2) compared to our previous report.[20] In addition, this coating layer is quite robust and resists cell uptake under adipogenic or osteogenic conditions for one week (Figure 3.3). These results indicated that the process generated a robust monolayer of AuNPs on the cell culture surface.[20] Since positively charged surfaces promote MSC adhesion and affect cell behavior,[21] we reasoned that MSCs could be further modulated through the combination of positive charge and other surface properties. Thus, we chose five different positively charged AuNPs, namely TTMA, C10, Arg, DAH and Benzyl for dip-coating (Figure 3.1). The ligands for TTMA, C10 and Benzyl AuNPs have different quaternary amine groups, respectively. Arg is functionalized by arginine-terminated ligands while DAH is based on a diaminohexane-terminated structure.

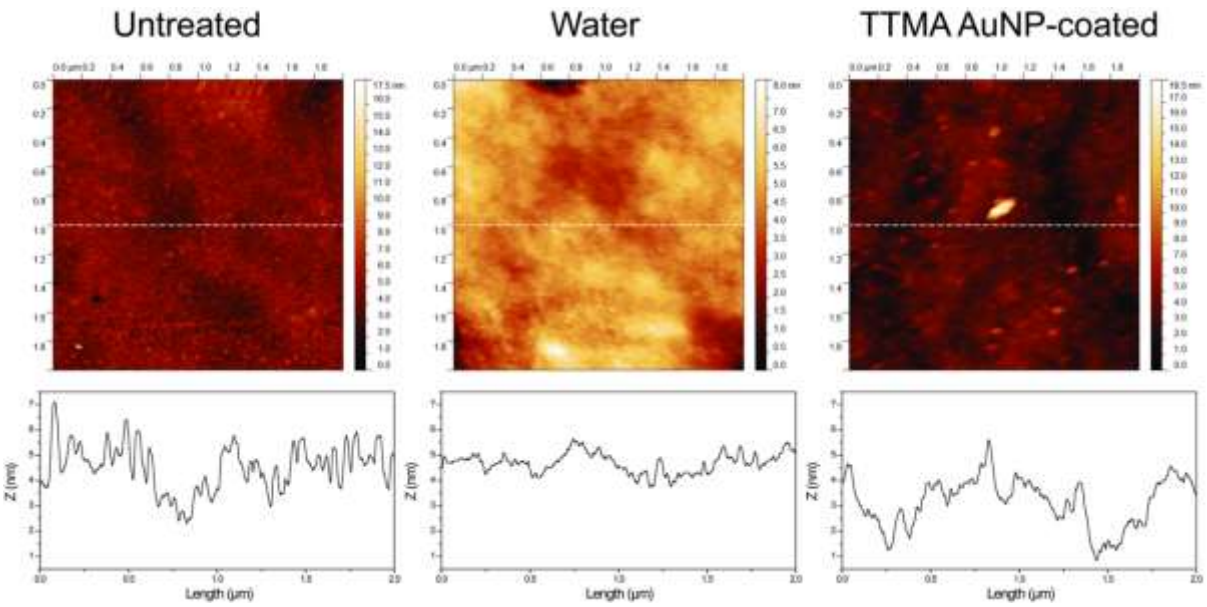

Figure 3.2. AFM image and cross section profile of untreated cell culture plate, water-treated cell culture plate and TTMA AuNP-treated cell culture plate. The RMS roughness was obtained from three cross section profiles in each image (0.5 nm ± 0.1 nm, 0.2 nm ± 0.1 nm, 0.2 nm ± 0.1 nm, respectively).

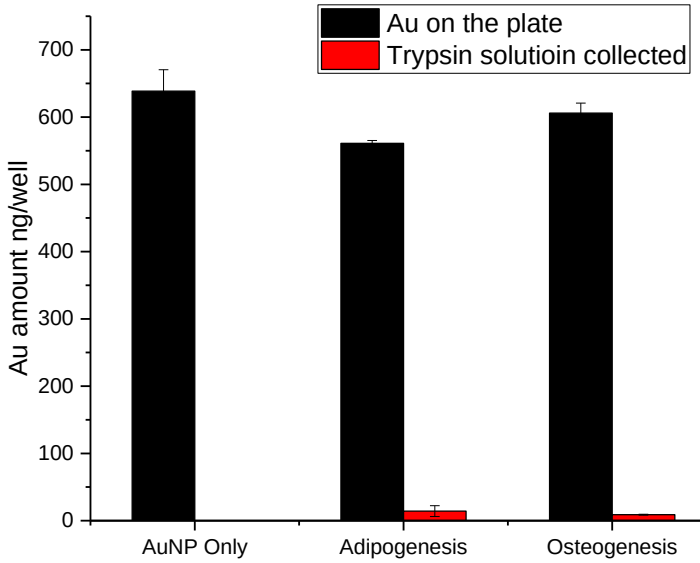

Figure 3.3. Cell-uptake test of TTMA AuNP monolayer. The cells were cultured on the TTMA AuNP monolayer in a 24-well plate under adipogenic or osteogenic induction conditions for one week. A 24-well plate coated with TTMA AuNPs without cells cultured on the surface was used as a control.

We performed a seven-day proliferation assay without induction to determine whether MSCs respond differently to the positively charged AuNP monolayers. After 1 h of incubation,

MSCs adhered to all surfaces (Figure 3.4), indicating biocompatibility of these surfaces. After 24 hrs, cells grown on AuNP monolayers showed similar morphology and viability than those cultured on a standard plastic surface (Figure 3.5 and Figure 3.6). However, dramatic differences were observed after 3 days of culture. TTMA, C10, Arg and DAH AuNP monolayers increased MSC proliferation by more than 50%, whereas the Benzyl AuNP monolayer inhibited cell proliferation. These results are in agreement with our previous finding that positively charged AuNP monolayers generally promote cell proliferation.[20] After 7 days, all except Benzyl AuNP monolayers (which prevented proliferation) showed similar proliferation trends (Figure 3.5). Further comparison of cell densities with those at 24 hrs revealed that such trend is presumably due to cell confluence (Figure 3.7). The results of proliferation assay and cell density analysis are consistent, indicating that positively charged surfaces generally enhance MSC proliferation, while the benzene ring on the surface of substrates strongly suppress MSC growth, possibly due to its hydrophobicity[22] or high MSC sensitivity to aromatic functionality.[21]

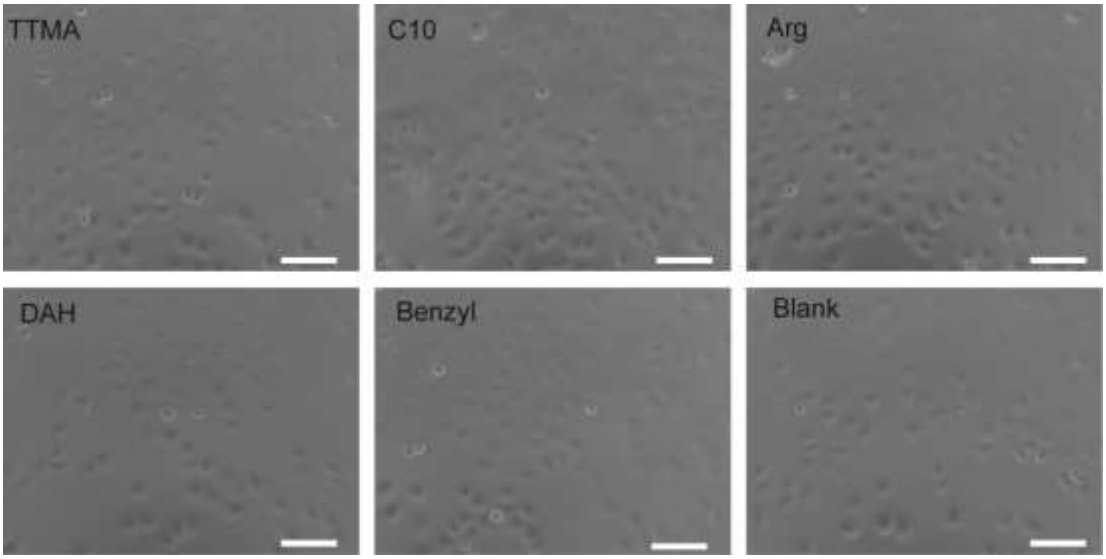

Figure 3.4. MSCs grown on differential functional positively charged AuNP-coated surfaces for 1 hr. Scale bars: 100 μm.

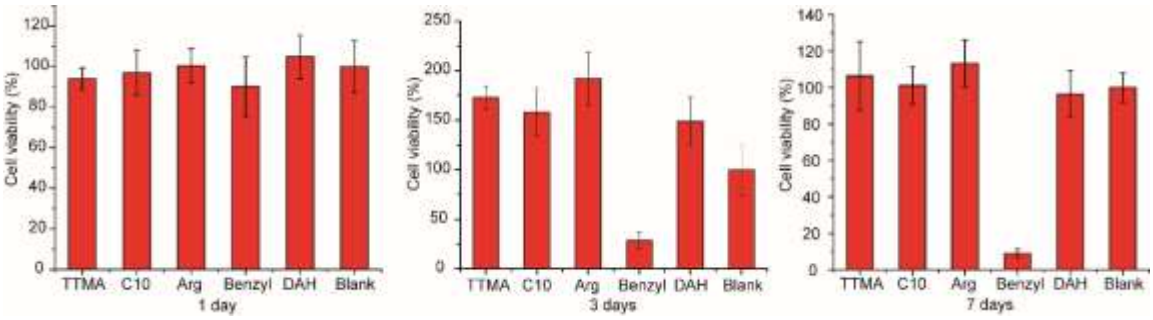

Figure 3.5. Proliferation assay of MSCs grown on surfaces functionalized with different positively charged AuNPs for 1 day, 3 days and 7 days.

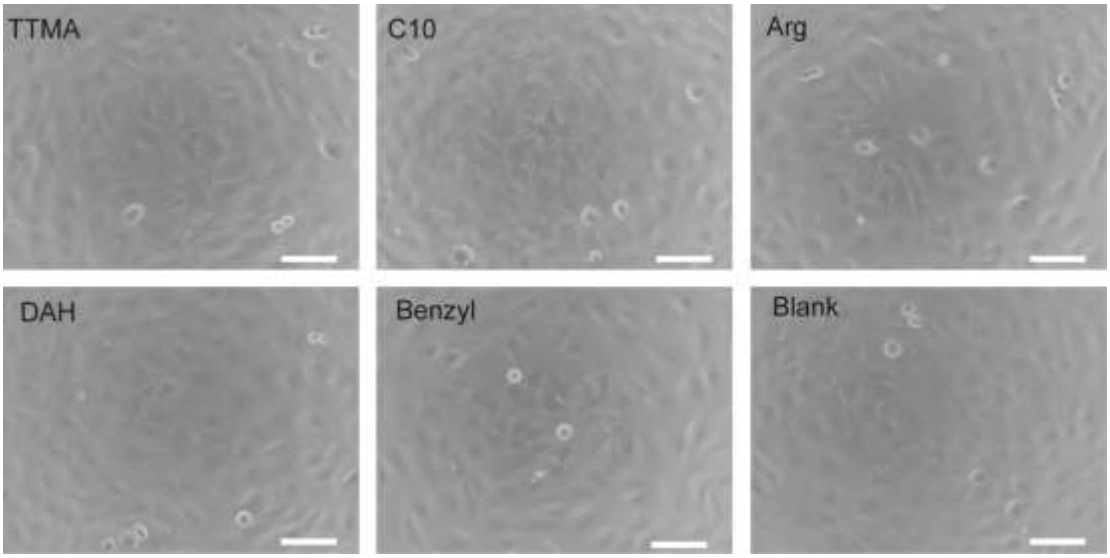

Figure 3.6. MSCs grown on differential functional positively charged AuNP-coated surfaces for 24 hr. Scale bars: 100 µm.

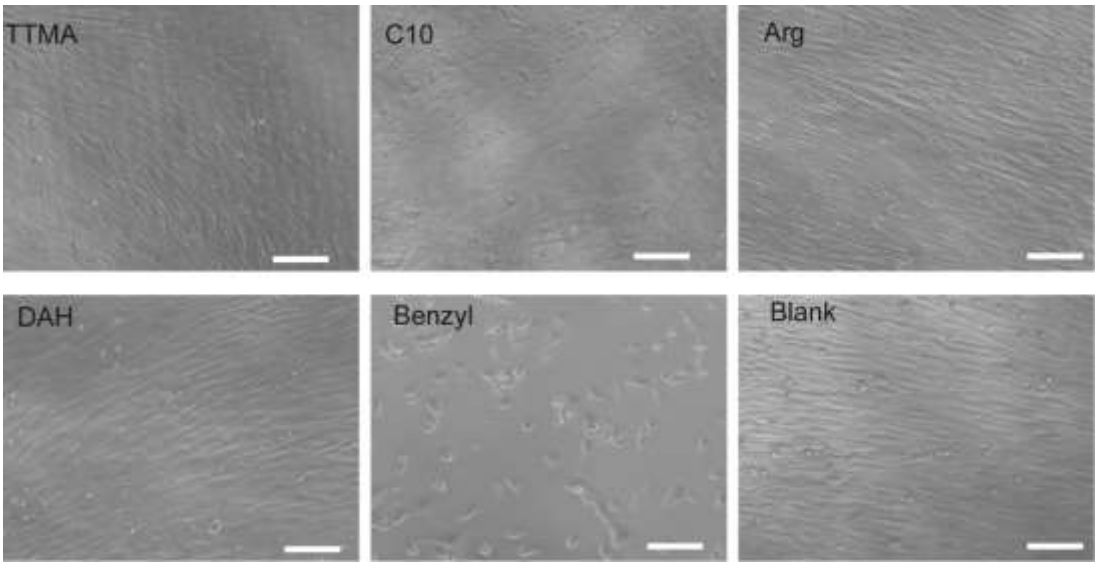

Figure 3.7. MSCs grown on differential functional positively charged AuNP-coated surfaces for 7 days. Scale bars: 100 μm.

We then performed a seven-day proliferation assay on MSCs under induced differentiation conditions. Prior to the differentiation, MSCs were allowed to adhere to the plates for 24 hrs. Next, the cells were cultured in either adipogenic or osteogenic media for 7 days. TTMA, Arg and DAH AuNP monolayers showed no toxicity to MSCs under differentiation conditions. However, under both induction conditions, MSCs grown on Benzyl AuNP monolayer did not survive (Figure 3.8). Thus, Benzyl AuNP monolayers not only affect cell proliferation negatively, but also induce cell death during differentiation. C10 AuNP monolayers induced almost complete cell death after 7 days in the presence of adipogenic but not osteogenic induction media. The structure of C10 AuNP resembles that of TTMA AuNP but with higher hydrophobicity. In fact, both these monolayers were similarly able of supporting MSC growth under non-differentiation or osteogenic condition. Hence, increased hydrophobicity of the supporting surface does not favor adipogenesis in MSCs. This property may have implications for the selective inhibition of adipocyte generation in the treatment of obesity and other diseases.

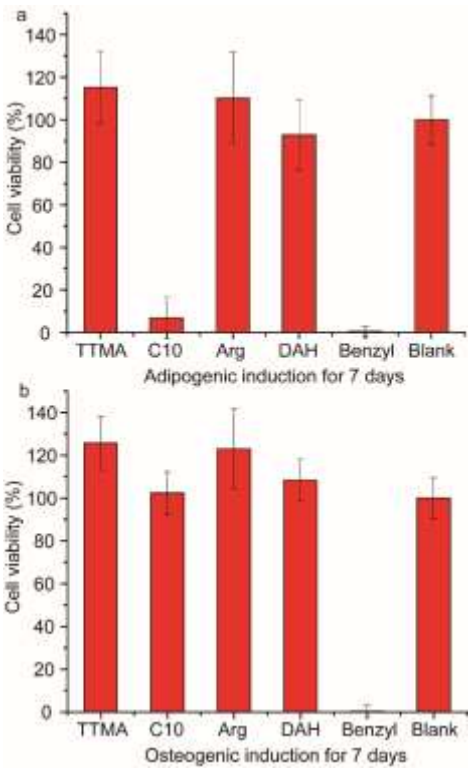

Figure 3.8. Proliferation assay of MSC on various positively charged AuNP-coated surfaces after 7 days induction in differentiation media: a) Adipogenic inducing media; b) Osteogenic inducing media.

We next investigated the modulatory capability of AuNP monolayers on osteogenic differentiation of MSCs. Osteogenesis plays an important role in bone maintenance and repair.[23] Impaired osteogenesis results in osteoporosis while excessive osteogenesis may cause hyperostosis.[24] Even though the modulation of MSC osteogenic differentiation has been achieved by tuning the stiffness of the supporting material,[25] chemical cues for osteogenesis control provide additional benefits, including precision at the atomic level, high-throughput screening and rapid modification. Herein, TTMA, C10, Arg and DAH AuNP monolayers were used to support cell growth and differentiation as functionalized surfaces. Neutral (OH) and negatively charged (COOH) AuNPs were utilized as controls, as well as the surface without AuNP coating. After osteogenic induction for 14 days, the cells were analyzed for alkaline phosphatase activity.

Alkaline phosphatase is a marker for MSC derived osteoblasts[26] (MSC progenitors do not express alkaline phosphatase[27]). After 14 days of osteogenic induction of MSC growth on the defined surfaces, a change in alkaline phosphatase activity was observed (Figure 3.9). Specifically, MSCs cultured on the DAH AuNP monolayer showed 40% higher alkaline phosphatase activity, when compared to cells grown on the surface without AuNP coating. On the other hand, in MSCs cultured on the TTMA AuNP monolayer, the alkaline phosphatase activity decreased 70% (Figure 3.10). Cells differentiated on other surfaces barely showed any difference with regard to alkaline phosphatase activity. These results indicate that chemically defined surfaces modulate osteogenic differentiation of MSCs.

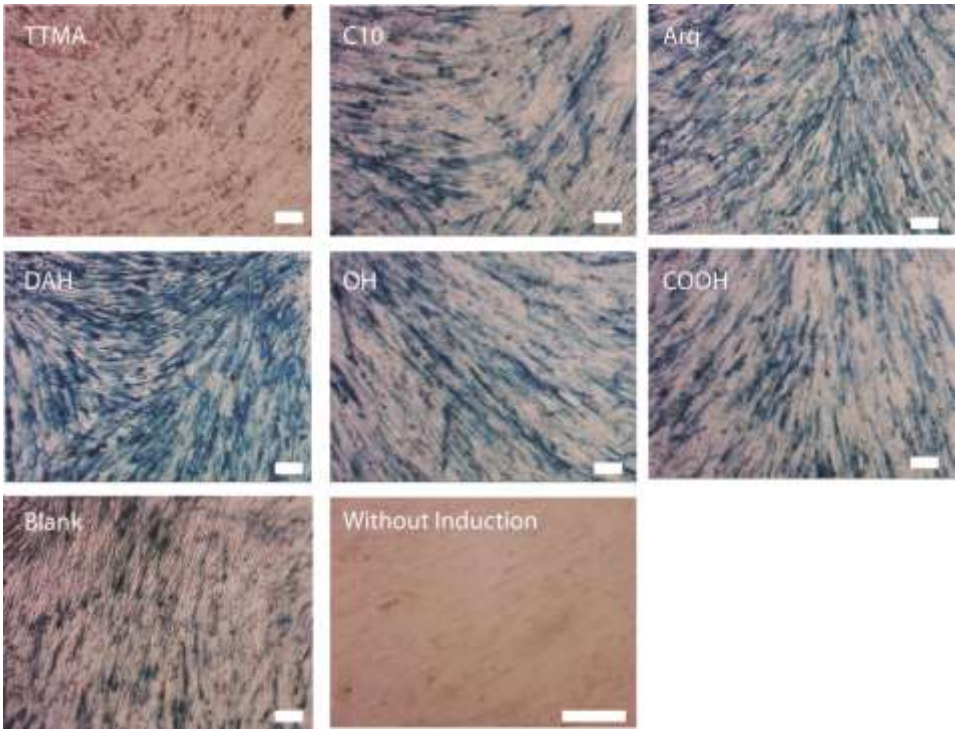

Figure 3.9. Vector® Blue staining for alkaline phosphatase activity after osteogenic induction for 14 days. Scale bars: 100 µm.

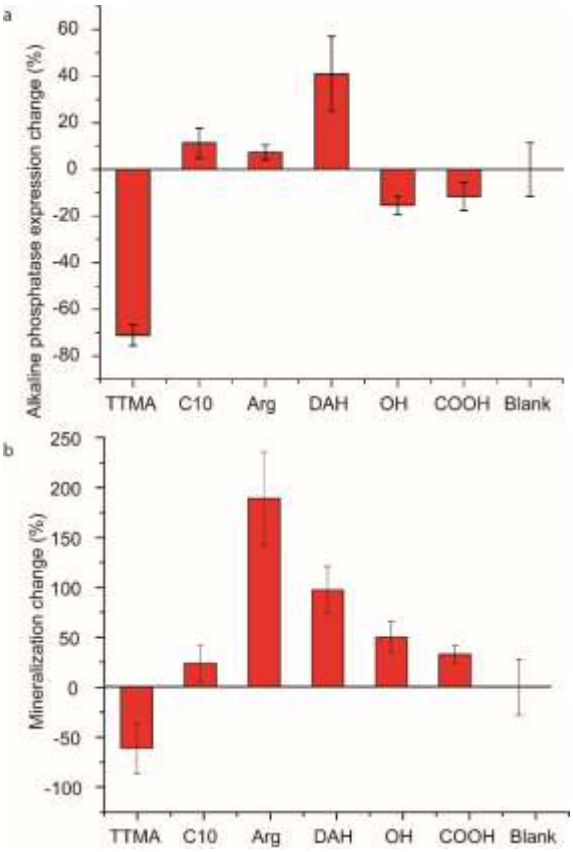

Figure 3.10. Osteogenesis of MSCs is modulated by AuNP-coated surfaces. a) Normalized differentiation ratio of induced cells grown on AuNP-coated surfaces after 14 days, marked by alkaline phosphatase expression level. b) Normalized calcium mineralization of osteoblasts, determined by Alizarin Red S staining.

To further confirm the osteogenic differentiation of MSCs, it is necessary to quantify the level of functional osteoblasts. Since mineralization of calcium is a key indicator of functional osteoblast, we then analyzed calcium deposition to evaluate MSC osteogenic differentiation. All surfaces were incubated with Alizarin Red S so that the calcium deposits were visible as red aggregates[28] (Figure 3.11). Quantitative analysis revealed that MSCs cultured on Arg and DAH monolayers produced more calcium deposits than the controls, whereas the TTMA AuNP monolayer inhibited calcium deposition. This result is in agreement with the alkaline phosphatase assays. The amine functional group has been reported to generally elevate the osteogenic

differentiation ratio.[16, 29] Our results further demonstrate that primary, but not quaternary, ammonium groups promotes MSC osteogenesis. Also, the increased calcium deposits with the Arg surface suggest that phenotypic control by the surface extends beyond differentiation.

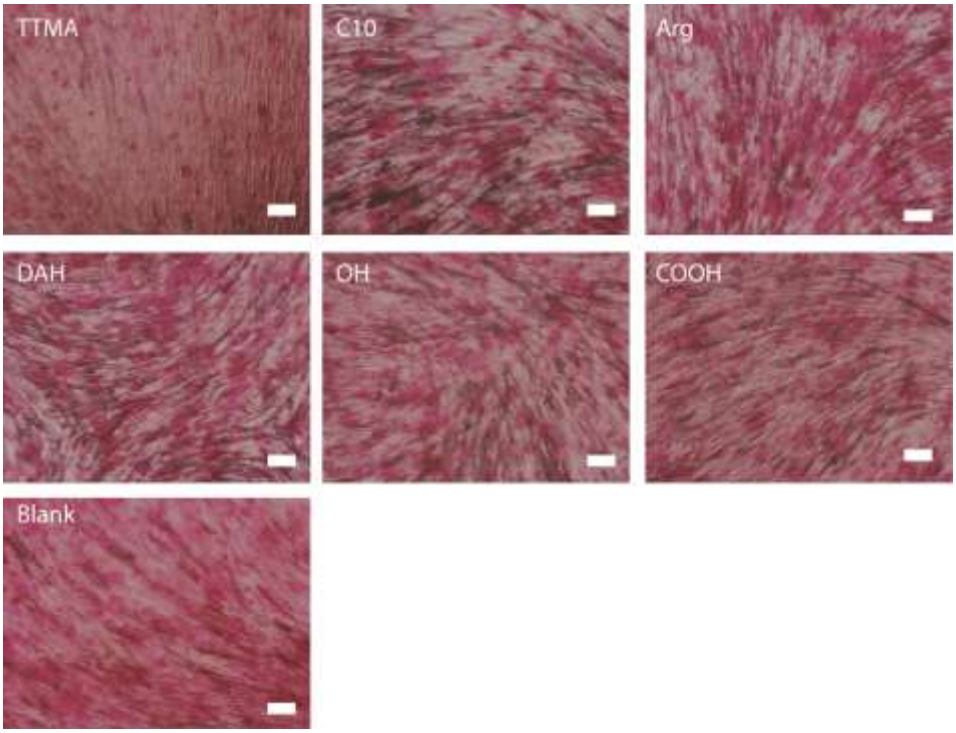

Figure 3.11. Cells stained with Alizarin S (red) and Vector® Blue (blue) after osteogenic induction for 14 days. Scale bars: 100 µm.

We then tested whether these AuNP monolayers were capable of modulating the adipogenic differentiation of MSCs. C10 and Benzyl AuNP monolayers were excluded from these experiments because of their toxicity in MSCs undergoing adipogenesis (Figure 3.8). Since the adipose-specific protein FABP4 is a known marker for adipogenesis,[30] the expression levels of FABP4 in MSCs were determined after 7 and 14 days of adipogenic differentiation (Figure 3.12a). At the seven-day point of differentiation, the expression level of FABP4 was elevated in MSCs grown on the TTMA AuNP monolayer. After 14 days of incubation, this enhancement was more pronounced (Figure 3.12b). Slight elevation of FABP4 expression was also observed in MSCs

cultured on the Arg AuNP monolayer, whereas MSCs cultured on the remaining surfaces expressed similar levels of FABP4 than controls.

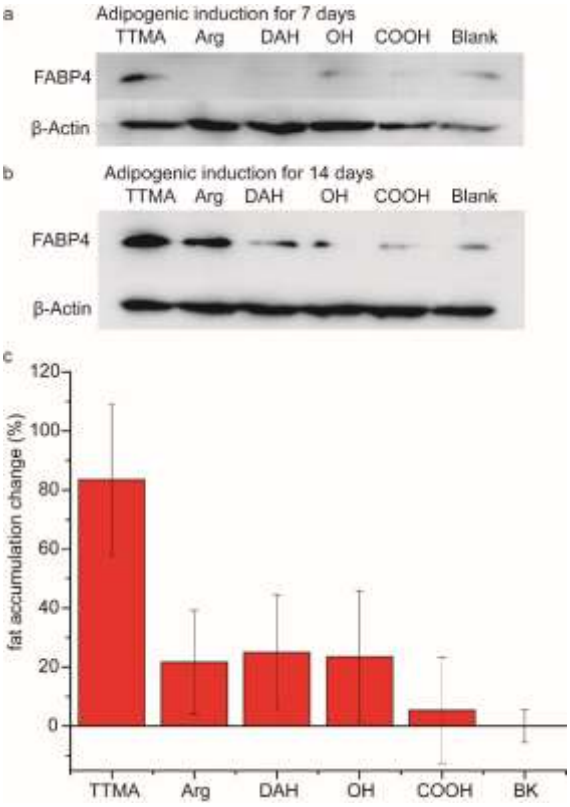

Figure 3.12. Adipogenesis of MSCs is modulated by AuNP-coated surfaces. a) FABP4 expression of induced cells grown on AuNP-coated surfaces after 7 days. b) FABP4 expression of induced cells grown on AuNP-coated surfaces after 14 days. c) Normalized differentiation ratio determined by Oil Red O staining.

Other than analyzing the expression marker, it is important to determine the function of adipocytes. Once adipocytes formed, fat droplets started to accumulate. As lipid droplets can be marked with Oil Red O;[28] this dye was used to detect and quantify MSC adipogenic differentiation. Microscope imaging revealed that numerous cells contained fat droplets after a 14-day induction (Figure 3.13). MSCs cultured on the TTMA AuNP monolayer exhibited the strongest Oil Red O staining. Quantitative analysis of Oil Red O indicated that adipogenic differentiation of MSCs grown on TTMA AuNP monolayers increased 83% when compared to surfaces without AuNP

(Figure 3.12c). In addition, the other AuNP monolayers did not show significant difference in Oil Red O staining when compared to the controls, which is consistent with the FABP4 expression results (see above). Taken together, our findings indicate that TTMA AuNP monolayers specifically enhance adipogenic differentiation of MSCs, in stark contrast to the anti-osteogenic properties of these surfaces.

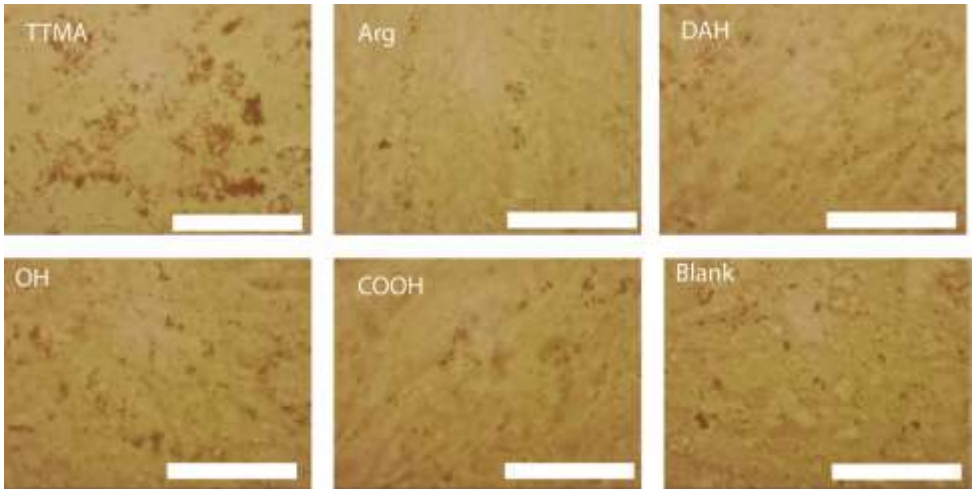

Figure 3.13. Oil Red O staining of cells after adipogenic induction for 14 days. Scale bars: 50 μm.

3.4 Conclusion

In summary, we have developed a facile and scalable strategy to modulate mesenchymal stem cell proliferation and differentiation. As shown in this study, the chemical properties of the surfaces are precisely tuned at the molecular level through deposition of engineered nanoparticles, allowing for further exploration of the modulatory capability of highly tunable surface chemistries in stem cell growth. Mechanistic studies on how stem cells response to subtle changes of their niches will also be able to be performed in vitro on these monolayers, including nanoparticle size, surface functionalization of nanoparticles, and functionalization density of nanoparticle ligands. The ability to promote modulated growth and differentiation offers great potential for the use of these surfaces on a variety of stem cells, as well as other cell types, in

medical applications such as wound healing and transplantation. Finally, because of their readily scalable deposition process, these surfaces will be easily adaptable for large-scale manufacturing.

3.5 References

1. S. J. Forbes, N. Rosenthal, *Nat. Med.* **2014**, *20*, 857.
2. A. G. Efthymiou, G. Chen, M. Rao, G. Chen, M. Boehm, *Expert Opin. Biol. Ther.* **2014**, *14*, 1333.
3. M. F. Brizzi, G. Tarone, P. Defilippi, *Curr. Opin. Cell Biol.* **2012**, *24*, 645.
4. F. M. Watt, W. T. S. Huck, *Nat. Rev. Mol. Cell Biol.* **2013**, *14*, 467.
5. H. Rashidi, J. Yang, K. M. Shakesheff, *Biomater. Sci.* **2014**, *2*, 1318.
6. J. H. Wen, L. G. Vincent, A. Fuhrmann, Y. S. Choi, K. C. Hribar, H. Taylor-Weiner, S. Chen, A. J. Engler, *Nat. Mater.* **2014**, *13*, 979.
7. A. B. Faia-Torres, S. Guimond-Lischer, M. Rottmar, M. Charnley, T. Goren, K. Maniura-Weber, N. D. Spencer, R. L. Reis, M. Textor, N. M. Neves, *Biomaterials* **2014**, *35*, 9023.
8. X. Hu, S.-H. Park, E. S. Gil, X.-X. Xia, A. S. Weiss, D. L. Kaplan, *Biomaterials* **2011**, *32*, 8979.
9. M. J. Dalby, N. Gadegaard, R. O. C. Oreffo, *Nat. Mater.* **2014**, *13*, 558.
10. B. K. K. Teo, S. T. Wong, C. K. Lim, T. Y. S. Kung, C. H. Yap, Y. Ramagopal, L. H. Romer, E. K. F. Yim, *ACS Nano* **2013**, *7*, 4785.
11. D. A. Brafman, C. W. Chang, A. Fernandez, K. Willert, S. Varghese, S. Chien, *Biomaterials* **2010**, *31*, 9135.
12. D. Grafahrend, K.-H. Heffels, M. V. Beer, P. Gasteier, M. Möller, G. Boehm, P. D. Dalton, J. Groll, *Nat. Mater.* **2010**, *10*, 67.
13. A. D. Celiz, J. G. W. Smith, R. Langer, D. G. Anderson, D. A. Winkler, D. A. Barrett, M. C. Davies, L. E. Young, C. Denning, M. R. Alexander, *Nat. Mater.* **2014**, *13*, 570.
14. P.-Y. Wang, L. R. Clements, H. Thissen, W.-B. Tsai, N. H. Voelcker, *Acta Biomater.* **2015**, *11*, 58.
15. H. Wang, D. T. K. Kwok, M. Xu, H. Shi, Z. Wu, W. Zhang, P. K. Chu, *Adv. Mater.* **2012**, *24*, 3315.
16. J. M. Curran, R. Chen, J. A. Hunt, *Biomaterials* **2006**, *27*, 4783.
17. J. M. Curran, R. Chen, J. A. Hunt, *Biomaterials* **2005**, *26*, 7057.
18. G. K. Toworfe, S. Bhattacharyya, R. J. Composto, C. S. Adams, I. M. Shapiro, P. Ducheyne, *J. Tissue Eng. Regen. Med.* **2009**, *3*, 26.
19. J. E. Phillips, T. A. Petrie, F. P. Creighton, A. J. García, *Acta Biomater.* **2010**, *6*, 12.
20. R. Tang, D. F. Moyano, C. Subramani, B. Yan, E. Jeoung, G. Y. Tonga, B. Duncan, Y.-C. Yeh, Z. Jiang, C. Kim, V. M. Rotello, *Adv. Mater.* **2014**, *26*, 3310.
21. L. Guo, N. Kawazoe, Y. Fan, Y. Ito, J. Tanaka, T. Tateishi, X. Zhang, G. Chen, *Biomaterials* **2008**, *29*, 23.
22. A. R. Murphy, P. S. John, D. L. Kaplan, *Biomaterials* **2008**, *29*, 2829.
23. W. Götz, C. Reichert, L. Canullo, A. Jäger, F. Heinemann, *Ann. Anat.* **2012**, *194*, 171.
24. Y. Mochizuki, K. Omura, H. Hideaki, T. Kugimoto, T. Osako, T. Taguch, *JIR* **2012**, 29.
25. A. J. Engler, S. Sen, H. L. Sweeney, D. E. Discher, *Cell* **2006**, *126*, 677.
26. R. S. Siffert, *J. Exp. Med.* **1951**, *93*, 415.
27. N. Jaiswal, S. E. Haynesworth, A. I. Caplan, S. P. Bruder, *J. Cell. Biochem.* **1997**, *64*, 295.

28. C. Bruedigam, M. v. Driel, M. Koedam, J. v. d. Peppel, B. C. J. van der Eerden, M. Eijken, J. P. T. M. van Leeuwen, in *Current Protocols in Stem Cell Biology*, Wiley-Blackwell, 2011.
29. X. Liu, Q. Feng, A. Bachhuka, K. Vasilev, *Appl. Surf. Sci.* **2013**, *270*, 473.
30. T. Shan, W. Liu, S. Kuang, *Faseb J.* **2012**, *27*, 277.

CHAPTER 4

DIRECT DELIVERY OF FUNCTIONAL PROTEINS AND ENZYMES TO THE CYTOSOL USING NANOPARTICLE-STABILIZED NANOCAPSULES

4.1 Introduction

Protein-based therapeutics are promising tools for numerous biomedical applications.[1] Intracellular delivery of functional proteins to replace missing, dysfunctional or poorly-expressed proteins, or antagonize key intracellular pathways is the fastest growing and a promising arm in modern drug development. Protein-based biologics have provided new therapeutic avenues for cancer,[2, 3] and have also been used to treat a range of disease states including inflammation,[4] lysosomal storage diseases,[5] and transient cerebrovascular disorders.[6] In addition to therapeutics, direct cytosolic delivery of functional proteins provides a potential tool for important biological applications including imaging,[7] signaling studies,[8, 9] cellular[10, 11] and stem cell engineering.[12]

A major complication in the use of protein-based drugs is the difficulty of delivering the unmodified, functional protein in an active conformation to the necessary site of action. Mechanical delivery methods, such as microinjection and electroporation have been used in research for decades.[13] These methods, however, are low-throughput, disruptive, and require specialized equipments to mechanically/physically puncture membranes, limiting their utility for in vivo applications. Another promising approach for delivering proteins utilizes covalent carriers[14, 15] that require irreversible modifications of the protein cargo. [16, 17] However, these covalent modifications of protein may impact protein function by interfering with protein folding.[18] Furthermore, covalent modification of proteins for delivery is not a general approach; in cases where this strategy works customized optimization protocols tailored to each specific protein are required.[14]

A major challenge in all the non-mechanical protein delivery strategies described above is access of the protein to the cytosol. Most delivery strategies rely on endocytic mechanisms of cellular uptake.[19] As a result, the delivered proteins are susceptible to degradation in the endosome/lysosome and are also unable to access key subcellular structures and machineries required for most applications.[15] Currently, prolonged incubation times, elevated concentrations of delivery agents, and lysosomotropic reagents (such as chloroquine) are required to increase the efficiency of endosomal escape of delivered proteins.[20, 21]

Supramolecular carrier-based delivery methods are modular, easy to formulate, and operate through reversible associations with target proteins.[22] In non-covalent strategies, proteins and delivery vectors self-assemble, allowing the transport of unmodified proteins into the cell and overcome the limitations of using covalently protein modification strategies.[14, 15]

We have recently developed a nanoparticle-stabilized capsule (NPSC) system for the delivery of hydrophobic drugs.[23] These NPSCs rapidly released small molecule payloads from their oil interior through a membrane fusion-like[24, 25] hydrophobic interaction with the cell membrane. We hypothesized that this vehicle could also be used for cytosolic protein delivery by incorporating functional proteins into the NPSC shell. In this report, we demonstrate rapid and efficient delivery of therapeutic and imaging proteins into the cytosol of HeLa cells using NPSCs. Caspase-3 (CASP3) was chosen to demonstrate therapeutic delivery of an active, biomedically important enzyme. Delivery of CASP3 is a particularly stringent test of the efficacy of this approach, as caspases are delicate enzymes that would be susceptible to inactivation during the delivery process. CASP3 was efficiently delivered into cells, resulting in effective induction of apoptosis. Green fluorescent protein (GFP) was used to determine the intracellular distribution of delivered proteins. The delivered GFP was distributed throughout the cell with identical cellular distribution to that of endogenously expressed red fluorescent protein (RFP). Further proof of

cytosolic access was demonstrated through efficient intracellular targeting of a GFP fusion protein to the peroxisome.[26]

4.2 Methods

4.2.1 Protein-NPSC complex preparation

The HKRK ligand protected AuNPs (HKRK AuNPs) were synthesized following reported method. To make the protein-NPSC complex, 2.5 μM HKRK AuNPs were incubated with 1 μM GFP in 30 μL phosphate buffer (5 mM, pH = 7.4) for 10 min. Then, 1 μL of the mixture of linoleic acid and decanoic acid (molar ratio = 1:1) was mixed with 500 μL of phosphate buffer (5 mM, pH = 7.4) containing 1 μM HKRK AuNPs and agitated by an amalgamator at 5000 rpm for 100 s to form emulsions. Finally, the mixture of the protein and HKRK AuNPs was diluted to 45 μL with phosphate buffer (5 mM, pH = 7.4) followed by the addition of 5 μL of the emulsion. The protein-NPSC complexes were ready to use after 10 min incubation at room temperature. The concentration of NPSC was 0.29 nM, calculated according to reported method. The final concentrations of HKRK AuNPs and GFP were 1.5 μM and 600 nM, respectively.

4.2.2 GFP expression and purification

Starter cultures from a glycerol stock of BL21(DE3) housing the gene for Enhanced GFP (EGFP) with an *N*-terminal 6-His tag in the pET21b expression vector (Novagen) with or without the peroxisomal-targeting sequence 1 (PTS1) were grown overnight in 50 mL of 2 × YT media with 50 μL of 1000× ampicillin (16 g tryptone, 10 g yeast extract, 5 g NaCl in 1 L water). The cultures were shaken overnight at 250 rpm at 37 °C. The following day, 10 mL of the starter cultures were added to a Fernbach flask containing 1 L of 2 × YT and 1 mL 1000× ampicillin and shaken until OD_{600} = 0.7 was reached. The protein expression was then induced by adding IPTG (1 mM, final concentration)

and shaken at 28 °C. After 3 h, the cells were harvested by centrifugation (5000 rpm for 15 min at 4 °C). The pellet was then resuspended in lysis buffer (2 mM imidazole, 50 mM NaH_2PO_4, 0.3 M NaCl) and the cells were lysed using a microfluidizer. Cell lysate was centrifuged at 15,000 rpm for 45 min at 4 °C. The GFP was purified from the supernatant using an imidazole gradient on a HisPur (Thermo Scientific) Cobalt column. The imidazole used for elution was removed from the GFP sample by dialysis in 5 mM sodium phosphate buffer (pH = 7.4).

4.2.3 Caspase-3 expression and purification

The caspase-3 full-length human gene in the pET23b vector (Addgene) was used for expression of caspase-3. The procedure is similar as GFP expression and purification. The supernatant was loaded onto a 5 mL HiTrap Ni-affinity column (GE Healthcare). The column was washed with a buffer of 50 mM Tris pH 8.5, 300 mM NaCl, 5% glycerol and 50 mM imidazole. The caspase-3 protein was eluted with a buffer containing 50 mM Tris pH 8.5, 300 mM NaCl, 5% glycerol and 250 mM imidazole. The eluted fraction was diluted 9-fold into a buffer containing 20 mM Tris pH 8.0 and 2 mM DTT to reduce the salt concentration. This protein sample was loaded onto a 5 mL Macro-Prep High Q column (Bio-Rad Laboratories, Inc.). The column was developed with a linear NaCl gradient and caspase-3 eluted in a buffer of 20 mM Tris pH 8.0, 120 mM NaCl and 2 mM DTT. The eluted protein was stored at -80 °C in the elution buffer conditions. Caspase-3, analyzed by SDS-PAGE to be ~98% pure was further analyzed by ESI-MS to confirm mass.

4.2.4 Cell culture

HeLa cells were cultured in a humidified atmosphere (5% CO_2) at 37 °C, and grown in Dulbecco's modified eagle's medium (DMEM, low glucose) supplemented with 10% fetal bovine serum (FBS) and 1% antibiotics (100 U/ml penicillin and 100 μg/ml streptomycin).

4.2.5 Cell transfection and selection

PCDNA3.1(-)-mcherry plasmid was cloned from pCHERRY3 plasmid, purchased from Addgene (ID: 24659). RFP-PTS plasmid was purchased from Origene. HeLa cells were transfected by lipofectamine 2000 according to manufacturer's protocols (Invitrogen). The transfected cells were then selected by geneticin (Invitrogen) at the concentration of 400 μg/mL in DMEM with 10% FBS until the stably transfected clones were obtained.

4.2.6 Fluorescence titration

In the fluorescent titration experiment between nanoparticles and GFP, the change of fluorescence intensity at 515 nm was measured with an excitation wavelength of 485 nm at various concentrations of NPs from 0 to 200 nM on a Molecular Devices SpectraMax M3 microplate reader (at 25 °C). Decay of fluorescence intensity arising from 100 nM GFP was observed with increasing NP concentration. Nonlinear least-squares curve fitting analysis was carried out to estimate the binding constant (Ks).[27]

4.2.7 GFP delivery

60,000 or 240,000 HeLa cells or transfected HeLa cells were cultured in a 24-well plate or confocal dish, respectively, for 24 h prior to delivery. The cells were washed by cold phosphate buffer saline (PBS) 3 times right before delivery. After the preparation of cells, GFP-NPSC complex solution (50 μL or 150 μL of the GFP-NPSC complex diluted by 450 μL or 1.35 mL of the DMEM without FBS, respectively) was incubated with the cells for 1 h in a 24-well plate or confocal dish, and followed by incubation with fresh DMEM with 10% FBS for 1h unless otherwise mentioned. To study the colocalization with Hoescht 33342 or Lysotracker, the reagent was introduced 20 min before the observation.

4.2.8 CASP3 delivery

The procedure of CASP3 delivery was similar to that of GFP delivery, except that 30,000 HeLa cells were incubated in a 24-well plate for 24 h prior to delivery. After the protein delivery, the cells were stained by Yopro-1 and 7-AAD for 30 min, followed by the observation under fluorescence microscope. The apoptotic ratio of each sample was calculated as the ratio of fluorescently stained cells over 100 cells.

4.2.9 Cell viability assay (Alamar Blue)

7,500 HeLa cells were cultured in a 96-well plate for 24 h prior to the experiment. The cells were washed by cold phosphate buffer saline (PBS) 3 times before the delivery, then different amounts of the GFP-NPSC complex (prepared as mentioned above) were diluted by DMEM and incubated with the cells for 1 h followed by the incubation with DMEM containing 10% FBS and 1% antibiotics for 23 h. After washing with PBS 3 times, the cells were then incubated with 200 µL DMEM containing 10% Alamar Blue for 3 h. Cell viability was calculated by measuring the fluorescence intensity of Alamar Blue at 590 nm, with an excitation of 535 nm.

4.2.10 In vitro caspase-3 activity assay

For kinetic measurements of caspase activity, 20 nM protein with and without 40 nM HKRK AuNPs were assayed over the course of 5 minutes in a caspase-3 activity-assay buffer containing 20 mM Tris (pH 7.5) and 5 mM TCEP. 150 µM substrate (DEVD-AMC [N-acetyl-Asp-Glu-Val-Asp-AMC], Enzo Lifesciences; Ex. 365 nm / Em. 495 nm) was added to initiate the reaction. Assays were performed in triplicate at 25°C in 100 µL volumes in 96-well microplate format using a Molecular Devices Spectramax spectrophotometer.

4.2.11 Live cell imaging

240 K HeLa cells were cultured in the confocal dish 24 hr prior to the experiment. Before live cell imaging, cells were washed by PBS for three times followed by the incubation with GFP-NPSC in cell culture media. The confocal dish was then placed in the live cell imaging chamber with 5% CO_2 and at 37 °C on the confocal microscope. A series of images were taken at certain time intervals.

4.3 Results and Discussions

4.3.1 Nanoparticle-stabilized capsule fabrication

The protein-NPSC (CASP3-NPSC and GFP-NPSC) complexes were generated using a convergent process (Figure 4.1a), where the HKRK AuNPs (see Figure 4.1a for the structure) provided a dual mode supramolecular stabilization of the capsule wall. Briefly, proteins and AuNPs were mixed and incubated at room temperature for 10 minutes. Template emulsions were formed by homogenizing AuNPs in phosphate buffer (5 mM, pH 7.4) and oil. Protein-NPSCs were formed by combining template emulsions and the protein-AuNP mixture. Combined hydrogen bonding and electrostatic interactions between the guanidinium moieties of the particles and the carboxylates of the oil[28, 29] pin the nanoparticles to the capsule surface. Lateral stabilization is provided through interactions of the cationic nanoparticles with the anionic proteins (GFP pI= 5.9, CASP3 pI= 6.1) to be transported (Figure 4.1a).[30] The capsule size is well-controlled and in a regime well suited for intracellular delivery[31] with GFP-NPSCs and CASP3-NPSCs possessing average diameters as determined by dynamic light scattering of 130 ± 40 nm and 140 ± 20 nm, respectively (Figure 4.1b and c, Figure 4.2).

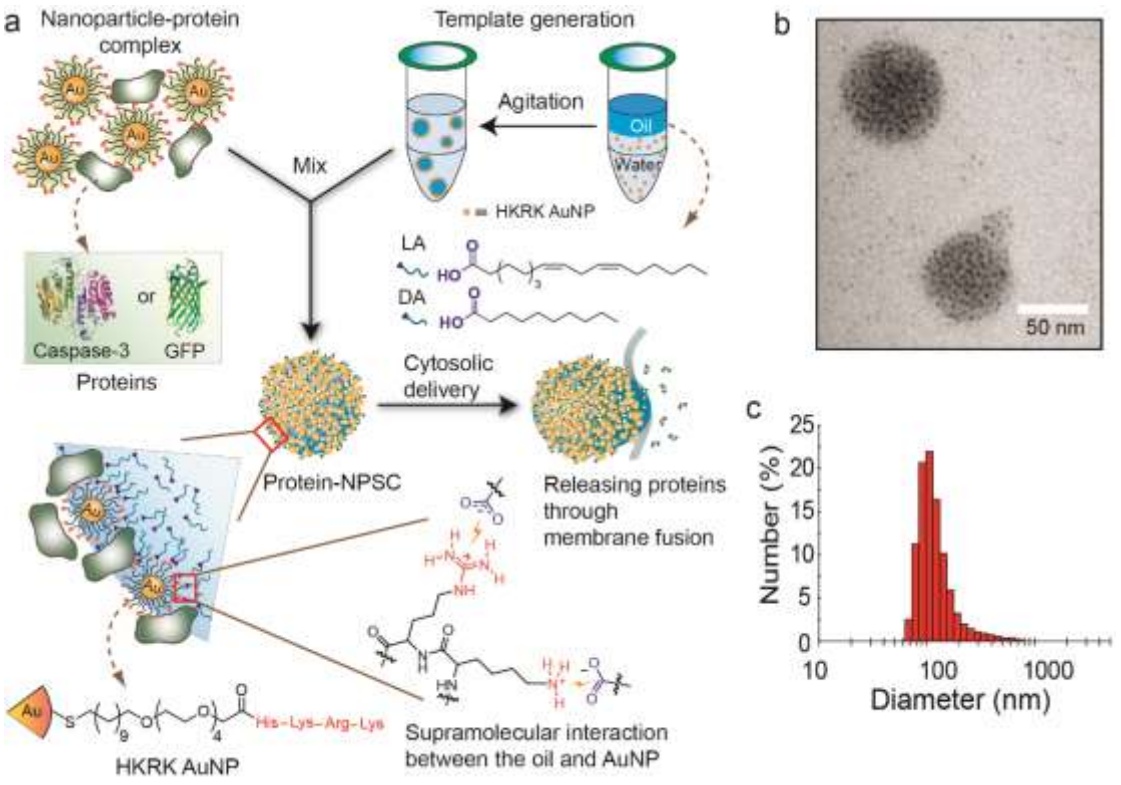

Figure 4.1. Design and preparation of nanoparticle-stabilized capsules (NPSCs). (a) Schematic showing the preparation of the protein-NPSC complex containing caspase-3 or GFP and proposed delivery mechanism. The oil was a 1:1 mixture of linoleic acid (LA) and decanoic acid (DA). (b) TEM image of the dried GFP-NPSC. (c) Dynamic light scattering (DLS) histogram of GFP-NPSCs indicating an average diameter of 130 ± 40 nm.

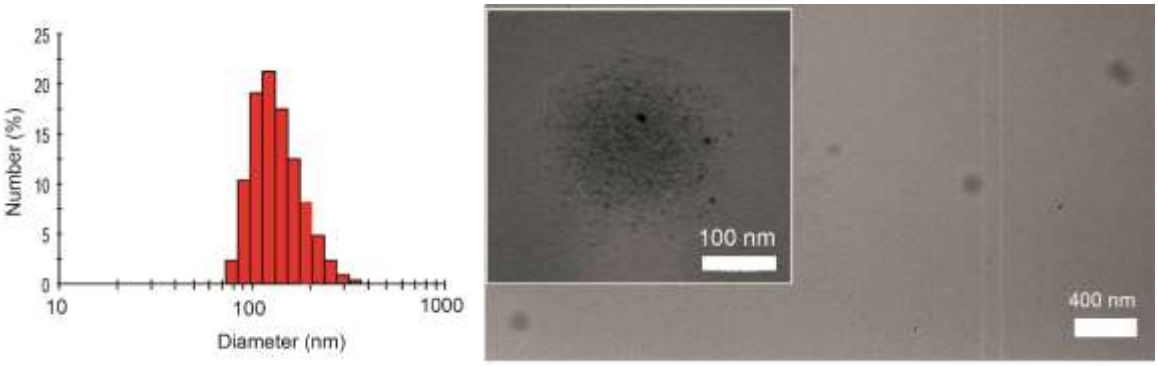

Figure 4.2. DLS (left) and TEM (right) results of CASP3-NPSCs.

A fluorescence titration was performed to measure the binding constant (K_s) between HKRK AuNPs and GFP, which was found to be 9×10^7 M^{-1}, indicating high affinity of HKRK AuNPs to the protein (Figure 4.3a). Screening of the electrostatic interactions through the use of 500 mM NaCl into the mixture of AuNPs with GFP at 1:1 molar ratio resulted in complete recovery of the GFP fluorescence (Figure 4.3b), indicating reversible electrostatic interactions between the HKRK AuNP and the protein. GFP is almost completely quenched upon complexation by AuNPs. NPSC formation, however, results in a partial restoration in fluorescence. This result indicates a change in the structure of GFP-AuNP complex when at the interface of the NPSCs. To further probe the nature of the interactions, the NPSCs were incubated in 0.5% Tween-20 and 500 mM NaCl solutions. The high salt solution resulted in no change in fluorescence, while Tween-20 resulted in increased in fluorescence. (79%; Figure 4.4a). These results suggest that other interactions are involved in NPSC assembly beyond simple electrostatics. For CASP3, enzyme activity was assessed after interaction with HKRK AuNPs. Activity assays *in vitro* showed that the interaction between CASP3 and HKRK AuNPs did not inhibit the enzymatic activity. In fact, HKRK AuNPs enhanced the CASP3 activity by 2.3 times, a phenomenon observed previously in other nanoparticle-protein systems[32] (Figure 4.4b). While efforts were made to assess activity of CASP3 in the NPSCS, the biphasic nature of the system prevented effective measurement of catalytic efficiency.

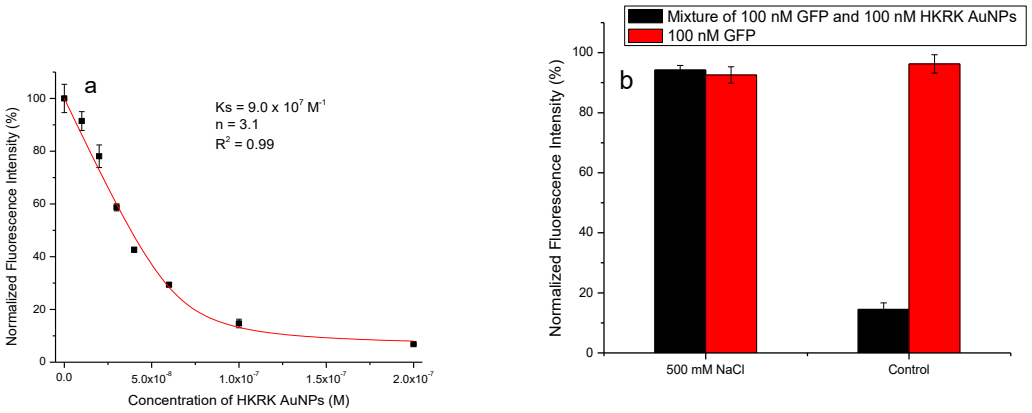

Figure 4.3. Determination of the interaction between GFP and HKRK AuNPs. (a) Fluorescence titration of HKRK AuNPs in the presence of 100 nM GFP in 5 mM phosphate buffer (pH = 7.4). The binding constant (Ks) and association stoichiometry (n) were calculated through the fitting using the model of single set of identical binding sites.[33] (b) Fluorescence recovery of 100 nM GFP quenched by 100 nM HKRK AuNPs in the presence of 500 mM NaCl or phosphate buffer (control).

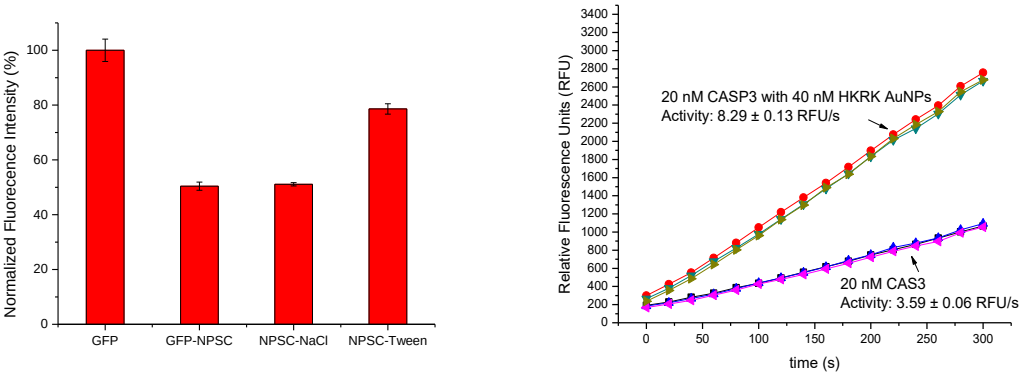

Figure 4.4. (a) Fluorescence recovery of GFP quenched by NPSC. The concentrations of both GFP and AuNP are 400 nM in 100 µL mixture. The concentration of NaCl is 500 mM and that of Tween-20 is 0.5% by volume. (b) In vitro activity assay of CASP3 in the presence or absence of HKRK AuNPs.

4.3.2 Therapeutic protein delivery with NPSCs

Effective use of therapeutic proteins for intracellular applications requires rapid delivery of the protein in the active form to the cytosol.[34, 35] CASP3 is a highly promising therapeutic

protein candidate[36] owing to its critical role in apoptosis.[37] Most tumor cells do not undergo appropriate apoptosis, which leads to unhindered cell growth.[38] In many tumor cells CASP3 function is blocked due to over expression of inhibitor of apoptosis (IAP) proteins that directly inhibit caspase function preventing apoptosis. Intracellular delivery of sufficient levels of active CASP3 into the cytosol of such tumor cells circumvents this blockage, allowing tumor cells to enter apoptosis. Delivery of active caspases is extremely challenging, however, due to the negative charge and heterotertrameric state of the protein, the susceptibility of the active site to oxidation and alkylation, and the fragile nature of the active site that is composed of four highly mobile loops.

Demonstration of effective delivery of active CASP3 was established through incubation of HeLa cells with CASP3-NPSCs. After 1 h incubation, 72.0 ± 5.5% of HeLa cells underwent apoptosis, confirmed by double staining with Yopro-1 (a dye to detect apoptotic cell nuclei)[39] and 7-AAD (a dye used to detect membrane disruption)[40] (Figure 4.5a). The NPSC itself (Figure 4.5b), CASP3 only (Figure 4.5c), or CASP3 with AuNPs induced minimal levels of cell apoptosis, demonstrating that CASP3-NPSCs deliver the protein in the active form required for therapeutic applications.

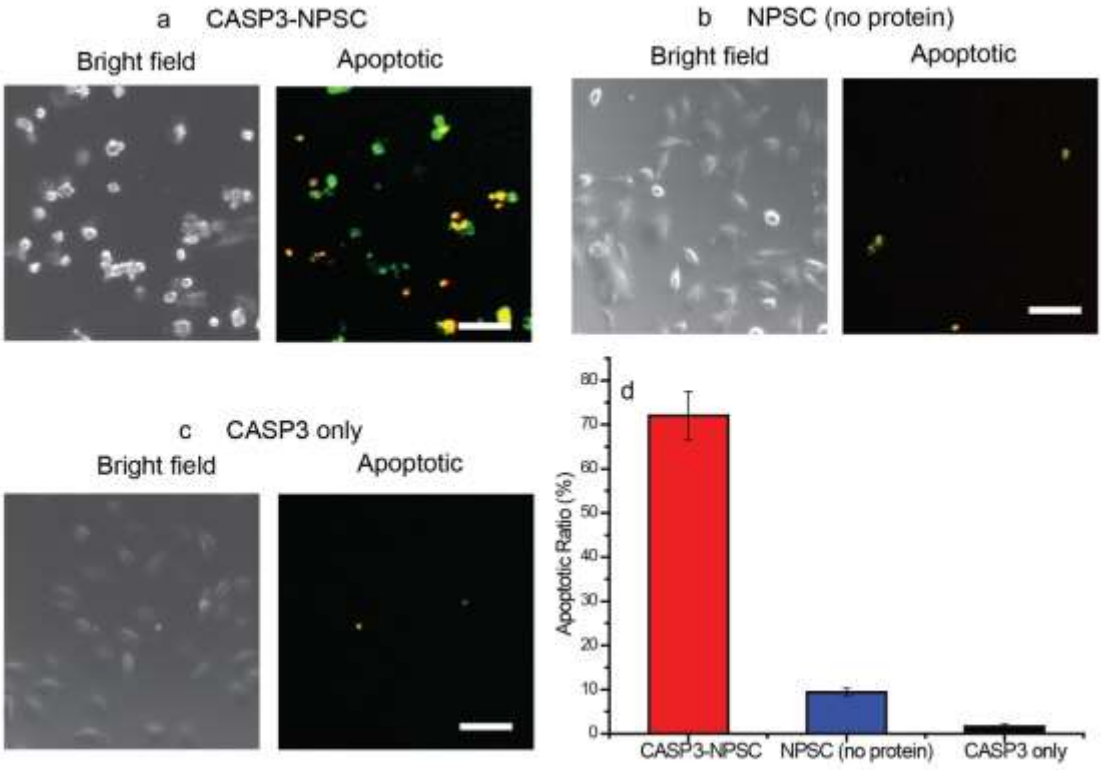

Figure 4.5. Delivery of caspase-3 into HeLa cells. Cells were incubated for 1 h with (a) CASP3-NPSC, (b) NPSC without CASP3, and (c) only CASP3 without NPSC. Subsequently, cells were stained using Yopro-1 (green fluorescence) and 7-AAD (red fluorescence) for 30 min, and the overlapped images are presented as apoptotic. (d) Apoptosis ratios of the cells after CASP3 delivery. Scale bars: 100 µm; the error bars represent the standard deviations of three parallel measurements.

4.3.3 GFP delivery using NPSCs

The effectiveness of the delivered caspase suggested access of the delivered protein to the cytosol. The capability of cytosolic delivery of NPSCs was verified using GFP. Imaging experiments were performed using live cells to provide an accurate determination of protein distribution inside the cell.[41] After 1 h incubation of GFP-NPSCs with HeLa cells, followed by 1 h incubation in fresh media, GFP was observed evenly distributed throughout the cytosol and nucleus (Figure 4.6a). In comparison, no delivery was observed by mixing empty NPSCs and GFP, indicating that the NPSCs serve as a carrier for the delivery cargo and not solely as a "hole

puncher" for membrane penetration (Figure 4.7). To further demonstrate the cytosolic distribution of GFP, NPSCs were used to deliver GFP into mCherry expressing HeLa cells.[42] Confocal images (Figure 4.6b and Figure 2.8) show GFP delivered *via* NPSCs to be evenly distributed throughout the cytosol and nucleus (with the exception of nucleoli) of HeLa cells, with no perceptible difference in distribution with respect to mCherry. Co-administration of Hoechst 33342 (a family of blue fluorescent dyes used to stain nuclei) confirmed that the delivered GFP had gained access to the nucleus, but not to the interiors of nucleoli (Figure 4.9), consistent with the distribution of cellularly expressed mCherry. Dispersal of GFP in the nucleus indicated that GFP was successfully delivered not just to the cytosol, but also to the nucleus by free diffusion through nuclear pores.[43] Taken together, these results demonstrate that the GFP was successfully delivered into the cytosol in a freely diffusing fashion.

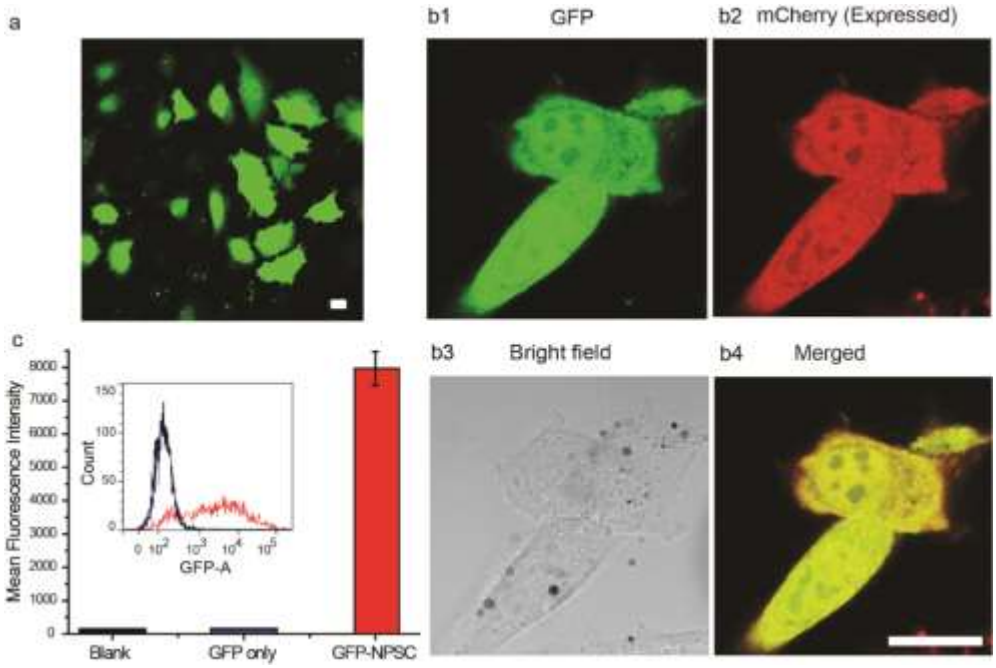

Figure 4.6. Delivery of GFP into HeLa cells. (a) Confocal image showing GFP delivery into HeLa cells by NPSCs. (b) Confocal images showing the colocalization of delivered GFP with expressed mCherry in HeLa cell. (c) Flow cytometry results of HeLa cells treated with GFP-NPSCs (red), or GFP alone (blue) for 2 h, using untreated HeLa cells as the control (black). Scale bars: 20 µm.

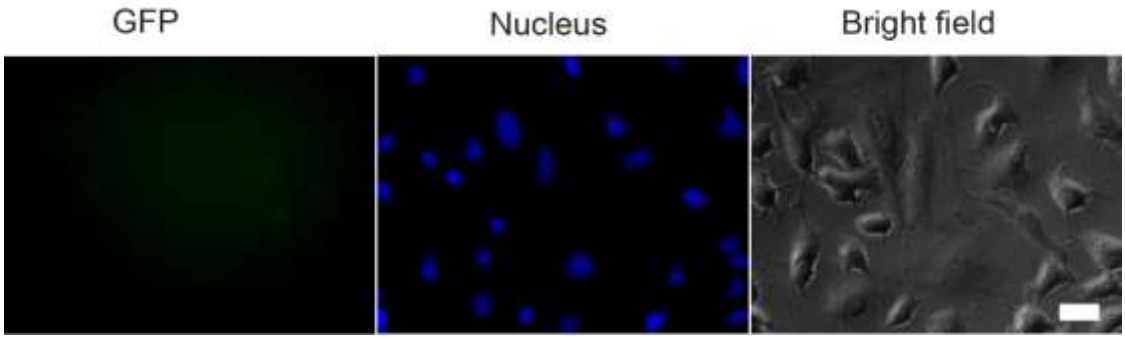

Figure 4.7. Co-incubation of empty NPSC and GFP with HeLa cells for 1 hr. The bar represent 20 µm.

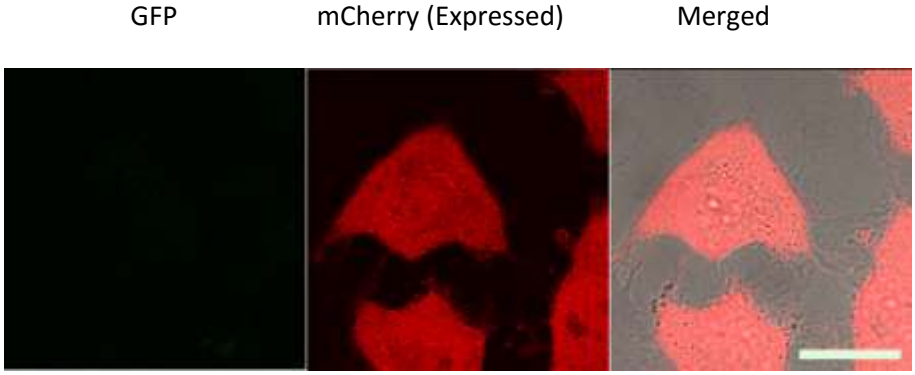

Figure 4.8. HeLa cells stably express mCherry (control group for Figure 2d in context). The scale bar represents 20 µm.

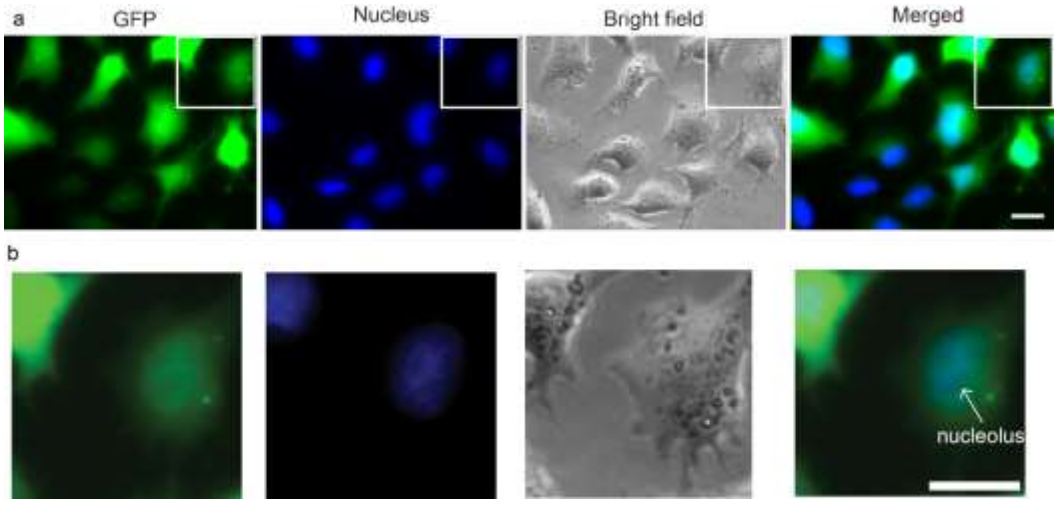

Figure 4.9. (a) Colocalization of GFP and Hoechst 33342 in a HeLa cell. (b) Magnified from boxes of Figure 4.9a. The scale bars represent 20 µm.

Flow cytometry was used to quantify the efficiency of GFP delivery into cells using NPSCs. The results showed that GFP was delivered to 77 ± 5% of cells in the GFP-NPSCs group (Figure 4.6c), consistent with the apoptosis induction observed with the CASP3-NPSCs. As expected, no delivery was observed for either the cells treated with GFP alone or untreated. Only low levels of delivery (20.6 ± 3.8%) were observed for GFP-HKRK AuNP complexes that were not in capsule form (Figure 4.10), with most of the delivered GFP remaining entrapped in late endosomes/lysosomes (Figure 4.11). The difference in GFP delivery efficiency and subcellular localization between the particle-only group and the NPSC group supports the hypothesis that the improved efficiency of the delivery process in the NPSC group resulted from a membrane fusion-delivery process, in agreement with previous studies.[44, 45] The NPSCs showed little cytotoxicity at the concentration (29 pM) used for the delivery studies (Figure 4.12).

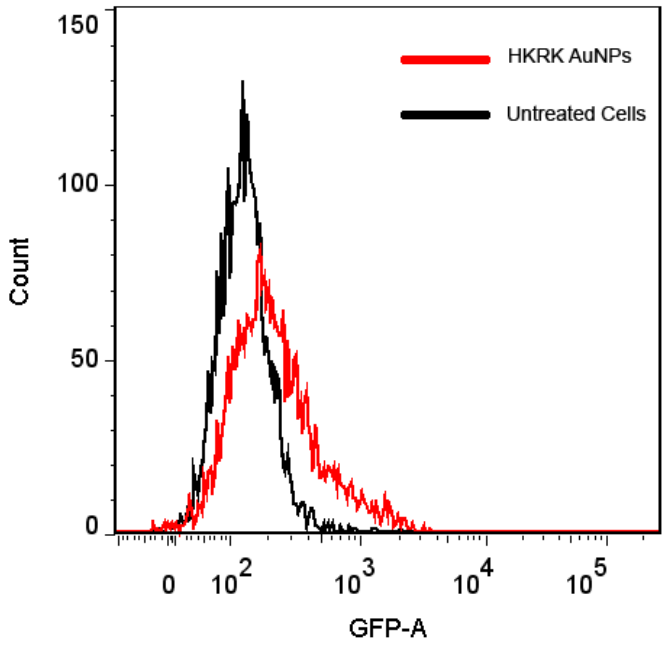

Figure 4.10. Flow cytometry results of HeLa cells cultured with GFP-HKRK AuNPs for 2 h, using untreated HeLa cells as the control.

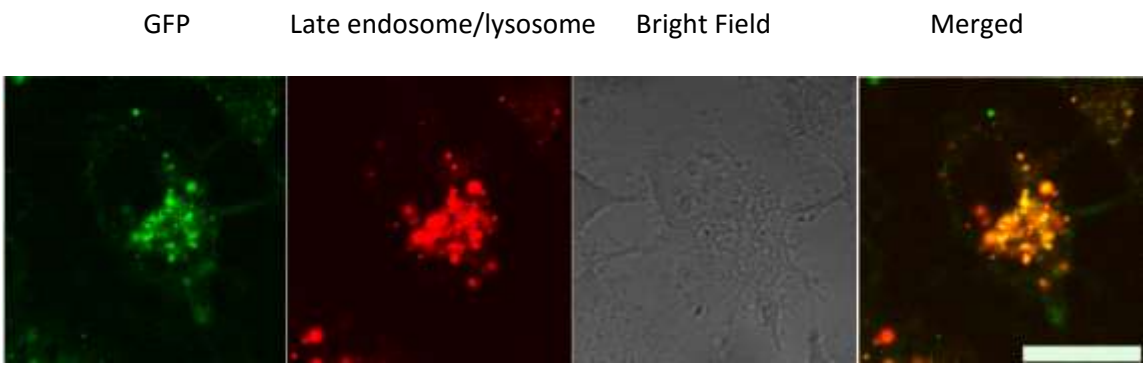

Figure 4.11. Confocal image of the colocalization of GFP with late endosomes and lysosomes after 1 hr of delivery by HKRK AuNPs. The scale bar represents 20 µm.

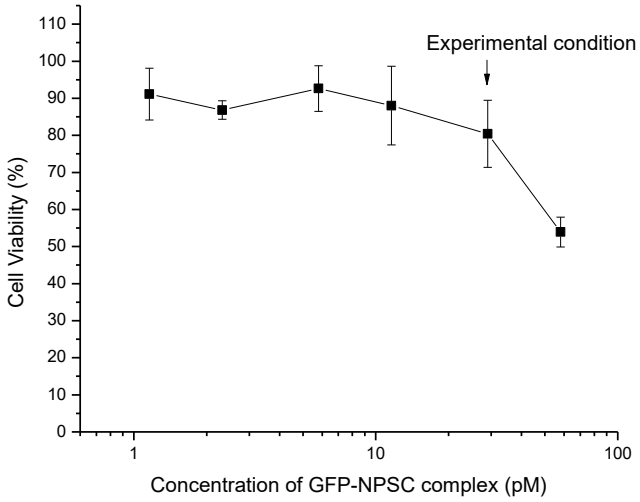

Figure 4.12. Viability of HeLa cells at different concentrations of GFP-NPSC complexes measured by Alamar Blue assay.

Live cell video imaging was then performed to track the intracellular release of protein payloads by NPSCs (Figure 4.13). As shown in Figure 4.13, GFP-NPSCs remain intact for the first few minutes after attaching to the cell, confirmed by the colocalization of GFP and the AuNPs. Then GFP was rapidly released into cytosol within. GFP was rapidly delivered, however the GFP-NPSC was not taken up as an intact entity by the cell. Taken together, these results strongly

support the membrane fusion mechanism of delivery while demonstrating that uptake does not occur through an endocytotic mechanism

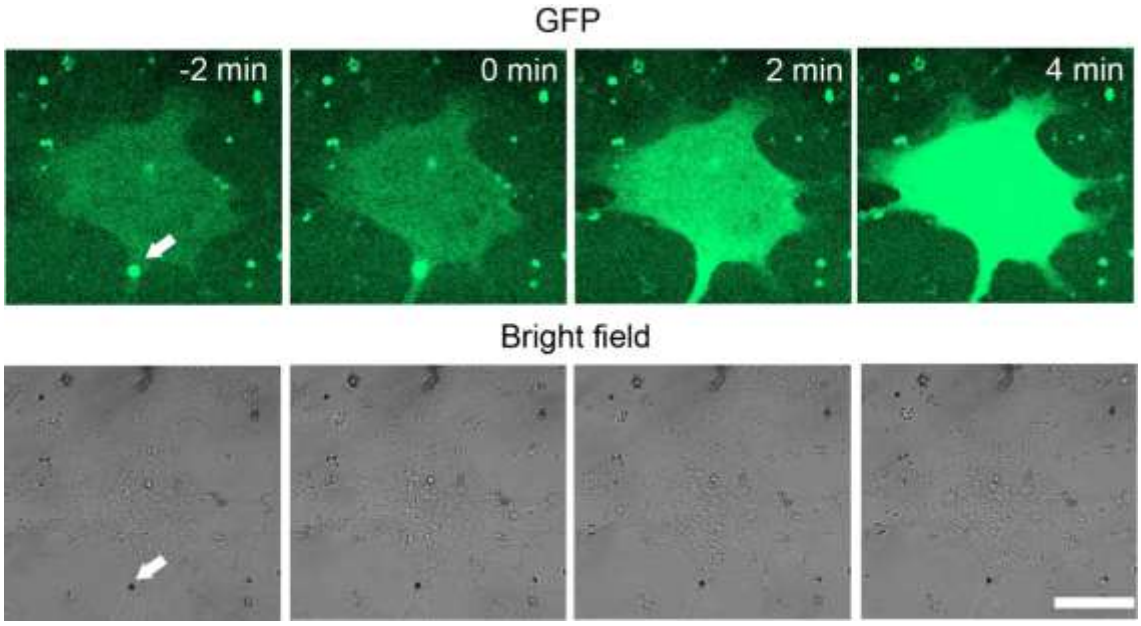

Figure 4.13. Live cell imaging of rapid GFP release into the cytosol of HeLa cell by NPSCs. "0 min" label represents the starting point of release. The arrow indicates a GFP-NPSC at the cell membrane prior to delivery of payload. Scale bar: 20 µm.

4.3.4 Intracellular targeting of delivered proteins

To further demonstrate the versatility of NPSC protein delivery for intracellular delivery and imaging, we fused a peroxisomal-targeting sequence 1 (PTS1) to GFP (Figure 2.14).[46] HeLa cells with stable expression of RFP bearing a C-terminal peroxisomal-targeting sequence were used to provide a fluorescence label for the peroxisomes. After 1 h incubation with GFP-PTS1-NPSC complexes, followed by 1 h incubation with fresh media, the confocal images clearly confirmed complete colocalization of the GFP-PTS1 fusion protein with the RFP-labeled peroxisomes (Figure 4.15a and Figure 4.16). In contrast, GFP without the PTS1 motif was evenly distributed throughout the cell as previously described (Figure 4.15b). These results clearly demonstrate that the protein delivered by the NPSCs gained complete access to the cytosol, and

that proteins delivered by NPSCs are capable of targeting subcellular organelles with essentially identical localization behavior to cellularly expressed proteins.

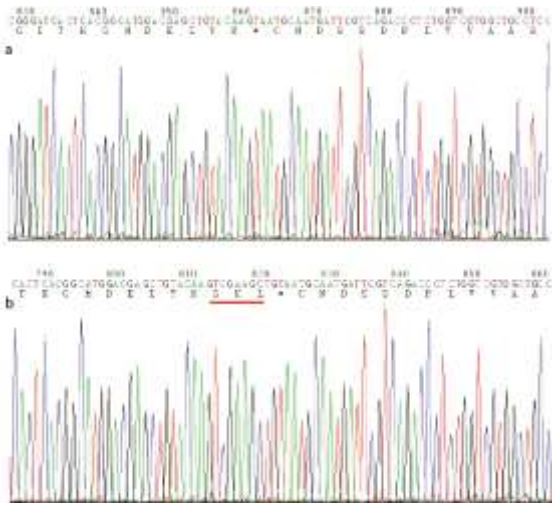

Figure 4.14. GFP fused with PTS1 motif.

(a) Sequence of C-terminal of GFP from the plasmid (sequence: MASHHHHHHMVSKGEELFTGVVPILVELDGDVNGHKFSVSGEGEGDATYGKLTLKFICTTGKLPVPWPTLVT TFTYGVQCFSRYPDHMKQHDFFKSAMPEGYVQERTIFFKDDGNYKTRAEVKFEGDTLVNRIELKGIDFKEDG NILGHKLEYNYNSHNVYIMADKQKNGIKVNFKIRHNIEDGSVQLADHYQQNTPIGDGPVLLPDNHYLSTQSAL SKDPNEKRDHMVLLEFVTAAGITHGMDELYK).

(b) Sequence of C-terminal of GFP fused with PTS1 motif from the plasmid (sequence: MASHHHHHHMVSKGEELFTGVVPILVELDGDVNGHKFSVSGEGEGDATYGKLTLKFICTTGKLPVPWPTLVT TFTYGVQCFSRYPDHMKQHDFFKSAMPEGYVQERTIFFKDDGNYKTRAEVKFEGDTLVNRIELKGIDFKEDG NILGHKLEYNYNSHNVYIMADKQKNGIKVNFKIRHNIEDGSVQLADHYQQNTPIGDGPVLLPDNHYLSTQSAL SKDPNEKRDHMVLLEFVTAAGITHGMDELYK**SKL**).

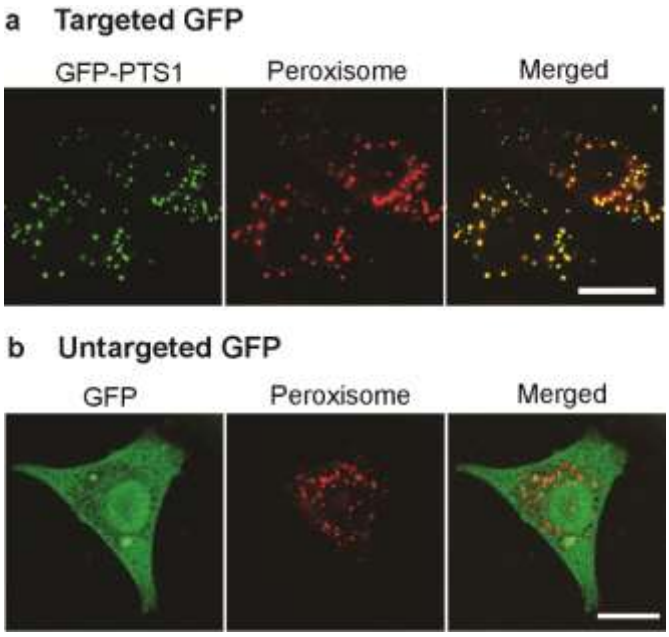

Figure 4.15. Peroxisome targeting in HeLa cells transfected with RFP-PTS1 plasmid. (a) Colocalization of GFP-PTS1 fusion protein with the peroxisomal indicator (RFP-PTS1) expressed by the cell. (b) No colocalization of GFP was observed without PTS1 motif. Scale bars: 20 µm.

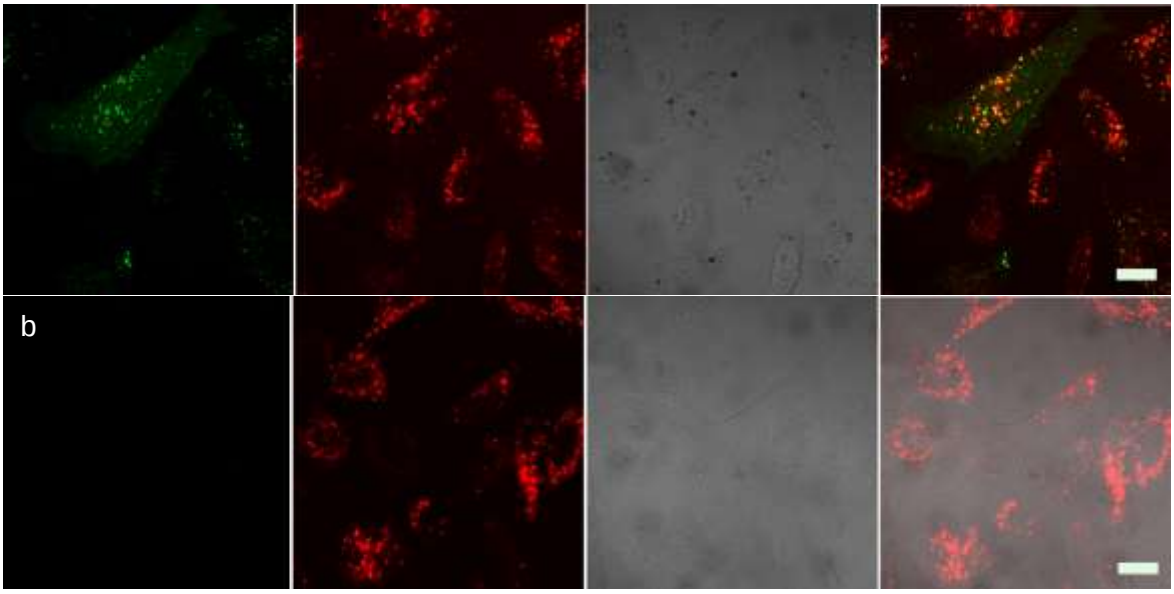

Figure 4.16. (a) Delivery of GFP-PTS1 into HeLa cells by NPSCs. (b) Untreated cells under the same exposure conditions. The scale bars represent 20 µm.

4.4 Conclusion

We have demonstrated a rapid and efficient protein delivery strategy using nanoparticle based supramolecular nanocapsules. This approach provides a generalized strategy for direct delivery of functional proteins in their native forms. The supramolecular structure of the NPSCs makes the system stable for delivery of proteins yet reversible for payload release. In contrast with particle based protein delivery systems, this method is capable of overcoming the major challenge of endosomal sequestration and thus holds great promise for effective protein therapy and imaging applications. We demonstrated the efficiency of the system by delivering a functional therapeutic protein, CASP3 into target cells to induce apoptosis. Delivery of fluorescent proteins demonstrated cytosolic distribution identical to that of a cellularly expressed counterpart, with delivery versatility further demonstrated by subcellular targeting of proteins. Taken together, the ability to incorporate active proteins on the capsule shell and efficiently deliver into the cytosol opens up new opportunities for protein replacement therapy, *in vivo* disease prognosis through imaging, cellular organelle labeling, and cellular engineering.

4.5 References

1. B. Leader, Q. J. Baca, D. E. Golan, *Nat. Rev. Drug Discov.* **2008**, *7*, 21.
2. Y. Yarden, M. X. Sliwkowski, *Nat. Rev. Mol. Cell Biol.* **2001**, *2*, 127.
3. P. F. Foltopoulou, A. S. Tsiftsoglou, I. D. Bonovolias, A. T. Ingendoh, L. C. Papadopoulou, *Biochim. Biophys. Acta-Mol. Basis Dis.* **2010**, *1802*, 497.
4. D. Jo, D. Y. Liu, S. Yao, R. D. Collins, J. Hawiger, *Nat. Med.* **2005**, *11*, 892.
5. M. Beck, *IUBMB Life* **2010**, *62*, 33.
6. T. Ogawa, S. Ono, T. Ichikawa, S. Arimitsu, K. Onoda, K. Tokunaga, K. Sugiu, K. Tomizawa, H. Matsui, I. Date, *Acta Med. Okayama* **2009**, *63*, 1.
7. Z. Cai, Z. Ye, X. Yang, Y. Chang, H. Wang, Y. Liu, A. Cao, *Nanoscale* **2011**, *3*, 1974.
8. Y. Ma, S. Cai, Q. Lv, Q. Jiang, Q. Zhang, Sodmergen, Z. Zhai, C. Zhang, *J. Cell Sci.* **2007**, *120*, 520.
9. D. A. Shah, S.-J. Kwon, S. S. Bale, A. Banerjee, J. S. Dordick, R. S. Kane, *Biomaterials* **2011**, *32*, 3210.
10. T. Gaj, J. Guo, Y. Kato, S. J. Sirk, C. F. Barbas, 3rd, *Nat. Methods* **2012**, *9*, 805.
11. C. Patsch, D. Kesseler, F. Edenhofer, *Methods* **2011**, *53*, 386.
12. H. Y. Zhou, S. L. Wu, J. Y. Joo, S. Y. Zhu, D. W. Han, T. X. Lin, S. Trauger, G. Bien, S. Yao, Y. Zhu, G. Siuzdak, H. R. Scholer, L. X. Duan, S. Ding, *Cell Stem Cell* **2009**, *4*, 581.

13. Y. Zhang, L.-C. Yu, *Curr. Opin. Biotechnol.* **2008**, *19*, 506.
14. S. L. Lo, S. Wang, *Macromol. Rapid Commun.* **2010**, *31*, 1134.
15. Z. Gu, A. Biswas, M. X. Zhao, Y. Tang, *Chem. Soc. Rev.* **2011**, *40*, 3638.
16. S. Foster, C. L. Duvall, E. F. Crownover, A. S. Hoffman, P. S. Stayton, *Bioconjugate Chem.* **2010**, *21*, 2205.
17. S. J. Kaczmarczyk, K. Sitaraman, H. A. Young, S. H. Hughes, D. K. Chatterjee, *Proc. Natl. Acad. Sci. U. S. A.* **2011**, *108*, 16998.
18. B. J. Bennion, V. Daggett, *Proc. Natl. Acad. Sci. U. S. A.* **2003**, *100*, 5142.
19. K. Melikov, L. Chernomordik, *Cell. Mol. Life Sci.* **2005**, *62*, 2739.
20. J. S. Wadia, R. V. Stan, S. F. Dowdy, *Nat. Med.* **2004**, *10*, 310.
21. J. J. Cronican, D. B. Thompson, K. T. Beier, B. R. McNaughton, C. L. Cepko, D. R. Liu, *ACS Chem. Biol.* **2010**, *5*, 747.
22. S. Salmaso, P. Caliceti, *Int. J. Pharm.* **2013**, *440*, 111.
23. X.-C. Yang, B. Samanta, S. S. Agasti, Y. Jeong, Z.-J. Zhu, S. Rana, O. R. Miranda, V. M. Rotello, *Angew. Chem. Int. Ed.* **2011**, *50*, 477.
24. S. J. Doxsey, J. Sambrook, A. Helenius, J. White, *J. Cell Biol.* **1985**, *101*, 19.
25. M. R. Almofti, H. Harashima, Y. Shinohara, A. Almofti, Y. Baba, H. Kiwada, *Arch. Biochem. Biophys.* **2003**, *410*, 246.
26. S. R. Terlecky, J. I. Koepke, *Adv. Drug Deliv. Rev.* **2007**, *59*, 739.
27. C.-C. You, M. De, G. Han, V. M. Rotello, *J. Am. Chem. Soc.* **2005**, *127*, 12873.
28. S. L. Wiskur, J. L. Lavigne, A. Metzger, S. L. Tobey, V. Lynch, E. V. Anslyn, *Chem.-Eur. J.* **2004**, *10*, 3792.
29. A. Zafar, R. Melendez, S. J. Geib, A. D. Hamilton, *Tetrahedron* **2002**, *58*, 683.
30. P. Ghosh, X. Yang, R. Arvizo, Z.-J. Zhu, S. S. Agasti, Z. Mo, V. M. Rotello, *J. Am. Chem. Soc.* **2010**, *132*, 2642.
31. K. Maruyama, *Adv. Drug Deliv. Rev.* **2011**, *63*, 161.
32. Y. Jeong, B. Duncan, M.-H. Park, C. Kim, V. M. Rotello, *Chem. Commun.* **2011**, *47*, 12077.
33. M. De, S. Rana, H. Akpinar, O. R. Miranda, R. R. Arvizo, U. H. F. Bunz, V. M. Rotello, *Nat. Chem.* **2009**, *1*, 461.
34. T. Yoshikawa, T. Sugita, Y. Mukai, Y. Abe, S. Nakagawa, H. Kamada, S.-i. Tsunoda, Y. Tsutsumi, *Biomaterials* **2009**, *30*, 3318.
35. O. Zelphati, Y. Wang, S. Kitada, J. C. Reed, P. L. Felgner, J. Corbeil, *J. Biol. Chem.* **2001**, *276*, 35103.
36. K. C. Cho, J. H. Jeong, H. J. Chung, C. O. Joe, S. W. Kim, T. G. Park, *J. Control. Release* **2005**, *108*, 121.
37. B. Zassler, I. E. Blasig, C. Humpel, *J. Neuro-Oncol.* **2005**, *71*, 127.
38. S. W. Lowe, A. W. Lin, *Carcinogenesis* **2000**, *21*, 485.
39. T. Idziorek, J. Estaquier, F. De Bels, J.-C. Ameisen, *J. Immunol. Methods* **1995**, *185*, 249.
40. M. Zimmermann, N. Meyer, *Methods Mol. Biol.* **2011**, *740*, 57.
41. J. P. Richard, K. Melikov, E. Vives, C. Ramos, B. Verbeure, M. J. Gait, L. V. Chernomordik, B. Lebleu, *J. Biol. Chem.* **2003**, *278*, 585.
42. P. Carroll, L. J. Schreuder, J. Muwanguzi-Karugaba, S. Wiles, B. D. Robertson, J. Ripoll, T. H. Ward, G. J. Bancroft, U. E. Schaible, T. Parish, *PLoS ONE* **2010**, *5*, e9823.
43. C. Dingwall, R. A. Laskey, *Annu. Rev. Cell Biol.* **1986**, *2*, 367.
44. S. T. Henriques, H. Costa, M. Castanho, *Biochemistry* **2005**, *44*, 10189.
45. H. Raagel, P. Saalik, M. Pooga, *Biochim. Biophys. Acta-Biomembr.* **2010**, *1798*, 2240.
46. S. J. Gould, G. A. Keller, N. Hosken, J. Wilkinson, S. Subramani, *J. Cell Biol.* **1989**, *108*, 1657.

CHAPTER 5

QUANTITATIVE TRACKING OF PROTEIN TRAFFICKING TO THE NUCLEUS ENABLED BY CYTOSOLIC PROTEIN DELIVERY

5.1 Introduction

Intracellular protein trafficking is central to all protein functions.[1] Aberrant localization of proteins is involved in the pathogenesis of diseases such as Alzheimer's, cancer and metabolic disorders.[2] Monitoring protein trafficking provides an effective way to investigate the spatial and temporal regulation of protein systems behind basic cellular functions.[3]

A key challenge in studying protein trafficking is to place the protein in the appropriate location of a cell. Conventionally, intracellular protein trafficking is monitored by cell permeabilization based methods.[4] In spite of being routinely used, cell permeabilization methods have been extensively criticized.[5] Permeabilized cells require exogenous supply of cytosol and ATP for subcellular transport of proteins. In particular, these methods deviate from *in vivo* conditions, and their unpredictable effects in extracting and relocating intracellular proteins in different cell types lead to artifacts.[5] Fluorescence recovery after photobleaching (FRAP) of expressed proteins is another widely used approach that provides insight on the diffusional properties of the protein.[6] However, this method also has its intrinsic limitations. Quantitative analysis of the localized protein is not feasible by this method because of pre-existing photobleached proteins. More importantly, photobleaching causes oxidative stress in the cell that can result in significant deviation from normal cellular homeostasis.[7]

Direct protein delivery provides an alternative path to overcome current challenges in the study of protein trafficking. Physical and mechanical approaches, such as microinjection and electroporation, have been used for decades.[3] However, these methods are quite disruptive to

cells.[8] Sudden and dramatic changes in intracellular homeostasis, including membrane potential and intracellular ionic concentrations, limit the use of these methods.[8] Endocytic pathways of cellular entry are slow and result in considerable protein degradation and sequestration,[9] providing a challenge for standard chemical and biological delivery strategies.

We have recently developed a protein delivery method using nanoparticle-stabilized capsules (NPSCs) that evades the endocytic pathway.[10] NPSCs contain a fatty acid core and a shell of HKRK AuNPs and payload proteins. In this process NPSCs rapidly deliver proteins directly to the cytosol *via* transient membrane fusion.[10, 11] This method allows us to deliver the targeted protein into the cytosol, and monitor nuclear protein trafficking in a non-disruptive fashion without complications arising from current strategies. (Figure 5.1a).

5.2 Results and Disscussions

We chose five nuclear localization signal (NLS) sequences (Figure 5.1b, Figure 5.2 and Tables 5.1 and 5.2), namely NLS^{SV40}, $NLS^{c\text{-}Myc}$, NLS^{NLP}, NLS^{TUS} and $NLS^{EGL\text{-}13}$ for monitoring nuclear protein trafficking and comparing nuclear targeting efficiencies of the above known NLSs. These NLS sequences are of different size, charge and origin. $NLS^{EGL\text{-}13}$, a 19-amino acid fragment derived from EGL-13 transcription factor,[12] was attached to the N-terminus of enhanced green fluorescent protein (eGFP), while NLS^{SV40}, $NLS^{c\text{-}Myc}$, NLS^{NLP} and NLS^{TUS} were fused to the C-terminus. NLS^{SV40} is the first NLS identified from the simian virus 40 (SV40) large T antigen whereas $NLS^{c\text{-}Myc}$, NLS^{NLP} and NLS^{TUS} are derived from c-Myc,[13] Nucleoplasmin[14] and Tus protein[15] respectively. For these studies, eGFP rather than any functional protein was chosen as a reporter protein since it is a well-accepted fluorescent reporter to study the distribution and dynamics of the nuclear protein

trafficking[16] that is small enough (27 kDa) to enter the nucleus.[17] Furthermore, eGFP is known not to interfere in cellular functions.

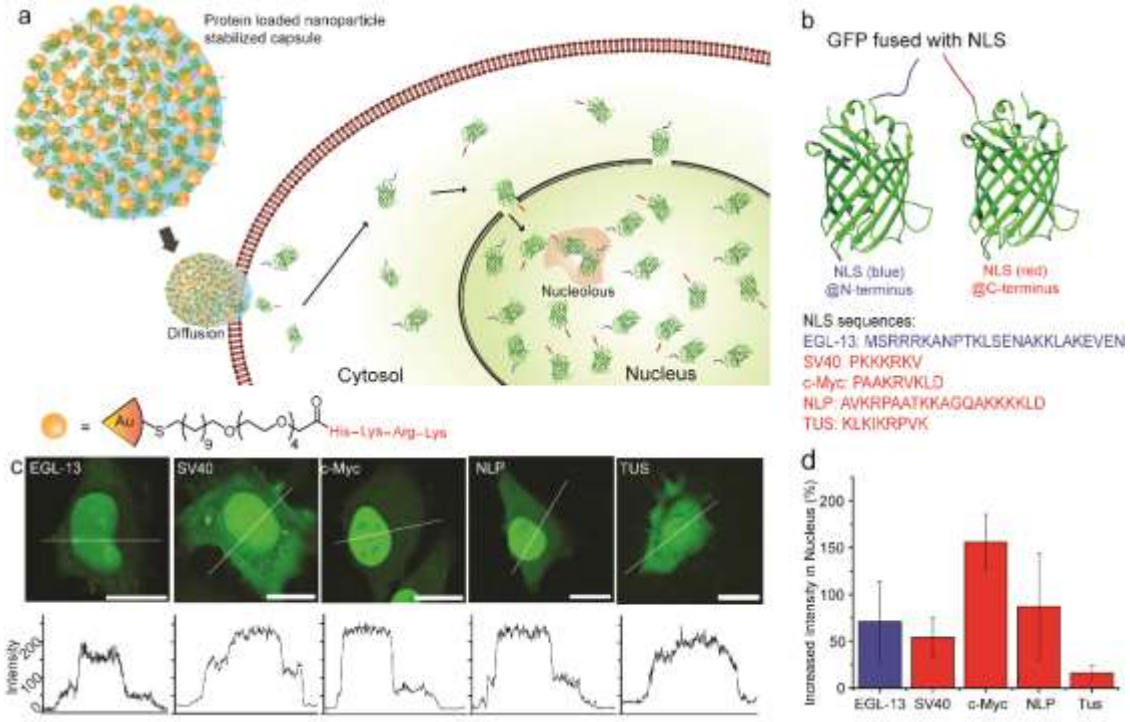

Figure 5.1. Delivery of eGFP fused with nuclear localization signals (NLS) to cells using NPSCs. (**a**) Schematic representing the cytosolic delivery and nuclear accumulation of proteins with NLSs. (**b**) Structure of eGFP fused with NLSs. (**c**) LSCM images showing different cellular distribution patterns of eGFP fused with NLSs. Bars: 20 µm. (**d**) Statistical analysis revealing nuclear importing efficiency (6 cells per group).

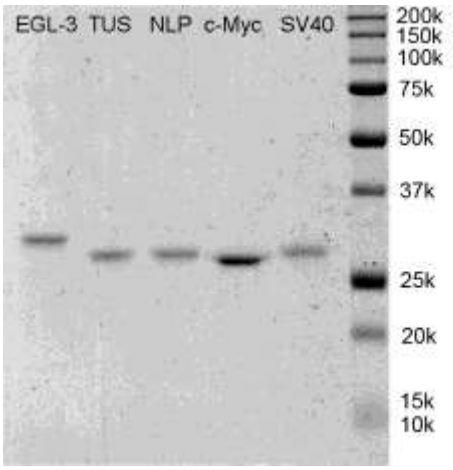

Figure 5.2. SDS-PAGE analysis of five NLS-eGFPs.

Table 5.1. Primers for PCR cloning

SV40	Forward	5’- ACGATGGATCCATGGTGAGCAAGGGCGAGGA -3’
	Reverse	5’-GTGTAAGCTTTTACAGTTCGCGTTTTTCTTTGG CCTTGTACAGCTCG -3’
NLP	Forward	5’-ACGATGGATCCATGGTGAGCAAGGGCGAGGA -3’
	Reverse first run	5’-GCTTTCTTAGTTGCGGCAGGGCGCTTAACAGC CTTGTACAGCTCGTCC-3’
	Reverse second run	5’-GTGTAAGCTTTTAATCTAGCTTTTTCTTTTTAGCC TGACCTGCTTTCTTAGTT-3’
c-Myc	Forward	5’- ACGATGGATCCATGGTGAGCAAGGGCGAGGA -3’
	Reverse	5’-GTGTAAGCTTTTAGTCTAGTTTAACGCGTTTGGC AGCAGGCTTGTACAGCTCGTCC-3’
Tus	Forward	5’- ACGATGGATCCATGGTGAGCAAGGGCGAGGA -3’
	Reverse	5’-GTGTAAGCTTTTACTTTACAGGCCGTTTTATCTTG AGTTTCTTGTACAGCTCGTCC-3’
EGL-13	Forward first run	5’- GAAAACGCGAAGAAGCTTGCCAAGGAAGTTGAA AATATGGTGAGCAAGGGCGAGGA-3’
	Forward second run	5’-ATATGGATCCATGAGCCGTAGACGAAAAGCGAAT CCGACAAAACTGAGTGAAAACGCGAAGAAGCTTG-3’
	Reverse	5’-TATAAAGCTTTTACTTGTACAGCTC-3’

Table 5.2. Sequences of NLS-eGFPs (NLSs have been labeled with color)

eGFP-SV40: MVSKGEELFTGVVPILVELDGDVNGHKFSVSGEGEGDATYGKLTLKFICTTGKLPVPWPTLVTTFXYGVQCF SRYPDHMKQHDFFKSAMPEGYVQERTIFFKDDGNYKTRAEVKFEGDTLVNRIELKGIDFKEDGNILGHKLE YNYNSHNVYIMADKQKNGIKVNFKIRHNIEDGSVQLADHYQQNTPIGDGPVLLPDNHYLSTQSALSKDPN EKRDHMVLLEFVTAAGITHGMDELYKPKKKRKV
eGFP-NLP: MRGSHHHHHHGSMVSKGEELFTGVVPILVELDGDVNGHKFSVSGEGEGDAXYGKLTLKFICTTGKLPVPW PTLVTTFXYGVQCFSRYPDHMKQHDFFKSAMPEGYVQERTIFFKDDGNYKTRAEVKFEGDTLVNRIELKGI DFKEDGNILGHKLEYNYNSHNVYIMADKQKNGIKVNFKIRHNIEDGSVQLADHYQQNTPIGDGPVLLPDN HYLSTQSALSKDPNEKRDHMVLLEFVTAAGITHGMDELYKAVKRPAATKKAGQAKKKKLD
eGFP-c-Myc: MRGSHHHHHHGSMVSKGEELFTGVVPILVELDGDVNGHKFSVSGEGEGDATYGKLTLKFICTTGKLPVPW PTLVTTFTYGVQCFSRYPDHMKQHDFFKSAMPEGYVQERTIFFKDDGNYKTRAEVKFEGDTLVNRIELKGI DFKEDGNILGHKLEYNYNSHNVYIMADKQKNGIKVNFKIRHNIEDGSVQLADHYQQNTPIGDGPVLLPDN HYLSTQSALSKDPNEKRDHMVLLEFVTAAGITHGMDELYKPAAKRVKLD
eGFP-TUS: MRGSHHHHHHGSMVSKGEELFTGVVPILVELDGDVNGHKFSVSGEGEGDAXYGKLTLKFICTTGKLPVPW PTLVTTFTYGVQCFSRYPDHMKQHDFFKSAMPEGYVQERTIFFKDDGNYKTRAEVKFEGDTLVNRIELKGI DFKEDGNILGHKLEYNYNSHNVYIMADKQKNGIKVNFKIRHNIEDGSVQLADHYQQNTPIGDGPVLLPDN HYLSTQSALSKDPNEKRDHMVLLEFVTAAGITHGMDELYKKLKIKRPVK
EGL-13-eGFP: MRGSHHHHHHGSMSRRRKANPTKLSENAKKLAKEVENMVSKGEELFTGVVPILVELDGDVNGHKFSVSG EGEGDATYGKLTLKFICTTGKLPVPWPTLVTTFXYGVQCFSRYPDHMKQHDFFKSAMPEGYVQERTIFFKD DGNYKTRAEVKFEGDTLVNRIELKGIDFKEDGNILGHKLEYNYNSHNVYIMADKQKNGIKVNFKIRHNIEDG SVQLADHYQQNTPIGDGPVLLPDNHYLSTQSALSKDPNEKRDHMVLLEFVTAAGITHGMDELYK

NPSCs containing the NLS-tagged eGFP-NPSC (NLS-eGFP-NPSC) were readily formed following previously reported methods[10] (Figure 5.3 and Figure 5.3). Effective delivery of NLS-eGFPs was established using laser scanning confocal microscopy (LSCM). After 1 h incubation of NLS-eGFP-NPSCs with HeLa cells, followed by 1 h incubation in fresh media, NLS-eGFP was distributed throughout the cell, with obvious accumulation in the nucleus Figure 5.1c and Figure

5.5). Quantitative comparison of the nuclear accumulation of the five NLS-eGFPs from LSCM results showed different nuclear import efficiencies (Figure 5.1d and Figure 5.6). Among the studied proteins, $NLS^{c\text{-}Myc}$-eGFP exhibited an increase in nuclear intensity by 160% compared to that in the cytosol while NLS^{SV40}-eGFP, one of the most routinely used NLS tags, exhibited an increase in intensity of only *ca.* 45%, with a substantial amount of protein remaining in the cytosol. This result is in agreement with the previous observation of nuclear accumulation of intracellularly expressed NLS^{SV40}-eGFP,[15] but differs strongly from cell permeabilization methods that showed that NLS^{SV40}-eGFP completely accumulated in nuclei.[18] This difference in outcomes presumably arises from alterations in the distribution of soluble intracellular proteins upon permeabilization.[19] The other three NLS-eGFPs showed significant nuclear accumulation ability. NLS^{NLP}-eGFP showed 85% higher nuclear intensity, while that of $NLS^{EGL\text{-}13}$-eGFP showed 70%. NLS^{TUS}-eGFP displayed only moderate nuclear targeting efficiency, with an increase of 30%. The varied nuclear intensities of NLS-eGFPs were due to the differences in the nuclear targeting efficiencies of the NLSs. In contrast, eGFP without any NLS tag was homogeneously distributed in the nucleus and cytosol after delivery. (Figure 5.7).

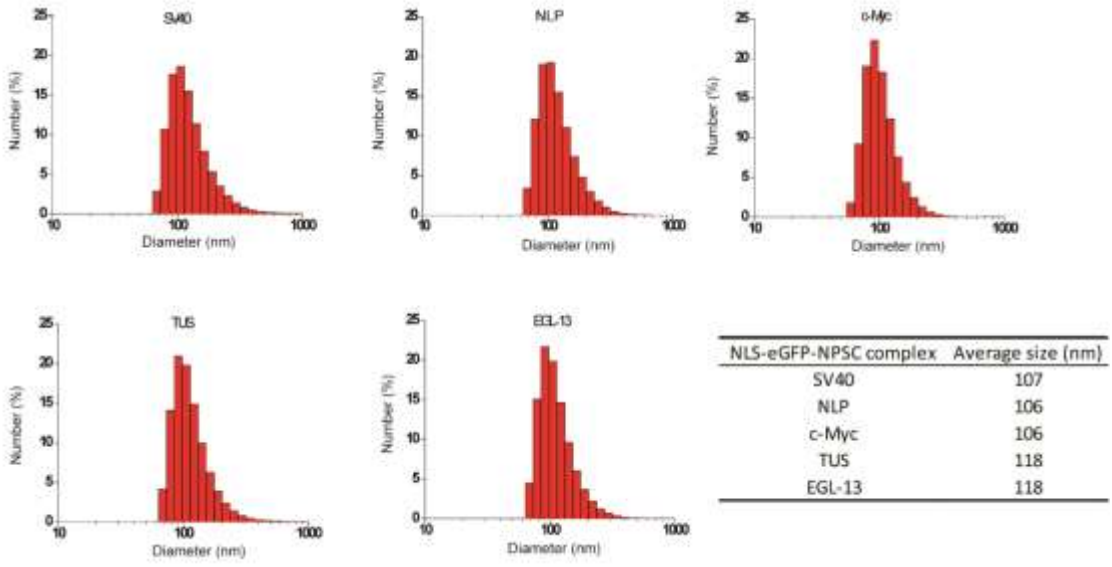

NLS-eGFP-NPSC complex	Average size (nm)
SV40	107
NLP	106
c-Myc	106
TUS	118
EGL-13	118

Figure 5.3. Dynamic Light Scattering measurements for NLS-eGFP-NPSC complexes

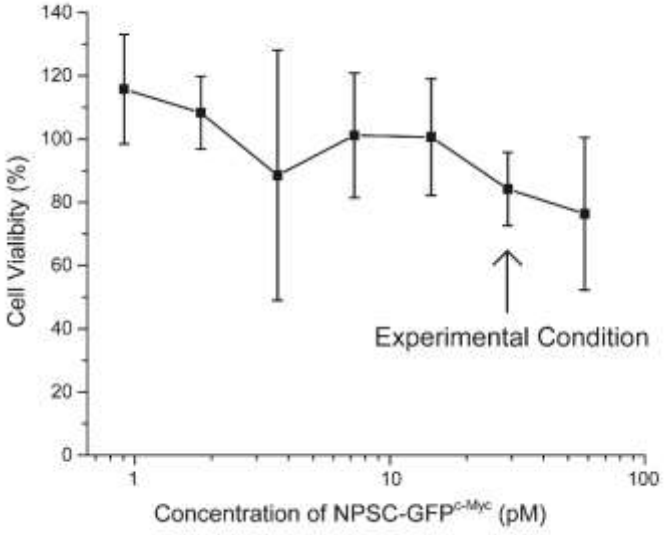

Figure 5.4. Viability of HeLa cells at different concentrations of NPSC-NLS$^{c\text{-}Myc}$-eGFP complexes measured by Alamar Blue assay.

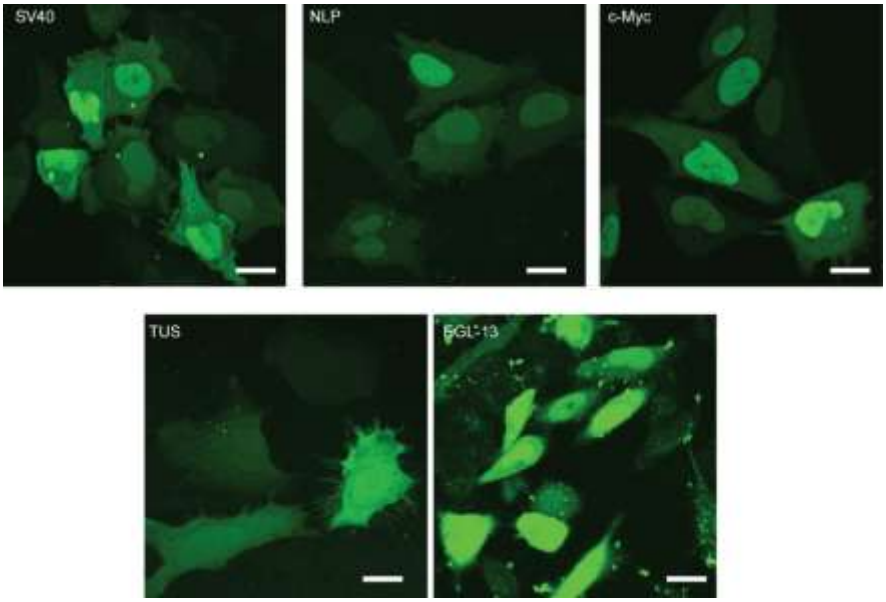

Figure 5.5. Large scale images of NLS-eGFPs delivered into HeLa cells. Bars: 20 µm.

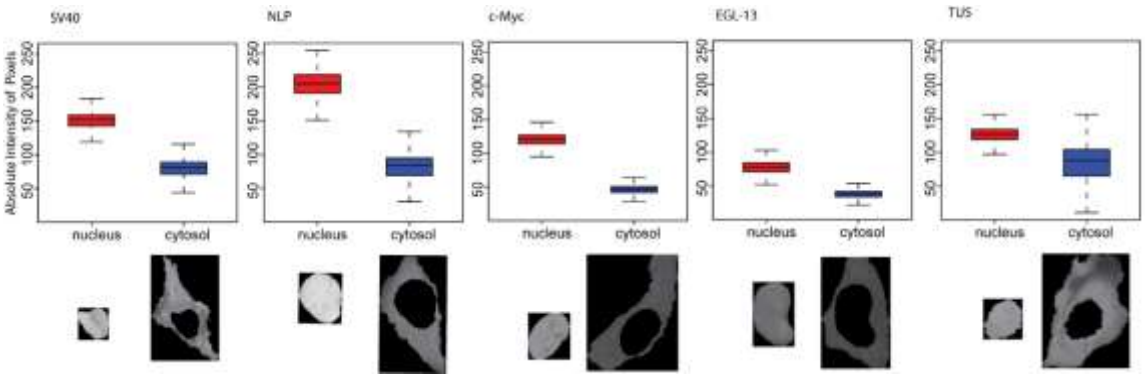

Figure 5.6. Typical results of quantitative fluorescence intensity analyses of NLS-eGFPs in single cells. Quartiles of pixel intensities were illustrated as box plots.

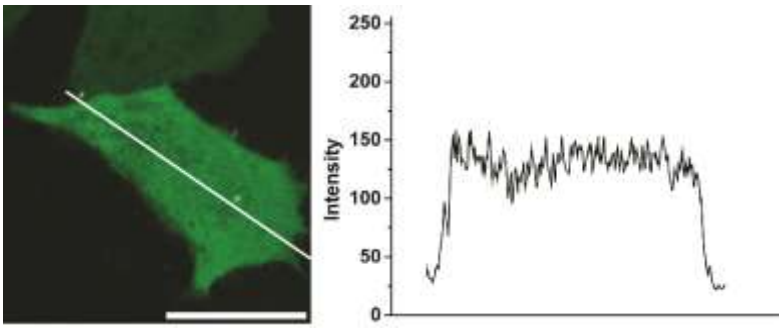

Figure 5.7. LSCM image showing cellular distribution pattern of eGFP without NLS. Bar: 20 μm.

We next tracked the dynamics of the nuclear accumulation of the NLS-eGFP in the cell through live cell video imaging. Since $NLS^{c\text{-}Myc}$-eGFP displayed maximal nuclear accumulation ability, we chose $NLS^{c\text{-}Myc}$-eGFP for these studies. Fluorescence imaging showed substantial accumulation of $NLS^{c\text{-}Myc}$-eGFP occurred in the nucleus within 60s of cytosolic delivery (Figure 5.8a). Time-lapse LSCM images at minute scale unveiled the kinetics of nuclear import of $NLS^{c\text{-}Myc}$-eGFP, as shown in Figure 5.8b. $NLS^{c\text{-}Myc}$-eGFP was delivered into the cytosol, with importation to the nucleus occurring immediately. (Figure 5.9). Within 6 min, nuclear import reached equilibrium (Figure 5.8c). This result is similar to previous measurement of *in vitro* nuclear protein import using permeabilized cells, in which half-saturation time ranges from 1.3 to 13.9 min.[20] As expected from the active transport process employed by the cell,[4] depletion of cellular ATP by NaN_3 and 2-deoxyglucose (DOG) resulted in no nuclear localization (Figure 5.8d), resembling the

distribution of the normal eGFP without NLS (Figure 5.10). Notably, delivery of NLS$^{c\text{-}Myc}$-eGFP to the cytosol was not disrupted by ATP depletion, indicating non-endocytic pathway involved in the delivery. This result was in agreement with our previous findings.

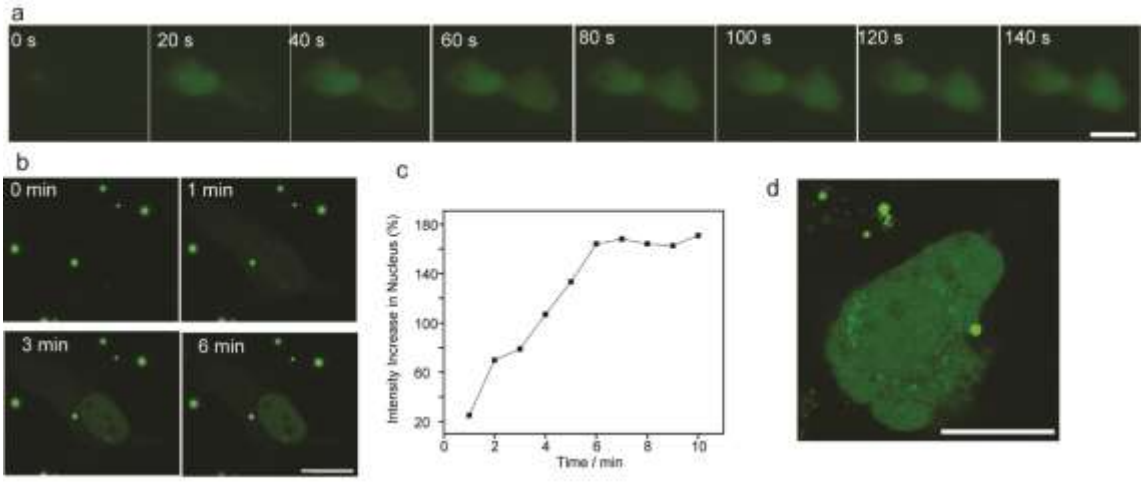

Figure 5.8. Nuclear import of eGFP fused with NLS is rapid and ATP dependent. (**a**) Time-lapse fluorescent microscopic images show nuclear accumulation of NLS$^{c\text{-}Myc}$-eGFP starts within 1 minute after presenting in cytosol. (**b,c**) Time-lapse LSCM images unveil the kinetics of nuclear import of NLS$^{c\text{-}Myc}$-eGFP. (**d**) No nuclear accumulation of NLS$^{c\text{-}Myc}$-eGFP is observed after the delivery following ATP depletion in the presence of 3 mg/mL NaN_3 and 50 mM 2-deoxyglucose. Bars: 20 µm.

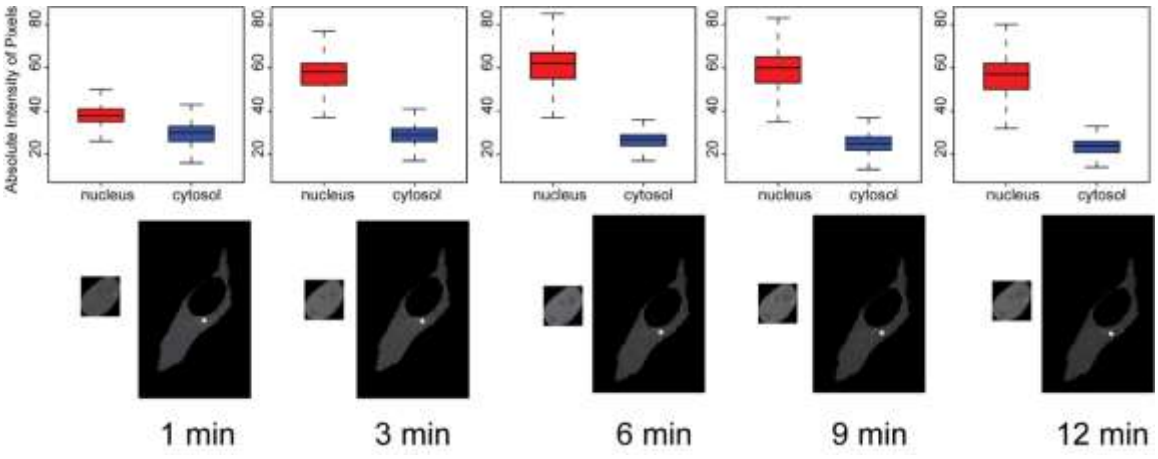

Figure 5.9. Typical results of quantitative fluorescence intensity analyses of NLSc-Myc-eGFPs in single cell at different time scales. Quartiles of pixel intensities were illustrated as box plots.

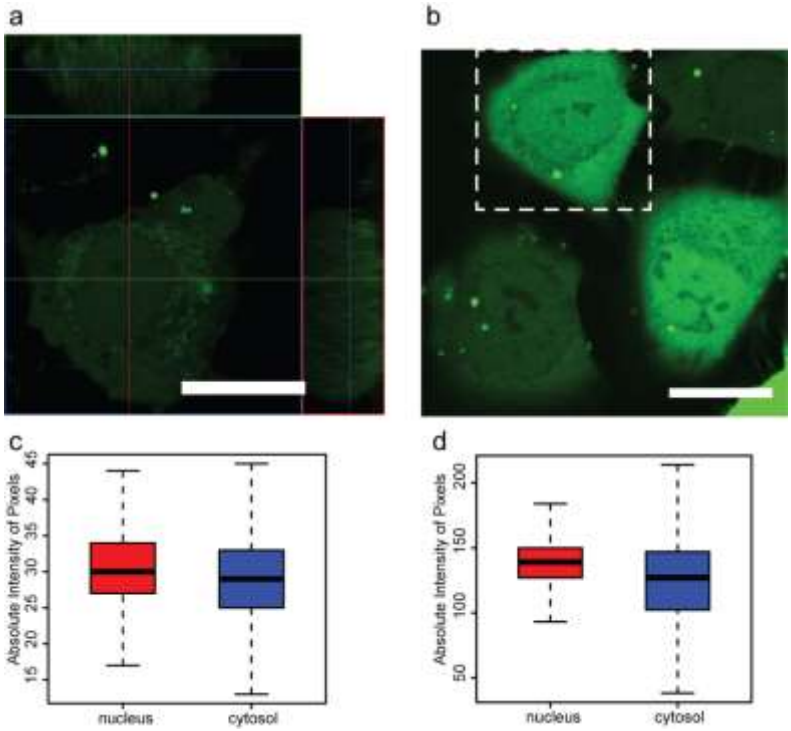

Figure 5.10. A comparison between the cytosolic delivery of (a) NLSc-Myc-eGFP at ATP depletion condition and (b) eGFP without NLS into HeLa cells. Bars: 20 µm. (c,d) Quartiles of pixel intensities were illustrated as box plots. For (d) Analysis of the boxed cell in b.

5.3 Methods

5.3.1 Construction of plasmids and *Escherichia coli* strains

6xHis-eGFP expression vector (pET21d-eGFP) was obtained from Novagen. Briefly, using 6xHis-eGFP as the template, PCR was performed with primers listed in the Table 5.3. Subsequently, PCR products were digested using BamHI and HindIII restriction enzymes and inserted into pQE80 vector, downstream of nucleotides for six histidine tag to construct pQE80-6xHis-NLS-eGFP or pQE80-6xHis-eGFP-NLS expression vectors. Successful cloning was confirmed by DNA sequencing.

Table 5.3. Primers for PCR cloning

SV40	Forward	5’- ACGATGGATCCATGGTGAGCAAGGGCGAGGA -3’
	Reverse	5’-GTGTAAGCTTTTACAGTTCGCGTTTTTCTTTGG CCTTGTACAGCTCG -3’
NLP	Forward	5’-ACGATGGATCCATGGTGAGCAAGGGCGAGGA -3’
	Reverse first run	5’-GCTTTCTTAGTTGCGGCAGGGCGCTTAACAGC CTTGTACAGCTCGTCC-3’
	Reverse second run	5’-GTGTAAGCTTTTAATCTAGCTTTTTCTTTTTAGCC TGACCTGCTTTCTTAGTT-3’
c-Myc	Forward	5’- ACGATGGATCCATGGTGAGCAAGGGCGAGGA -3’
	Reverse	5’-GTGTAAGCTTTTAGTCTAGTTTAACGCGTTTGGC AGCAGGCTTGTACAGCTCGTCC-3’
Tus	Forward	5’- ACGATGGATCCATGGTGAGCAAGGGCGAGGA -3’
	Reverse	5’-GTGTAAGCTTTTACTTTACAGGCCGTTTTATCTTG AGTTTCTTGTACAGCTCGTCC-3’
EGL-13	Forward first run	5’- GAAAACGCGAAGAAGCTTGCCAAGGAAGTTGAA AATATGGTGAGCAAGGGCGAGGA-3’
	Forward second run	5’-ATATGGATCCATGAGCCGTAGACGAAAAGCGAAT CCGACAAAACTGAGTGAAAACGCGAAGAAGCTTG-3’
	Reverse	5’-TATAAAGCTTTTACTTGTACAGCTC-3’

5.3.2 Protein Expression

To produce recombinant proteins, plasmids carrying 6xHis-NLS-eGFP or 6xHis-eGFP-NLS were transformed into *Escherichia coli* BL21 (DE3) strain. A transformed colony was picked up to grow small cultures in 50 mL 2XYT media at 37°C overnight. The following day, 15 mL of grown culture was inoculated into 1 L 2XYT media and allowed to grow at 37°C until OD reaches 0.6. At this point, the protein expression was induced by adding isopropyl-*β*-D-thiogalactopyranoside (IPTG; 1 mM final concentration) at 25°C. After 16 hours of induction, the cells were harvested and the pellets were lysed using a microfluidizer. His-tagged fluorescent proteins were purified from the lysed supernatant using His-Pur cobalt columns. The integrity and the purity of native

protein were determined by 12% sodium dodecyl sulfate polyacrylamide gel electrophoresis (SDS-PAGE). **Figure 5.2** shows the SDS-PAGE gel of the purified proteins.

5.3.3 Protein-NPSC Complex Formation

HKRK gold nanoparticles (HKRK AuNPs) were synthesized according to a previous report.[10] To make the NLS-eGFP-NPSC complex, 2.5 µM HKRK AuNPs were incubated with 1 µM eGFP in 30 µL of phosphate buffer (5 mM, pH = 7.4) for 10 min. Then, 1 µL of linoleic acid was mixed with 500 µL of phosphate buffer (5 mM, pH = 7.4) containing 1 µM HKRK AuNPs and agitated by an amalgamator (Yinya New Materials Co. Ltd, Hangzhou, China) at 5000 rpm for 100 s to form emulsions. Finally, the mixture of the protein and HKRK AuNPs was diluted to 45 µL with phosphate buffer (5 mM, pH = 7.4) followed by the addition of 5 µL of the emulsion. The NLS-eGFP-NPSC complexes were ready to use after 10 min incubation at room temperature. The final concentrations of HKRK AuNPs and eGFP were 1.5 µM and 600 nM, respectively.

5.3.4 Cell viability assay (Alamar Blue)

15,000 HeLa cells were cultured in a 96-well plate for 24 h prior to the experiment. The cells were washed by cold phosphate buffer saline (PBS) 3 times before the delivery, then different amounts of the eGFP-NPSC complex (prepared as mentioned above) were diluted by DMEM and incubated with the cells for 1 h followed by the incubation with DMEM containing 10% FBS and 1% antibiotics for 23 h. After washing with PBS 3 times, the cells were then incubated with 200 µL DMEM containing 10% Alamar Blue for 3 h. Cell viability was calculated by measuring the fluorescence intensity of Alamar Blue at 590 nm, with an excitation of 535 nm.

5.3.5 Cell culture

HeLa cells were cultured in a humidified atmosphere (5% CO_2) at 37°C and grown in Dulbecco's modified eagle's medium (DMEM, low glucose) supplemented with 10% fetal bovine serum (FBS) and 1% antibiotics (100 U/ml penicillin and 100 μg/ml streptomycin).

5.3.6 NLS-eGFP Delivery

A total of 60,000 or 240,000 HeLa cells were cultured in a 24-well plate or confocal dish, respectively, for 24 h prior to delivery. The cells were washed by cold phosphate buffer saline (PBS) three times right before delivery. After the preparation of cells, NLS-eGFP-NPSC complex solution (50 or 150 μL of the NLS-eGFP-NPSC complex diluted by 450 μL or 1.35 mL of the DMEM without FBS, respectively) was incubated with the cells for 1 h in a 24-well plate or confocal dish, followed by incubation with fresh DMEM with 10% FBS for 1 h unless otherwise mentioned.

5.3.7 Cell Imaging

240,000 HeLa cells were cultured in the confocal dish for 24 h prior to the experiment. Before imaging, cells were washed by PBS for three times followed by the incubation with NLS-eGFP-NPSC in cell culture media. The cells were then observed by LSCM (LSM 510, Zeiss, Germany) microscope.

5.3.8 Live Cell Imaging

240,000 HeLa cells were cultured in the confocal dish for 24 h prior to delivery. Before imaging, cell culture media were replaced PBS with 10% FBS to eliminate the fluorescence of media. The confocal dish was then placed in the live cell imaging chamber with 5% CO_2 and at 37°C on the fluorescent (IX51, Olympus, Japan) or LSCM (LSM 510, Zeiss, Germany) microscope.

A series of images were taken at 4 s interval on fluorescent microscope or 1 min interval on LSCM microscope.

5.3.9 ATP Depletion

Cells were treated with cell culture media containing 3 mg/mL NaN_3/50 mM 2-deoxyglucose 1 h prior to delivery. NLS-eGFP was then delivered using the same method mentioned above. However, during the delivery, 3 mg/mL NaN_3 and 50 mM 2-deoxyglucose were supplemented in the media to maintain the ATP depleted status of cells.

5.3.10 Image Analysis

Images obtained from LSCM were in 8-bit grayscale format containing both fluorescent and bright field channels. The fluorescent channel was extracted by ImageJ. The pixel intensity profile along line segment was also performed by ImageJ. The cytosol and nucleus of each cell were separated by Photoshop and saved as 8-bit grayscale Tiff files with black backgound without any intensity adjustment. The resulted images were processed and plotted by R.

5.4 Conclusion

In summary, we have developed an effective, straightforward and non-invasive method for quantitative monitoring of intracellular trafficking of proteins. We demonstrated the efficacy of this method using NLS-mediated nuclear delivery, however, this strategy can be readily generalized to other trafficking processes, providing a new tool for probing the dynamics of cellular processes.

5.5 References

1. Z. Cao, S. Geng, L. Li, C. Lu, *Chem. Sci.* **2014**, *5*, 2530.
2. M. C. Hung, W. Link, *J. Cell Sci.* **2011**, *124*, 3381.
3. D. J. Stephens, R. Pepperkok, *Proc. Natl. Acad. Sci. U. S. A.* **2001**, *98*, 4295.
4. M. Lu, J. Zak, S. Chen, L. Sanchez-Pulido, David T. Severson, J. Endicott, Chris P. Ponting, Christopher J. Schofield, X. Lu, *Cell* **2014**, *157*, 1130.
5. U. Schnell, F. Dijk, K. A. Sjollema, B. N. G. Giepmans, *Nat. Methods* **2012**, *9*, 152.
6. J. Lippincott-Schwartz, E. Snapp, A. Kenworthy, *Nat. Rev. Mol. Cell Biol.* **2001**, *2*, 444.
7. H. C. Ishikawa-Ankerhold, R. Ankerhold, G. P. C. Drummen, *Molecules* **2012**, *17*, 4047.
8. I. Laffaflan, M. B. Hallett, *Blood* **2000**, *95*, 3270.
9. A. Erazo-Oliveras, K. Najjar, L. Dayani, T.-Y. Wang, G. A. Johnson, J.-P. Pellois, *Nat. Methods* **2014**, *11*, 861.
10. R. Tang, C. S. Kim, D. J. Solfiell, S. Rana, R. Mout, E. M. Velázquez-Delgado, A. Chompoosor, Y. Jeong, B. Yan, Z.-J. Zhu, C. Kim, J. A. Hardy, V. M. Rotello, *ACS Nano* **2013**, *7*, 6667.
11. Y. Jiang, R. Tang, B. Duncan, Z. Jiang, B. Yan, R. Mout, V. M. Rotello, *Angew. Chem. Int. Ed.* **2015**, *54*, 506.
12. W. Hanna-Rose, M. Han, *Development* **1999**, *126*, 169.
13. C. V. Dang, W. M. Lee, *Mol. Cell. Biol.* **1988**, *8*, 4048.
14. J. Robbins, S. M. Dilwortht, R. A. Laskey, C. Dingwall, *Cell* **1991**, *64*, 615.
15. S. J. Kaczmarczyk, K. Sitaraman, T. Hill, J. L. Hartley, D. K. Chatterjee, *PLoS ONE* **2010**, *5*, e8889.
16. H. Ogawa, S. Inouye, F. I. Tsuji, K. Yasuda, K. Umesono, *Proc. Natl. Acad. Sci. U. S. A.* **1995**, *92*, 11899.
17. X. Wei, V. G. Henke, C. Strübing, E. B. Brown, D. E. Clapham, *Biophys. J.* **2003**, *84*, 1317.
18. S. A. Adam, *J. Cell Biol.* **1990**, *111*, 807.
19. M. A. Melan, G. Sluder, *J. Cell Sci.* **1992**, *101*, 731.
20. W. Hu, B. E. Kemp, D. A. Jans, *J. Cell. Biochem.* **2005**, *95*, 782.

CHAPTER 6

EFFECTIVE NUCLEAR LOCALIZATION OF PROTEINS WITH BORONATE TARGETING SIGNALS

6.1 Introduction

The localization of proteins to proper subcellular positions is essential for their function.[1] This targeting process relies on specific signals that interact with sorting factors and/or organelle receptors to guide proteins to their final destination.[2] Taking advantage of such cellular distribution systems, proteins have been engineered for intracellular targeting and drug delivery.[3] As many drug targets are localized to particular subcellular compartments, these intracellularly-targeted therapeutic strategies significantly reduce side effects while increasing drug efficacy.[4]

The development of intracellular targeting systems is, however, currently limited to a set of known peptide localization signals.[5] By mimicking biological pathways, synthetic systems provide an alternative strategy for intracellular targeting that offers more versatility for drug development and biological research. Synthetic targeting elements would also sidestep the challenges of fusing natural signaling peptides to proteins by genetic engineering, where many proteins are difficult to express recombinantly, or adopt distorted conformations in foreign hosts.

Currently, there are few non-peptidic signals suitable for subcellular localization of biomacromolecules. The one widely recognized example is the triphenylphosphonium (TPP) group. TPP conjugates are used for both mitochondrial labeling and targeted delivery driven by large mitochondrial membrane potential, and not through active transport.[6] However, synthetic targeting to other organelles through either active or passive means are currently unavailable.

There are two key challenges for developing synthetic signals for subcellular localization of proteins in live cells: cytosolic access[7] and targeting efficiency.[8] Previously, we have developed an HKRK nanoparticle stabilized capsule (NPSC) platform for cytosolic delivery of negatively

charged proteins[9, 10] and an aromatic boronic acid (4-nitrophenyl 4-(4,4,5,5-tetramethyl-1,3,2-dioxaborolan-2-yl)benzyl carbonate; NBC) tag for facile protein modification.[11] Herein, we report that the NBC tag directs proteins to the nucleus after cytosolic delivery using an NPSC system with low toxicity (Figure 6.1 and Figure 6.2). This is, to our knowledge, the first fully synthetic nuclear localization signal to be described. Proteins modified with this nuclear NBC label, including ribonuclease A (RNase A) and fluorescent proteins, were rapidly delivered into cells using NPSCs and significantly accumulated in nuclei. Similar to its various natural counterparts, NBC-mediated nuclear import is governed by importin α/β, with passive adsorption directed by the aromatic moiety also contributing to the nuclear accumulation. Numerous important cellular processes, with their associated drug targets, localize to the nucleus. Developing synthetic signals for protein nuclear localization not only charts an alternative pathway for biochemical research, but also holds great promise for designing better therapeutic strategies.[4]

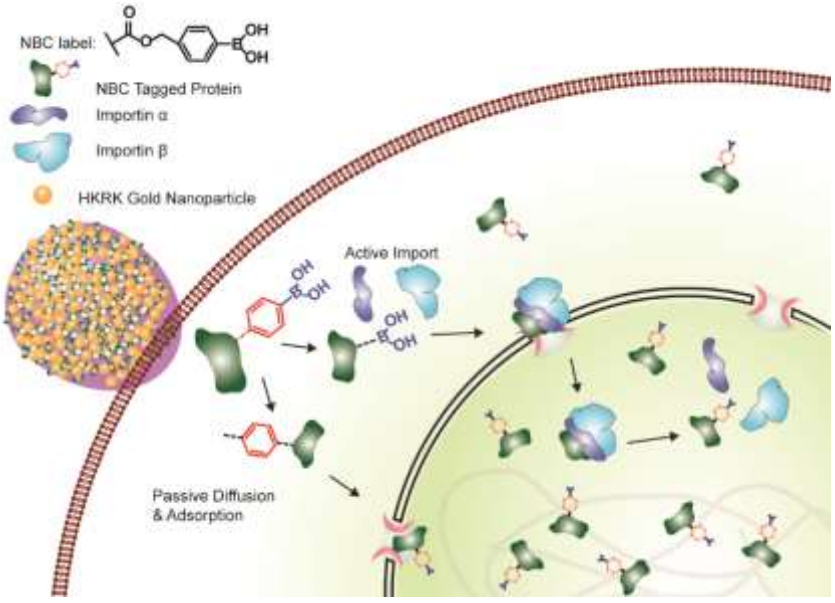

Figure 6.1. Schematic diagram showing delivery of RNase A-NBC-NPSC complex to the cytosol and into the nucleus of cells.

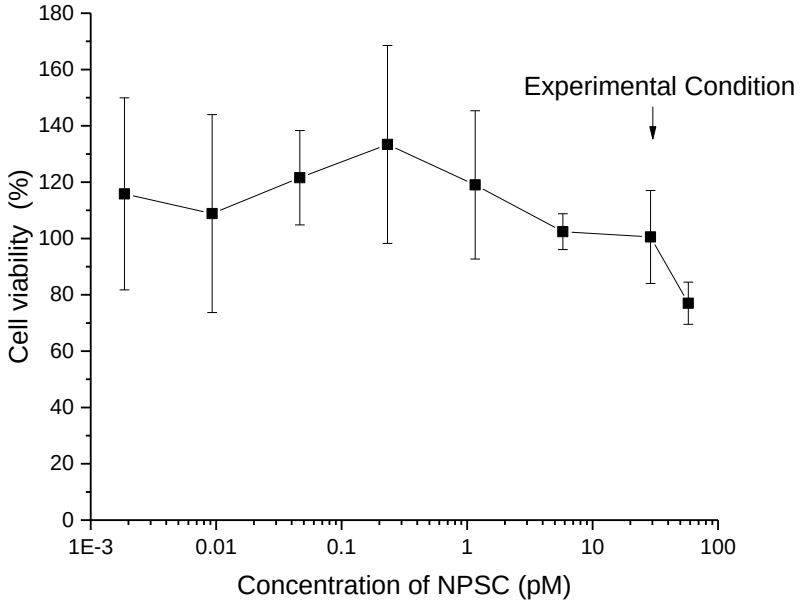

Figure 6.2. Viability of HeLa cells at different concentrations of NPSC measured by Alamar Blue assay.

6.2 Methods

6.2.1 GFP expression

To produce recombinant proteins, a plasmid carrying 6xHis-eGFP was transformed into the Escherichia coli BL21 (DE3) strain. A transformed colony was picked up to grow small cultures in 50 mL 2XYT media at 37°C overnight. The following day, 15 mL of grown culture was inoculated into one liter of 2XYT media and allowed to grow at 37°C until OD reaches 0.6. At this point, the protein expression was induced by adding isopropyl-b-D-thiogalactopyranoside (IPTG; 1 mM final concentration) at 25°C. After 16 hours of induction, the cells were harvested and the pellets were lysed using a microfluidizer. His-tagged fluorescent proteins were purified from the lysed supernatant using His-Pur cobalt columns.

6.2.2 Protein modification

Fluorescent FITC-labeled RNase A-NBC was described previously.[11] EGFP-NBC or EGFP-NC were prepared by reacting eGFP with an excess amount of NBC or NC according to our previous report.[11] Briefly, 1.3 mg/mL eGFP (in 0.1 M $NaHCO_3$ buffer solution, pH = 8.5, 0.72 mg protein in total) was mixed with 150 µL DMSO solution containing 0.25 mg NBC or NC. The reaction mixtures were then stirred at room temperature for an additional 10 h with protection from light, followed by ultrafiltration purification using Amicon® Ultra Centrifugal Filters (MWCO = 10,000, Millipore, MA). EGFP-CPB was prepared by mixing eGFP with N-hydroxysuccinimide (NHS)-activated 4-carboxyphenyl-boronic acid (CPB) in a similar way to that of eGFP-NBC modification. The NHS ester of CPB was prepared by adding N-hydroxysuccinimide (0.23 mg, 1.98 µmol), EDC (0.38 mg, 1.98 µmol), DMAP (0.046 mg, 0.38 µmol) into a DMSO solution of 4-carboxyphenylboronic acid (0.32 mg, 1.89 µmol), followed by an additional 12 h of incubation before mixing with eGFP. The protein molecular weight was determined using MALDI-TOF mass spectrometry. Proteins labeled with three NBC tags were used in this research (data shown in Figure 6.3 and 6.9). The tetramer structure of dsRed with NBC tag was confirmed by denaturing (monomer) and semi-denaturing (tetramer) SDS-PAGE analysis. For denaturing SDS-PAGE analysis, protein samples were mixed with 5x sample buffer including 5% 2-mercaptoethanol and heated at 95 °C for 5 min prior to loading. For semi-denaturing condition, protein samples were directed loaded after mixing with 5x sample buffer without 2-mercaptoethanol or heating.

6.2.3 Protein-NPSC Complex Formation

HKRK gold nanoparticles (HKRK AuNPs) were synthesized according to a previous report.[9] To make the protein-NPSC complex, 2.5 µM HKRK AuNPs were incubated with 1.5 µM of protein in 60 µL of phosphate buffer (5 mM, pH = 7.4) for 10 min. Then, 1 µL of linoleic acid was mixed

with 500 μL of phosphate buffer (5 mM, pH = 7.4) containing 1 μM HKRK AuNPs and agitated by an amalgamator (Yinya New Materials Co. Ltd, Hangzhou, China) at 5000 rpm for 100 s to form emulsions. Finally, the mixture of the protein and HKRK AuNPs was diluted to 135 μL with phosphate buffer (5 mM, pH = 7.4) followed by the addition of 15 μL of the emulsion. The protein-NPSC complexes were ready to use after 10 min of incubation at room temperature. The final concentrations of HKRK AuNPs and the protein were 1.5 μM Figure 6.300 nM, respectively. The preparation procedure of Arginine AuNP NPSCs is the same expect the use of Arginine AuNPs instead of HKRK AuNPs.

6.2.4 Cell culture

HeLa cells were cultured in a humidified atmosphere (5% CO2) at 37°C and grown in Dulbecco's modified eagle's medium (DMEM, low glucose) supplemented with 10% fetal bovine serum (FBS) and 1% antibiotics (100 U/ml penicillin and 100 μg/ml streptomycin).

6.2.5 Cell synchronization

For G0/G1 phase arrest, HeLa cells were cultured in DMEM without FBS for 72 hr prior to the experiment. For S phase synchronization, HeLa cells were arrested in DMEM with 2 mM thymidine for 17 hr, then released by culture in DMEM without thymidine. After that, cells were arrested again in DMEM with 2 mM thymidine for 17 hr. Before flow cytometry, cells were trypsinized, fixed with 66% ethanol for 2 hr and stained with propidium iodide (PI) in the presence of RNase A.

6.2.6 Cell viability assay (Alamar Blue)

15,000 HeLa cells were cultured in a 96-well plate for 24 hr prior to the experiment. The cells were washed by cold phosphate buffer saline (PBS) three times before the delivery, then different amounts of the NPSC complex (prepared as mentioned above) were diluted by DMEM and incubated with the cells for 1 hr followed by the incubation with DMEM containing 10% FBS and 1% antibiotics for 23 hr. After washing with PBS three times, the cells were then incubated with 200 μL DMEM containing 10% Alamar Blue for 3 h. Cell viability was calculated by measuring the fluorescence intensity of Alamar Blue at 590 nm, with an excitation of 535 nm.

6.2.7 Protein delivery

A total of 240,000 cells were cultured in a confocal dish for 24 hr prior to delivery. The cells were washed in cold phosphate buffer saline (PBS) thrice right before delivery. After preparation, the cells were incubated in protein-NBC-NPSC complex solution (150 μL of the complex diluted by 1.35 mL of the DMEM without FBS) for 1 hr, followed by incubation with fresh DMEM with 10% FBS for 10 min, unless otherwise mentioned. The cells were then kept in PBS and imaged in a LSCM (LSM 510, Zeiss, Germany or Nikon Ti, Japan) microscope. For flow cytometry analysis, cells were washed by PBS for three times and collected after trypsinization.

6.2.8 Importin α/β inhibition

Cells were treated with cell culture media containing 25 μM ivermectin 1 hr prior to delivery. The protein was then delivered using the same method mentioned above. During the delivery, 25 μM ivermectin were supplemented to the media to maintain the Importin α/β inhibition status of cells. The inhibition condition was kept during imaging.

6.2.10 ATP Depletion

Cells were treated with cell culture media containing 3 mg/mL of NaN_3/50 mM 2-deoxyglucose 30 min prior to delivery. The protein was then delivered using the same method mentioned above. During the delivery, 3 mg/mL NaN_3 and 50 mM 2-deoxyglucose were supplemented to the media to maintain the ATP depleted status of the cells. The ATP depletion condition was kept during imaging.

6.2.11 Image Analysis

Images obtained with the LSCM were in 8-bit grayscale format. The fluorescent channel was extracted by ImageJ. The background, cytosol, nucleus and nuclear granules (if any) of each cell were separated by Photoshop and saved as 8-bit grayscale Tiff files without any intensity adjustment. The resulted images were processed and plotted by R. Six individual cells were analyzed in each group.

6.3 Results

6.3.1 RNase A-NBC accumulates in the nucleus after NPSC delivery

RNase A and its homologues have therapeutic implications for various diseases, such as cancer[12] and AIDS.[13] Delivery of RNase A and its homologues into cells, and especially into the nucleus, results in intracellular RNA degradation, thus compromising cell function and viability.[14] To determine the cellular behavior of the NBC tag, we conjugated fluorescein isothiocyanate (FITC) to RNase A-NBC (Figure 6.3). Consistent with our previous reports,[9, 15] NPSCs containing FITC labeled RNase A-NBC were readily formed and delivered into HeLa cells (Figure 6.3b). RNase A-NBC that was released into the cytosol was imaged by laser scanning confocal microscopy (LSCM). One hour after delivery RNase A-NBC was strongly accumulated in the nucleus (Figure

6.4a and Figure 6.5). Within the nucleus, RNase-A-NBC further accumulated into granule-like structures (indicated by arrows in Figure 6.4a) that were distinct from the nucleoplasm. In comparison, RNase A conjugated with *cis*-aconitic acid (ACO tag; structure shown in Figure 6.5) revealed only limited nuclear enrichment after cytosolic delivery (Figure 6.5), with the same fluorescent granular structure inside nucleus as the NBC-tagged system. This result indicates that RNase A is capable of accessing nucleus due to its small size[16] and can be retained there with intranuclear structures or substrates. However, in the presence of NBC tag, the accumulation of RNase A in the nucleus dramatically increased. Noting that this delivery is based on supramolecular interactions, a few extracellular aggregates can be observed due to instability of a small portion of delivery vehicles.[17, 18]

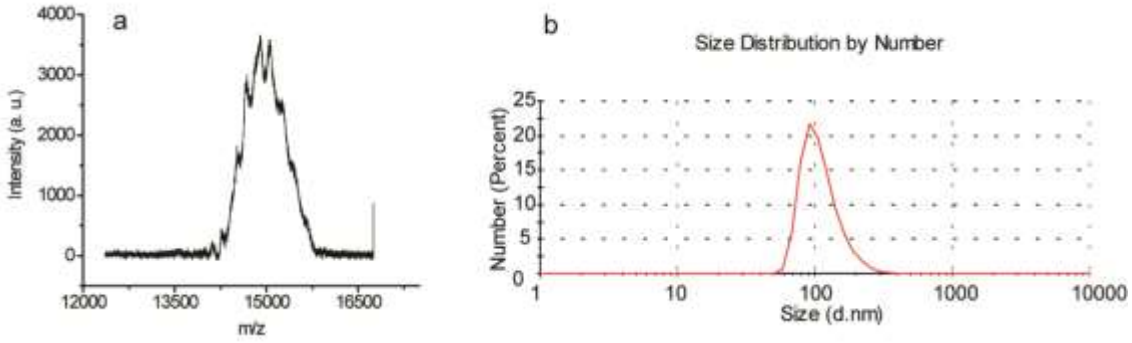

Figure 6.3. Delivery complex of RNase A-NBC labeled with FITC and NPSCs. (a) Mass spectrometry of RNase A-NBC labeled with FITC. (b) Dynamics light scattering results of the size of the delivery complex.

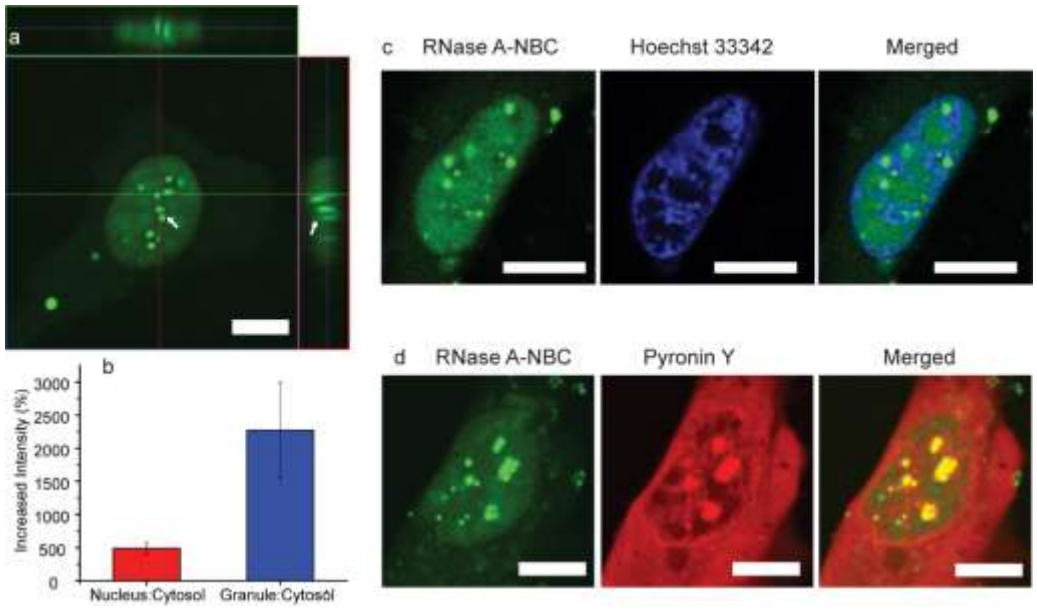

Figure 6.4. Delivery of RNase A-NBC into HeLa cells using the NPSC delivery platform. (a) LSCM image showing RNase A-NBC delivery into HeLa cells by NPSCs. Arrows indicate granular structures of RNase A-NBC formed in the nucleus. (b) Quantitative analysis of fluorescence intensities in a. (c) Colocalization of RNase A-NBC with Hoechst 33342, a DNA staining dye. (d) Colocalization of RNase A-NBC with Pyronin Y, a dsRNA staining dye. Scale bars: 10 μm.

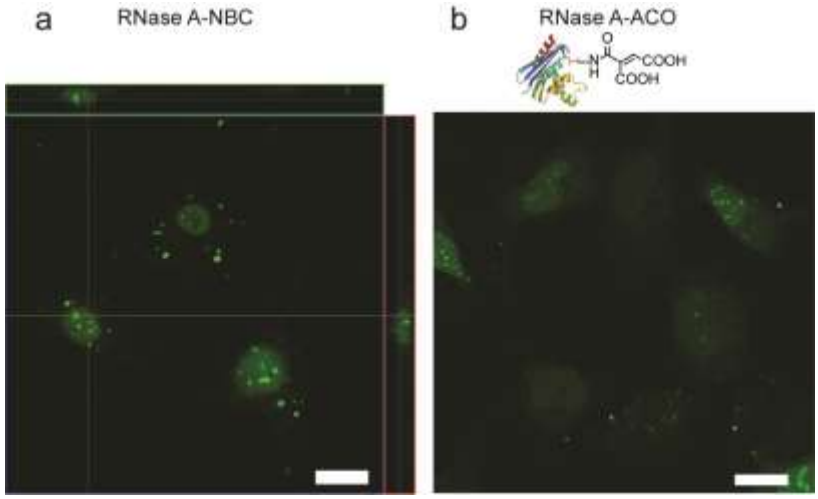

Figure 6.5. LSCM image showing RNase A delivery into HeLa cells by NPSCs: (a) RNase A-NBC and (b) RNase A-ACO. Scale bar: 20 μm.

Quantitative analysis (Figure 6.6) of LSCM images revealed that the fluorescence intensity of RNase A-NBC in the nucleoplasm was 490% ± 94% higher than in the cytosol. The intensity of RNase A-NBC fluorescence in the nuclear granules was 2300% ± 730% higher than in the cytosol (Figure 6.4b and Table 6.1). In contrast, the intensity of RNase A-ACO in the nucleus was only 130% ± 30% higher than in the cytosol (Table 6.2). Although RNase A is a small protein and might naturally penetrate into the nucleus in the presence of NBC tag, the concentration increase of RNase A in the nucleus is almost four-fold higher than that of the control group, indicating efficient targeting to the nucleus.

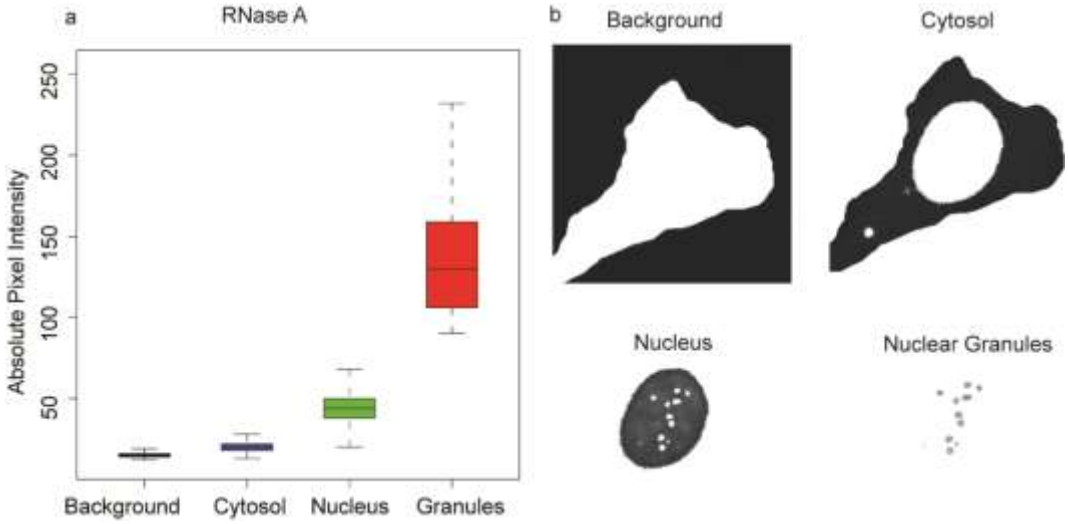

Figure 6.6. Quantitative analysis of an individual cell in Figure 1b after RNase A-NBC delivery. (a) Analysis result after R processing. (b) Different parts of the image were split for the analysis.

Table 6.1. Quantitative analysis of individual cells after RNase A-NBC delivery.

	Absolute median intensity of one cell				Enhanced fluorescence intensity (%)	
	Background	Cytosol	Nucleus	Granules	Nucleus:Cytosol	Granules:Cytosol
1	15	20	44	130	480	2200
2	15	21	58	212	617	3183
3	14	17	27	94	333	2567
4	13	20	57	210	529	2714
5	18	28	80	215	520	1870
6	16	32	108	211	461	1085
				Average	490	2300
				SD	94	730

Absolute median intensities were obtained from R.
The percentage of enhanced fluorescence intensity was calculated using the following equations:

$Nucleus\% = [(I_{nu} - I_{bk})/(I_{cyto} - I_{bk}) - 1] \times 100\%$

$Granule\% = [(I_{gr} - I_{bk})/(I_{nu} - I_{bk}) - 1] \times 100\%$

Where *Nucleus%* corresponds to the percentage of enhanced fluorescence intensity in the nucleus when compared to the cytosol, and *Granule%* in the nuclear granules when compared to the nucleus. I_{bk} is the median fluorescence of the background. I_{cyto} is the median fluorescence of the cytosol. I_{nu} is the median fluorescence of the nucleus. I_{gr} is the median fluorescence of nuclear granules.

Table 6.2. Quantitative analyses of individual cells after RNase A-ACO delivery

	Median median intensity of one cell			Enhanced fluorescence intensity in nucleus (%)
	Background	Cytosol	Nucleus	
1	17	41	70	121
2	17	34	61	159
3	17	30	44	108
4	17	35	56	117
5	17	33	52	119
6	17	36	71	184
			Average	135
			SD	30

We next determined the subnuclear localization of the RNase A-NBC. After RNase A-NBC delivery we stained the cells with either Hoechst 33342 (Figure 6.4c), a blue fluorescent dye for DNA staining, or Pyronin Y, a red fluorescent dye specific for visualizing double stranded RNA (Figure 6.4d). The Hoechst 33342 experiments revealed that RNase A-NBC distributed throughout the nucleoplasm and nucleolus (Figure 6.4c). The Pyronin Y experiments, however, clearly showed that the RNase A-NBC nuclear granules co-localize with condensed nuclear RNAs (Figure 6.4d and Figure 6.7). A number of nuclear RNAs, including rRNA and mRNA, are stored in nucleoli, suggesting that RNase A-NBC may provide a powerful therapeutic tool for RNA regulation.

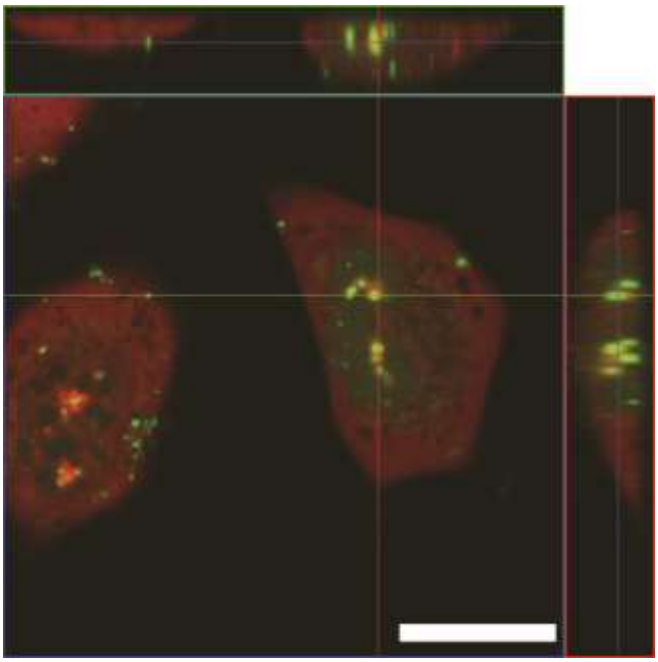

Figure 6.7. Z-stack overlap of RNase A-NBC with Pyronin Y. Green: RNase A-NBc; Red: Pyronin Y. Scale bar: 20 μm.

6.3.2 NBC tag drives nuclear accumulation

Although RNase A-NBC showed an obvious nuclear accumulation, its natural ability to be enriched in the nucleus complicated our analysis. We removed these possibilities by conjugating the NBC tag to eGFP (eGFP-NBC; Figure 6.8a and Figure 6.9). EGFP was chosen for two reasons: (i) The fluorescence of eGFP depends on the conformation and integrity of the protein; structural change or degradation of eGFP therefore results in substantial fluorescence loss;[19] (ii) EGFP does not interfere with the nuclear importing machinery inside cells.[20]

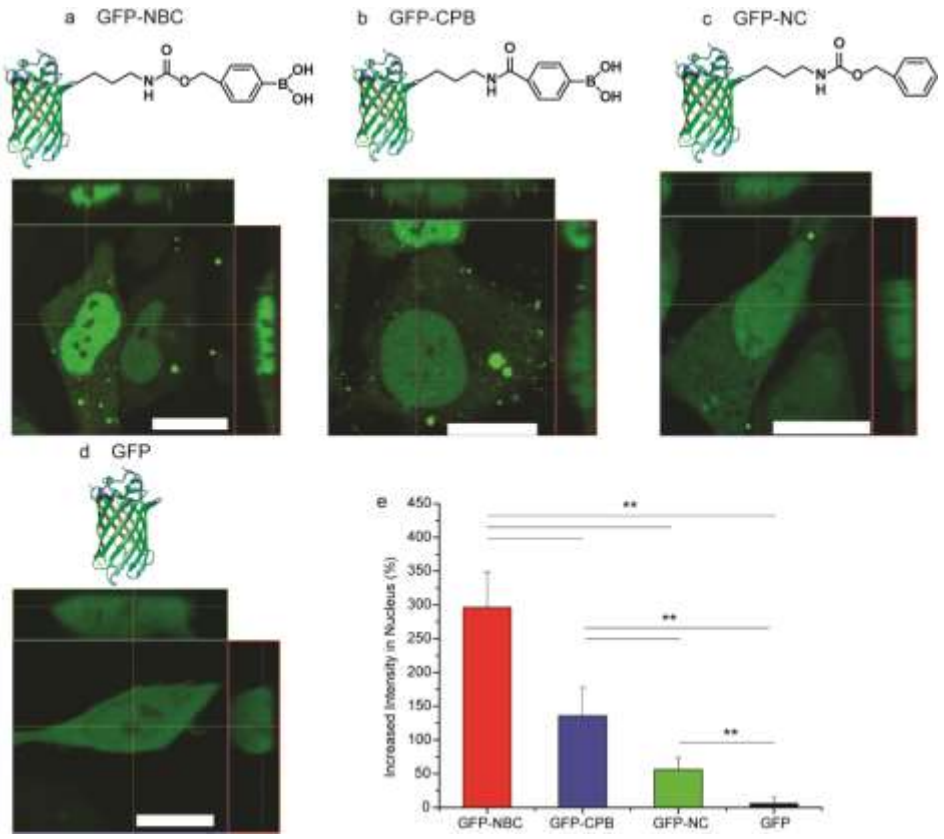

Figure 6.8. Nuclear accumulation of eGFP relies on the NBC label. (a) LSCM image of a HeLa cell after the delivery of eGFP-NBC. (b) LSCM image of a HeLa cell after the delivery of eGFP-CPB. (c) LSCM image of a HeLa cell after the delivery of eGFP-NC. (d) LSCM image of a HeLa cell after the delivery of normal eGFP. Scale bars: 20 μm. (e) Quantitative analysis of the increased fluorescence intensity of eGFP in the nucleus. Six random cells representing different intensities were analyzed in each group. ** indicates P value of t-test less than 0.01.

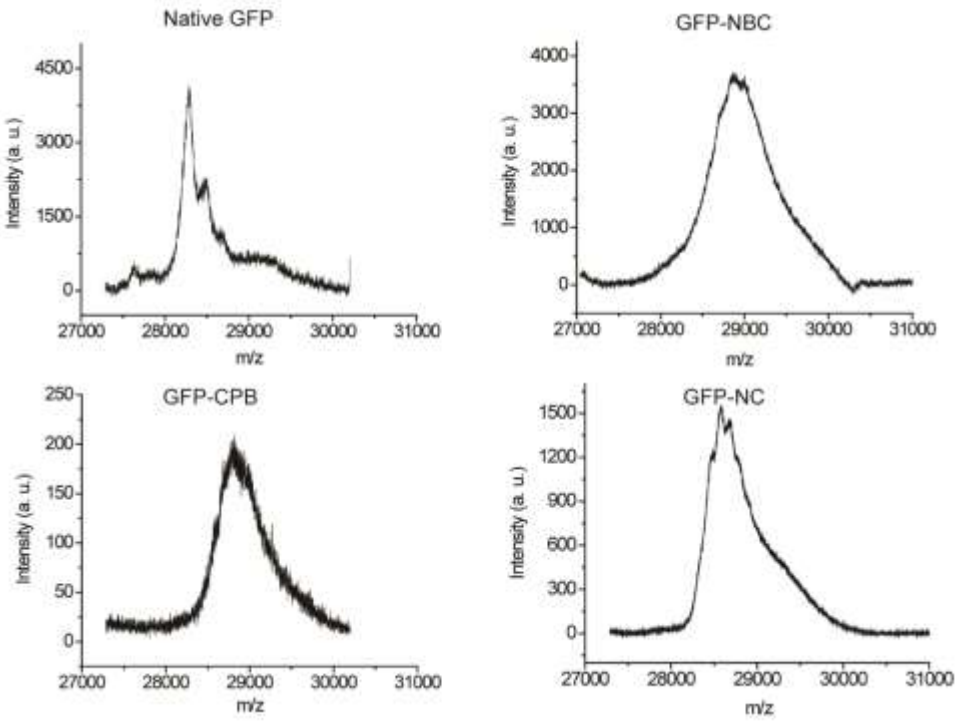

Figure 6.9. Mass spectrometry of both native and tagged GFP.

As expected, eGFP without NBC tag is homogeneously distributed by the NPSC platform throughout the cell, including the nucleus (Figure 6.8d). One hour after delivery, however, eGFP-NBC was highly localized in the nucleus, similarly to RNase A-NBC (Figure 6.8a and Figure 6.10). Quantitative analysis of the LSCM image revealed that the average concentration of eGFP-NBC was 300% ± 50% higher in the nucleus than in the cytosol (Figure 6.11a and Table 6.3). In our previous study, we have compared the nuclear localization efficiencies of a series of nuclear localization signals.[21] The signal derived from c-Myc protein revealed highest efficiency. However, the efficiency of the NBC tag is almost two-fold to that of c-Myc signal investigated on the same delivery platform and with the same protein. Nonetheless, eGFP-NBC was not concentrated in nucleoli or nuclear granules (Figure 6.12). This difference in localization between eGFP-NBC and RNase A-NBC is likely to result from their distinct functional activities. RNase A is an enzyme

specifically targeting RNA, and might therefore become enriched by its substrate after accessing the nucleus. On the other hand, eGFP is a fluorescent protein without other known cellular function.

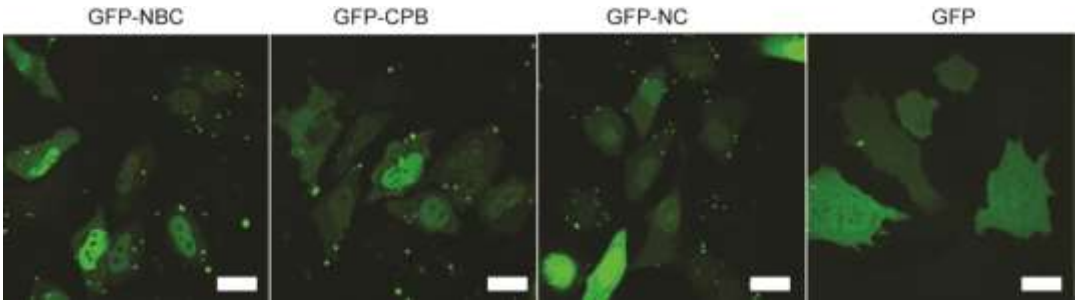

Figure 6.10. Large scale LSCM images of HeLa cells after delivery of GFP with different labels. Native GFP was delivered as a control. Scale bars: 20 μm.

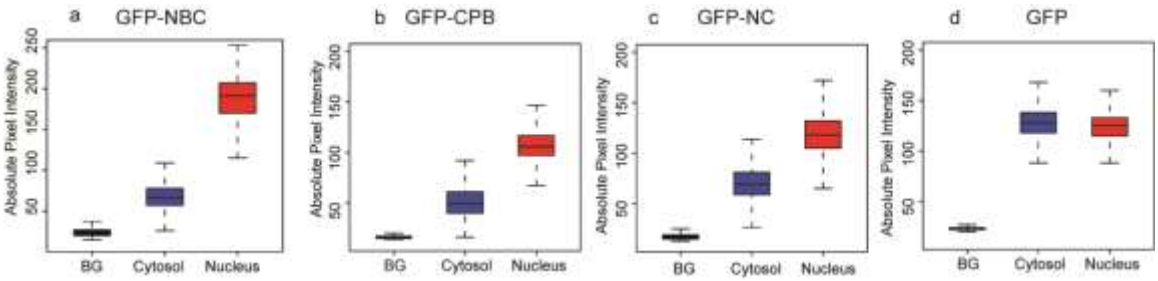

Figure 6.11. Quantitative analysis of individual cells in Figure 6.8.

Table 6.3. Quantitative analyses of individual cells after GFP-NBC delivery

	Median median intensity of one cell			Enhanced fluorescence intensity in nucleus (%)
	Background	Cytosol	Nucleus	
1	19	30	53	209
2	23	67	191	282
3	23	40	89	288
4	18	57	173	297
5	18	29	68	355
6	21	32	70	345
			Average	300
			SD	50

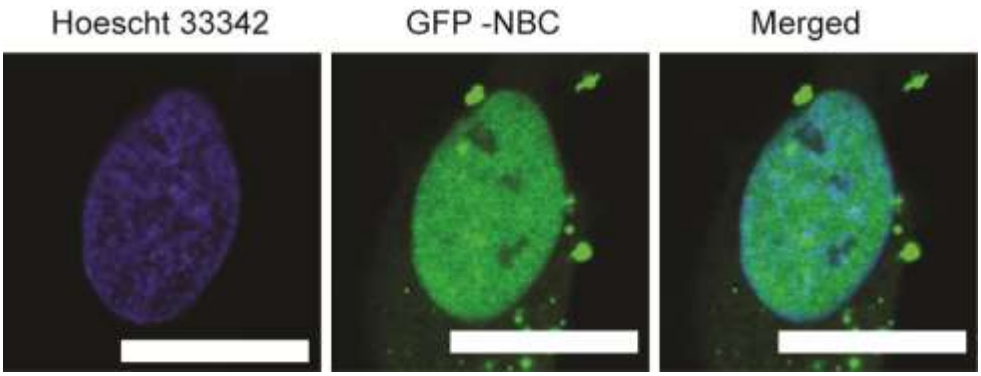

Figure 6.12. GFP-NBC dose not accumulate into nucleoli of the HeLa cell. Scale bars: 20 µm.

We next performed preliminary structure-activity studies to identify the features of NBC conjugation that facilitate nuclear targeting of proteins. In addition to the NBC tag, 4-carboxyphenylboronic acid (CPB, Figure 6.8b and Figure 6.9) and benzyl 4-nitrophenyl carbonate (NC, Figure 6.8c and Figure 6.9) were conjugated to eGFP. CPB is similar in structure to the NBC tag, but is somewhat more electron deficient due to the amide moiety. With its lack of boronate functionality, NC allowed for the evaluation of the role of the aromatic group in nuclear targeting.

LSCM images showed enhanced nuclear accumulation of both CPB and NC conjugates, albeit with lower efficiency than observed with NBC. The intensity of eGFP in the nucleus relative to the cytosol was 140% ± 40% higher for eGFP-CPB, (Figure 6.11b and Table 6.4), and 60% ± 20% higher for eGFP-NC (Figure 6.11c and Table 6.5). Statistical analyses confirmed that there is a significant difference in nuclear accumulation between eGFP-NBC, eGFP-CPB and eGFP-NC ($P < 0.01$; Figure 6.8e). Moreover, eGFP tagged with NBC, CPB or NC has significantly stronger nuclear accumulation when compared to native eGFP (Figure 6.8d, Figure 6.11d and Table 6), as measured by eGFP fluorescence intensity ($P < 0.01$; Figure 6.8e). Flow cytometry analysis (Figure 6.13) revealed that successful GFP delivery occurred in 70% to 90% of the cells in all delivery groups.

Furthermore, the decrease of average fluorescence intensity of cells (Figure 6.13c) is associated with the increase of nuclear condensation of GFP. This decrease is presumably due to the localization of GFP that inhibits the fluorescence emission. These results show that the boronate and the aromatic moieties contribute synergistically to nuclear localization. In addition, although boronate can covalently bind with glycoproteins at high pH, this reaction is not favored under physiological condition and is hence not expected to inhibit the nuclear import of tagged proteins.[22]

Table 6.4. Quantitative analysis of individual cells after GFP-CPB delivery

	Median median intensity of one cell			Enhanced fluorescence intensity in nucleus (%)
	Background	Cytosol	Nucleus	
1	16	49	106	173
2	16	73	163	158
3	19	47	94	168
4	14	57	98	95
5	14	39	57	72
6	16	72	155	148
			Average	140
			SD	40

Table 6.5. Quantitative analysis of individual cells after GFP-NC delivery

	Median median intensity of one cell			Enhanced fluorescence intensity in nucleus (%)
	Background	Cytosol	Nucleus	
1	17	69	118	94
2	21	92	148	79
3	19	56	75	51
4	25	111	139	33
5	24	44	52	40
6	31	143	213	63
			Average	60
			SD	20

Table 6.6. Quantitative analysis of individual cells after GFP delivery

	Median median intensity of one cell			Enhanced fluorescence intensity in nucleus (%)
	Background	Cytosol	Nucleus	
1	23	128	125	-2.9
2	22	43	45	9.5
3	25	106	108	2.5
4	23	127	137	9.6
5	22	58	65	19.4
6	22	84	82	-3.2
			Average	6
			SD	9

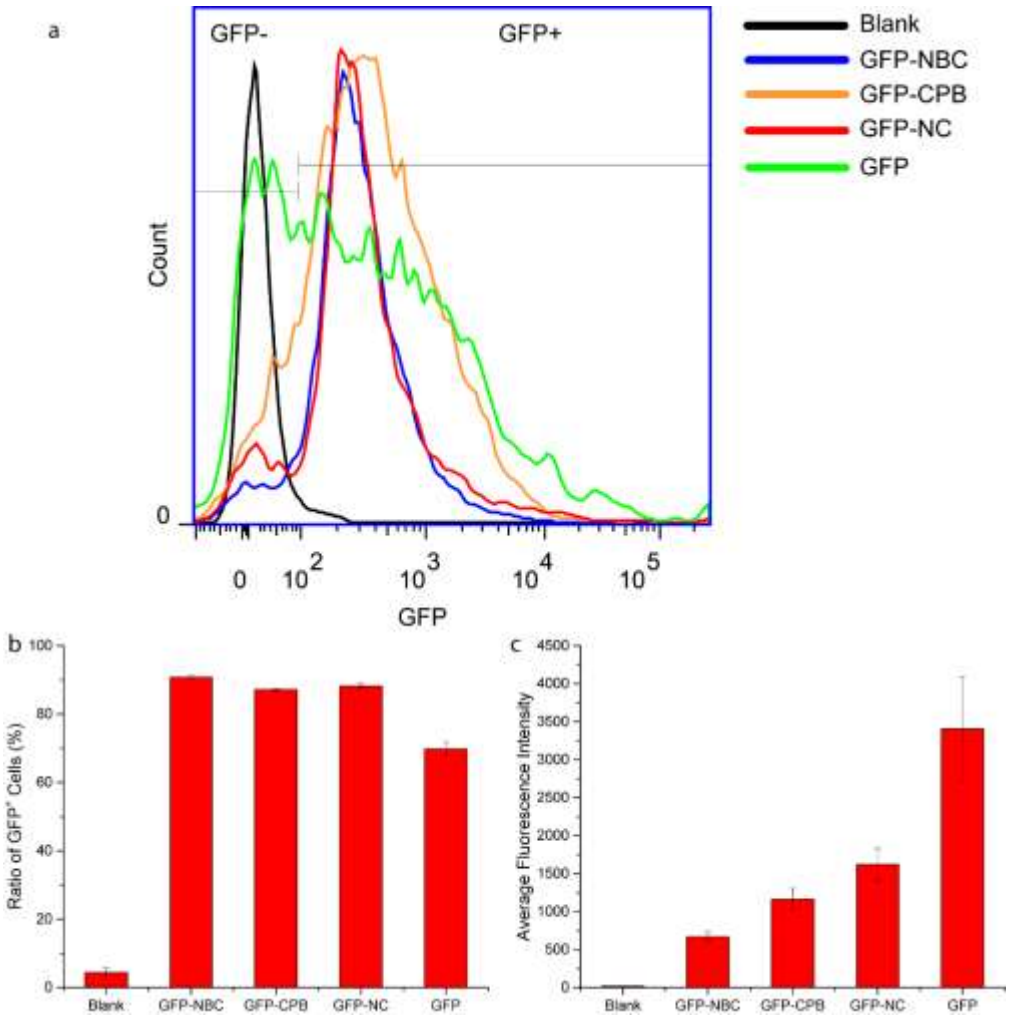

Figure 6.13. Flow cytometry results of GFP delivery with or with without tags to HeLa cells. (a) Flow cytometry data. (b) Ratio of GFP positive cells in each group. (c) Average fluorescence intensity of cells in each group.

Proteins with molecular weight greater than 60 kD cannot passively diffuse into the nucleus, making large proteins excellent testbeds for demonstrating active transport. To demonstrate whether active import is involved in the nuclear localization of proteins mediated by our NBC ligand, we employed dsRed, a tetramer fluorescent protein with the molecular weight of 112 kD (Figure 6.14a and b). DsRed has been shown to access the nucleus only in the presence of nuclear localization signals.[23] After 1 hr delivery, dsRed labeled with NBC tag (dsRed-NBC) was strongly accumulated in nucleus (Figure 6.15a and Figure 6.14c). In contrast, dsRed without NBC tag did not enter nucleus due to its large size (Figure 6.15b and Figure 6.14d). After 8 hr culture, obvious nuclear localization of dsRed-NBC in HeLa cell with was still observed (Figure 6.15c). Together these results substantiate an active import mechanism of NBC tagged proteins.

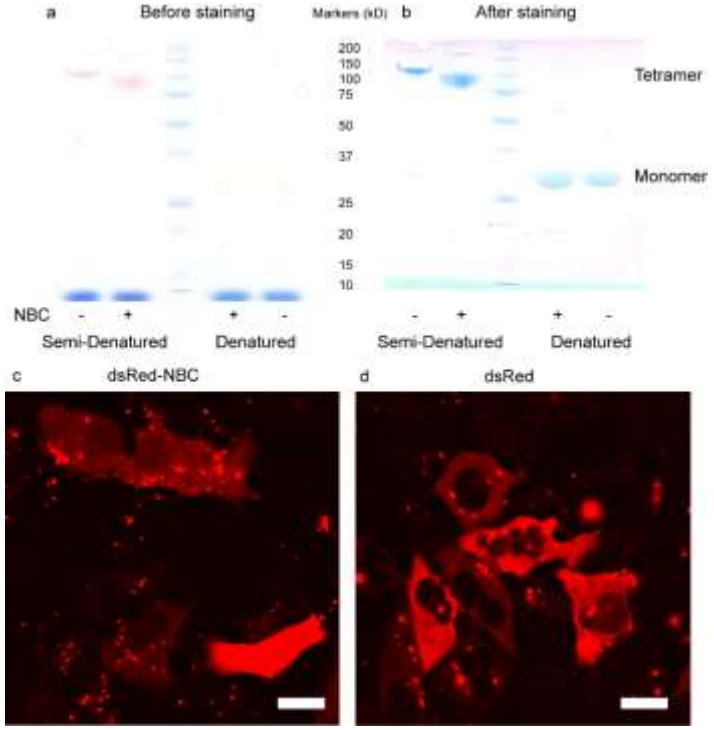

Figure 6.14. Delivery of dsRed with or without NBC tag to HeLa cells. (a) SDS-PAGE gel of dsRed before Brilliant Blue staining. (b) SDS-PAGE gel after Brilliant Blue staining. Under denaturing condition to break the tetramer structure, samples were denatured with 2-mercaptoethanol at 95 °C for 5 min. Under semi-denaturing condition to keep the tetramer structure, samples were loaded without treatment of 2-mercaptoethanol or heating. Protein amount for each lane: 20 µg. (c) Large scale LSCM images of HeLa cells after 1 hr delivery of dsRed with NBC tag. (d) Large scale LSCM images of HeLa cells after 1hr delivery of dsRed without NBC tag. Scale bars: 20 µm.

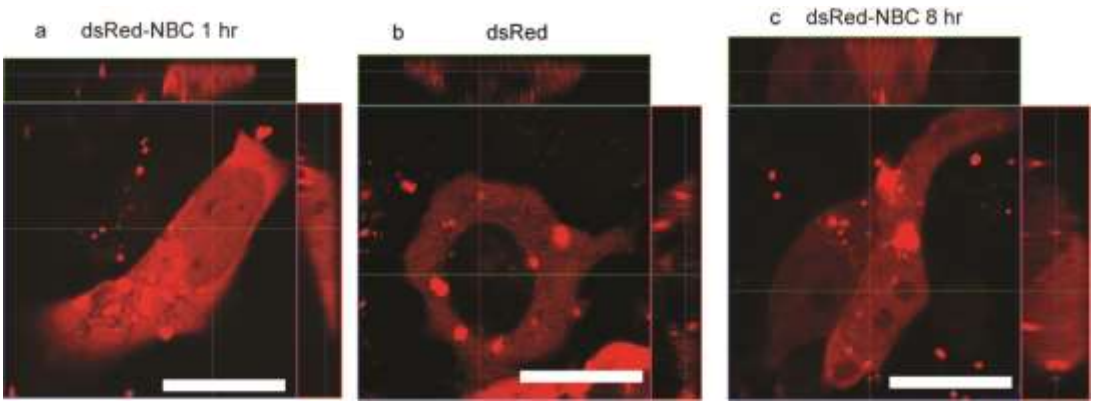

Figure 6.15. Large fluorescent protein dsRed was accumulated in nucleus after labeling with NBC tag. (a) deRed-NBC accessed nucleus of HeLa cell after 1 hr delivery. (b) dsRed without NBC tag did not enter nucleus of HeLa cell after 1 hr delivery. (c) 8 hr after dsRed-NBC delivery to HeLa cells. Scale bars: 20 μm.

6.3.3 NBC mediated nuclear localization is independent of cell synchronization, cell type, delivery vehicle and protein size

To analyze whether nuclear localization of eGFP-NBC is cell cycle dependent, we synchronized HeLa cells to G0/G1 phase by serum starvation for 72 hr or to the beginning of S phase by double thymidine block prior to delivery (Figure 6.16). After 1 hr delivery, we observed that eGFP-NBC accumulated in nuclei of cells regardless of cell phase (Figure 6.17a, b). This result indicates that NBC mediated nuclear import is at least partially independent of cell cycle.

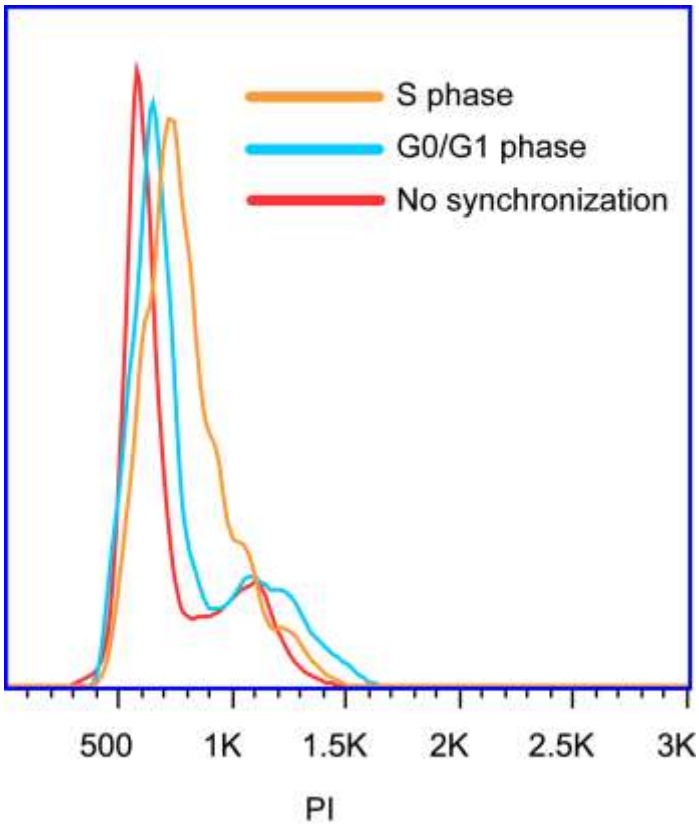

Figure 6.16. Flow cytometry after cell synchronizations.

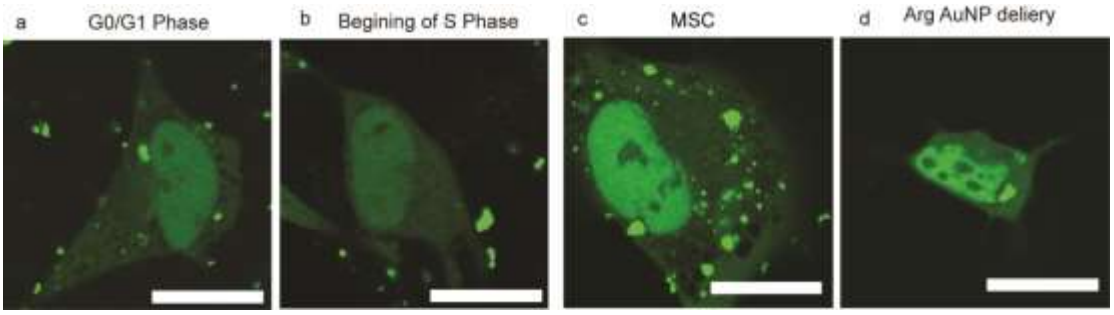

Figure 6.17. NBC mediated nuclear localization is independent of cell synchronization, cell type and delivery vehicle. (a) eGFP-NBC delivery after cells being synchronized to G0/G1 phase and (b) to the beginning of S phase. (c) eGFP-NBC delivery to human mesenchymal stem cell. (d) eGFP-NBC delivery using Arginine AuNP NPSCs as the vehicle. Scale bars: 20 µm.

We next determined the behavior of NBC tag in human mesenchymal stem cells (MSC), a cell type with high potential in clinical use that is often prepared for use *ex vivo*. As expected, obvious nuclear accumulation of eGFP-NBC was observed after 1 hr delivery (Figure 6.17c and Figure 6.18). MSC is important for tissue engineering and disease therapy,[24] therefore, delivery of NBC tagged proteins to nucleus of MSCs offers new opportunities for the regulation of this cell type.

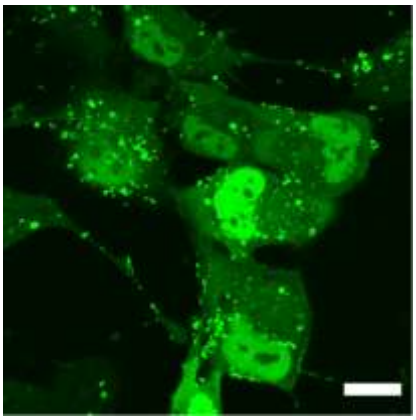

Figure 6.18. Large scale LSCM images of MSCs after delivery of GFP tagged with NBC. Scale bar: 20 μm.

Since HKRK peptide resembles the structure of SV40 nuclear localization signal (PKKKRKV),[25] we wanted to eliminate the possibility that HKRK ligand on AuNP surface helped nuclear localization of proteins, even though eGFP without NBC tag was not enriched in nucleus (Figure 6.8d). Previously, we have developed an arginine-terminated AuNP based NPSC system for the cytosolic delivery of siRNA.[15] Although this platform is not optimized for proteins, certain proteins can still be delivered to cell cytosol. Using this platform, we completely ruled out the possible function of HKRK peptide in nuclear localization of proteins. As shown in Figure 6.17d, after 1 hr delivery, eGFP-NBC efficientlyy accumulated in nucleus, similar to that delivered by

HKRK NPSCs. This result further confirmed that the nuclear localization of proteins is due to the NBC tag, not the delivery vehicle.

6.3.4 Pathways involved in NBC nuclear accumulation

Nuclear accumulation of proteins can be mediated by either active import or passive diffusion.[26] We first treated HeLa cells with ivermectin,[27] a specific inhibitor of the importin α/β pathway to assess active transport. Nuclear localization of eGFP-NBC was still observed after ivermectin treatment, (Figure 6.19a, b) however the enhancement of nuclear localization decreased dramatically to 60% ± 30% (Figure 6.19e, Figure 6.20a and Table 7). This result indicates that active transport through the importin α/β pathway is responsible for the majority of the nuclear localization observed with NBC tagged proteins. To test whether other active import pathways are involved in the nuclear accumulation of eGFP-NBC, we depleted ATP from HeLa cells before and during delivery. ATP is a prerequisite for both importin-dependent[28] and other[29] pathways. One hour after delivery in the ATP depleted condition, nuclear accumulation was observed (Figure 6.19c). Fluorescence intensity enhancement in the nucleus was 95% ± 20% (Figure 6.19g, Figure 6.20b and Table 8), similar to that achieved after ivermectin treatment, indicating that importin was the major driver of active transport.

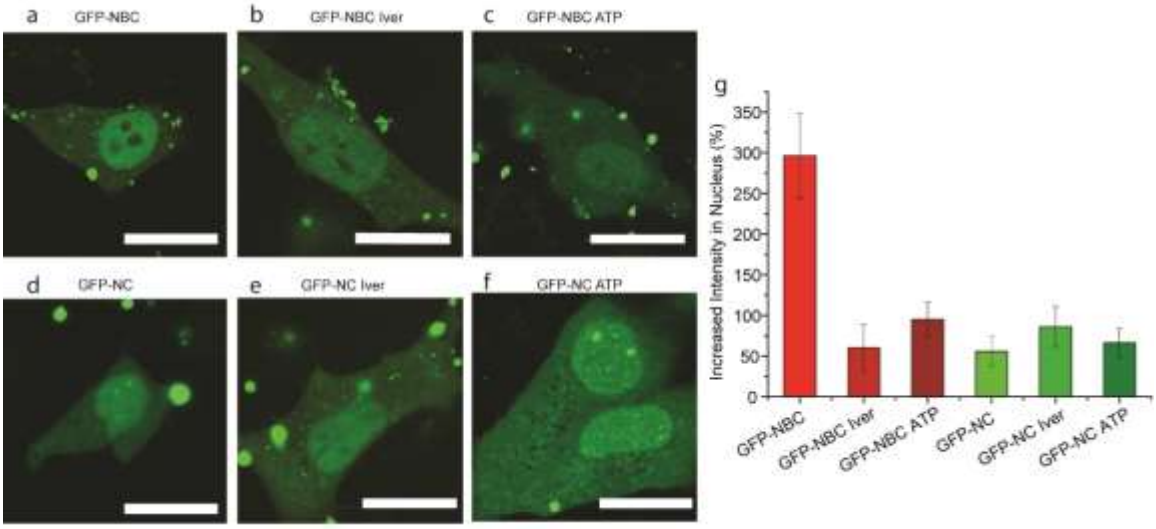

Figure 6.19. Inhibition of active import to nucleus significantly reduces nuclear accumulation of NBC-tagged eGFP. (a) eGFP-NBC delivery before and (b) after inhibition of importin α/β pathway. (c) eGFP-NBC delivery after inhibition of all active import pathway by ATP depletion. (d) eGFP-NC delivery before and (e) after inhibition of importin α/β pathway. (f) eGFP-NC delivery after inhibition of all active import pathway by ATP depletion. Scale bars: 20 μm. (g) Quantitative analysis of increased fluorescence intensity of eGFP-NBC and eGFP-NC in the nucleus after delivery with or without pretreatment using six cells in each group.

Table 6.7. Quantitative analysis of individual cells after GFP-NBC delivery in the presence of ivermectin.

	Median median intensity of one cell			Enhanced fluorescence intensity in nucleus (%)
	Background	Cytosol	Nucleus	
1	20	39	53	74
2	17	32	41	60
3	16	40	52	50
4	15	30	46	107
5	17	32	35	20
6	16	44	58	50
			Average	60
			SD	30

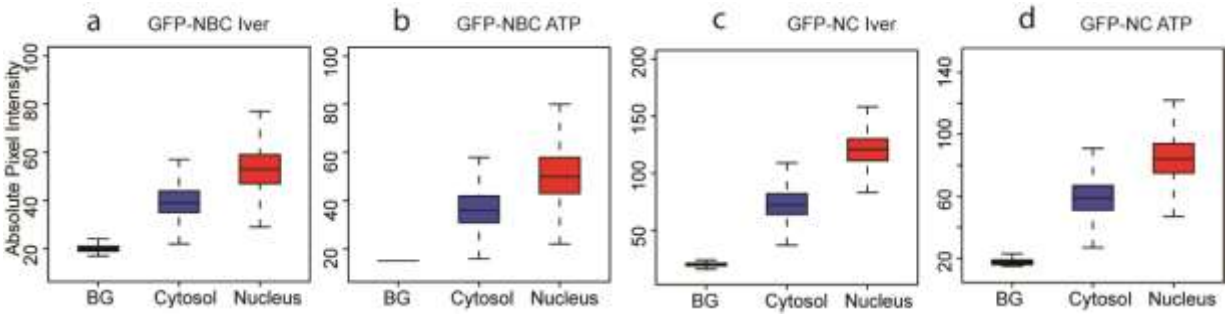

Figure 6.20. Quantitative analyses of individual cells in Figure 6.19.

Table 6.8. Quantitative analysis of individual cells after GFP-NBC delivery with ATP depletion.

	Median median intensity of one cell			Enhanced fluorescence intensity in nucleus (%)
	Background	Cytosol	Nucleus	
1	15	36	50	67
2	15	27	37	83
3	16	33	49	94
4	16	32	47	94
5	17	94	193	129
6	17	39	62	105
			Average	95
			SD	20

Significant (and similar) nuclear localization was observed when importin was inhibited and from the non-boronate NC system, suggesting a passive mechanism dependent on the aromatic substitution. To test this hypothesis, we delivered eGFP-NC into HeLa cells either in the presence of ivermectin (Figure 6.19d, e) or under ATP depletion (Figure 6.19f). As expected, nuclear accumulation of eGFP-NC was observed in both conditions. Compared to eGFP-NBC delivery, there was no substantial difference between eGFP-NC delivery with or without either pretreatment (Figure 6.19g, Figure 6.20c, d and Tables 6.9, 6.10). These results corroborate our observation that the benzene ring is involved in nuclear accumulation, with localization

potentially arising from hydrophobic interactions mediated by aromatic substituents. While aromatic rings naturally exist in some amino acids, they are usually not presented on the exposed outer surface of proteins. In contrast, NBC and NC tags are directly conjugated to the protein surface[11] enabling hydrophobic interactions with the contents of nucleus, in analogy with passive nuclear localization during viral infection.[30]

Table 6.9. Quantitative analysis of individual cells after GFP-NC delivery in the presence of ivermectin.

	Median median intensity of one cell			Enhanced fluorescence intensity in nucleus (%)
	Background	Cytosol	Nucleus	
1	20	72	121	94
2	17	51	87	106
3	16	56	80	60
4	15	32	46	82
5	16	39	66	117
6	17	35	45	56
			Average	85
			SD	25

6.4 Discussion

As discussed previously, RNase A-NBC has only a slight activity decrease compared to native RNase A.[11] In our current study study, we did not observe obvious structural damage or activity loss of fluorescent proteins after conjugation with NBC tag. Furthermore, the tag can be designed as permanent or cleavable under certain stimuli.[11] We expect that a permanent tag can be used for irreversible nuclear import of proteins and a cleavable tag may be applied in case reversible nuclear import of proteins is desired.

Our inhibition study demonstrated that after cytosolic release nuclear accumulation of NBC tagged proteins occurs via two distinct mechanisms: (i) Active transportation into the nucleus

via interaction between boronic acid and importin α/β; (ii) Passive diffusion into the nucleus and adsorption via hydrophobic interaction with the benzene ring on the protein surface. According to the import mechanism of importin α/β pathway, NBC tags on payload protein presumably bind with importin α of importin α/β heterodimer and importin β targets nuclear pore complexes for subsequent nuclear translocation of NBC tagged proteins.[31]

In summary, we describe the use of aromatic boronic acids (NBC) for synergistic active and passive targeting of proteins for delivery to the nucleus. Our mechanistic experiments show that the boronic acid mediates active nuclear import, while the benzene ring contributes to passive accumulation of proteins into the nucleus. These two moieties can therefore be combined or individually used to control protein nuclear targeting. Unlike TPP, which solely relies on membrane potential, the NBC tag is a synthetic signal that takes advantage of the intracellular transportation machinery for subcellular localization. This finding suggests that transport machineries for other subcellular destinations could also be recruited by synthetic tags, paving the way for the development of more versatile and efficient intracellular targeting strategies for therapeutic and imaging applications.

6.5 References

1. M. C. Hung, W. Link, *J. Cell Sci.* **2011**, *124*, 3381.
2. S. W. Hicks, J. E. Galan, *Nat. Rev. Microbiol.* **2013**, *11*, 316.
3. L. Rajendran, H. J. Knolker, K. Simons, *Nat. Rev. Drug Discov.* **2010**, *9*, 29.
4. N. M. Sakhrani, H. Padh, *Drug Des. Dev. Ther.* **2013**, *7*, 585.
5. R. Nair, P. Carter, B. Rost, *Nucleic Acids Res.* **2003**, *31*, 397.
6. A. Mukhopadhyay, H. Weiner, *Adv. Drug Deliv. Rev.* **2007**, *59*, 729.
7. A. Fu, R. Tang, J. Hardie, M. E. Farkas, V. M. Rotello, *Bioconjugate Chem.* **2014**, *25*, 1602.
8. S. R. Terlecky, J. I. Koepke, *Adv. Drug Deliv. Rev.* **2007**, *59*, 739.
9. R. Tang, C. S. Kim, D. J. Solfiell, S. Rana, R. Mout, E. M. Velázquez-Delgado, A. Chompoosor, Y. Jeong, B. Yan, Z.-J. Zhu, C. Kim, J. A. Hardy, V. M. Rotello, *ACS Nano* **2013**, *7*, 6667.
10. Y. C. Yeh, R. Tang, R. Mout, Y. Jeong, V. M. Rotello, *Angew. Chem. Int. Ed.* **2014**, *53*, 5137.
11. M. Wang, S. Sun, C. I. Neufeld, B. Perez-Ramirez, Q. Xu, *Angew. Chem. Int. Ed.* **2014**, *53*, 13444.

12. M. Borriello, P. Laccetti, G. Terrazzano, G. D'Alessio, C. De Lorenzo, *Br. J. Cancer* **2011**, *104*, 1716.
13. R. F. Turcotte, R. T. Raines, *Aids Res. Hum. Retrovir.* **2008**, *24*, 1357.
14. M. Bosch, A. Benito, M. Ribó, T. Puig, B. Beaumelle, M. Vilanova, *Biochemistry* **2004**, *43*, 2167.
15. Y. Jiang, R. Tang, B. Duncan, Z. Jiang, B. Yan, R. Mout, V. M. Rotello, *Angew. Chem. Int. Ed.* **2015**, *54*, 506.
16. C. Dingwall, R. A. Laskey, *Annu. Rev. Cell Biol.* **1986**, *2*, 367.
17. M. Yan, J. Du, Z. Gu, M. Liang, Y. Hu, W. Zhang, S. Priceman, L. Wu, Z. H. Zhou, Z. Liu, T. Segura, Y. Tang, Y. Lu, *Nat. Nanotechnol.* **2010**, *5*, 48.
18. S. J. Kaczmarczyk, K. Sitaraman, H. A. Young, S. H. Hughes, D. K. Chatterjee, *Proc. Natl. Acad. Sci. U. S. A.* **2011**, *108*, 16998.
19. P. Corish, C. Tyler-Smith, *Protein Engineering* **1999**, *12*, 1035.
20. Y. Miyamoto, T. Saiwaki, J. Yamashita, Y. Yasuda, I. Kotera, S. Shibata, M. Shigeta, Y. Hiraoka, T. Haraguchi, Y. Yoneda, *J. Cell Biol.* **2004**, *165*, 617.
21. M. Ray, R. Tang, Z. Jiang, V. M. Rotello, *Bioconjugate Chem.* **2015**, *26*, 1004.
22. B. Pappin, M. J. Kiefel, T. A. Houston, *Carbohydrates - Comprehensive Studies on Glycobiology and Glycotechnology Ch. 3*, InTech, Rijeka 2012.
23. F. Rodrigues, M. van Hemert, H. Y. Steensma, M. Côrte-Real, C. Leão, *J. Bacteriol.* **2001**, *183*, 3791.
24. C. Nombela-Arrieta, J. Ritz, L. E. Silberstein, *Nat. Rev. Mol. Cell Biol.* **2011**, *12*, 126.
25. D. Kalderon, B. L. Roberts, W. D. Richardson, A. E. Smith, *Cell* **1984**, *39*, 499.
26. N. Freitas, C. Cunha, *Curr. Genomics* **2009**, *10*, 550.
27. K. M. Wagstaff, S. M. Rawlinson, A. C. Hearps, D. A. Jans, *J. Biomol. Screen* **2011**, *16*, 192.
28. S. Kose, N. Imamoto, Y. Yoneda, *FEBS Lett.* **1999**, *463*, 327.
29. M. Lu, J. Zak, S. Chen, L. Sanchez-Pulido, David T. Severson, J. Endicott, Chris P. Ponting, Christopher J. Schofield, X. Lu, *Cell* **2014**, *157*, 1130.
30. Z. Onder, J. Moroianu, *Virology* **2014**, *449*, 150.
31. H. Fried, U. Kutay, *Cellular and Molecular Life Sciences CMLS*, *60*, 1659.

CHAPTER 7

INTRACELLULAR DELIVERY OF LARGE PROTEINS USING NANOPARTICLE-STABILIZED CAPSULES

7.1 Introduction

Protein-based therapeutics have widespread applications in biomedical engineering,[1] cell engineering[2, 3] and regenerative medicine.[4, 5] An increasing number of proteins, including signaling proteins,[6] antibodies[7, 8] and functional enzymes[9, 10] have been preclinically or clinically tested for the treatment of diseases. The vast majority of these studies, however, have focused on extracellular delivery.

Intracellular delivery of proteins provides a transient and non-integrative means for the regulation of cellular protein functions, and it has recently attracted the interest of researchers and clinicians. However, despite significant advances in the development of intracellular protein delivery tools major challenges still remain.[11] A key aspect that remains unresolved is the rate of cytosolic release of the macromolecule in its active form; unlike small molecules, proteins display a wide diversity of size and conformations that may inhibit cytosolic access, typically through entrapment in the endosomal/lysosomal pathway.[12] To address this problem, a number of delivery platforms have been developed.[13] For instance, endosomal escape agents, cell penetrating peptides, and endosomal lysis agents such as chloroquine[14] have been effective at facilitating protein delivery into cells.[15] Nevertheless, the delivery performance of these traditional methods is still limited in efficiency,[16] in particular for proteins of large size.[17, 18]

Membrane fusion is an alternative approach that conveys rapid release of cargo proteins into the cytosol by bypassing endosomal entrapment.[19] We have previously developed a nanoparticle-stabilized capsule (NPSC) platform for intracellular protein delivery through direct membrane fusion[20, 21] wherein the terminal functional group on the gold nanoparticles (AuNPs) is

a tetrapeptide, His-Lys-Arg-Lys (HKRK). Despite their high efficiency, tight binding of HKRK AuNPs to proteins of large size resulted in ineffective payload release into the cytosol. We hypothesized that decreasing the overall charge of the terminal group on the AuNPs could reduce their interaction with proteins, thereby improving delivery efficiency for larger systems. We used 1-guanidino-2-(4-imidazole)propionic acid (GIPA, Figure 7.1) as the terminal group of the AuNP ligand, providing effective cytosolic delivery of large proteins, including dsRed and *β*-galactosidase (*β*-gal), into the cytosol. Notably, the synthesis of the GIPA ligand was far more facile than the peptide-based ligand.

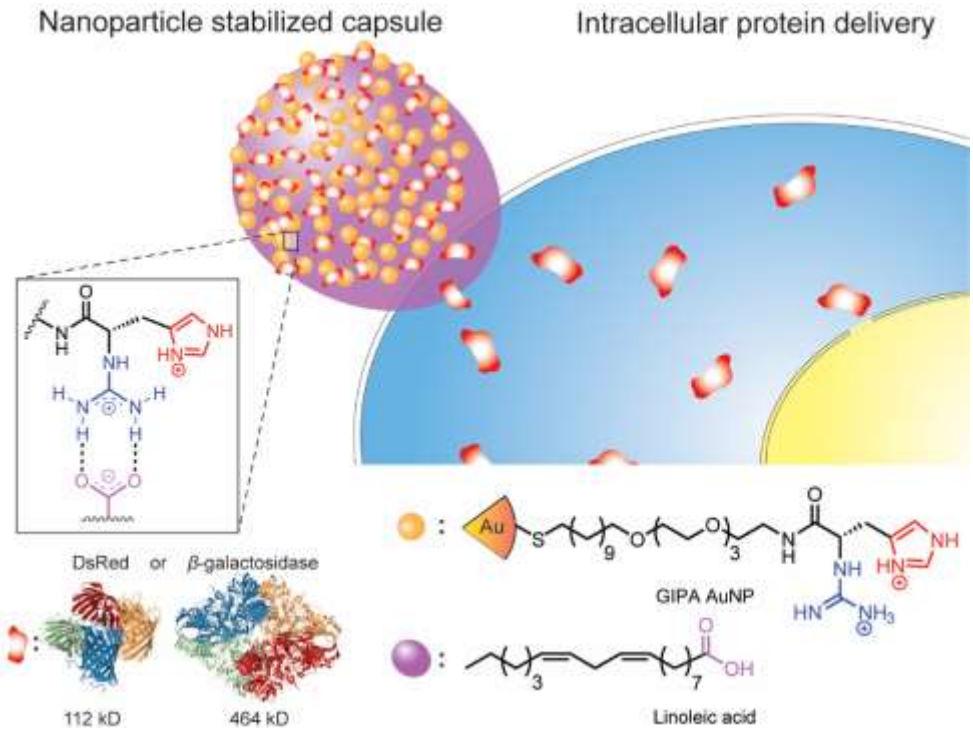

Figure 7.1. Schematic illustration of a new platform of intracellular protein (dsRed and *β*-galactosidase) delivery using GIPA AuNPs-stabilized capsule.

7.2 Methods

7.2.1 Preparation of GIPA Ligand

Synthesis of Compound 1

1-(Triphenylmethyl)-L-histidine (1.50 g, 3.77 mmol) was dispersed in 20 mL methanol and mixed with triethylamine (382 mg, 0.53 mL, 3.77mmol). The suspension was stirred at room temperature for 10 min. Ethyl trifluoroacetate (698 mg, 0.58 mL, 4.91mmol) was added into the white suspension dropwise. The suspension turned into clear brownish solution after 1 h stirring at room temperature. The stirring was continued for another 5 hrs. Then the pH of the solution was adjusted to 1-2 with 1 M HCl at 0 °C. The aqueous solution was extracted with chloroform for 5 times. The combined organic layer was dried over Na_2SO_4 and concentrated *in vacuo*. The white solid was dissolved with a minimal amount of methanol and diethyl ether mixture (v/v = 1:1) and further recrystallized with *n*-hexanes at 4 °C. The product was filtered and dried under vacuum as white solid (1.55 g, 3.14 mmol, 83.3%) (Compound **1**, Figure 7.2). ^{1}H NMR (400 MHz, DMSO-d_6): δ 9.57 (s, 1H), 7.44 – 7.33 (m, 9H), 7.28 (d, *J* = 1.4 Hz, 1H), 7.10 – 7.00 (m, 6H), 6.66 (d, *J* = 1.3 Hz, 1H), 4.48 (s, 1H), 3.03 (dd, *J* = 14.7, 4.1 Hz, 1H), 2.90 (dd, J = 14.6, 10.3 Hz, 1H). MALDI-MS *m/z* calculated for $C_{27}H_{22}F_3N_3O_3$ $[M + H]^+$ 493.16, found 493.53.

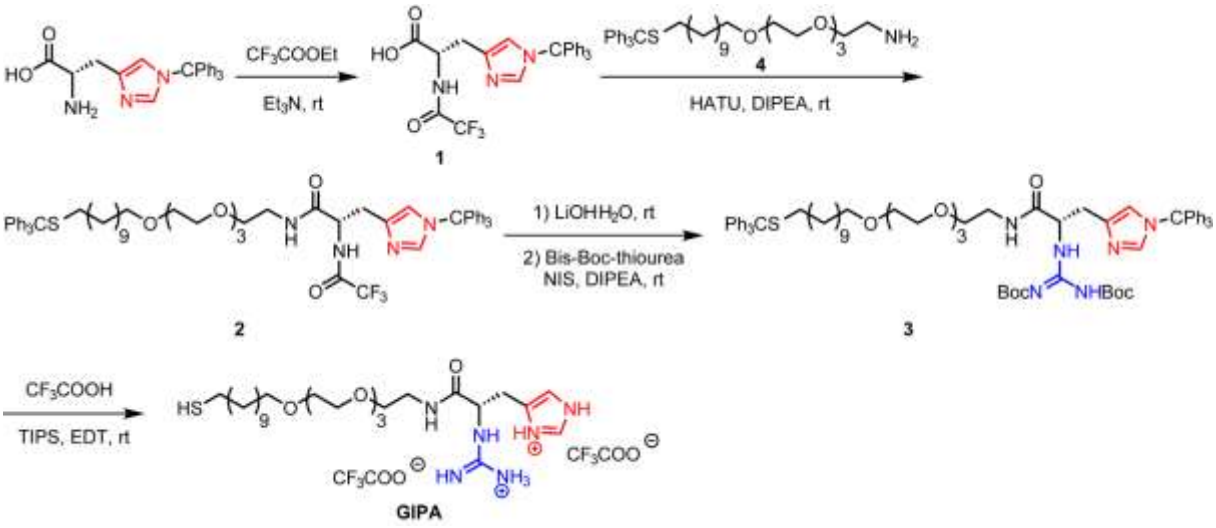

Figure 7.2. Synthetic scheme of GIPA ligand.

Synthesis of Compound 2

Compound **4** (Figure 7.2) was synthesized according to previously reported procedure.[22] Compound **1** (650 mg, 1.32 mmol), Compound **4** (982 mg, 1.58 mmol), and diisopropylamine (DIPEA, 511 mg, 0.69 mL, 3.95 mmol) were dissolved in 15 mL dimethylformamide (DMF) and stirred for 10 min at 0 °C. 1-[Bis(dimethylamino)methylene]-1H-1,2,3-triazolo[4,5-b]pyridinium 3-oxid hexafluorophosphate (HATU, 601 mg, 1.58 mmol) was dissolved in 3 mL DMF and added into the previous mixture dropwise. Then the solution was warmed up to room temperature and stirred for 2 hrs. The reaction was quenched with 5 mL deionized water and diluted with 100 mL ethyl acetate. The organic layer was washed with 0.1 M HCl for 3 times, saturated $NaHCO_3$ solution for 3 times, and saturated NaCl solution for 5 times. Then the organic layer was separated and dried over Na_2SO_4. The mixture was concentrated and purified by column chromatography over silica gel with Ethyl acetate and subsequently ethyl acetate–methanol (95:5). The product was concentrated *in vacuo* and obtained as pale yellow oil (1.19 g, 1.08 mmol, 81.8%) (Compound **2**, Figure 7.2). ^{1}H NMR (400 MHz, $CDCl_3$): δ 8.67 (d, *J* = 7.0 Hz, 1H), 7.56 (s, 1H), 7.47 – 7.38 (m, 7H), 7.38 – 7.33 (m, 9H), 7.33 – 7.26 (m, 5H), 7.25 – 7.18 (m, 3H), 7.16 – 7.07 (m, 6H), 4.72 (q, *J* = 6.0 Hz, 1H), 3.69 – 3.60 (m, 6H), 3.60 – 3.55 (m, 6H), 3.55 – 3.48 (m, 2H), 3.48 – 3.35 (m, 4H), 3.10 (dd, *J* = 15.0, 4.8 Hz, 1H), 3.02 – 2.94 (m, 1H), 2.14 (t, *J* = 7.4 Hz, 2H), 1.63 – 1.52 (m, 2H), 1.40 (p, *J* = 7.2 Hz, 2H), 1.35 – 1.08 (m, 14H). MALDI-MS *m/z* calculated for $C_{65}H_{75}F_3N_4O_6S$ $[M + Na]^+$ 1119.54, found 1119.63.

Synthesis of Compound 3

Compound **2** (1.19 g, 1.08 mmol) was dissolved in 2 mL methanol. $LiOH{\cdot}H_2O$ (228 mg, 5.42 mmol) was dissolved in 2 mL deionized water and added into the methanol solution in one portion at room temperature. The mixture was stirred for 15 hrs. $CHCl_3$ was used to extract the solution for 6 times. The combined organic layer was dried over $MgSO_4$ and concentrated *in vacuo* without further purification. The deprotected product (680 mg) was directly used for the next step. The

product after deprotection (272 mg, 0.27 mmol), *N,N*'-di-(tert-butoxycarbonyl)thiourea (Bis-Boc-thiourea, 63 mg, 0.23 mmol), and DIPEA (0.1 mL, 0.57 mmol) were dissolved in 2 mL dichloromethane (DCM) while being flushed with N_2. *N*-Iodosuccinimide (NIS, 51 mg, 0.23 mmol)[23] was dispersed in 2 mL DCM and added into the mixture in one portion at 0°C. The reaction was then warmed up to room temperature and stirred for 15 hrs. $Na_2S_2O_4$ (10 mL 1 M) solution was added to quench the reaction and stirred for another 15 min. Afterwards, the mixture was diluted with 100 mL ethyl acetate and washed with saturated NaCl solution for 3 times. The organic layer was separated and dried over Na_2SO_4. The mixture was concentrated and purified by column chromatography over silica gel with ethyl acetate–methanol (95:5). The product was obtained as yellow oil (198 mg, 0.16 mmol, 44.0%) (Compound **3**, Figure 7.2). ^{1}H NMR (400 MHz, $CDCl_3$): δ 9.00 (d, *J* = 7.2 Hz, 1H), 7.44 (t, *J* = 1.8 Hz, 2H), 7.43 – 7.40 (m, 3H), 7.34 (td, *J* = 4.4, 1.8 Hz, 9H), 7.31 (q, *J* = 1.9, 1.5 Hz, 2H), 7.30 – 7.26 (m, 6H), 7.24 (t, *J* = 1.3 Hz, 1H), 7.22 (d, *J* = 2.2 Hz, 1H), 7.20 (t, *J* = 1.3 Hz, 1H), 7.16 – 7.10 (m, 5H), 3.70 – 3.61 (m, 6H), 3.59 (dq, *J* = 6.2, 4.0, 2.9 Hz, 5H), 3.51 (t, *J* = 5.4 Hz, 2H), 3.45 (t, *J* = 6.9 Hz, 3H), 2.15 (t, *J* = 7.3 Hz, 2H), 1.58 (p, *J* = 6.9 Hz, 3H), 1.52 (s, 7H), 1.46 (d, *J* = 1.6 Hz, 8H), 1.39 (q, *J* = 7.5 Hz, 2H), 1.25 (d, *J* = 23.0 Hz, 16H). ESI-MS *m/z* calculated for $C_{74}H_{94}N_6O_9S$ $[M + H]^+$ 1243.7, $[M + H + CH_3OH]^+$ 1275.7, found 1243.5, 1275.5.

Synthesis of GIPA Ligand

Compound **3** (198 mg, 0.16 mmol) was dissolved in 2 mL anhydrous DCM and stirred at room temperature with N_2 flushed. A mixture containing 9.25 mL trifluoroacetic acid (TFA), 0.25 mL 1,2-ethanedithiol (EDT), 0.25 mL triisopropylsilane (TIPS), and 0.25 mL deionized H_2O was made and added into the DCM solution. The mixture was then stirred at room temperature for 1 hr under N_2 protection. The solvent was evaporated afterwards and the residue was washed with *n*-hexanes for 2 times, *n*-hexanes–diethyl ether (v/v = 4:1) for 4 times. The residue was dried under vacuum and the product was obtained as pale yellow oil (105 mg, 0.13 mmol, 83.1%) (**GIPA**

Ligand, Figure 7.2). ^{1}H NMR (400 MHz, $CDCl_3$): δ 8.82 – 8.46 (m, 2H), 8.28 (d, *J* = 63.0 Hz, 2H), 7.38 (s, 2H), 7.27 (s, 2H), 4.77 (s, 1H), 3.61 (t, *J* = 13.6 Hz, 16H), 3.43 (p, *J* = 21.3, 17.8 Hz, 8H), 2.51 (q, *J* = 7.4 Hz, 2H), 1.56 (dp, *J* = 20.4, 6.6 Hz, 5H), 1.43 – 1.15 (m, 19H). MALDI-MS *m/z* calculated for $C_{26}H_{50}N_6O_5S$ $[M + H]^+$ 559.36, found 559.50.

7.2.2 Gold nanoparticle (AuNP) synthesis and functionalization with GIPA Ligand

The AuNPs (*ca.* 2 nm core size) were synthesized according to previously reported procedures.[24] The 1-pentanethiol-stablized AuNPs were functionalized with GIPA Ligand via place-exchange reactions[25.] Briefly, 20 mg AuNP stabilized with 1-pentanethiol was dissolved in 2 mL anhydrous DCM and stirred at room temperature with N_2 flushed. GIPA Ligand (60 mg) was dissolved in 2 mL DCM–methanol mixture (v/v = 9:1) and added into the AuNP solution. The mixture was then stirred at room temperature for 96 hrs under N_2 protection. The solvent was evaporated afterwards and the residue was washed with *n*-hexanes–DCM (v/v = 9:1) for 5 times. Then the functionalized AuNPs were dispersed in *Mili-Q* water and dialyzed using 10,000 MWCO SnakeSkin Dialysis Tubing (Thermo Scientific, USA) for 120 hrs. The concentration of the AuNP solution was measured according to a reported method by UV spectroscopy on a Molecular Devices SpectraMax M2 at 506 nm.[26] Transmission electron microscopy (TEM) of AuNPs was performed on a JEOL 2000FX electron microscope (Figure 7.3). Dynamic light scattering (DLS) profiles (Figure 7.4) and zeta potential were carried out on a Malvern Zetasizer Nano ZS. The surface zeta potential of GIPA-AuNPs was (14.6 ± 0.4) mV.

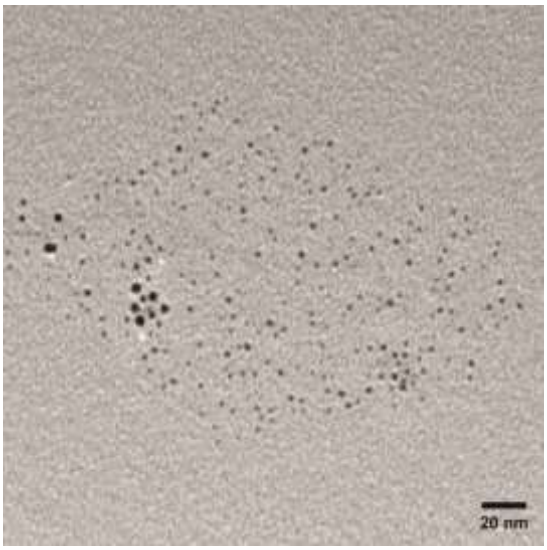

Figure 7.3. TEM image of GIPA-functionalized AuNPs. The black scale bar is 20 nm as denoted.

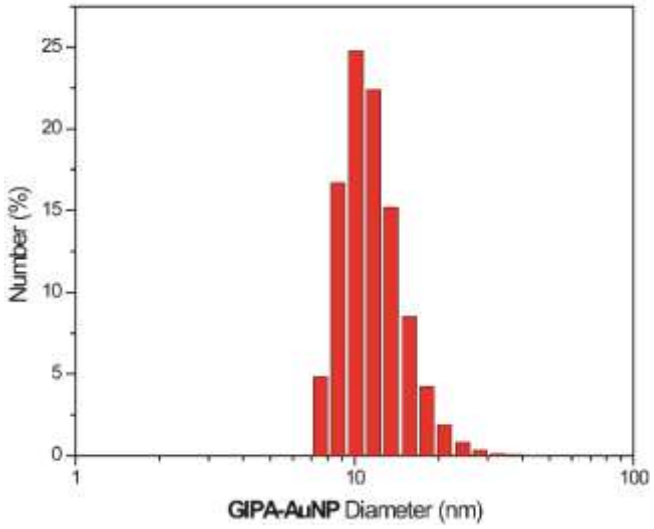

Figure 7.4. DLS histogram of GIPA-functionalized AuNPs, demonstrating the hydrodynamic diameter distribution of nanoparticles.

7.2.3 Cell culture

HeLa cells were cultured in a humidified atmosphere (5% CO_2) at 37 °C, and grown in Dulbecco's modified eagle's medium (DMEM, low glucose) supplemented with 10% fetal bovine serum (FBS) and 1% antibiotics (100 $U \cdot mL^{-1}$ penicillin and 100 $\mu g \cdot mL^{-1}$ streptomycin).

7.2.4 Fluorescence titration

In the fluorescent titration experiment between nanoparticles and GFP, the change of fluorescence intensity at 515 nm was measured with an excitation wavelength of 485 nm at various concentrations of AuNPs from 0 to 200 nM on a Molecular Devices SpectraMax M2 microplate reader (at 25 °C). Decay of fluorescence intensity arising from 100 nM GFP was observed with increasing NP concentration. Nonlinear least-squares curve fitting analysis was carried out to estimate the binding constant (K_s).[27] The fluorescent titration between nanoparticles and dsRed was performed similarly except the excitation wavelength of 561 nm and emission wavelength of 585 nm.

7.2.5 Protein-NPSC complex formation

To make the protein-NPSC complex, 2.5 μM GIPA AuNPs were incubated with 1.5 μM of protein in 60 μL of phosphate buffer (5 mM, pH = 7.4) for 10 min. Then, 1 μL of linoleic acid was mixed with 500 μL of phosphate buffer (5 mM, pH = 7.4) containing 1 μM GIPA AuNPs and agitated with an amalgamator (Yinya New Materials Co. Ltd, Hangzhou, China) at 5000 rpm for 100 s to form emulsions. Finally, the mixture of the protein and GIPA AuNPs were diluted to 135 μL with phosphate buffer (5 mM, pH = 7.4) followed by the addition of 15 μL of the emulsion. The protein-NPSC complexes were ready to use after 10 min of incubation at room temperature. The final concentrations of GIPA AuNPs and the protein were 1.5 μM and 600 nM, respectively.

7.2.6 Protein delivery

A total of 240,000 HeLa cells were cultured in a confocal dish for 24 hrs prior to delivery. The cells were washed with cold phosphate buffer saline (PBS) thrice right before delivery. After preparation, the cells were incubated in protein-NPSC complex solution (150 μL of the complex diluted by 1.35 mL of the DMEM without FBS) for 1 hr, followed by incubating with fresh DMEM

(with 10% FBS) for 10 min, unless otherwise mentioned. The cells were then kept in PBS and imaged by a laser scanning confocal microscope (LSM 510, Zeiss, Germany).

7.2.7 X-gal staining

Cells were stained according to the assay kit (Genlantis, USA). Briefly, cells were washed with PBS once and fixed with the fixation solution followed by 4 hrs of staining. Cells were then washed once with PBS and observed under an optical microscope. Experiments were performed in triplicate.

7.3 Results and Discussion

The key design parameters for NPSC formation is the presence of a guanidinium group to pin the particle to the fatty acid droplet through hydrogen bonding and electrostatic interactions.[28] The short peptide HKRK on the ligand terminal of our NPSC delivery platform contains two lysine residues that increase positive charge density. As strong electrostatic interaction may result in inefficient release of proteins with high molecular weight, we truncated the structure of HKRK, leaving only imidazole and guanidine groups on the ligand. We synthesized the terminal based on a histidine derivative, adding the guanidine group to mimic a peptide terminal with reduced charge density (Figure 7.2). The imidazole residue on the histidine derivative provides a positive charge equally distributed between two nitrogen atoms at physiological pH. Moreover, it facilitates delivery due to a proton sponge function that promotes protein release if the payload is entrapped in endosomes.[29] The guanidine group interacts with both the protein payload and the oil core to stabilize the NPSC structure.[30]

GIPA AuNPs were prepared using 2 nm AuNPs (Figures 7.3, 7.4) through a place-exchange reaction. From TEM results, there was no obvious difference in the core sizes before and after GIPA ligand exchange. The zeta-potential of GIPA AuNPs was measured to determine the surface charge. As expected, although these AuNPs are positively charged (zeta potential: 15 ± 1 mV), their surface charge density was lower than HKRK AuNPs (zeta potential: 32 ± 1 mV).[31] The reduced charge density of AuNPs would be expected to weaken the interaction of the NP with proteins; fluorescent protein dsRed (a tetramer with a molecular weight of 112 kD)[32] was titrated with GIPA AuNPs. When AuNPs bind with dsRed, the protein fluorescence is quenched[33] due to the energy transfer from the photo-excited fluorescent proteins to AuNPs.[34, 35] The titration[27] results revealed that the binding constants of AuNPs to dsRed were different (Figure 7.5). The binding constant (Ks) of HKRK AuNPs dsRed was (1.9 ± 0.9) × 10^{10} M^{-1}, whereas the binding constant of GIPA AuNPs with dsRed was (1.3 ± 0.4) × 10^{8} M^{-1}.

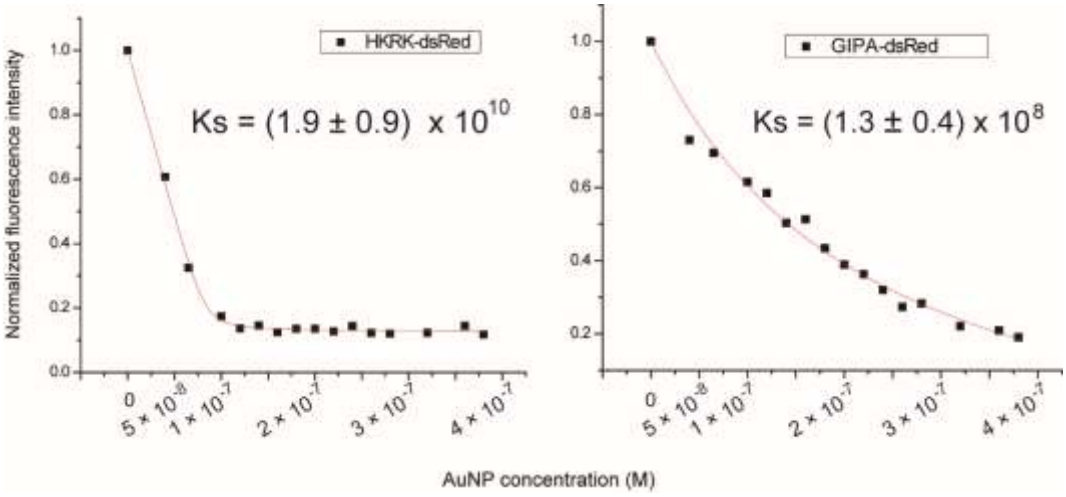

Figure 7.5. Fluorescence titrations of AuNPs in the presence of fluorescent proteins.

DsRed was likewise an advantageous protein to test the efficacy of GIPA NPSC-based protein delivery due to its strong fluorescence and large size. After the formation of dsRed-NPSCs,

the overall capsule diameter was 130 ± 55 nm (Figure 7.6), similarly to what we have previously reported.[20] The NPSCs were diluted with Dulbecco's Modified Eagle Medium for cell culture experiments, and after 1 hr incubation, we measured the efficiency of dsRed delivery into cells. Flow cytometry results indicated that 65% cells were stained with dsRed (Figure 7.7). The average fluorescence intensity was 7 times higher than control groups. In comparison, only 18% cells showed uptake of dsRed when delivered with HKRK NPSCs, indicating poor performance of this platform delivering proteins of large size. Notably, dsRed was observed evenly distributed throughout the cytosol, but not in nucleus (Figure 7.7e). 3D image projections further confirmed this cytoplasmic distribution of dsRed (Figure 7.7f). As proteins with molecular weight higher than 60 kD cannot diffuse passively into the nucleus,[36] these results show that dsRed is in its native tetramer structure. Together these data demonstrate that GIPA AuNPs are able of efficiently delivering large proteins into the cytosol without affecting their structure.

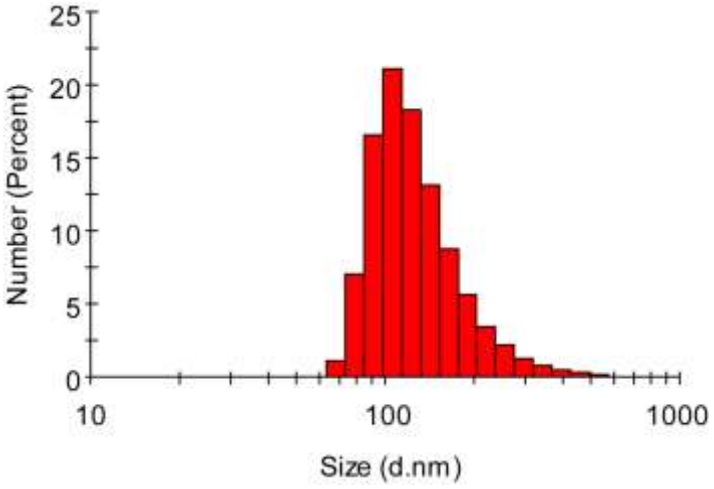

Figure 7.6. DLS histogram of dsRed-NPSCs indicating an average diameter of 130 ± 50 nm.

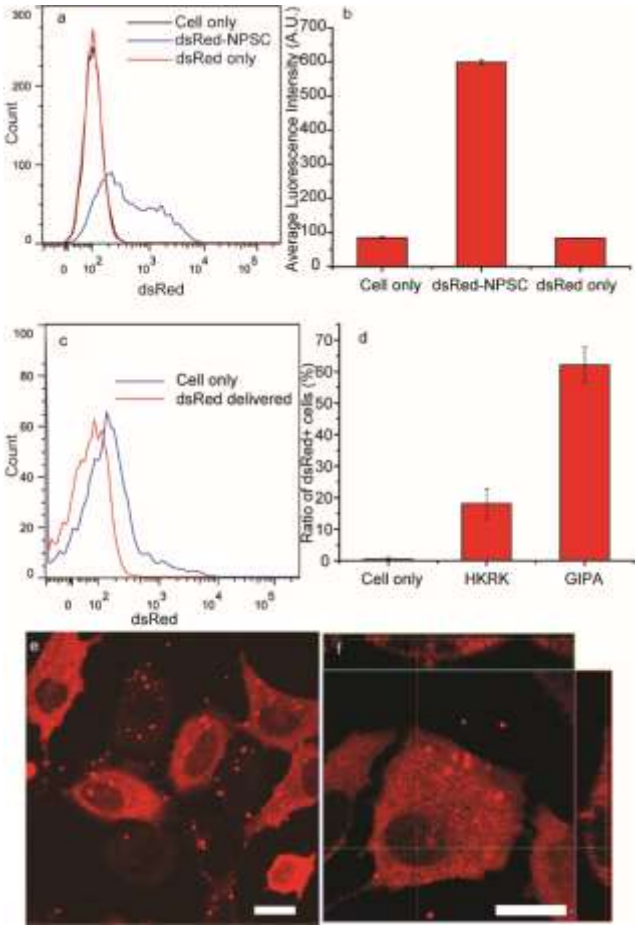

Figure 7.7. Delivery of dsRed to cytosol of HeLa cells. a) Flow cytometry results of dsRed delivery by GIPA NPSCs. b) Quantification of average fluorescence intensity of cells. c) Flow cytometry results of dsRed delivery by HKRK NPSCs. d) Quantification indicates GIPA NPSC has much higher efficiency for the delivery of dsRed. e) LSCM image showing dsRed delivery into HeLa cells by GIPA NPSCs. f) Z-stack image of dsRed delivery. Scale bars: 20 µm.

Delivery of enzymes into cells is a promising strategy for enzyme replacement and prodrug activation therapies. While we have demonstrated that caspase-3, an apoptotic enzyme of small size, can be rapidly delivered into the cytosol using a NPSC platform,[20] the creation of delivery platform for enzymes of higher molecular weight would greatly expand the utility of this strategy. Rapid delivery of *β*-gal to the cytosol is a promising approach for efficient prodrug activation therapy in cancer cells,[37, 38] yet the large size of this enzyme (464 kD) in its tetrameric

form is an obstacle for cytosolic access.[18] We assessed whether the GIPA NPSC platform was capable of efficiently delivering *β*-gal into the cytosol in HeLa. The size of *β*-gal-GIPA NPSCs is 110 ± 50 nm when measured by dynamic light scattering (DLS; Figure 7.8). Delivery of fluorescein isothiocyanate labeled *β*-gal (FITC-*β*-gal) revealed the cytosolic but not nuclear distribution of the protein after 1 hr delivery (Figure 7.9a), similar to that of dsRed. Due to its large size, *β*-gal cannot passively diffuse into nucleus. By delivering FITC-*β*-gal we were able to confirm that GIPA NPSCs efficiently deliver *β*-gal specifically into the cytosol. X-gal staining was then used to demonstrate retention of enzymatic activity of delivered *β*-gal. After delivery, the media was removed and cells were stained with X-gal for 4 hr. Notably, *β*-gal bound to GIPA NPSCs, but not *β*-gal alone, was efficiently delivered to the cell (Figure 7.9 b-d). Thus, GIPA NPSC platforms are capable of delivering functional enzymes of large size into cells without hampering their structure or function.

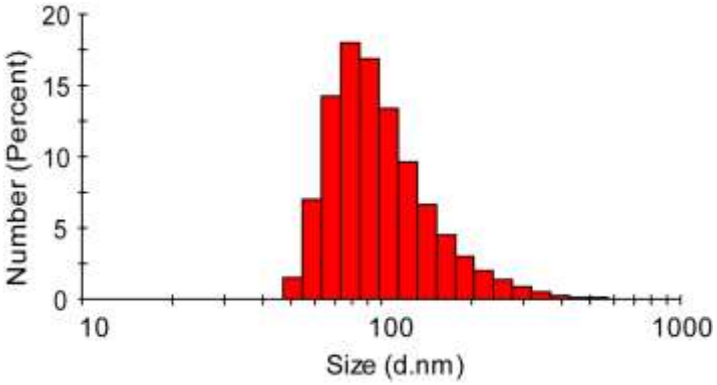

Figure 7.8. DLS histogram of *β*-Gal-NPSCs indicating an average diameter of 110 ± 50 nm.

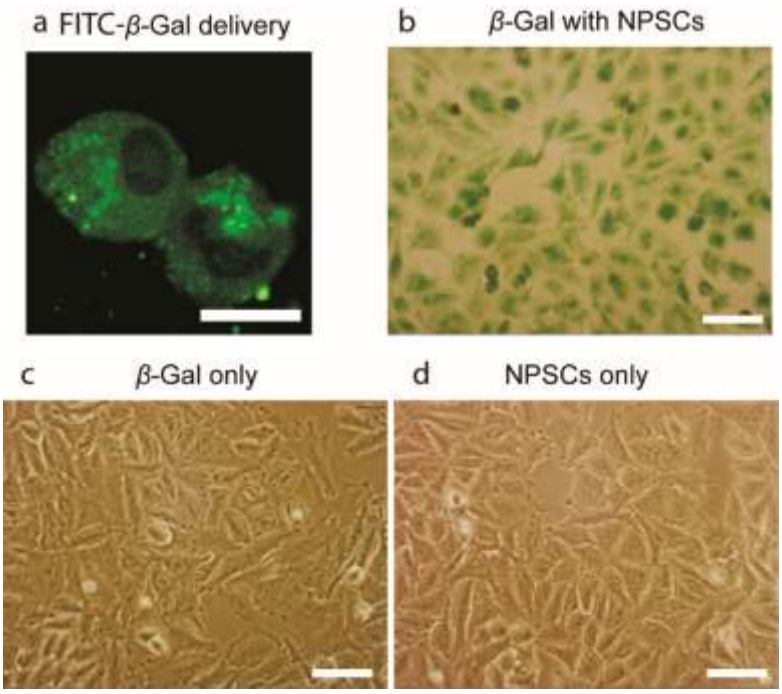

Figure 7.9. Distribution of *β*-gal in HeLa cells after delivery. a) LSCM image showing FITC- *β*-gal delivery. Scale bar: 10 µm. b) X-gal staining of delivered *β*-gal in HeLa cells. c) X-gal staining of cells incubated with free *β*-gal alone. d) X-gal staining of cells incubated with NPSCs alone. Scale bars: 100 µm.

7.4 Conclusion

In summary, we have developed an effective intracellular delivery strategy for proteins of high molecular weight using GIPA AuNPs stabilized capsules. GIPA AuNPs interact weakly with proteins and rapidly deliver the payload into the cytosol via a protein-GIPA NPSC complex. Both dsRed and *β*-galactosidase are effectively transduced into cells without hampering their native structures and functions. These studies demonstrate the use of supramolecular chemistry to tune the interaction between ligands of nanoparticles and proteins, providing a strategy for optimizing nanomaterial delivery vehicles.

7.5 References

1. S. Kobsa, W. M. Saltzman, *Pediatr. Res.* **2008**, *63*, 513.

2. J. A. Zuris, D. B. Thompson, Y. Shu, J. P. Guilinger, J. L. Bessen, J. H. Hu, M. L. Maeder, J. K. Joung, Z.-Y. Chen, D. R. Liu, *Nat. Biotechnol.* **2015**, *33*, 73.
3. M. Peitz, K. Pfannkuche, K. Rajewsky, F. Edenhofer, *Proc. Natl. Acad. Sci. U. S. A.* **2002**, *99*, 4489.
4. H. Zhou, S. Wu, J. Y. Joo, S. Zhu, D. W. Han, T. Lin, S. Trauger, G. Bien, S. Yao, Y. Zhu, G. Siuzdak, H. R. Schöler, L. Duan, S. Ding, *Cell Stem Cell* **2009**, *4*, 381.
5. E. R. Lorden, H. M. Levinson, K. W. Leong, *Drug Deliv. Transl. Res.* **2013**, *5*, 168.
6. S. Barrientos, H. Brem, O. Stojadinovic, M. Tomic-Canic, *Wound Repair Regen.* **2014**, *22*, 569.
7. I. Sassoon, V. Blanc, in *Antibody-Drug Conjugates*, Vol. 1045 (Ed: L. Ducry), Humana Press, 2013, 1.
8. C. Peters, S. Brown, *Biosci. Rep.* **2015**, *35*.
9. S.-h. Kan, M. Aoyagi-Scharber, S. Q. Le, J. Vincelette, K. Ohmi, S. Bullens, D. J. Wendt, T. M. Christianson, P. M. N. Tiger, J. R. Brown, R. Lawrence, B. K. Yip, J. Holtzinger, A. Bagri, D. Crippen-Harmon, K. N. Vondrak, Z. Chen, C. M. Hague, J. C. Woloszynek, D. S. Cheung, K. A. Webster, E. G. Adintori, M. J. Lo, W. Wong, P. A. Fitzpatrick, J. H. LeBowitz, B. E. Crawford, S. Bunting, P. I. Dickson, E. F. Neufeld, *Proc. Natl. Acad. Sci. U. S. A.* **2014**, *111*, 14870.
10. W. Ardelt, K. Shogen, Z. Darzynkiewicz, *Curr. Pharm. Biotechnol.* **2008**, *9*, 215.
11. Y. Lu, W. Sun, Z. Gu, *J. Control. Release* **2014**, *194*, 1.
12. Z. Gu, A. Biswas, M. Zhao, Y. Tang, *Chem. Soc. Rev.* **2011**, *40*, 3638.
13. W. Sun, Y. Lu, Z. Gu, *Part. Part. Syst. Charact.* **2014**, *31*, 1204.
14. Y.-C. Yeh, R. Tang, R. Mout, Y. Jeong, V. M. Rotello, *Angew. Chem. Int. Ed.* **2014**, *53*, 5137.
15. H. Räägel, P. Säälik, M. Pooga, *BBA-Biomembranes* **2010**, *1798*, 2240.
16. M. P. Stewart, A. Lorenz, J. Dahlman, G. Sahay, *Wiley Interdisciplinary Reviews: Nanomedicine and Nanobiotechnology* **2015**, n/a.
17. A. Erazo-Oliveras, N. Muthukrishnan, R. Baker, T.-Y. Wang, J.-P. Pellois, *Pharmaceuticals* **2012**, *5*, 1177.
18. J. D. Brodin, A. J. Sprangers, J. R. McMillan, C. A. Mirkin, *J. Am. Chem. Soc.* **2015**, *137*, 14838.
19. A. Watabe, T. Yamaguchi, T. Kawanishi, E. Uchida, A. Eguchi, H. Mizuguchi, T. Mayumi, M. Nakanishi, T. Hayakawa, *BBA-Biomembranes* **1999**, *1416*, 339.
20. R. Tang, C. S. Kim, D. J. Solfiell, S. Rana, R. Mout, E. M. Velázquez-Delgado, A. Chompoosor, Y. Jeong, B. Yan, Z.-J. Zhu, C. Kim, J. A. Hardy, V. M. Rotello, *ACS Nano* **2013**, *7*, 6667.
21. M. Ray, R. Tang, Z. Jiang, V. M. Rotello, *Bioconjugate Chem.* **2015**, *26*, 1004.
22. A. Chompoosor, G. Han, V. M. Rotello, *Bioconjugate Chem.* **2008**, *19*, 1342.
23. K. Ohara, J. J. Vasseur, M. Smietana, *Tetrahedron Lett.* **2009**, *50*, 1463.
24. M. Brust, M. Walker, D. Bethell, D. J. Schiffrin, R. Whyman, *J. Chem. Soc, Chem. Commun.* **1994**, 801.
25. M. J. Hostetler, A. C. Templeton, R. W. Murray, *Langmuir* **1999**, *15*, 3782.
26. X. O. Liu, M. Atwater, J. H. Wang, Q. Huo, *Colloid Surf. B-Biointerfaces* **2007**, *58*, 3.
27. C.-C. You, M. De, G. Han, V. M. Rotello, *J. Am. Chem. Soc.* **2005**, *127*, 12873.
28. A. T. Wright, M. J. Griffin, Z. Zhong, S. C. McCleskey, E. V. Anslyn, J. T. McDevitt, *Angewandte Chemie* **2005**, *117*, 6533.
29. P. Midoux, C. Pichon, J.-J. Yaouanc, P.-A. Jaffrès, *Br. J. Pharmacol.* **2009**, *157*, 166.
30. X.-C. Yang, B. Samanta, S. S. Agasti, Y. Jeong, Z.-J. Zhu, S. Rana, O. R. Miranda, V. M. Rotello, *Angew. Chem. Int. Ed.* **2011**, *50*, 477.
31. P. Ghosh, X. Yang, R. Arvizo, Z.-J. Zhu, S. S. Agasti, Z. Mo, V. M. Rotello, *J. Am. Chem. Soc.* **2010**, *132*, 2642.
32. B. Lounis, J. Deich, F. I. Rosell, S. G. Boxer, W. E. Moerner, *J. Phys. Chem. B* **2001**, *105*, 5048.

33. R. Mout, G. Y. Tonga, M. Ray, D. F. Moyano, Y. Xing, V. M. Rotello, *Nanoscale* **2014**, *6*, 8873.
34. Z. Jiang, N. D. B. Le, A. Gupta, V. M. Rotello, *Chem. Soc. Rev.* **2015**, *44*, 4264.
35. S. Saraswat, A. Desireddy, D. Zheng, L. Guo, H. P. Lu, T. P. Bigioni, D. Isailovic, *J. Phys. Chem. C* **2011**, *115*, 17587.
36. C. Dingwall, R. A. Laskey, *Annu. Rev. Cell Biol.* **1986**, *2*, 367.
37. T. Legigan, J. Clarhaut, I. Tranoy-Opalinski, A. Monvoisin, B. Renoux, M. Thomas, A. Le Pape, S. Lerondel, S. Papot, *Angew. Chem. Int. Ed.* **2012**, *51*, 11606.
38. L. F. Tietze, B. Krewer, *Chem. Biol. Drug Des.* **2009**, *74*, 205.

BIBLIOGRAPHY

S. A. Adam, Nuclear protein import in permeabilized mammalian cells requires soluble cytoplasmic factors. *J. Cell Biol.* **1990**, *111*, 807.

S. S. Agasti, A. Chompoosor, C. C. You, P. Ghosh, C. K. Kim, V. M. Rotello, Photoregulated Release of Caged Anticancer Drugs from Gold Nanoparticles. *J. Am. Chem. Soc.* **2009**, *131*, 5728.

M. R. Almofti, H. Harashima, Y. Shinohara, A. Almofti, Y. Baba, H. Kiwada, Cationic liposome-mediated gene delivery: Biophysical study and mechanism of internalization. *Arch. Biochem. Biophys.* **2003**, *410*, 246.

W. Ardelt, K. Shogen, Z. Darzynkiewicz, Onconase and Amphinase, the Antitumor Ribonucleases from Rana pipiens Oocytes. *Curr. Pharm. Biotechnol.* **2008**, *9*, 215.

Y. Arima, H. Iwata, Effect of wettability and surface functional groups on protein adsorption and cell adhesion using well-defined mixed self-assembled monolayers. *Biomaterials* **2007**, *28*, 3074.

L. Bacakova, E. Filova, M. Parizek, T. Ruml, V. Svorcik, Modulation of cell adhesion, proliferation and differentiation on materials designed for body implants. *Biotechnol. Adv.* **2011**, *29*, 739.

T. L. Barr, *Modern ESCA: the Principles and Practice of X-Ray Photoelectron Spectroscopy*, CRC Press, Boca Raton 1994.

S. Barrientos, H. Brem, O. Stojadinovic, M. Tomic-Canic, Clinical application of growth factors and cytokines in wound healing. *Wound Repair Regen.* **2014**, *22*, 569.

H. Bayraktar, P. S. Ghosh, V. M. Rotello, M. J. Knapp, Disruption of protein-protein interactions using nanoparticles: inhibition of cytochrome c peroxidase. *Chem. Commun.* **2006**, 1390.

M. Beck, Therapy for lysosomal storage disorders. *IUBMB Life* **2010**, *62*, 33.

B. J. Bennion, V. Daggett, The molecular basis for the chemical denaturation of proteins by urea. *Proc. Natl. Acad. Sci. U. S. A.* **2003**, *100*, 5142.

J. M. Berg, J. L. Tymoczko, L. Stryer, Springer Science + Business Media, 2013.

C. C. Berton-Carabin, K. Schroen, Pickering Emulsions for Food Applications: Background, Trends, and Challenges. *Annu. Rev. Food Sci. Technol.* **2015**, *6*, 263.

S. Blanco, M. Frye, Role of RNA methyltransferases in tissue renewal and pathology. *Curr. Opin. Cell Biol.* **2014**, *31*, 1.

M. Borriello, P. Laccetti, G. Terrazzano, G. D'Alessio, C. De Lorenzo, A novel fully human antitumour immunoRNase targeting ErbB2-positive tumours. *Br. J. Cancer* **2011**, *104*, 1716.

M. Bosch, A. Benito, M. Ribó, T. Puig, B. Beaumelle, M. Vilanova, A Nuclear Localization Sequence Endows Human Pancreatic Ribonuclease with Cytotoxic Activity. *Biochemistry* **2004**, *43*, 2167.

D. A. Brafman, C. W. Chang, A. Fernandez, K. Willert, S. Varghese, S. Chien, Long-term human pluripotent stem cell self-renewal on synthetic polymer surfaces. *Biomaterials* **2010**, *31*, 9135.

M. F. Brizzi, G. Tarone, P. Defilippi, Extracellular matrix, integrins, and growth factors as tailors of the stem cell niche. *Curr. Opin. Cell Biol.* **2012**, *24*, 645.

J. D. Brodin, A. J. Sprangers, J. R. McMillan, C. A. Mirkin, DNA-Mediated Cellular Delivery of Functional Enzymes. *J. Am. Chem. Soc.* **2015**, *137*, 14838.

Y. Y. Broza, H. Haick, Nanomaterial-based sensors for detection of disease by volatile organic compounds. *Nanomedicine* **2013**, *8*, 785.

C. Bruedigam, M. v. Driel, M. Koedam, J. v. d. Peppel, B. C. J. van der Eerden, M. Eijken, J. P. T. M. van Leeuwen, in *Current Protocols in Stem Cell Biology*, Wiley-Blackwell, 2011.

M. Brust, M. Walker, D. Bethell, D. J. Schiffrin, R. Whyman, Synthesis of thiol-derivatised gold nanoparticles in a two-phase Liquid-Liquid system. *J. Cheml Soci. Chem. Commun.* **1994**, 801.

Z. Cai, Z. Ye, X. Yang, Y. Chang, H. Wang, Y. Liu, A. Cao, Encapsulated enhanced green fluorescence protein in silica nanoparticle for cellular imaging. *Nanoscale* **2011**, *3*, 1974.

Z. Cao, S. Geng, L. Li, C. Lu, Detecting intracellular translocation of native proteins quantitatively at the single cell level. *Chem. Sci.* **2014**, *5*, 2530.

P. Carroll, L. J. Schreuder, J. Muwanguzi-Karugaba, S. Wiles, B. D. Robertson, J. Ripoll, T. H. Ward, G. J. Bancroft, U. E. Schaible, T. Parish, Sensitive detection of gene expression in mycobacteria under replicating and non-replicating conditions using optimized far-red reporters. *PLoS One* **2010**, *5*, e9823.

A. D. Celiz, J. G. W. Smith, R. Langer, D. G. Anderson, D. A. Winkler, D. A. Barrett, M. C. Davies, L. E. Young, C. Denning, M. R. Alexander, Materials for stem cell factories of the future. *Nat. Mater.* **2014**, *13*, 570.

M. E. Cerf, Beta Cell Dysfunction and Insulin Resistance. *Frontiers in Endocrinology* **2013**, *4*, 37.

H.-I. Chang, M.-K. Yeh, Clinical development of liposome-based drugs: formulation, characterization, and therapeutic efficacy. *Int. J. Nanomed.* **2012**, *7*, 49.

Y. Chevalier, M. A. Bolzinger, Emulsions stabilized with solid nanoparticles: Pickering emulsions. *Colloid Surf. A-Physicochem. Eng. Asp.* **2013**, *439*, 23.

K. C. Cho, J. H. Jeong, H. J. Chung, C. O. Joe, S. W. Kim, T. G. Park, Folate receptor-mediated intracellular delivery of recombinant caspase-3 for inducing apoptosis. *J. Control. Release* **2005**, *108*, 121.

A. Chompoosor, G. Han, V. M. Rotello, Charge dependence of ligand release and monolayer stability of gold nanoparticles by biogenic thiols. *Bioconjugate Chem.* **2008**, *19*, 1342.

P. Corish, C. Tyler-Smith, Attenuation of green fluorescent protein half-life in mammalian cells. *Protein Engineering* **1999**, *12*, 1035.

J. J. Cronican, D. B. Thompson, K. T. Beier, B. R. McNaughton, C. L. Cepko, D. R. Liu, Potent delivery of functional proteins into mammalian cells in vitro and in vivo using a supercharged protein. *ACS Chem. Biol.* **2010**, *5*, 747.

J. M. Curran, R. Chen, J. A. Hunt, Controlling the phenotype and function of mesenchymal stem cells in vitro by adhesion to silane-modified clean glass surfaces. *Biomaterials* **2005**, *26*, 7057.

J. M. Curran, R. Chen, J. A. Hunt, The guidance of human mesenchymal stem cell differentiation in vitro by controlled modifications to the cell substrate. *Biomaterials* **2006**, *27*, 4783.

C. A. Custodio, R. L. Reis, J. F. Mano, Engineering Biomolecular Microenvironments for Cell Instructive Biomaterials. *Adv. Healthcare Mater.* **2014**, *3*, 797.

V. M. R. D. F. Moyano, *Cellular and subcellular nanotechnology : methods and protocols*, Humana Press ; Springer, New York 2013.

R. M. P. da Silva, J. F. Mano, R. L. Reis, Smart thermoresponsive coatings and surfaces for tissue engineering: switching cell-material boundaries. *Trends Biotechnol.* **2007**, *25*, 577.

M. J. Dalby, N. Gadegaard, R. O. C. Oreffo, Harnessing nanotopography and integrin–matrix interactions to influence stem cell fate. *Nat. Mater.* **2014**, *13*, 558.

C. V. Dang, W. M. Lee, Identification of the human c-myc protein nuclear translocation signal. *Mol. Cell. Biol.* **1988**, *8*, 4048.

W. H. De Jong, P. J. A. Borm, Drug delivery and nanoparticles: Applications and hazards. *Int. J. Nanomed.* **2008**, *3*, 133.
E. J. de la Rosa, F. de Pablo, Cell death in early neural development: beyond the neurotrophic theory. *Trends Neurosci.* **2000**, *23*, 454.
M. De, S. Rana, H. Akpinar, O. R. Miranda, R. R. Arvizo, U. H. F. Bunz, V. M. Rotello, Sensing of proteins in human serum using conjugates of nanoparticles and green fluorescent protein. *Nat. Chem.* **2009**, *1*, 461.
Y. Ding, Z. Jiang, K. Saha, C. S. Kim, S. T. Kim, R. F. Landis, V. M. Rotello, Gold Nanoparticles for Nucleic Acid Delivery. *Mol. Ther.* **2014**, *22*, 1075.
C. Dingwall, R. A. Laskey, Protein import into the cell nucleus. *Annu. Rev. Cell Biol.* **1986**, *2*, 367.
A. D. Dinsmore, M. F. Hsu, M. G. Nikolaides, M. Marquez, A. R. Bausch, D. A. Weitz, Colloidosomes: Selectively permeable capsules composed of colloidal particles. *Science* **2002**, *298*, 1006.
A. A. Dominguez, W. A. Lim, L. S. Qi, Beyond editing: repurposing CRISPR-Cas9 for precision genome regulation and interrogation. *Nat. Rev. Mol. Cell Biol.* **2016**, *17*, 5.
G. Doria, J. Conde, B. Veigas, L. Giestas, C. Almeida, M. Assunção, J. Rosa, P. V. Baptista, Noble Metal Nanoparticles for Biosensing Applications. *Sensors* **2012**, *12*, 1657.
S. J. Doxsey, J. Sambrook, A. Helenius, J. White, An efficient method for introducing macromolecules into living cells. *J. Cell Biol.* **1985**, *101*, 19.
B. Duncan, X. Li, R. F. Landis, S. T. Kim, A. Gupta, L.-S. Wang, R. Ramanathan, R. Tang, J. A. Boerth, V. M. Rotello, Nanoparticle-Stabilized Capsules for the Treatment of Bacterial Biofilms. *ACS Nano* **2015**, *9*, 7775.
A. Dzimitrowicz, P. Jamroz, K. Greda, P. Nowak, M. Nyk, P. Pohl, The influence of stabilizers on the production of gold nanoparticles by direct current atmospheric pressure glow microdischarge generated in contact with liquid flowing cathode. *J. Nanopart. Res.* **2015**, *17*, 185.
A. G. Efthymiou, G. Chen, M. Rao, G. Chen, M. Boehm, Self-renewal and cell lineage differentiation strategies in human embryonic stem cells and induced pluripotent stem cells. *Expert Opin. Biol. Ther.* **2014**, *14*, 1333.
S. G. Elci, D. F. Moyano, S. Rana, G. Y. Tonga, R. L. Phillips, U. H. F. Bunz, V. M. Rotello, Recognition of glycosaminoglycan chemical patterns using an unbiased sensor array. *Chem. Sci.* **2013**, *4*, 2076.
M. R. Elliott, K. S. Ravichandran, Clearance of apoptotic cells: implications in health and disease. *J. Cell Biol.* **2010**, *189*, 1059.
Y. Engel, J. D. Schiffman, J. M. Goddard, V. M. Rotello, Nanomanufacturing of biomaterials. *Mater. Today* **2012**, *15*, 478.
A. J. Engler, S. Sen, H. L. Sweeney, D. E. Discher, Matrix Elasticity Directs Stem Cell Lineage Specification. *Cell* **2006**, *126*, 677.
A. Erazo-Oliveras, N. Muthukrishnan, R. Baker, T.-Y. Wang, J.-P. Pellois, Improving the Endosomal Escape of Cell-Penetrating Peptides and Their Cargos: Strategies and Challenges. *Pharmaceuticals* **2012**, *5*, 1177.
A. Erazo-Oliveras, K. Najjar, L. Dayani, T.-Y. Wang, G. A. Johnson, J.-P. Pellois, Protein delivery into live cells by incubation with an endosomolytic agent. *Nat. Methods* **2014**, *11*, 861.
J. Estelrich, M. J. Sánchez-Martín, M. A. Busquets, Nanoparticles in magnetic resonance imaging: from simple to dual contrast agents. *Int. J. Nanomed.* **2015**, *10*, 1727.

A. B. Faia-Torres, S. Guimond-Lischer, M. Rottmar, M. Charnley, T. Goren, K. Maniura-Weber, N. D. Spencer, R. L. Reis, M. Textor, N. M. Neves, Differential regulation of osteogenic differentiation of stem cells on surface roughness gradients. *Biomaterials* **2014**, *35*, 9023.

P. F. Foltopoulou, A. S. Tsiftsoglou, I. D. Bonovolias, A. T. Ingendoh, L. C. Papadopoulou, Intracellular delivery of full length recombinant human mitochondrial L-Sco2 protein into the mitochondria of permanent cell lines and SCO2 deficient patient's primary cells. *Biochim. Biophys. Acta-Mol. Basis Dis.* **2010**, *1802*, 497.

S. J. Forbes, N. Rosenthal, Preparing the ground for tissue regeneration: from mechanism to therapy. *Nat. Med.* **2014**, *20*, 857.

S. Foster, C. L. Duvall, E. F. Crownover, A. S. Hoffman, P. S. Stayton, Intracellular delivery of a protein antigen with an endosomal-releasing polymer enhances CD8 T-cell production and prophylactic vaccine efficacy. *Bioconjugate Chem.* **2010**, *21*, 2205.

C. Frantz, K. M. Stewart, V. M. Weaver, The extracellular matrix at a glance. *J. Cell Sci.* **2010**, *123*, 4195.

N. Freitas, C. Cunha, Mechanisms and Signals for the Nuclear Import of Proteins. *Curr. Genomics* **2009**, *10*, 550.

H. Fried, U. Kutay, Nucleocytoplasmic transport: taking an inventory. *Cellular and Molecular Life Sciences CMLS*, *60*, 1659.

A. Fu, R. Tang, J. Hardie, M. E. Farkas, V. M. Rotello, Promises and Pitfalls of Intracellular Delivery of Proteins. *Bioconjugate Chem.* **2014**, *25*, 1602.

J. Fukuda, A. Khademhosseini, J. Yeh, G. Eng, J. Cheng, O. C. Farokhzad, R. Langer, Micropatterned cell co-cultures using layer-by-layer deposition of extracellular matrix components. *Biomaterials* **2006**, *27*, 1479.

T. Gaj, J. Guo, Y. Kato, S. J. Sirk, C. F. Barbas, 3rd, Targeted gene knockout by direct delivery of zinc-finger nuclease proteins. *Nat. Methods* **2012**, *9*, 805.

J. L. García, A. Asadinezhad, J. Pacherník, M. Lehocký, I. Junkar, P. Humpolíček, P. Sáha, P. Valášek, Cell Proliferation of HaCaT Keratinocytes on Collagen Films Modified by Argon Plasma Treatment. *Molecules* **2010**, *15*, 2845.

G. Ghiaur, S. Yegnasubramanian, B. Perkins, J. L. Gucwa, J. M. Gerber, R. J. Jones, Regulation of human hematopoietic stem cell self-renewal by the microenvironment's control of retinoic acid signaling. *Proc. Natl. Acad. Sci. U. S. A.* **2013**, *110*, 16121.

P. Ghosh, X. C. Yang, R. Arvizo, Z. J. Zhu, S. S. Agasti, Z. H. Mo, V. M. Rotello, Intracellular Delivery of a Membrane-Impermeable Enzyme in Active Form Using Functionalized Gold Nanoparticles. *J. Am. Chem. Soc.* **2010**, *132*, 2642.

P. S. Ghosh, C. K. Kim, G. Han, N. S. Forbes, V. M. Rotello, Efficient Gene Delivery Vectors by Tuning the Surface Charge Density of Amino Acid-Functionalized Gold Nanoparticles. *ACS Nano* **2008**, *2*, 2213.

W. Götz, C. Reichert, L. Canullo, A. Jäger, F. Heinemann, Coupling of osteogenesis and angiogenesis in bone substitute healing – A brief overview. *Ann. Anat.* **2012**, *194*, 171.

S. J. Gould, G. A. Keller, N. Hosken, J. Wilkinson, S. Subramani, A conserved tripeptide sorts proteins to peroxisomes. *J. Cell Biol.* **1989**, *108*, 1657.

D. Grafahrend, K.-H. Heffels, M. V. Beer, P. Gasteier, M. Möller, G. Boehm, P. D. Dalton, J. Groll, Degradable polyester scaffolds with controlled surface chemistry combining minimal protein adsorption with specific bioactivation. *Nat. Mater.* **2010**, *10*, 67.

Z. Gu, A. Biswas, M. X. Zhao, Y. Tang, Tailoring nanocarriers for intracellular protein delivery. *Chem. Soc. Rev.* **2011**, *40*, 3638.

L. Guo, N. Kawazoe, Y. Fan, Y. Ito, J. Tanaka, T. Tateishi, X. Zhang, G. Chen, Chondrogenic differentiation of human mesenchymal stem cells on photoreactive polymer-modified surfaces. *Biomaterials* **2008**, *29*, 23.

G. Han, N. S. Chari, A. Verma, R. Hong, C. T. Martin, V. M. Rotello, Controlled recovery of the transcription of nanoparticle-bound DNA by intracellular concentrations of glutathione. *Bioconjugate Chem.* **2005**, *16*, 1356.

G. Han, C. C. You, B. J. Kim, R. S. Turingan, N. S. Forbes, C. T. Martin, V. M. Rotello, Light-regulated release of DNA and its delivery to nuclei by means of photolabile gold nanoparticles. *Angew Chem Int Edit* **2006**, *45*, 3165.

W. Hanna-Rose, M. Han, COG-2, a Sox domain protein necessary for establishing a functional vulval-uterine connection in Caenorhabditis elegans. *Development* **1999**, *126*, 169.

Z. He, J. J. Li, C. H. Zhen, L. Y. Feng, X. Y. Ding, Effect of leukemia inhibitory factor on embryonic stem cell differentiation: implications for supporting neuronal differentiation. *Acta Pharmacol. Sin.* **2006**, *27*, 80.

S. T. Henriques, H. Costa, M. Castanho, Translocation of beta-galactosidase mediated by the cell-penetrating peptide pep-1 into lipid vesicles and human HeLa cells is driven by membrane electrostatic potential. *Biochemistry* **2005**, *44*, 10189.

U. Hersel, C. Dahmen, H. Kessler, RGD modified polymers: biomaterials for stimulated cell adhesion and beyond. *Biomaterials* **2003**, *24*, 4385.

S. W. Hicks, J. E. Galan, Exploitation of eukaryotic subcellular targeting mechanisms by bacterial effectors. *Nat. Rev. Microbiol.* **2013**, *11*, 316.

M. J. Hostetler, S. J. Green, J. J. Stokes, R. W. Murray, Monolayers in Three Dimensions: Synthesis and Electrochemistry of ω-Functionalized Alkanethiolate-Stabilized Gold Cluster Compounds. *J. Am. Chem. Soc.* **1996**, *118*, 4212.

M. J. Hostetler, A. C. Templeton, R. W. Murray, Dynamics of Place-Exchange Reactions on Monolayer-Protected Gold Cluster Molecules. *Langmuir* **1999**, *15*, 3782.

P. Hou, Y. Li, X. Zhang, C. Liu, J. Guan, H. Li, T. Zhao, J. Ye, W. Yang, K. Liu, J. Ge, J. Xu, Q. Zhang, Y. Zhao, H. Deng, Pluripotent Stem Cells Induced from Mouse Somatic Cells by Small-Molecule Compounds. *Science* **2013**, *341*, 651.

T.-L. Hsu, Y.-C. Chang, S.-J. Chen, Y.-J. Liu, A. W. Chiu, C.-C. Chio, L. Chen, S.-L. Hsieh, Modulation of Dendritic Cell Differentiation and Maturation by Decoy Receptor 3. *J. Immunol.* **2002**, *168*, 4846.

W. Hu, B. E. Kemp, D. A. Jans, Kinetic properties of nuclear transport conferred by the retinoblastoma (Rb) NLS. *J. Cell. Biochem.* **2005**, *95*, 782.

X. Hu, S.-H. Park, E. S. Gil, X.-X. Xia, A. S. Weiss, D. L. Kaplan, The influence of elasticity and surface roughness on myogenic and osteogenic-differentiation of cells on silk-elastin biomaterials. *Biomaterials* **2011**, *32*, 8979.

J. Huang, Y. Yang, M. Al-Mozaini, P. S. Burke, J. Beamon, M. F. Carrington, K. Seiss, J. Rychert, E. S. Rosenberg, M. Lichterfeld, X. G. Yu, Dendritic Cell Dysfunction During Primary HIV-1 Infection. *J. Infect. Dis.* **2011**, *204*, 1557.

X. Huang, M. A. El-Sayed, Gold nanoparticles: Optical properties and implementations in cancer diagnosis and photothermal therapy. *J. Adv. Res.* **2010**, *1*, 13.

N. Huebsch, E. Lippens, K. Lee, M. Mehta, S. T. Koshy, M. C. Darnell, R. M. Desai, C. M. Madl, M. Xu, X. Zhao, O. Chaudhuri, C. Verbeke, W. S. Kim, K. Alim, A. Mammoto, D. E. Ingber, G. N. Duda, D. J. Mooney, Matrix elasticity of void-forming hydrogels controls transplanted-stem-cell-mediated bone formation. *Nat. Mater.* **2015**, *14*, 1269.

M. C. Hung, W. Link, Protein localization in disease and therapy. *J. Cell Sci.* **2011**, *124*, 3381.

T. Idziorek, J. Estaquier, F. De Bels, J.-C. Ameisen, YOPRO-1 permits cytofluorometric analysis of programmed cell death (apoptosis) without interfering with cell viability. *J. Immunol. Methods* **1995**, *185*, 249.

H. C. Ishikawa-Ankerhold, R. Ankerhold, G. P. C. Drummen, Advanced Fluorescence Microscopy Techniques—FRAP, FLIP, FLAP, FRET and FLIM. *Molecules* **2012**, *17*, 4047.

N. Jaiswal, S. E. Haynesworth, A. I. Caplan, S. P. Bruder, Osteogenic differentiation of purified, culture-expanded human mesenchymal stem cells in vitro. *J. Cell. Biochem.* **1997**, *64*, 295.

Y. Jeong, B. Duncan, M.-H. Park, C. Kim, V. M. Rotello, Reusable biocatalytic crosslinked microparticles self-assembled from enzyme-nanoparticle complexes. *Chem. Commun.* **2011**, *47*, 12077.

Y. Jiang, R. Tang, B. Duncan, Z. Jiang, B. Yan, R. Mout, V. M. Rotello, Direct Cytosolic Delivery of siRNA Using Nanoparticle-Stabilized Nanocapsules. *Angew Chem Int Edit* **2015**, *54*, 506.

Z. Jiang, N. D. B. Le, A. Gupta, V. M. Rotello, Cell surface-based sensing with metallic nanoparticles. *Chem. Soc. Rev.* **2015**, *44*, 4264.

Y.-P. Jiao, F.-Z. Cui, Surface modification of polyester biomaterials for tissue engineering. *Biomed. Mater.* **2007**, *2*, R24.

D. Jo, D. Y. Liu, S. Yao, R. D. Collins, J. Hawiger, Intracellular protein therapy with SOCS3 inhibits inflammation and apoptosis. *Nat. Med.* **2005**, *11*, 892.

B. J. Jordan, R. Hong, B. Gider, J. Hill, T. Emrick, V. M. Rotello, Stabilization of alpha-chymotrypsin at air-water interface through surface binding to gold nanoparticle scaffolds. *Soft Matter* **2006**, *2*, 558.

S. J. Kaczmarczyk, K. Sitaraman, T. Hill, J. L. Hartley, D. K. Chatterjee, Tus, an E. coli Protein, Contains Mammalian Nuclear Targeting and Exporting Signals. *PLoS One* **2010**, *5*, e8889.

S. J. Kaczmarczyk, K. Sitaraman, H. A. Young, S. H. Hughes, D. K. Chatterjee, Protein delivery using engineered virus-like particles. *Proc. Natl. Acad. Sci. U. S. A.* **2011**, *108*, 16998.

D. Kalderon, B. L. Roberts, W. D. Richardson, A. E. Smith, A short amino acid sequence able to specify nuclear location. *Cell* **1984**, *39*, 499.

S.-h. Kan, M. Aoyagi-Scharber, S. Q. Le, J. Vincelette, K. Ohmi, S. Bullens, D. J. Wendt, T. M. Christianson, P. M. N. Tiger, J. R. Brown, R. Lawrence, B. K. Yip, J. Holtzinger, A. Bagri, D. Crippen-Harmon, K. N. Vondrak, Z. Chen, C. M. Hague, J. C. Woloszynek, D. S. Cheung, K. A. Webster, E. G. Adintori, M. J. Lo, W. Wong, P. A. Fitzpatrick, J. H. LeBowitz, B. E. Crawford, S. Bunting, P. I. Dickson, E. F. Neufeld, Delivery of an enzyme-IGFII fusion protein to the mouse brain is therapeutic for mucopolysaccharidosis type IIIB. *Proc. Natl. Acad. Sci. U. S. A.* **2014**, *111*, 14870.

M. Kawamura, M. R. Urist, Growth-Factors, Mitogens, Cytokines, and Bone Morphogenetic Protein in Induced Chondrogenesis in Tissue-Culture. *Dev. Biol.* **1988**, *130*, 435.

T. Kawano, Y. Nakamichi, S. Fujinami, K. Nakajima, H. Yabu, M. Shimomura, Mechanical Regulation of Cellular Adhesion onto Honeycomb-Patterned Porous Scaffolds by Altering the Elasticity of Material Surfaces. *Biomacromolecules* **2013**, *14*, 1208.

S.-J. Kee, Y.-S. Kwon, Y.-W. Park, Y.-N. Cho, S.-J. Lee, T.-J. Kim, S.-S. Lee, H.-C. Jang, M.-G. Shin, J.-H. Shin, S.-P. Suh, D.-W. Ryang, Dysfunction of Natural Killer T Cells in Patients with Active Mycobacterium tuberculosis Infection. *Infect. Immun.* **2012**, *80*, 2100.

C. S. Kim, R. Mout, Y. Zhao, Y.-C. Yeh, R. Tang, Y. Jeong, B. Duncan, J. A. Hardy, V. M. Rotello, Co-Delivery of Protein and Small Molecule Therapeutics Using Nanoparticle-Stabilized Nanocapsules. *Bioconjugate Chem.* **2015**, *26*, 950.

S. Kobsa, W. M. Saltzman, Bioengineering Approaches to Controlled Protein Delivery. *Pediatr. Res.* **2008**, *63*, 513.
S. Kose, N. Imamoto, Y. Yoneda, Distinct energy requirement for nuclear import and export of importin β in living cells. *FEBS Lett.* **1999**, *463*, 327.
A. Kunze, P. Tseng, C. Godzich, C. Murray, A. Caputo, F. E. Schweizer, D. Di Carlo, Engineering cortical neuron polarity with nanomagnets on a chip. *ACS Nano* **2015**, *9*, 3664.
S. Kyle, S. Saha, Nanotechnology for the detection and therapy of stroke. *Adv. Healthcare Mater.* **2014**, *3*, 1703.
I. Laffaflan, M. B. Hallett, Gentle microinjection for myeloid cells using SLAM. *Blood* **2000**, *95*, 3270.
R. F. Landis, R. Tang, S. Hou, M. Yazdani, Y. Lee, V. M. Rotello, Zwitterionic Ligands Bound to Cdse/Zns Quantum Dots Prevent Adhesion to Mammalian Cells. *Phosphorus Sulfur Silicon Relat. Elem.* **2015**, *190*, 2302.
S. W. Lane, D. A. Williams, F. M. Watt, Modulating the stem cell niche for tissue regeneration. *Nat Biotech* **2014**, *32*, 795.
B. Leader, Q. J. Baca, D. E. Golan, Protein therapeutics: a summary and pharmacological classification. *Nat. Rev. Drug Discov.* **2008**, *7*, 21.
H. Lee, Y. Jang, J. Seo, J.-M. Nam, K. Char, Nanoparticle-Functionalized Polymer Platform for Controlling Metastatic Cancer Cell Adhesion, Shape, and Motility. *ACS Nano* **2011**, *5*, 5444.
J. H. Lee, H. L. Jang, K. M. Lee, H.-R. Baek, K. Jin, K. S. Hong, J. H. Noh, H.-K. Lee, In vitro and in vivo evaluation of the bioactivity of hydroxyapatite-coated polyetheretherketone biocomposites created by cold spray technology. *Acta Biomater.* **2013**, *9*, 6177.
T. Legigan, J. Clarhaut, I. Tranoy-Opalinski, A. Monvoisin, B. Renoux, M. Thomas, A. Le Pape, S. Lerondel, S. Papot, The First Generation of β-Galactosidase-Responsive Prodrugs Designed for the Selective Treatment of Solid Tumors in Prodrug Monotherapy. *Angew. Chem. Int. Ed.* **2012**, *51*, 11606.
S. A. Lelièvre, M. J. Bissell, in *Reviews in Cell Biology and Molecular Medicine*, Wiley-VCH Verlag GmbH & Co. KGaA, 2006.
A. Lerman, A. M. Zeiher, Endothelial Function: Cardiac Events. *Circulation* **2005**, *111*, 363.
N. Li, X. Zhang, Q. Song, R. Su, Q. Zhang, T. Kong, L. Liu, G. Jin, M. Tang, G. Cheng, The promotion of neurite sprouting and outgrowth of mouse hippocampal cells in culture by graphene substrates. *Biomaterials* **2011**, *32*, 9374.
S. Li, A. L. J. Symonds, T. Miao, I. Sanderson, P. Wang, Modulation of Antigen-Specific T-Cells as Immune Therapy for Chronic Infectious Diseases and Cancer. *Frontiers in Immunology* **2014**, *5*, 293.
J. Lippincott-Schwartz, E. Snapp, A. Kenworthy, Studying protein dynamics in living cells. *Nat. Rev. Mol. Cell Biol.* **2001**, *2*, 444.
X. Liu, Q. Feng, A. Bachhuka, K. Vasilev, Surface chemical functionalities affect the behavior of human adipose-derived stem cells in vitro. *Appl. Surf. Sci.* **2013**, *270*, 473.
X. O. Liu, M. Atwater, J. H. Wang, Q. Huo, Extinction coefficient of gold nanoparticles with different sizes and different capping ligands. *Colloid Surf. B-Biointerfaces* **2007**, *58*, 3.
S. L. Lo, S. Wang, Intracellular protein delivery systems formed by noncovalent bonding interactions between amphipathic peptide carriers and protein cargos. *Macromol. Rapid Commun.* **2010**, *31*, 1134.
E. R. Lorden, H. M. Levinson, K. W. Leong, Integration of drug, protein, and gene delivery systems with regenerative medicine. *Drug Deliv. Transl. Res.* **2013**, *5*, 168.

B. Lounis, J. Deich, F. I. Rosell, S. G. Boxer, W. E. Moerner, Photophysics of DsRed, a red fluorescent protein, from the ensemble to the single-molecule level. *J. Phys. Chem. B* **2001**, *105*, 5048.
S. W. Lowe, A. W. Lin, Apoptosis in cancer. *Carcinogenesis* **2000**, *21*, 485.
M. Lu, J. Zak, S. Chen, L. Sanchez-Pulido, David T. Severson, J. Endicott, Chris P. Ponting, Christopher J. Schofield, X. Lu, A Code for RanGDP Binding in Ankyrin Repeats Defines a Nuclear Import Pathway. *Cell* **2014**, *157*, 1130.
Y. Lu, W. Sun, Z. Gu, Stimuli-responsive nanomaterials for therapeutic protein delivery. *J. Control. Release* **2014**, *194*, 1.
A. Lujambio, To clear, or not to clear (senescent cells)? That is the question. *Inside the Cell* **2016**, *1*, 87.
Y. Ma, S. Cai, Q. Lv, Q. Jiang, Q. Zhang, Sodmergen, Z. Zhai, C. Zhang, Lamin B receptor plays a role in stimulating nuclear envelope production and targeting membrane vesicles to chromatin during nuclear envelope assembly through direct interaction with importin β. *J. Cell Sci.* **2007**, *120*, 520.
Z. Ma, Z. Mao, C. Gao, Surface modification and property analysis of biomedical polymers used for tissue engineering. *Colloids Surf. B* **2007**, *60*, 137.
N. Malik, M. S. Rao, A Review of the Methods for Human iPSC Derivation. *Methods Mol. Biol. (Clifton, N.J.)* **2013**, *997*, 23.
K. Maruyama, Intracellular targeting delivery of liposomal drugs to solid tumors based on EPR effects. *Adv. Drug Deliv. Rev.* **2011**, *63*, 161.
R. Matesanz, in *Stem Cell Transplantation*, (Eds: C. López-Larrea, A. López-Vázquez, B. Suárez-Álvarez), Springer US, New York, NY 2012, 1.
D. Mazia, Adhesion of cells to surfaces coated with polylysine. Applications to electron microscopy. *J. Cell Biol.* **1975**, *66*, 198.
T. M. Meese, Y. Hu, R. W. Nowak, K. G. Marra, Surface studies of coated polymer microspheres and protein release from tissue-engineered scaffolds. *J. Biomater. Sci.- Polym. Ed.* **2002**, *13*, 141.
M. A. Melan, G. Sluder, Redistribution and Differential Extraction of Soluble-Proteins in Permeabilized Cultured-Cells - Implications for Immunofluorescence Microscopy. *J. Cell Sci.* **1992**, *101*, 731.
K. Melikov, L. Chernomordik, Arginine-rich cell penetrating peptides: from endosomal uptake to nuclear delivery. *Cell. Mol. Life Sci.* **2005**, *62*, 2739.
P. Midoux, C. Pichon, J.-J. Yaouanc, P.-A. Jaffrès, Chemical vectors for gene delivery: a current review on polymers, peptides and lipids containing histidine or imidazole as nucleic acids carriers. *Br. J. Pharmacol.* **2009**, *157*, 166.
A. I. Mihajlović, V. Thamodaran, A. W. Bruce, The first two cell-fate decisions of preimplantation mouse embryo development are not functionally independent. *Sci Rep* **2015**, *5*, 15034.
O. R. Miranda, H.-T. Chen, C.-C. You, D. E. Mortenson, X.-C. Yang, U. H. F. Bunz, V. M. Rotello, Enzyme-Amplified Array Sensing of Proteins in Solution and in Biofluids. *J. Am. Chem. Soc.* **2010**, *132*, 5285.
O. R. Miranda, X. N. Li, L. Garcia-Gonzalez, Z. J. Zhu, B. Yan, U. H. F. Bunz, V. M. Rotello, Colorimetric Bacteria Sensing Using a Supramolecular Enzyme-Nanoparticle Biosensor. *J. Am. Chem. Soc.* **2011**, *133*, 9650.
Y. Miyamoto, T. Saiwaki, J. Yamashita, Y. Yasuda, I. Kotera, S. Shibata, M. Shigeta, Y. Hiraoka, T. Haraguchi, Y. Yoneda, Cellular stresses induce the nuclear accumulation of importin α and cause a conventional nuclear import block. *J. Cell Biol.* **2004**, *165*, 617.

Y. Mochizuki, K. Omura, H. Hideaki, T. Kugimoto, T. Osako, T. Taguch, Chronic mandibular osteomyelitis with suspected underlying synovitis, acne, pustulosis, hyperostosis, and osteitis (SAPHO) syndrome: a case report. *JIR* **2012**, 29.

R. Mout, G. Y. Tonga, M. Ray, D. F. Moyano, Y. Xing, V. M. Rotello, Environmentally responsive histidine-carboxylate zipper formation between proteins and nanoparticles. *Nanoscale* **2014**, *6*, 8873.

R. Mout, G. Y. Tonga, M. Ray, D. F. Moyano, Y. Q. Xing, V. M. Rotello, Environmentally responsive histidine-carboxylate zipper formation between proteins and nanoparticles. *Nanoscale* **2014**, *6*, 8873.

D. F. Moyano, V. M. Rotello, Nano Meets Biology: Structure and Function at the Nanoparticle Interface. *Langmuir* **2011**, *27*, 10376.

M. Mrksich, A surface chemistry approach to studying cell adhesion. *Chem. Soc. Rev.* **2000**, *29*, 267.

S. R. Mudshinge, A. B. Deore, S. Patil, C. M. Bhalgat, Nanoparticles: Emerging carriers for drug delivery. *Saudi Pharm. J.* **2011**, *19*, 129.

A. Mukhopadhyay, H. Weiner, Delivery of Drugs and Macromolecules to Mitochondria. *Adv. Drug Deliv. Rev.* **2007**, *59*, 729.

A. R. Murphy, P. S. John, D. L. Kaplan, Modification of silk fibroin using diazonium coupling chemistry and the effects on hMSC proliferation and differentiation. *Biomaterials* **2008**, *29*, 2829.

B. S. Murty, P. Shankar, B. Raj, B. B. Rath, J. Murday, in *Textbook of Nanoscience and Nanotechnology*, Springer Berlin Heidelberg, Berlin, Heidelberg 2013, 29.

R. Nair, P. Carter, B. Rost, NLSdb: database of nuclear localization signals. *Nucleic Acids Res.* **2003**, *31*, 397.

C. Nombela-Arrieta, J. Ritz, L. E. Silberstein, The elusive nature and function of mesenchymal stem cells. *Nat. Rev. Mol. Cell Biol.* **2011**, *12*, 126.

H. Ogawa, S. Inouye, F. I. Tsuji, K. Yasuda, K. Umesono, Localization, trafficking, and temperature-dependence of the Aequorea green fluorescent protein in cultured vertebrate cells. *Proc. Natl. Acad. Sci. U. S. A.* **1995**, *92*, 11899.

T. Ogawa, S. Ono, T. Ichikawa, S. Arimitsu, K. Onoda, K. Tokunaga, K. Sugiu, K. Tomizawa, H. Matsui, I. Date, Protein transduction method for cerebrovascular disorders. *Acta Med. Okayama* **2009**, *63*, 1.

K. Ohara, J. J. Vasseur, M. Smietana, NIS-promoted guanylation of amines. *Tetrahedron Lett.* **2009**, *50*, 1463.

Z. Onder, J. Moroianu, Nuclear import of cutaneous beta genus HPV8 E7 oncoprotein is mediated by hydrophobic interactions between its zinc-binding domain and FG nucleoporins. *Virology* **2014**, *449*, 150.

H. C. Ott, T. S. Matthiesen, S.-K. Goh, L. D. Black, S. M. Kren, T. I. Netoff, D. A. Taylor, Perfusion-decellularized matrix: using nature's platform to engineer a bioartificial heart. *Nat. Med.* **2008**, *14*, 213.

V. Pansare, S. Hejazi, W. Faenza, R. K. Prud'homme, Review of Long-Wavelength Optical and NIR Imaging Materials: Contrast Agents, Fluorophores and Multifunctional Nano Carriers. *Chem. Mat.* **2012**, *24*, 812.

B. Pappin, M. J. Kiefel, T. A. Houston, *Carbohydrates - Comprehensive Studies on Glycobiology and Glycotechnology Ch. 3*, InTech, Rijeka 2012.

M.-H. Park, C. Subramani, S. Rana, V. M. Rotello, Chemoselective Nanoporous Membranes via Chemically Directed Assembly of Nanoparticles and Dendrimers. *Adv. Mater.* **2012**, *24*, 5862.

C. Patsch, D. Kesseler, F. Edenhofer, Genetic engineering of mammalian cells by direct delivery of FLP recombinase protein. *Methods* **2011**, *53*, 386.

M. Peitz, K. Pfannkuche, K. Rajewsky, F. Edenhofer, Ability of the hydrophobic FGF and basic TAT peptides to promote cellular uptake of recombinant Cre recombinase: A tool for efficient genetic engineering of mammalian genomes. *Proc. Natl. Acad. Sci. U. S. A.* **2002**, *99*, 4489.

C. Peters, S. Brown, Antibody–drug conjugates as novel anti-cancer chemotherapeutics. *Biosci. Rep.* **2015**, *35*.

J. E. Phillips, T. A. Petrie, F. P. Creighton, A. J. García, Human mesenchymal stem cell differentiation on self-assembled monolayers presenting different surface chemistries. *Acta Biomater.* **2010**, *6*, 12.

P. Pieranski, Two-Dimensional Interfacial Colloidal Crystals. *Phys. Rev. Lett.* **1980**, *45*, 569.

G. Pillai, Nanomedicines for Cancer Therapy: An Update of FDA Approved and Those under Various Stages of Development. *SOJ Pharm. Pharm. Sci.* **2014**, *1*, 13.

A. Pinzon-Charry, T. Maxwell, J. A. Lopez, Dendritic cell dysfunction in cancer: A mechanism for immunosuppression. *Immunol. Cell Biol.* **2005**, *83*, 451.

A. Pinzon-Charry, T. Woodberry, V. Kienzle, V. McPhun, G. Minigo, D. A. Lampah, E. Kenangalem, C. Engwerda, J. A. López, N. M. Anstey, M. F. Good, Apoptosis and dysfunction of blood dendritic cells in patients with falciparum and vivax malaria. *J. Exp. Med.* **2013**, *210*, 1635.

L. Qi, N. Li, R. Huang, Q. Song, L. Wang, Q. Zhang, R. Su, T. Kong, M. Tang, G. Cheng, The effects of topographical patterns and sizes on neural stem cell behavior. *PLoS One* **2013**, *8*, e59022.

H. Raagel, P. Saalik, M. Pooga, Peptide-mediated protein delivery-Which pathways are penetrable? *Biochim. Biophys. Acta-Biomembr.* **2010**, *1798*, 2240.

H. Räägel, P. Säälik, M. Pooga, Peptide-mediated protein delivery—Which pathways are penetrable? *BBA-Biomembranes* **2010**, *1798*, 2240.

L. Rajendran, H. J. Knolker, K. Simons, Subcellular targeting strategies for drug design and delivery. *Nat. Rev. Drug Discov.* **2010**, *9*, 29.

S. Rana, A. Bajaj, R. Mout, V. M. Rotello, Monolayer coated gold nanoparticles for delivery applications. *Adv. Drug Deliv. Rev.* **2012**, *64*, 200.

S. Rana, A. K. Singla, A. Bajaj, S. G. Elci, O. R. Miranda, R. Mout, B. Yan, F. R. Jirik, V. M. Rotello, Array-Based Sensing of Metastatic Cells and Tissues Using Nanoparticle-Fluorescent Protein Conjugates. *ACS Nano* **2012**, *6*, 8233.

H. Rashidi, J. Yang, K. M. Shakesheff, Surface engineering of synthetic polymer materials for tissue engineering and regenerative medicine applications. *Biomater. Sci.* **2014**, *2*, 1318.

M. Ray, R. Tang, Z. Jiang, V. M. Rotello, Quantitative Tracking of Protein Trafficking to the Nucleus Using Cytosolic Protein Delivery by Nanoparticle-Stabilized Nanocapsules. *Bioconjugate Chem.* **2015**, *26*, 1004.

J. P. Richard, K. Melikov, E. Vives, C. Ramos, B. Verbeure, M. J. Gait, L. V. Chernomordik, B. Lebleu, Cell-penetrating peptides - A reevaluation of the mechanism of cellular uptake. *J. Biol. Chem.* **2003**, *278*, 585.

L. Richert, F. Vetrone, J. H. Yi, S. F. Zalzal, J. D. Wuest, F. Rosei, A. Nanci, Surface nanopatterning to control cell growth. *Adv. Mater.* **2008**, *20*, 1488.

J. Robbins, S. M. Dilworthtt, R. A. Laskey, C. Dingwall, Two interdependent basic domains in nucleoplasmin nuclear targeting sequence: Identification of a class of bipartite nuclear targeting sequence. *Cell* **1991**, *64*, 615.
M. P. Rodero, K. Khosrotehrani, Skin wound healing modulation by macrophages. *Int. J. Clin. Exp. Pathol.* **2010**, *3*, 643.
F. Rodrigues, M. van Hemert, H. Y. Steensma, M. Côrte-Real, C. Leão, Red Fluorescent Protein (DsRed) as a Reporter in Saccharomyces cerevisiae. *J. Bacteriol.* **2001**, *183*, 3791.
S. I. Roohani-Esfahani, S. Nouri-Khorasani, Z. F. Lu, M. H. Fathi, M. Razavi, R. C. Appleyard, H. Zreiqat, Modification of porous calcium phosphate surfaces with different geometries of bioactive glass nanoparticles. *Mater. Sci. Eng. C* **2012**, *32*, 830.
I. Rousalova, E. Krepela, Granzyme B-induced apoptosis in cancer cells and its regulation (review). *Int. J. Oncol.* **2010**, *37*, 1361.
N. M. Sakhrani, H. Padh, Organelle targeting: third level of drug targeting. *Drug Des. Dev. Ther.* **2013**, *7*, 585.
S. Salmaso, P. Caliceti, Self assembling nanocomposites for protein delivery: Supramolecular interactions of soluble polymers with protein drugs. *Int. J. Pharm.* **2013**, *440*, 111.
V. Sanna, N. Pala, G. Dessì, P. Manconi, A. Mariani, S. Dedola, M. Rassu, C. Crosio, C. Iaccarino, M. Sechi, Single-step green synthesis and characterization of gold-conjugated polyphenol nanoparticles with antioxidant and biological activities. *Int. J. Nanomed.* **2014**, *9*, 4935.
S. Saraswat, A. Desireddy, D. Zheng, L. Guo, H. P. Lu, T. P. Bigioni, D. Isailovic, Energy Transfer from Fluorescent Proteins to Metal Nanoparticles. *J. Phys. Chem. C* **2011**, *115*, 17587.
I. Sassoon, V. Blanc, in *Antibody-Drug Conjugates*, Vol. 1045 (Ed: L. Ducry), Humana Press, 2013, 1.
T. Satoh, S. Kakimoto, H. Kano, M. Nakatani, S. Shinkai, T. Nagasaki, In vitro gene delivery to HepG2 cells using galactosylated 6-amino-6-deoxychitosan as a DNA carrier. *Carbohydr. Res.* **2007**, *342*, 1427.
C. Schäfer, B. Borm, S. Born, C. Möhl, E.-M. Eibl, B. Hoffmann, One step ahead: Role of filopodia in adhesion formation during cell migration of keratinocytes. *Exp. Cell Res.* **2009**, *315*, 1212.
U. Schnell, F. Dijk, K. A. Sjollema, B. N. G. Giepmans, Immunolabeling artifacts and the need for live-cell imaging. *Nat. Methods* **2012**, *9*, 152.
L. M. Schwiebert, R. P. Schleimer, S. F. Radka, S. J. Ono, Modulation of MHC class II expression in human cells by dexamethasone. *Cell. Immunol.* **1995**, *165*, 12.
P. Sciau, *Nanoparticles in Ancient Materials: The Metallic Lustre Decorations of Medieval Ceramics*, Vol. 115, INTECH Open Access Publisher, 2012.
D. A. Shah, S.-J. Kwon, S. S. Bale, A. Banerjee, J. S. Dordick, R. S. Kane, Regulation of stem cell signaling by nanoparticle-mediated intracellular protein delivery. *Biomaterials* **2011**, *32*, 3210.
T. Shan, W. Liu, S. Kuang, Fatty acid binding protein 4 expression marks a population of adipocyte progenitors in white and brown adipose tissues. *Faseb J.* **2012**, *27*, 277.
R. S. Siffert, THE ROLE OF ALKALINE PHOSPHATASE IN OSTEOGENESIS. *J. Exp. Med.* **1951**, *93*, 415.
R. Sipehia, G. Martucci, J. Lipscombe, Transplantation of Human Endothelial Cell Monolayer on Artificial Vascular Prosthesis: The Effect of Growth-Support Surface Chemistry, Cell Seeding Density, Ecm Protein Coating, and Growth Factors. *Artificial Cells, Blood Substitutes, and Biotechnology* **1996**, *24*, 51.

A. Skardal, D. Mack, A. Atala, S. Soker, Substrate elasticity controls cell proliferation, surface marker expression and motile phenotype in amniotic fluid-derived stem cells. *J. Mech. Behav. Biomed. Mater.* **2013**, *17*, 307.

R. A. Sperling, P. Rivera Gil, F. Zhang, M. Zanella, W. J. Parak, Biological applications of gold nanoparticles. *Chem. Soc. Rev.* **2008**, *37*, 1896.

C. M. Stanford, Surface Modification of Biomedical and Dental Implants and the Processes of Inflammation, Wound Healing and Bone Formation. *Int. J. Mol. Sci.* **2010**, *11*, 354.

D. J. Stephens, R. Pepperkok, The many ways to cross the plasma membrane. *Proc. Natl. Acad. Sci. U. S. A.* **2001**, *98*, 4295.

M. P. Stewart, A. Lorenz, J. Dahlman, G. Sahay, Challenges in carrier-mediated intracellular delivery: moving beyond endosomal barriers. *Wiley Interdisciplinary Reviews: Nanomedicine and Nanobiotechnology* **2015**, n/a.

J. L. Stilwell, R. J. Samulski, Role of Viral Vectors and Virion Shells in Cellular Gene Expression. *Mol. Ther.* **2004**, *9*, 337.

C. Subramani, K. Saha, B. Creran, A. Bajaj, D. F. Moyano, H. Wang, V. M. Rotello, Cell Alignment using Patterned Biocompatible Gold Nanoparticle Templates. *Small* **2012**, *8*, 1209.

W. Sun, Y. Lu, Z. Gu, Advances in Anticancer Protein Delivery using Micro-/Nanoparticles. *Part. Part. Syst. Charact.* **2014**, *31*, 1204.

K. B. Sutradhar, M. L. Amin, Nanotechnology in Cancer Drug Delivery and Selective Targeting. *ISRN Nanotechnology* **2014**, *2014*, 12.

K. Takahashi, S. Yamanaka, Induction of Pluripotent Stem Cells from Mouse Embryonic and Adult Fibroblast Cultures by Defined Factors. *Cell*, *126*, 663.

Y. Takahashi, M. Shintani, N. Takase, Y. Kazo, F. Kawamura, H. Hara, H. Nishida, K. Okada, H. Yamane, H. Nojiri, Modulation of primary cell function of host Pseudomonas bacteria by the conjugative plasmid pCAR1. *Environ. Microbiol.* **2015**, *17*, 134.

R. Tang, C. S. Kim, D. J. Solfiell, S. Rana, R. Mout, E. M. Velázquez-Delgado, A. Chompoosor, Y. Jeong, B. Yan, Z.-J. Zhu, C. Kim, J. A. Hardy, V. M. Rotello, Direct Delivery of Functional Proteins and Enzymes to the Cytosol Using Nanoparticle-Stabilized Nanocapsules. *ACS Nano* **2013**, *7*, 6667.

R. Tang, D. F. Moyano, C. Subramani, B. Yan, E. Jeoung, G. Y. Tonga, B. Duncan, Y.-C. Yeh, Z. Jiang, C. Kim, V. M. Rotello, Rapid Coating of Surfaces with Functionalized Nanoparticles for Regulation of Cell Behavior. *Adv. Mater.* **2014**, *26*, 3310.

B. K. K. Teo, S. T. Wong, C. K. Lim, T. Y. S. Kung, C. H. Yap, Y. Ramagopal, L. H. Romer, E. K. F. Yim, Nanotopography Modulates Mechanotransduction of Stem Cells and Induces Differentiation through Focal Adhesion Kinase. *ACS Nano* **2013**, *7*, 4785.

S. R. Terlecky, J. I. Koepke, Drug delivery to peroxisomes: Employing unique trafficking mechanisms to target protein therapeutics. *Adv. Drug Deliv. Rev.* **2007**, *59*, 739.

A. S. Thakor, J. Jokerst, C. Zavaleta, T. F. Massoud, S. S. Gambhir, Gold Nanoparticles: A Revival in Precious Metal Administration to Patients. *Nano Lett.* **2011**, *11*, 4029.

K. L. Thompson, M. Williams, S. P. Armes, Colloidosomes: Synthesis, properties and applications. *J. Colloid Interface Sci.* **2015**, *447*, 217.

L. F. Tietze, B. Krewer, Antibody-Directed Enzyme Prodrug Therapy: A Promising Approach for a Selective Treatment of Cancer Based on Prodrugs and Monoclonal Antibodies. *Chem. Biol. Drug Des.* **2009**, *74*, 205.

G. K. Toworfe, S. Bhattacharyya, R. J. Composto, C. S. Adams, I. M. Shapiro, P. Ducheyne, Effect of functional end groups of silane self-assembled monolayer surfaces on apatite formation, fibronectin adsorption and osteoblast cell function. *J. Tissue Eng. Regen. Med.* **2009**, *3*, 26.

H. C. Tsui, K. L. Lankford, W. L. Klein, Differentiation of neuronal growth cones: specialization of filopodial tips for adhesive interactions. *Proc. Natl. Acad. Sci. U. S. A.* **1985**, *82*, 8256.

R. F. Turcotte, R. T. Raines, Design and Characterization of an HIV-Specific Ribonuclease Zymogen. *Aids Res. Hum. Retrovir.* **2008**, *24*, 1357.

B. Valamehr, S. J. Jonas, J. Polleux, R. Qiao, S. Guo, E. H. Gschweng, B. Stiles, K. Kam, T.-J. M. Luo, O. N. Witte, X. Liu, B. Dunn, H. Wu, Hydrophobic surfaces for enhanced differentiation of embryonic stem cell-derived embryoid bodies. *Proc. Natl. Acad. Sci. U. S. A.* **2008**, *105*, 14459.

F. Variola, J. B. Brunski, G. Orsini, P. Tambasco de Oliveira, R. Wazen, A. Nanci, Nanoscale surface modifications of medically relevant metals: state-of-the art and perspectives. *Nanoscale* **2011**, *3*, 335.

T. Vignaud, R. Galland, Q. Tseng, L. Blanchoin, J. Colombelli, M. Thery, Reprogramming cell shape with laser nano-patterning. *J. Cell Sci.* **2012**, *125*, 2134.

J. S. Wadia, R. V. Stan, S. F. Dowdy, Transducible TAT-HA fusogenic peptide enhances escape of TAT-fusion proteins after lipid raft macropinocytosis. *Nat. Med.* **2004**, *10*, 310.

K. M. Wagstaff, S. M. Rawlinson, A. C. Hearps, D. A. Jans, An AlphaScreen®-Based Assay for High-Throughput Screening for Specific Inhibitors of Nuclear Import. *J. Biomol. Screen* **2011**, *16*, 192.

H. Wang, D. T. K. Kwok, M. Xu, H. Shi, Z. Wu, W. Zhang, P. K. Chu, Tailoring of Mesenchymal Stem Cells Behavior on Plasma-Modified Polytetrafluoroethylene. *Adv. Mater.* **2012**, *24*, 3315.

M. Wang, S. Sun, C. I. Neufeld, B. Perez-Ramirez, Q. Xu, Reactive Oxygen Species-Responsive Protein Modification and Its Intracellular Delivery for Targeted Cancer Therapy. *Angew Chem Int Edit* **2014**, *53*, 13444.

P.-Y. Wang, L. R. Clements, H. Thissen, W.-B. Tsai, N. H. Voelcker, Screening rat mesenchymal stem cell attachment and differentiation on surface chemistries using plasma polymer gradients. *Acta Biomater.* **2015**, *11*, 58.

R. B. Wang, P. S. Billone, W. M. Mullett, Nanomedicine in Action: An Overview of Cancer Nanomedicine on the Market and in Clinical Trials. *J. Nanomater.* **2013**.

X. Wang, S. Li, C. Yan, P. Liu, J. Ding, Fabrication of RGD micro/nanopattern and corresponding study of stem cell differentiation. *Nano Lett.* **2015**, *15*, 1457.

A. Watabe, T. Yamaguchi, T. Kawanishi, E. Uchida, A. Eguchi, H. Mizuguchi, T. Mayumi, M. Nakanishi, T. Hayakawa, Target-cell specificity of fusogenic liposomes: Membrane fusion-mediated macromolecule delivery into human blood mononuclear cells. *BBA-Biomembranes* **1999**, *1416*, 339.

F. M. Watt, W. T. S. Huck, Role of the extracellular matrix in regulating stem cell fate. *Nat. Rev. Mol. Cell Biol.* **2013**, *14*, 467.

X. Wei, V. G. Henke, C. Strübing, E. B. Brown, D. E. Clapham, Real-Time Imaging of Nuclear Permeation by EGFP in Single Intact Cells. *Biophys. J.* **2003**, *84*, 1317.

J. Wen, G. Somorjai, F. Lim, R. Ward, XPS Study of Surface Composition of a Segmented Polyurethane Block Copolymer Modified by PDMS End Groups and Its Blends with Phenoxy. *Macromolecules* **1997**, *30*, 7206.

J. H. Wen, L. G. Vincent, A. Fuhrmann, Y. S. Choi, K. C. Hribar, H. Taylor-Weiner, S. Chen, A. J. Engler, Interplay of matrix stiffness and protein tethering in stem cell differentiation. *Nat. Mater.* **2014**, *13*, 979.

S. L. Wiskur, J. L. Lavigne, A. Metzger, S. L. Tobey, V. Lynch, E. V. Anslyn, Thermodynamic analysis of receptors based on guanidinium/boronic acid groups for the complexation of carboxylates, alpha-hydroxycarboxylates, and diols: Driving force for binding and cooperativity. *Chem.-Eur. J.* **2004**, *10*, 3792.

A. T. Wright, M. J. Griffin, Z. Zhong, S. C. McCleskey, E. V. Anslyn, J. T. McDevitt, Differential Receptors Create Patterns That Distinguish Various Proteins. *Angewandte Chemie* **2005**, *117*, 6533.

Y. Wu, Z. Ai, K. Yao, L. Cao, J. Du, X. Shi, Z. Guo, Y. Zhang, CHIR99021 promotes self-renewal of mouse embryonic stem cells by modulation of protein-encoding gene and long intergenic non-coding RNA expression. *Exp. Cell Res.* **2013**, *319*, 2684.

Y. N. Xia, P. D. Yang, Y. G. Sun, Y. Y. Wu, B. Mayers, B. Gates, Y. D. Yin, F. Kim, Y. Q. Yan, One-dimensional nanostructures: Synthesis, characterization, and applications. *Adv. Mater.* **2003**, *15*, 353.

M. Yamamoto, K. Yamamoto, T. Noumura, Type I Collagen Promotes Modulation of Cultured Rabbit Arterial Smooth Muscle Cells from a Contractile to a Synthetic Phenotype. *Exp. Cell Res.* **1993**, *204*, 121.

K. Yamanouchi, Y. Gotoh, M. Nagayama, Dexamethasone enhances differentiation of human osteoblastic cells in vitro. *J. Bone Miner. Metab.*, *15*, 23.

M. Yan, J. Du, Z. Gu, M. Liang, Y. Hu, W. Zhang, S. Priceman, L. Wu, Z. H. Zhou, Z. Liu, T. Segura, Y. Tang, Y. Lu, A novel intracellular protein delivery platform based on single-protein nanocapsules. *Nat. Nanotechnol.* **2010**, *5*, 48.

X.-C. Yang, B. Samanta, S. S. Agasti, Y. Jeong, Z.-J. Zhu, S. Rana, O. R. Miranda, V. M. Rotello, Drug Delivery Using Nanoparticle-Stabilized Nanocapsules. *Angew Chem Int Edit* **2010**, *50*, 477.

X.-C. Yang, B. Samanta, S. S. Agasti, Y. Jeong, Z.-J. Zhu, S. Rana, O. R. Miranda, V. M. Rotello, Drug Delivery Using Nanoparticle-Stabilized Nanocapsules. *Angew Chem Int Edit* **2011**, *50*, 477.

Y. Yarden, M. X. Sliwkowski, Untangling the ErbB signalling network. *Nat. Rev. Mol. Cell Biol.* **2001**, *2*, 127.

K. Ye, X. Wang, L. Cao, S. Li, Z. Li, L. Yu, J. Ding, Matrix Stiffness and Nanoscale Spatial Organization of Cell-Adhesive Ligands Direct Stem Cell Fate. *Nano Lett.* **2015**, *15*, 4720.

Y. C. Yeh, B. Creran, V. M. Rotello, Gold nanoparticles: preparation, properties, and applications in bionanotechnology. *Nanoscale* **2012**, *4*, 1871.

Y. C. Yeh, R. Tang, R. Mout, Y. Jeong, V. M. Rotello, Fabrication of Multiresponsive Bioactive Nanocapsules through Orthogonal Self-Assembly. *Angew Chem Int Edit* **2014**, *53*, 5137.

T. Yoshikawa, T. Sugita, Y. Mukai, Y. Abe, S. Nakagawa, H. Kamada, S.-i. Tsunoda, Y. Tsutsumi, The augmentation of intracellular delivery of peptide therapeutics by artificial protein transduction domains. *Biomaterials* **2009**, *30*, 3318.

C.-C. You, M. De, G. Han, V. M. Rotello, Tunable inhibition and denaturation of α-chymotrypsin with amino acid-functionalized gold nanoparticles. *J. Am. Chem. Soc.* **2005**, *127*, 12873.

C.-C. You, O. R. Miranda, B. Gider, P. S. Ghosh, I.-B. Kim, B. Erdogan, S. A. Krovi, U. H. F. Bunz, V. M. Rotello, Detection and identification of proteins using nanoparticle-fluorescent polymer chemical nose sensors. *Nat. Nanotechnol.* **2007**, *2*, 318.

A. Zafar, R. Melendez, S. J. Geib, A. D. Hamilton, Hydrogen bond controlled aggregation of guanidinium-carboxylate derivatives in the solid state. *Tetrahedron* **2002**, *58*, 683.
B. Zassler, I. E. Blasig, C. Humpel, Protein delivery of caspase-3 induces cell death in malignant C6 glioma, primary astrocytes and immortalized and primary brain capillary endothelial cells. *J. Neuro-Oncol.* **2005**, *71*, 127.
O. Zelphati, Y. Wang, S. Kitada, J. C. Reed, P. L. Felgner, J. Corbeil, Intracellular delivery of proteins with a new lipid-mediated delivery system. *J. Biol. Chem.* **2001**, *276*, 35103.
X. Zhang, Gold Nanoparticles: Recent Advances in the Biomedical Applications. *Cell Biochem. Biophys.* **2015**.
Y. Zhang, L.-C. Yu, Microinjection as a tool of mechanical delivery. *Curr. Opin. Biotechnol.* **2008**, *19*, 506.
X.-M. Zhao, Y. Xia, G. M. Whitesides, Soft lithographic methods for nano-fabrication. *J. Mater. Chem.* **1997**, *7*, 1069.
W. F. Zheng, W. Zhang, X. Y. Jiang, Precise Control of Cell Adhesion by Combination of Surface Chemistry and Soft Lithography. *Advanced Healthcare Materials* **2013**, *2*, 95.
H. Zhou, S. Wu, J. Y. Joo, S. Zhu, D. W. Han, T. Lin, S. Trauger, G. Bien, S. Yao, Y. Zhu, G. Siuzdak, H. R. Schöler, L. Duan, S. Ding, Generation of Induced Pluripotent Stem Cells Using Recombinant Proteins. *Cell Stem Cell* **2009**, *4*, 381.
H. Y. Zhou, S. L. Wu, J. Y. Joo, S. Y. Zhu, D. W. Han, T. X. Lin, S. Trauger, G. Bien, S. Yao, Y. Zhu, G. Siuzdak, H. R. Scholer, L. X. Duan, S. Ding, Generation of induced pluripotent stem cells using recombinant proteins. *Cell Stem Cell* **2009**, *4*, 581.
Z.-J. Zhu, R. Carboni, M. J. Quercio, B. Yan, O. R. Miranda, D. L. Anderton, K. F. Arcaro, V. M. Rotello, R. W. Vachet, Surface Properties Dictate Uptake, Distribution, Excretion, and Toxicity of Nanoparticles in Fish. *Small* **2010**, *6*, 2261.
M. Zimmermann, N. Meyer, Annexin V/7-AAD staining in keratinocytes. *Methods Mol. Biol.* **2011**, *740*, 57.
J. A. Zuris, D. B. Thompson, Y. Shu, J. P. Guilinger, J. L. Bessen, J. H. Hu, M. L. Maeder, J. K. Joung, Z.-Y. Chen, D. R. Liu, Cationic lipid-mediated delivery of proteins enables efficient protein-based genome editing in vitro and in vivo. *Nat. Biotechnol.* **2015**, *33*, 73.